FUNCTIONAL ANALYSIS OF P63-YB1 INTERACTION IN NORMAL AND TRANSFORMED EPITHELIAL CELLS: DEVELOPMENT OF NOVEL MOLECULAR TOOLS FOR SQUAMOUS CANCER DIAGNOSIS AND THERAPY

ANNAELENA TROIANO

Dottorato in Scienze Biotecnologiche – XXVII ciclo
Indirizzo Biotecnologie Industriali e Molecolari
Università di Napoli Federico II

Dottorato in Scienze Biotecnologiche – XXVII ciclo
Indirizzo Biotecnologie Industriali e Molecolari
Università di Napoli Federico II

FUNCTIONAL ANALYSIS OF P63-YB1 INTERACTION IN NORMAL AND TRANSFORMED EPITHELIAL CELLS: DEVELOPMENT OF NOVEL MOLECULAR TOOLS FOR SQUAMOUS CANCER DIAGNOSIS AND THERAPY

ANNAELENA TROIANO

Dottoranda: Dr.ssa Annaelena Troiano

Relatore: Prof.ssa Viola Calabrò

Coordinatore: Prof. Giovanni Sannia

INDEX

Riassunto

L'epidermide è un tessuto epiteliale pluristratificato la cui omeostasi dipende da un preciso equilibrio fra proliferazione, differenziamento e morte cellulare. Lo studio dei meccanismi che regolano la vitalità e la crescita delle cellule che lo compongono ha un forte impatto su una serie di settori di interesse biotecnologico come la cosmesi e la riparazione tissutale.
Gli epiteli pluristratificati sono costituiti da più ordini di cellule sovrapposte e svolgono funzioni di rivestimento e di protezione.
Nell'epidermide si distinguono, dalla profondità alla superficie, uno *strato basale*, uno *strato spinoso*, uno *strato granuloso*, uno *strato lucido* e uno *strato corneo*. Come in tutti gli epiteli, le cellule basali, tipicamente staminali, si moltiplicano per mitosi e danno origine a nuove cellule che, differenziando, si spostano verso la superficie. Le cellule che risalgono negli strati sovrabasali non proliferano più, si modificano nella struttura e nella funzione ed esprimono particolari proteine, le *cheratine*, che si accumulano nel citoplasma sottoforma di filamenti intermedi. Il processo ha termine con la formazione di lamelle cornee appiattite. Questo fenomeno prende il nome di cheratinizzazione e le cellule coinvolte sono chiamate *cheratinociti* (*Rosati and Colombo*, 2003.)
La pelle è un organo complesso, metabolicamente attivo e che svolge diverse funzioni. Essa, infatti, costituisce una barriera fisica dell'organismo verso l'ambiente esterno, regola il passaggio di acqua e di altre sostanze, fornisce protezione contro micro-organismi, agenti tossici, raggi ultravioletti e insulti meccanici (*Randall*, 2006).
Alterazioni a carico dei processi che regolano l'omeostasi dell'epidermide possono contribuire all'insorgenza di tumori. I tumori della pelle sono classificati in *non-melanoma skin cancer* (NMSC) e *melanoma*. I primi sono suddivisi in epiteliali o *squamous cell carcinoma* (SCC) e non epiteliali o *basal cell carcinoma* (BBC) (*Yun-Hsuan Ouyang*, 2010).
Il carcinoma squamoso (SCC) è un tumore resistente ai trattamenti terapeutici che si origina negli epiteli della pelle, dell'esofago, del polmone e delle cavità orali ed è frequentemente associato ad inattivazione mutazionale di p53 e ad over-espressione dell'oncoproteina ΔNp63α, codificata dal locus genico di TP63 (*Hibi*, 2000). Questo locus, mediante l'uso di promotori alternativi, origina due categorie di isoforme, chiamate *TA* e *ΔN* (*Yang*, 1998), mentre eventi di *splicing* alternativo al C-terminale generano almeno tre varianti di p63 (α, β e γ) in ciascuna classe (*Blanpain and Fuchs*, 2007). Il locus di TP63 risulta amplificato nell'88% dei tumori al polmone e nell'80% dei carcinomi squamosi cutanei e ΔNp63α è la principale isoforma iperespressa (*Hibi*, 2000; *Reis-Filho*, 2002; *Rocco*, 2006).
In condizioni fisiologiche ΔNp63α è espressa in modo predominante nello strato basale dell'epidermide adulta ed è un importante fattore pro-proliferativo nonchè un marker della staminalità. Durante il differenziamento del cheratinocita la sua espressione si riduce fino a scomparire e se, a causa di alterazioni del programma differenziativo, ciò non si verifica si determina iperplasia che predispone alla trasformazione maligna (*Moll*, 2004).
In studi comparativi sull'espressione di p63 tra tumori primari e metastatici ΔNp63α risulta iper-espressa nell'89% dei tumori primari della pelle, ma solo nell'11% delle metastasi cutanee (*Kanitakis*, 2007). E' stato inoltre dimostrato che l'inattivazione delle funzioni di p63 incrementa il potenziale metastatico mediato da TGFβ (*Adorno*, 2009) e ciò sostiene l'ipotesi che la perdita, piuttosto che l'over-espressione, di ΔNp63α sia associata al fenomeno della metastasi (*Rocco*, 2006).

L'espressione di ΔNp63α può essere indotta da diversi "pathway" di trasduzione del segnale come quello dell'FGFR2 (*Ramsey*, 2013), di PI3K (*Barbieri*, 2003) e dell'EGFR (*Ripamonti*, 2013). Tuttavia, l' inibizione di ciascuno di questi "signaling" non si è rivelata efficace nel trattamento del carcinoma squamoso (*Ramsey*, 2013). Nel complesso queste osservazioni suggeriscono che potrebbe essere interessante valutare i "partner" molecolari di ΔNp63α per comprendere meglio le funzioni della proteina nel controllo della proliferazione e valutare nuovi approcci terapeutici per le neoplasie caratterizzate dalla sua iper-espressione. Ciò ha spinto il gruppo di ricerca presso il quale ho svolto il mio progetto di dottorato ad intraprendere un approccio di proteomica funzionale che ha portato alla identificazione della proteina YB-1 come potenziale interattore di ΔNp63α (*Amoresano*, 2010).
YB-1 o YBX-1 (*Y Box Binding protein 1*) è una proteina espressa nella maggior parte dei tessuti umani e il suo knockout in topi è letale a livello embrionale per anomalie nella chiusura del tubo neurale (*Uchiumi*, 2006). YB-1 è una proteina che si muove tra il citoplasma e il nucleo in risposta ad un'ampia varietà di stimoli, quali quelli di crescita, di stress e di danno al DNA (*Kim*, 2013). In studi clinici è stato dimostrato che la sua localizzazione nucleare è associata alla progressione tumorale e a prognosi negativa, in particolare nei tumori ovarici (*Panupinthu,* 2013), nel glioblastoma (*Faury*, 2007), nel melanoma (*Shittek*, 2007) e nel carcinoma squamoso (*Lasham*, 2013). YB-1, infatti, è un fattore di trascrizione di geni correlati alla proliferazione delle cellule staminali tumorali come CD44 e CD49f , reprime l'oncosoppressore $p16^{INK4A}$ e attiva geni pro-proliferativi quali PCNA, MDR1, EGFR e la ciclina B1 (*To*, 2010; *Fotovati*, 2011; *Lasham*, 2013).
Nel citoplasma, invece, YB-1 agisce come regolatore negativo della proliferazione inibendo la traduzione cap-dipendente di molti mRNA correlati alla crescita, quali le cicline D1 ed E, c-myc, c-jun, c-fos, PDGFR-α, TGF-α (*Sutherland*, 2005). Nel contempo la componente citoplasmatica della proteina YB-1 è responsabile dell'incremento del potenziale metastatico di cellule di carcinoma mammario, inducendo la traduzione IRES-dipendente di mRNA coinvolti nella transizione epitelio-mesenchima come Snail1, Slug e Twist (*Evdokimova*, 2006).
Infine dati recenti dimostrano l'esistenza di frammenti proteolitici di YB-1 secreti da cellule mesangiali, monocitiche e renali in seguito a stimoli infiammatori che interagendo con il recettore Notch-3 (*Rauen*, 2009) possono avere effetti mitogenici e promigratori (*Frye*, 2009).
Dal momento che la proteina YB-1 è coinvolta in diversi "pathway" oncogenici e pro-infiammatori essa è ritenuta un interessante target terapeutico. In particolare, sono stati sviluppati differenti approcci molecolari per interferire direttamente con la funzione della proteina o con quella di alcuni suoi regolatori (*Law*, 2010; *Shen*, 2011). Un esempio interessante e molto recente è la scoperta di una molecola ricavata da alcuni frutti e vegetali, chiamata FISETIN, che agisce come inibitore di YB-1 in cellule di carcinoma prostatico riducendone la proliferazione (*Khan*, 2014).

Sulla base di tutte queste considerazioni il mio progetto di dottorato ha avuto lo scopo di caratterizzare le relazioni funzionali tra le proteine ΔNp63α e YB-1 nella patogenesi dei carcinomi squamosi al fine di implementarne gli approcci terapeutici.
Durante lo svolgimento del mio progetto di dottorato ho contribuito a validare l'esistenza dell'interazione fisica tra ΔNp63α e YB-1 in cheratinociti primari immortalizzati (HaCaT) ed in cellule di carcinoma squamoso (SCC011). Ho verificato che tale specifica associazione fisica comporta l'accumulo nucleare di YB-1 ed influenza le funzioni che YB-1 svolge in questo compartimento. Ho inoltre dimostrato

che l'assenza di ΔNp63α in cellule di carcinoma squamoso aumenta la migrazione cellulare attraverso un meccanismo YB-1 dipendente (*Di Costanzo,* 2012).
In secondo luogo, il mio progetto di ricerca si è focalizzato sullo studio degli effetti dell'assenza di YB-1 in cheratinociti proliferanti e in differenziamento. Il silenziamento di YB-1 in cheratinociti immortalizzati ed in cellule di carcinoma squamoso non metastatiche influenza drammaticamente la vitalità e l'adesione cellulare, con concomitante diminuzione dei livelli di espressione di ΔNp63α e di CD44. Al contrario, in cellule di carcinoma squamoso altamente metastatiche, come le SCC022, ho osservato un effetto diametralmente opposto: l'assenza di YB-1 comporta l'attivazione del pathway di sopravvivenza cellulare PI3K/AKT. Questa parte della mia attività sperimentale ha contribuito alla conoscenza del network molecolare che governa la sopravvivenza e l'adesione delle cellule epiteliali e alla consapevolezza che ΔNp63α e YB-1 possono essere rilevanti nella patogenesi dei tumori squamosi (*Troiano*, 2014)

Ho trascorso parte del secondo anno di dottorato presso il Blizard Institute dell'univeristà Queen Mary di Londra per avviare un progetto di collaborazione con il gruppo di ricerca del professor Daniele Bergamaschi. Egli e i suoi collaboratori avevano recentemente dimostrato, per la prima volta, la stabilizzazione delle isoforme TA e ΔN di p63 nel nucleo e nei mitocondri di cellule di melanoma, in risposta a stress genotossici. In particolare, avevano osservato che l'espressione di entrambe le isoforme è associata a fenomeni di chemioresistenza in questo tipo di tumore (*Matin*, 2013).
Il melanoma è una forma tumorale particolarmente aggressiva che insorge nei melanociti della pelle, la cui incidenza è rapidamente incrementata nelle ultime decadi. Come in altri tumori, anche in melanoma la proteina YB-1 risulta iper-espressa e la sua traslocazione nucleare è associata alla progressione, alla migrazione e alla chemioresistenza del tumore (*Shittek*, 2007).
La collaborazione con il gruppo del Prof. Bergamaschi è nata al fine di verificare se p63 e YB-1 fossero coinvolti anche nella patogenesi e/o progressione del melanoma cutaneo.
Sebbene i dati da me ottenuti siano ancora preliminari, essi dimostrano l'esistenza in cellule di melanoma di peptidi di YB-1 a basso peso molecolare, la cui abbondanza e localizzazione dipende dall'espressione di p63. Questi peptidi-limite sono particolarmente interessanti e indubbiamente necessitano di essere studiati in maniera più approfondita, ad esempio valutandone il potenziale pro-proliferativo come già osservato in altri sistemi. Inoltre, i miei esperimenti di silenziamento di YB-1 in cellule di melanoma hanno dimostrato che, anche in queste cellule, esiste un cross-talk fra YB-1 e p63 importante per il controllo della vitalità e sopravvivenza delle cellule di melanoma.

Durante lo svolgimento del mio progetto di dottorato ho avuto l'opportunità di collaborare con la Prof.ssa Piera Quesada, esperta studiosa dell'enzima PARP (polyADP-ribose-polymerase) e del suo ruolo nel "signaling" indotto dal danno al DNA. La nostra collaborazione è nata allo scopo di valutare la risposta dei membri della famiglia di p53 all'uso di inibitori di PARP e di Topoisomerasi I in cellule di carcinoma mammario e squamoso. In particolare, il nostro obiettivo è stato quello di descrivere possibili meccanismi di chemioresistenza in cui fossero coinvolte alcune isoforme di p63.

L'enzima PARP è il principale membro di una famiglia di 18 proteine multifunzionali in grado di catalizzare la reazione di ADP-ribosilazione su proteine bersaglio (*O'Brien*, 2006).
La poli-ADP-ribosilazione è una modifica post-traduzionale dipendente dal danno al DNA, caratteristica di alcuni istoni e proteine nucleari e che contribuisce alla sopravvivenza cellulare. La proteina PARP ha un ruolo critico nel meccanismo di riparo del danno a singolo filamento del DNA; essa infatti lega il sito di rottura a singolo filamento, modifica le proteine nelle vicinanze e recluta in prossimità del sito di taglio il complesso di enzimi coinvolti nella riparazione del DNA (*Davar*, 2012).
Gli inibitori di PARP sono il frutto più recente del paradigma terapeutico della letalità sintetica nello sviluppo di farmaci anti-tumorali, ovvero la teoria secondo la quale due difetti considerati benigni in cellule tumorali possono diventare letali se combinati (*Davar*, 2012). Se, infatti, danni a singolo filamento non vengono riparati, durante la duplicazione cellulare, possono diventare danni a doppia catena che innescano la risposta di altri meccanismi specifici di riparo del DNA. Se, però, gli inibitori di PARP sono usati in cellule in cui uno di questi meccanismi è già compromesso, la loro combinazione può diventare letale per la cellula tumorale. Gli inibitori di PARP sono utilizzati in monoterapia nei carcinomi mammari di tipo 1 e 2 (BRCA1 e BRCA2) o in combinazione con altri agenti chemioterapici di danno al DNA, come la Camptotecina (CPT) e il suo derivato Topotecano (TPT), noti inibitori della Topoisomerasi I (*Malanga*, 2004).
Il mio lavoro ha messo in evidenza che in cellule di carcinoma mammario MCF7 il trattamento combinato dell'inibitore di PARP, PJ34, con l'inibitore della Topoisomerasi I, TPT, causa un forte incremento dei livelli delle isoforme TAp63α e γ; in particolare, TAp63γ è un potente induttore di apoptosi. Inoltre, ho contribuito a chiarire i meccanismi molecolari innescati dai trattamenti singoli e combinati di tali inibitori. E' stato, infatti, dimostrato che, mentre il singolo trattamento con TPT induce il reclutamento di p53 sul promotore di p21WAF e ne attiva la trascrizione, il trattamento combinato TPT+PJ34 imprime un cambiamento nel destino cellulare inducendo l'espressione di geni pro-apoptotici come BAX.
Infine, ho osservato che nelle cellule di carcinoma squamoso SCC022 che non esprimono p53, il trattamento TPT+PJ34 comporta la degradazione della proteina ΔNp63α , senza però indurre apoptosi. Se, però, il trattamento combinato è concomitante all' iper-espressione dell' isoforma TAp63γ la cellula recupera la sua capacità di andare in apoptosi inducendo geni pro-apoptotici come BAX.
I dati da me ottenuti per questa parte del progetto sono confluiti in due pubblicazioni dal titolo "p63 involvement in poly(ADP-ribose) polymerase 1 signaling of topoisomerase I-dependent DNA damage in carcinoma cells" e "Effect of poly(ADP-ribose) polymerase and DNA topoisomerase I inhibitors on the p53/p63-dependent survival of carcinoma cells" (*Montariello*, 2013; *Montariello*, 2015).

SUMMARY

Skin homeostasis is dependent on a tightly coordinated network of signaling pathways, resulting in a spatial and temporal balance of proliferation, growth arrest, differentiation, senescence and apoptosis. The knowledge of mechanisms that regulate keratinocyte growth and proliferation is attractive for several biotechnological fields, such as cosmetics, tissue engineering and skin regeneration.

ΔNp63α, as critical pro-proliferative factor and marker of epidermal stemness, is essential for morphogenesis of organs/tissues developing by epithelial-mesenchimal interactions such as the epidermis, teeth, hair and glands (*Mills*, 1999). Using a proteomic approach my research group had identified YB-1 as a ΔNp63α molecular partner (*Amoresano*, 2010). Y Box Binding protein 1 (YB-1) is a transcription/translation factor involved in a wide variety of cellular functions, including cell proliferation and migration, DNA repair, multidrug resistance and stress response to extracellular signals (*Lyabin*, 2014).

My PhD project was aimed to advance in the characterization of the functional interplay between ΔNp63α and Y-box binding 1 proteins using *in cell* approaches to elucidate their roles in skin proliferation.

First, I have validated ΔNp63α-YB-1 interaction in distinct cell contexts and demonstrated that this interaction causes accumulation of YB-1 into the nuclear compartment and influences its localization-dependent functions (*Di Costanzo*, 2012).

Then, I extended our knowledge on the YB-1 and ΔNp63α functional interplay demonstrating that, being able to sustain ΔNp63α gene expression, YB-1 is part of a complex molecular network linking ΔNp63α to the PI3K/AKT/PTEN pathway and that establishment of a positive feedback loop, coupling induction of ΔNp63α expression with PI3K/AKT activation, may be a relevant step in the progression of squamous carcinogenesis (*Troiano*, 2015).

During my PhD program, I have spent six months at the Blizard Institute - Queen Mary University of London collaborating with Professor Bergamaschi's team. Based on my experience on squamous carcinoma I explored if p63 and YB-1 are also involved in melanoma pathogenesis and/or progression.

Although my data are still preliminary, they show that ΔNp63α controls YB-1 protein integrity and nuclear localization also in melanoma cells and their functional cross-talk plays a role in melanoma cell survival.

Finally, thanks to the collaboration with Prof. Piera Quesada's team, I had the opportunity to perform experiments aimed to investigate on the role of p53 family members in the response of cancer cells to Topoisomerase I and poly(ADP-ribose)polymerase (PARP1) inhibitors.

My results point to a role for p63 in the cell response to treatment with TOP I and PARP-1 inhibitors. Highlighting the different outcome (i.e cell cycle arrest *vs* apoptosis) of PARP-1 activation/inhibition, my studies give right of the use of PARP inhibitor as chemotherapic adjuvant and/or in monotherapy also in TAp63/ΔNp63α proficient cancer cells (*Montariello*, 2013; *Montariello*, 2015).

1.INTRODUCTION

1.1 STRATIFIED SQUAMOUS EPITHELIA

A stratified epithelium consists of many layers of epithelial cells; in a stratified squamous epithelium the cells of the outer layers are flat (squamous). Stratified squamous epithelia function as coats in order to withstand abrasion and shear forces (*Rosati and Colombo*, 2003). Cells of the basal layer are small and cuboidal-to-columnar, however they gradually become larger and flat as the cells migrate to the apical layer. Cells of the apical layer are continuously replaced by the epithelial cells of deeper layers (*Randall*, 2006).
In the human body there are two major subtypes of stratified squamous epithelia:

Non-keratinizing: The apical surface of this epithelium is bathed by *mucus,* derived from glands and the cells lack large quantities of the protein *keratin,* therefore it is able to protect the underlying tissue only against relatively mild or moderate degree of abrasion. A non - keratinizing stratified squamous epithelium is found lining three prominent sites in the human body:

- the esophagus, the pharynx
- the sides and floor of the oral cavity
- the vagina, male and female urethra

Keratinizing: The surface of this epithelium is characteristically dry and free of mucus and keratinocytes represent the vast majority of cells in this epithelium. They actively synthesize keratin, a mechanically tough and fibrillar protein of the intermediate filament family of cytoskeletal proteins (*Bensouillah*, 2012), which enables the tissue to withstand high degrees of mechanical stresses. The cells also produce and secrete glycolipids that adsorb to the extracellular surface of the plasma membrane to fill interstitial spaces, making the tissue waterproof (*Bensouillah*, 2012)

The most important keratinizing squamous epithelium is the epidermis, the outer layer of the skin.

1.1.1 Skin anatomy

The skin is the largest organ of the body, making up 16% of body weight, with a surface area of 1.8 m^2 (*Bensouillah*, 2012). In the skin there are three structural

layers: the epidermis, the dermis and subcutis. Hair, nails, sebaceous, sweat and apocrine glands are regarded as derivatives of skin.
The epidermis is the outer layer, serving as the physical and chemical barrier between the interior body and exterior environment; the dermis is the deeper layer providing the structural support of the skin; the subcutis or hypodermis is an important site of fat storage (*Bensouillah*, 2012).

Epidermis
Epidermal keratinocytes are connected by protein bridges called desmosomes. They are in a constant state of transition from the deeper layers to the superficial one. Moving from the inner layer to the surface, the four strata of the epidermis are named (Figure A):
- stratum basale (basal or germinativum)
- stratum spinosum (spinous or prickle)
- stratum granulosum (granular)
- stratum corneum (horny)

FIGURE A

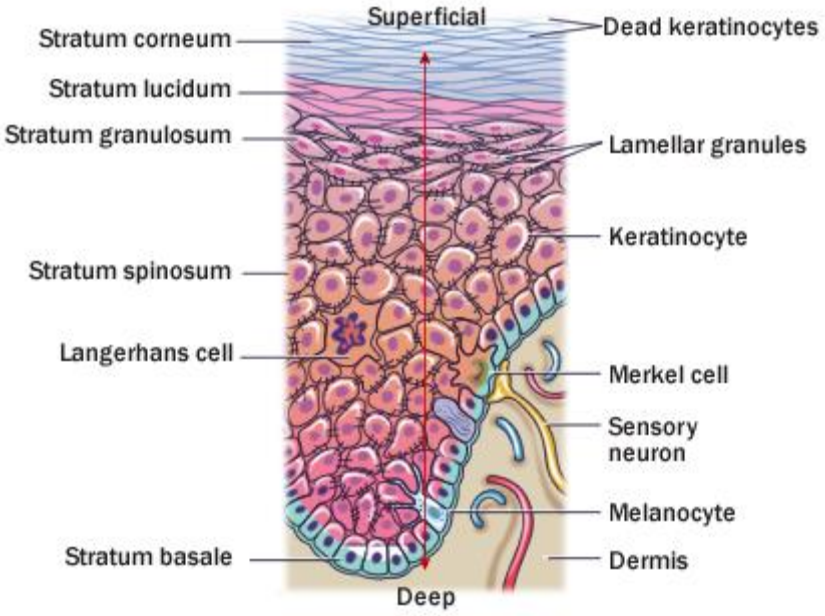

By Blueddor Pubblishing 2011

FIGURE A. REPRESENTATIVE SCHEME OF EPIDERMIS

In addition, the stratum lucidum is a thin layer of translucent cells seen in thick epidermis. It represents a transition from the stratum granulosum and stratum corneum and is not usually seen in thin epidermis. Together, the stratum spinosum and stratum granulosum are sometimes referred to as the Malpighian layer (*Rosati and Colombo*, 2003).

Stratum basale
In this layer, cells have stemness features and high rate of proliferation. The basal layer is adjacent to the dermis and includes dividing and non-dividing keratinocytes, attached to the basement membrane by hemi-desmosomes and inter-connected by

desmosomes. As keratinocytes divide, one cell remains in the basal layer and the other one differentiates, moving towards the surface. The process of differentiation starts with the loss of integrins, which mediate the adhesion to the basal membrane. The basal layer also contains Merkel cells. They are closely associated with cutaneous nerves and seem to be involved in light touch sensation (*Bensouillah*, 2012)

Stratum spinosum

As basal cells reproduce and mature, they move upwards forming the stratum spinosum. Under light microscope the cells seem to be connected by intercellular bridges, which appear as `prickles', from whose the name of the layer. Instead, electronic microscopy has shown that cells are not connected by cytoplasmic protrusions, but rather by fibril structures. The outset cells of the stratum spinosum start to produce involucrin, the main component of cornified lining, typical of terminal differentiated keratinocytes (*Randall*, 2006).

A small proportion of the cell population in the basal and spinosum layer is represented by melanocytes, which produce the pigment melanin. Melanin accumulates in melanosomes that are transferred to the adjacent keratinocytes, where they remain as granules. Melanin pigment provides protection against ultraviolet (UV) radiation, in fact, chronic exposure to light increases the ratio of melanocytes to keratinocytes. The number of melanocytes is the same in equivalent body sites in white and black skin, but the distribution and rate of production of melanin is different (*Bensouillah*, 2012).

Moreover, the inner layers of the epidermis contain Langerhans cells, derived from hematopoietic progenitors of bone marrow. They are specialized in antigen presentation and belong to the skin immune system (SIS). Actually, they acquire antigens in peripheral tissues, transport them to regional lymph nodes, present to naive T cells and initiate adaptive immune response (*Romani*, 2012).

Stratum granulosum

Continuing their transition to the surface, the cells continue to flatten, lose their nuclei and their cytoplasm and acquire a granular aspect. In this layer, the cells are able to secrete the filaggrin, a phosphorylated protein which interacts with keratin fibers and is essential for the regulation of epidermal homeostasis (*Bensouillah*, 2012; *Steinert*, 1993).

Stratum corneum

The final outcome of keratinocyte maturation is found in the stratum corneum, made up of layers of hexagonal-shaped, non-viable cornified cells, known as corneocytes. Each corneocyte is surrounded by a protein envelope, is filled with water-retaining keratin proteins and in the extracellular space there are overlapping layers of lipids (*Bensouillah*, 2012; *Steinert*, 1993). The resulting structure provides the natural physical and water-retaining barrier of the skin. The movement of epidermal cells to this layer usually takes about 28 days and is known as the epidermal transit time (*Bensouillah*, 2012).

1.1.2 Skin functions

The skin is a complex metabolically active organ and has several functions, in fact it creates a physical barrier to the environment, allowing and limiting the inward and outward passage of water, electrolytes and other substances and it provides protection against micro-organisms, ultraviolet radiation, toxic agents and mechanical insults (*Bensouillah*, 2012).
Fillagrin and keratin molecules are responsible for skin barrier function. In the granular layer the protein fillagrin complexed with keratin and, as the degenerating cells move towards the stratum corneum, enzymes break down the keratin-fillagrin complex: fillagrin forms on the outside of the corneocytes, while the water retaining keratin remains inside (*Bensouillah*, 2012). When the skin is dry, fillagrin breaks down in order to control the osmotic pressure and the amount of water it holds. The free amino acids of fillagrin, along with other components such as lactic acid, urea and salts, are known as `natural moisturising factors' (NMF) and are responsible for keeping the skin moist and pliable due to their ability to attract and hold water (*Randall*, 2006). Shedding of the corneocytes is an important factor in maintaining skin integrity and smoothness and in normal healthy skin there is a balance between the production and shedding of these cells. In diseases such as psoriasis, characterized by increased corneocyte production and decrease in their shedding, the skin results dry and rough, as the corneocytes accumulate (*Bensouillah*, 2012).
Moreover, in the inner layers of the epidermis melanocytes and melanin, creating a protective shield over the nuclei of the keratinocytes, have important roles in the UV protection, which induce keratinocyte proliferation and DNA damage.
Finally, skin plays an important role in the immunological surveillance, containing all the elements of cellular immunity, with the exception of B cells and in the thermoregulation, maintaining a constant body temperature (*Bensouillah*, 2012).

1.1.3 Skin cancer

Skin homeostasis, as well as for every tissue, is dependent on a tightly coordinated network of signaling pathways, resulting in a spatial and temporal balance of proliferation, growth arrest, differentiation, senescence and apoptosis. Aberrant regulation of any of these biological processes can contribute to the onset and progression of tumorigenesis (*Weinberg*, 2002).
Skin cancer is the most common malignancy in the United States and makes up about one third of all cancers diagnosed.
The common skin cancers are divided into non-melanoma skin cancers (NMSCs) and melanoma. NMSCs are classified in two subcategories: epithelial and non-epithelial skin cancers. Squamous cell carcinoma (SCC) and basal cell carcinoma (BCC) are, by far, the most frequent pathologic types of NMSC, included in non-epithelial skin cancers (*Marks*, 1995).

The most important factor involved in the pathogenesis of NMSC is the cumulative amount of exposure to ultraviolet radiation (UVR), in particular the wavelength range 290 to 320 nm is the most carcinogenic (*Buzzell*, 1993). Other risk factors including radiation exposure, long-term intake of arsenic or fair-skinned people may contribute to the development of NMSC. In addition, NMSC may arise from preexisting conditions such as scars, chronic ulcers (Marjolin's ulcer), sinuses (*Johnson*, 1992) or

two rare genetic syndromes—xeroderma pigmentosa and nevoid basal cell carcinoma syndrome (*Shumrick*, 1993). Finally, an increased incidence of NMSC, especially SCC, of the head and neck has also been found in transplant recipients. These SCCs are more likely to behave aggressively and have a high rate of metastasis (*Padgett*, 2001).

Basal Cell Carcinoma

The most common skin cancer is BCC, accounting for 70 to 75% of skin cancers. There are five clinical types of BCC (*Yun-Hsuan Ouyang*, 2010):

- nodulo-ulcerative
- superficial
- morpheaform
- pigmented
- fibroadenoma.

The first three of these are mentioned with the greatest frequency. The nodulo-ulcerative lesions are the most common type, accounting for 75% of cases of BCC. The typical clinical appearance is a well-circumscribed nodule or plaque with pearly border and overlying telangiectasia and may be combined with rodent ulcer. Superficial BCC represents ~10% of BCC. The clinical presentation is discrete erythematous macules or plaques with scaly change and a thin rolled border (*Yun-Hsuan Ouyang*, 2010; *Kirkuam*, 2005).

BCC tends to share the common histopathologic features of a predominant basal cell type, peripheral palisading of lesional cell nuclei, and a mucinous stroma with artificial cleft between the epithelial island and the stroma. In addition, there are variable degrees of cytologic atypia and mitotic activity (*Kirkuam*, 2005).

The incidence of metastasis in BCC is very rare, occurring in 0.0028 to 0.1% of patients. Review of the literature shows that morpheaform, adenocystic, metatypical, and basosquamous types of BCC have a relatively high local recurrence rate (*Ratushny*, 2012).

Squamous Cell Carcinoma

Squamous cell carcinoma (**SCC**) is a treatment-refractory malignancy arising within the epithelium of the skin, lung, esophagus, oral cavity and upper aero-digestive tract.

In particular, cutaneous squamous cell carcinoma (cSCC) is the second most common human cancer with over 250.000 new cases annually in the US and is second in incidence only to basal cell carcinoma. cSCC typically manifests as a spectrum of progressively advanced malignancies, ranging from a precursor actinic keratosis (AK) to squamous cell carcinoma (SCC) in situ (SCCIS), invasive cSCC and finally metastatic SCC (*Yun-Hsuan Ouyang*, 2010).

AKs are defined at the histological level by dysplasia and consist of keratinocytes manifesting atypical nuclei that are enlarged, irregular and hypercromatic. AKs are also display disorganized growth, abnormal differentiation with thickened stratum corneum (*Ratushny*, 2012).

According to the classic multistep model of carcinogenesis the progression from AK to cSCC may be described as several and consequent steps: mutation in one gene,

often a tumor suppressor, may lead to the development of a precursor lesion with increased genetic instability or loss of cell cycle control. Additional mutations in other drivers oncogenes allow the emergence of more neoplastic properties, leading to invasive carcinoma. The number of genetic changes required to transition from benign epithelium to metastatic carcinoma internal malignancies is thought to range from four to six (*Ratko, 2014*).
In contrast to several internal malignancies, where p53 mutation is a late event in neoplastic evolution, in keratinocytes genomic instability results mainly from UVB-induced inactivation of p53. In fact p53 is commonly mutated in AKs indicating that p53 loss occurred in pre-neoplastic lesions (*Baker,* 1990). Aberrant activation of EGFR and Fyn, a Src-family tyrosine kinase, and Ras activating mutations or amplification have also been commonly found in SCC. Important determinants of tumorigenesis in cSCC are the interactions between tumor cells, their extracellular matrix and the basement membrane zone (*Loyo*, 2013; *Ramsey* , 2013).
Finally, one common finding in SCCs is the overexpression of the p63 protein, that is associated with amplification of the p63 locus at chromosome 3q27-29. Accordingly, p63 genomic sequence was found to be amplified in lung (88%), head and neck (80%) and cutaneous squamous carcinomas and the predominant splice variant of p63 expressed was ΔNp63α (*Hibi*, 2000; *Reis-Filho*, 2002; *Rocco*, 2006).

1.2 TP63

1.2.1 p63 gene and protein structure

The human TP63 locus spreads over about 220 kB on chromosome 3q27–29 and it belongs to p53 gene family. The locus consists of 15 exons and has two different promoters, the first located upstream the exon 1 and the second on the third intron. The promoters give rise to two categories of isoforms, TA- or ΔN- aminotermini transcripts, with an acidic transactivation domain or without it, respectively. The complexity of the locus is enriched by alternative splicing at the carboxy-terminal (C-terminal) which generates at least three p63 variants (α, β and γ) in each class. The different C-termini of α, β, and γ isoforms contribute to the diversity of p63 proteins; α, but not β and γ, isoforms contain a Sterile Alpha-Motif (SAM) domain that functions as a protein–protein interaction module in other proteins (*Yang*, 1998; *Thanos*, 1999; *Barbieri*, 2006).
All p63 proteins show a DNA-binding domain which is approximately 60% identical at the aminoacid level to the DNA binding domain of p53, and an oligomerization domain with about 37% identity to that of p53. According to their high structural homology to p53 in the DNA binding domain, p63 proteins can bind to p53 DNA binding sites *in vitro* and *in vivo* (*Westfall*, 2003; *Flores,* 2002).
The TA isoforms also have a N-terminal transactivation domain similar to p53, and can transactivate genes through a canonical p53-responsive element. ΔNp63 proteins lack this domain and can act as dominant negative against p53 and TAp63 proteins (*Yang*, 1998). Recent studies have shown that ΔNp63 also possess transcriptional activity (*Ghioni*, 2002).

1.2.2 p63 in development and maintenance of squamous epithelia

The critical role of p63 in limb morphogenesis and stratified tissue development was unveiled by studies on p63 knockout mice (*Mills*, 1999; *Yang*, 1999). p63 -/- mice die shortly after birth, because of their striking developmental defects. They lack all stratified squamous epithelia and their derivatives, such as epidermal appendages and mammary, lacrimal, and salivary glands (*Mills*, 1999; *Yang*, 1999). In addition, p63 −/− mice display truncated limb due to the inability to maintain or differentiate the apical ectodermal ridge, a structure required for limb outgrowth. Moreover, these mice exhibit craniofacial abnormalities, including cleft lip and palate and a lack of teeth (*Mills*, 1999; *Yang*, 1999).
Similarly to what observed in mice, disruption of ΔNp63 in zebrafish resulted in lack of epidermal morphogenesis and fin truncations (*Lee*, 2002).

Mutations in the p63 gene cause at least five autosomal dominantly inherited human syndromes, with a strong genotype-phenotype correlation. The p63 syndrome family includes the EEC, AEC, ADULT, LSM and SHFM syndromes[1] which present various combinations of limb abnormalities, orofacial clefting and ectodermal dysplasia (*Brunner*, 2002). The mutations patterns are characteristic for each of these disorders, for example, EEC syndrome is caused by missense mutations in the p63 DNA binding domain, whilst AEC syndrome is associated with missense or frameshift mutations in the SAM domain (*Celli*, 1999; *McGrath,* 2001).
Finally, regarding the correlation with the environment, the phenotypes associated to p63 mutations can be affected by other modifying genetic or external factors as suggested by their incomplete penetrance and variable expressivity (*van Bokhoven*, 2001). All together these observations indicate that different p63 mutations can affect distinct developmental events, all ascribable to ectodermal developmental defects.

In normal adults, p63 protein expression lies in the basal layers of the stratified epithelial structures, such as epidermis, oral mucosa, and cervical epithelium, as well as transitional epithelium in the mucosa of the urinary bladder and complex glands, including the prostate and mammary, salivary, and lacrimal glands. Remarkably, p63 is often over-expressed in cancers derived from these tissues (*Di Como*, 2002).
During epidermal morphogenesis ΔNp63 isoforms are expressed at higher levels than the TAp63 isoforms (*McDade and McCance*, 2010) and interestingly, depletion of ΔNp63 isoforms produces tissue hypoplasia and defects in the expression of skin differentiation markers as following pan-p63 siRNA. On the contrary, knockdown of TAp63 isoforms give no detectable effects on proliferation, but only incomplete differentiation of the granular layer and stratum corneum (*Truong*, 2006).
ΔNp63α is the predominant isoform in the basal layer of adult skin, where it plays a role in maintaining the viability and proliferative capacity of basal epithelial cells. Keratinocyte differentiation results in the down-regulation of ΔNp63α transcript,

[1] EEC = ectrodactyly, ectodermal dysplasia, facial clefting (MIM 129900); AEC = ankylopblepharon, ectodermal dysplasia and clefting (MIM 106260); ADULT = acro-dermato-ungual-lacrimal-tooth syndrome (MIM 103285); LSM = limb-mammary syndrome (MIM 603543); SHFM = split hand/foot malformation (MIM 183600).

consistent with the loss of p63 protein in the more differentiated suprabasal layers of the epidermis (*Westfall*, 2003).
Additional mechanisms have been proposed to reduce ΔNp63α level during the differentiation process as proteolysis (*Melino,* 2006; *Di Costanzo,* 2011) or microRNA *mir-203-mediated silencing* (*Yi*, 2008).
The PI3K/Akt survival pathway, instead, prevents downregulation of ΔNp63α expression and inhibits keratinocyte terminal differentiation (*Barbieri,* 2003; *Vivanco*, 2002)

1.2.3 *ΔNp63α and cancer*

Several studies on human patient-derived tumours have been performed to explore the role of p63 in cancer. p63 was found to be highly expressed in the nucleus of different tumour types, such as head and neck cancers (*Rocco*, 2006), B cell lymphoma (*Hedvat*, 2005), bladder carcinoma (*Compèrat*, 2007), but also in the cytoplasm of prostate carcinoma cells (*Weinstein*, 2002). To distinguish between TA and ΔNp63 proteins, antibodies against different p63 epitopes or isoform-specific PCR primers have been used in order to understand the role of the distinct p63 isoforms in cancer pathogenesis and progression. Taken together, the results obtained point to the oncogenic role of ΔNp63, in fact these isoforms are highly expressed in tumors (*Nylander,* 2002; *Barbieri*, 2006) while TAp63 isoforms are absent or barely detectable (*Compérat,* 2007).
Among all ΔNp63 isoforms, ΔNp63α is the predominant isoform found in cancer, although its role in tumorigenesis is still controversial. ΔNp63α protein is over-expressed in basal cell skin carcinoma and up to 80% of primary Squamous Cell Carcinomas (SCCs) of the head and neck, cervix, lung and esophagus (*Hibi*, 2000).
Multiple mechanisms can sustain high and persistent levels of ΔNp63α expression. Expression of ΔNp63α is known to be induced by the FGFR2 (*Ramsey*, 2013), the EGFR/STAT3 (*Ripamonti*, 2013) and PI3K pathways (*Barbieri*, 2003) although the time, the tissue context and precise stimuli triggering one or the other pathways have still to be defined. In contrast to a role in promoting tumorigenesis, ΔNp63α expression is a positive prognostic factor in cancer progression and is associated with favorable prognosis in patients with lung cancers (*Massion*, 2003). Lately, an increasing number of data are coming out claiming that ΔNp63α is a metastasis suppressor. For instance, ΔNp63α knockdown in squamous carcinoma cells was associated to a loss of cell adhesion and metastatic spread (*Barbieri*, 2006), while in prostate and breast, where only basal myoepithelial cells display intense ΔNp63α staining, invasive breast carcinomas are consistently devoid of nuclear p63 (*Barbareschi*, 2001). Barbieri and colleagues hypothesize that ΔNp63α acts to promote early steps in tumorigenesis by protecting cells from growth arrest and apoptosis, while at same time acts as a metastasis suppressor by maintenance of the epithelial characteristics of cancer cells (*Barbieri*, 2006).

1.2.4 p63 and its molecular partners

Proteins usually play their functions in the cell as macromolecular complexes. Interaction with distinct factors might arrange the protein structure, specify its

subcellular localization or binding affinity to nucleic acids and/or cellular structure and ultimately define its functions.
To get insights into the p63 biology it is important to identify and characterize its molecular partners. This field of p63 biology has only been very partially explored, Itch/AIP4, Fbw7, PIN are some p63 interactors that have been characterized to regulate p63 stability and function (*Rossi*, 2006; *Galli*, 2010).
My research group using a functional proteomic approach by mass spectrometry has revealed a set of 50 potential ΔNp63α partner in HaCaT keratinocytes (*Amoresano*, 2010). Among the potential interactors there was a set of RNA-binding proteins, including the multifunctional Y-box binding protein 1.

1.3 YB-1

1.3.1 YB-1 protein structure

The YB-1 gene resides on chromosome 1p34, it is structured in 8 exons (*Toh*, 1998) with a long 5′ UTR, involved in the regulation of gene expression (*Kohno*, 2003). The mRNA of YB-1, 1.5 kb long, encodes a protein of 324 amino acids with an expected molecular weight of 36 kDa (*Didier*, 1988; *Kuwano*, 2004.). However, its apparent molecular weight in SDS-PAGE is 50 kDa. The Y-box-binding protein 1 (YB-1, YBX1) is a member of the DNA/RNA binding protein family, with an evolutionarily ancient and conserved cold shock domain (*Kohno*, 2003).
YB-1 protein consists of three domains: the alanine/proline-rich N-terminal domain (A/P domain), the cold shock domain (CSD) and the large C-terminal domain (CTD) with alternating clusters of positively and negatively charged amino acid residues (*Lyabin*, 2014).
The CSD structure is represented by five-stranded *β*-barrel with consensus sequences RNP-1 (K/N-G-F/Y-G-F-I/V) and RNP-2 (V-F-V-H-F) through which it binds to RNA and DNA (*Lasham*, 2013).
Instead, the A/P domain and the CTD have no regular secondary structure; neverthless, YB-1 realizes the interactions with the majority of its protein partners through the CTD domain by a poly(Pro) II conformation (*Rath*, 2005), as well as by its positively charged amino acid residues arranged as clusters (*Lyabin*, 2014).
The carboxyl-terminal domain has, also, multiple phosphorylation, acetylation and ubiquitylation sites involved in the regulation of various protein functions (*Inoue*, 2011).

About the role of YB-1 as a RNA-binding protein, it has been reported an interesting study which illustrates how its structure is well suitable to different cellular mechanisms. The authors explain that at a comparatively low YB-1/mRNA ratio, typical of translated polysomal mRNPs, monomeric YB-1 interacts with RNA through both its CSD and CTD and causes mRNP unwinding. In these complexes, mRNA has its termini exposed to both translation initiation factors and ribosomes. At a high YB-1/mRNA ratio, typical for free untranslated mRNPs, YB-1 undergoes multimerization through its CTD, while its CSD remains mRNA-bound. A large YB-1 multimeric complex composed of 15-18 molecules accommodates at its surface an RNA segment of about 600-700 nt. Long mRNAs can be accommodated at several multimers (*Skabkin*, 2004; *Lyabin*, 2014).

YB-1 has also the ability to produce fibrils which may underlie formation of RNA granules, such as stress granules and P-bodies in the cell (*Guryanov*, 2012; *Lyabin*, 2014). In particular, under conditions of a high ionic strength, YB-1 forms reversible amyloid-like fibrils (*Selivanova*, 2010) and its disordered terminal domains modulate this process: the A/P domain stimulates fibril formation, while the first part of CTD suppresses it at any level of ionic strength (*Guryanov and Selivanova*, 2012). This ability is presumably explained by its low stability, because its melting temperature is as low as 39◦C and at physiological temperature its best part remains in a non-native state (*Guryanov*, 2012).
Finally, YB-1 was first recognized as a protein bound to promoters of the HLA-DR gene and to Epidermal Growth Factor enhancer (*Didier*, 1988; *Sakura*, 1988). These genomic regions are characterized by the presence of the so-called Y-box sequence (5'CTGATTGGC/TCTTAA-3'), to whom YB-1 owes its name. Later, YB-1 was found to bind and regulate the expression of genes with or without the Y-box sequence in their regulative regions. A slight specificity of YB-1 to the Y-box can be observed *in vitro*, however YB-1 appears to bind strongly to single-and double-stranded GGGG, CACC and CATC motifs (*Zasedateleva*, 2002). In a recent manuscript by Dolfini and Mantovani (*Dolfini*, 2013), using the ChIP-on ChIP and ChIP-Seq bioinformatic data, it has been reported that YB-1 has no particular specificity for the canonical Y-box sequence.

1.3.2 YB-1 functions

YB-1 belongs to a group of intrinsically disordered proteins that do not follow the classical rule "one protein-one function". It is an example the novel principle claiming that a disordered structure may suggest many functions. In fact, YB-1 has several functions and it is involved in many cellular processes due to (i) its ability to interact with nucleic acids, (ii) its ability to form complexes with other proteins and, moreover, (iii) its capacity to shuttle between the nucleus and the cytoplasm under particular stimuli such as heat (*Stein*, 2001), anticancer drugs, and ultraviolet (UV) irradiation (*Bargou*, 1997; *Koike*, 1997; *Fujita*, 2005) or during G1/S phase transition (*Lyabin*, 2014; *Inoue*, 2011)

Proliferation

Several studies have linked the expression of YB-1 with the cell proliferative activity. Distinct team have observed that knockout of mouse *YB-1* causes abnormalities in neurotubule formation during the early embryonic development, fetal growth retardation and prenatal deaths (*Lu*, 2005; *Uchiumi,* 2006).
Interestingly, overexpresson of YB-1 has been observed in primary melanoma (*Schittek*, 2007), prostate cancer (*Giménez-Bonafé*, 2004), glioblastoma (*Faury*, 2007) and neuroblastoma (*Wachowiak*, 2010). Reduction of YB-1 expression, instead, causes growth inhibition or apoptosis in a broad range of cancer cells both *in vitro* and *in vivo (Lasham, 2013).* Targeted overexpression of YB-1 in the mammary gland of a transgenic mouse results in the formation of breast cancer (*Bergmann*, 2005).

YB-1 appears to be involved in the control of cell proliferation through different mechanisms:

- YB-1 has the ability to control the expression of different E2F family members and it directly binds to the promoters of several canonical E2F1-regulated genes (*Lasham*, 2012).
- YB-1 regulates the *PI3KCA* gene encoding the catalytic subunit p110α of PI3K enzymes. This gene is frequently amplified or mutated in cancers. The PI3K pathway signals through the multifunctional protein kinase Akt, which in turn regulates mTOR, control several oncogenic mechanisms, including proliferation, survival, metabolism and metastasis (*Dazert*, 2011).
- YB-1 plays an integral role in the PI3K/Akt/mTOR pathway and depends on Akt for its nuclear translocation following phosphorylation at Ser^{102} in a number of cell lines, including basal-like breast cancer cells (*Sutherland*, 2005) ovarian cancer cells (*Basaki*, 2007) and melanoma cells (*Sinnberg*, 2012)
- YB-1 represses transcription of the *TP53* gene (*Lasham*, 2003) and it can disable the p53 pathway by regulating its activity. In addition, it has been shown that YB-1 controls the expression of upstream regulators of RB, like cyclins D1, *CDK1* and *CDK2* (*Lasham*, 2013).

Invasion and metastasis

YB-1 regulates pathways involved in invasion and metastasis. *In vitro* studies have shown that YB-1 potentiates the invasive properties of several cancer cell lines (*Lovett*, 2010). Several mechanisms have been proposed to explain YB-1 pro-metastatic property:

- YB-1 has been shown to promote the translation of mRNAs encoding *E-cadherin*-repressing factors such as Snail, Lef 1 and Twist (*Evdokimova*, 2009). The cadherins are involved in maintaining cell–cell adhesion in the tumour mass and they are frequently inactivated during metastasis progression (*Jamora*, 2003).
- YB-1 induces transcription of a number of matrix metalloproteinases (MMPs), including MMP-2, MMP-12 and MMP-13 responsible for the dissociation BM/ECM (basement membrane/extracellular matrix) (*Samuel*, 2007).
- YB-1 appears to regulate the translation of TGFβ1(*Fraser*, 2008) and to bind to the promoters of Wnt pathway proteins, involved also in angiogenesis.
- YB-1 is a transcriptional activator of the CD44 gene (*To*, 2010), an important membrane-bound protein that plays a relevant role in metastasis.

Chemoresistance

In the presence of genotoxic agents, such as anti-cancer drugs and ultraviolet irradiation, YB-1 upregulates the transcription of the Multidrug Resistance 1 (*MDR1)* gene, resulting in the increased expression of P-glycoprotein (*Ohga*, 1998). The P-glycoprotein, a member of the ATP-binding cassette (ABC) transporter

superfamily, is known to mediate the efflux of xenobiotics in the cell (*Litman*, 2001) affecting the sensitivity of the cancer cell to chemoterapic agents.
In particular, nuclear YB-1 influences the transcription of chemoresistance genes, decreasing chemosensitivity of cancer cells to a wide range of anticancer drugs, such as cisplatin (*Ohga*, 1996), doxorubicin (*Bargou*, 1997), paclitaxel (*Fujita*, 2005) and mitomycin C (*Shibahara*, 2004). Cisplatin-resistant human head and neck cancer KB epidermoid cancer cells and ovarian cancer cells exhibited higher nuclear expression of YB-1 than the drug-sensitive wild type cancer cells (*Yahata*, 2002). Moreover, it has recently shown that YB-1 is able to increase the expression of *CD44* and *CD49f* genes associated with cancer stem cells (*To*, 2010), both genes induce chemoresistance in MDA-MB-231 breast cancer cells (*Fillmore*, 2008). CD44, in fact, interacts with hyaluronan and activates drug-resistant genes such as *MDR1* (*Inoue*, 2011).

Inflammation

Some of the pathways and players linked to YB-1 and previously described such as EGFR, STAT3, MMP-2 and CD44 promote cancer cell inflammation. In addition to these, YB-1 has been found correlated with other inflammatory pathways:

- In mesangial inflammatory cells and HK2 and HEK293 kidney epithelial cells, oxidative stress and cytokines like PDGF-BB, interferon-γ and lipopolysaccharide trigger YB-1 secretion. Extracellular YB-1 associates with outer cell membrane components and interacts with extracellular Notch-3 receptor domains. YB-1 secretion and Notch-3 receptor expression/activation may amplify the inflammatory response of mesangial cells (MC) conferred by the Jak/STAT (signal transducers and activators of transcription) pathway (*Rauen*, 2009).
- In a Scientific EMBO Report, Frye BC and colleagues describe that lipopolysaccharide induces YB-1 secretion in primary monocytic cells and that extracellular YB-1 exerts a potent proliferative response in different cell types and promotes cell migration (*Frye*, 2009).
- YB-1 peptides have been found in serum of sepsis patients and urine of patients affected by different forms of tumors (*Hanssen*, 2013). The specific role of these peptides is still unknown.

1.3.3 YB-1 AS A THERAPEUTIC TARGET

YB-1 is upstream of several molecular pathways involved in tumorigenesis and inflammatory diseases, therefore YB-1 appears to be a very attractive therapeutic target. In the last decade different approaches to target YB-1 have been employed, including targeting of YB-1 directly, interfering with the activation of YB-1 or targeting the regulators that activate YB-1.
First, a molecule of nucleic acid was successfully employed in different cultured cancer cells as a decoy to sequester YB-1 protein, resulting in inhibition of tumour cell growth and p53-mediated apoptosis (*Homer*, 2005). The use of nucleic acids as therapeutics has been slowed by issues of delivery, although rapid advances are now being made (*Seton-Rogers*, 2012).

Another therapeutic approach to directly target YB-1 could be the use of siRNAs. Anti-YB-1 siRNAs have been shown to suppress tumour cell invasion, proliferation, insensitivity to chemotherapy and to promote apoptosis (*Gao*, 2009). The delivery of siRNAs in humans is still a challenge for chemistry and pharmacology due to their discussed problems of stability and bioavailability (*Seton-Rogers*, 2012).
In a therapeutic strategy it is important to remind that YB- 1 functions as transcription factor when phosphorylated at Ser^{102}, which stimulates nuclear translocation and DNA binding (*Southerland*, 2005). S102A YB-1 mutants exhibited reduced cell proliferation and an interference peptide, designed as another type of 'molecular decoy' that competes with YB-1 for phosphorylation by RSK and Akt, has been found successfully inhibiting proliferation of breast and prostate cancer cells in culture (*Law*, 2010). Thus peptide-based delivery systems could be a promising method to inhibit YB-1 therapeutically.
A potential method to suppress YB-1 activity could be also the use of 'signal transduction' inhibitors. A side effect of blocking kinases such as PDK-1, Akt and RSK is quenching of YB-1 phosphorylation at Ser^{102} and thereby reduction of its transactivation activity. In fact, RSK inhibition with siRNA or small molecules, such as BI-D1870 and SL0101, completely suppress the activation of YB-1 (*Stratford*, 2008). Likewise, the MEK inhibitor PD098059 blocks RSK and suppresses the nuclear localization of YB-1 (*Shen*, 2011) as well as YB-1 blockade may potentially underlie a significant part of the activity of these inhibitors.
Very recently, Khan and colleagues have identified Fisetin (3,7,3',4'-tetrahydroxyflavone) as a new potential inhibitor of YB-1 activation in PCa cells. Fisetin belongs to such a flavonol subgroup of flavonoids along with quercetin, myricetin and kaempferol. It is present in many fruits and vegetables most notably strawberries, apples, persimmons, kiwis, cucumbers and onions. Computational docking and molecular dynamics suggested that fisetin binds to the residues from β1 - β4 strands of CSD, hindering Akt's interaction with YB-1. Fisetin also inhibited EGF induced YB-1 phosphorylation and appear to reduce the expression of EMT markers both *in vitro* and *in vivo* (*Khan*, 2014).

AIMS OF THE THESIS

Squamous cell carcinoma (SCC) is a treatment-refractory malignancy arising within the epithelium of the skin, lung, esophagus, oral cavity and upper aero-digestive tract. SCCs are frequently associated with mutational inactivation of the p53 tumor suppressor and overexpression of ΔNp63α oncoprotein.
ΔNp63α expression is known to be induced by FGFR2 (*Ramsey*, 2013), PI3K/Akt (*Barbieri*, 2003) and EGFR/STAT3 (*Ripamonti*, 2013) signaling pathways. However, therapeutically targeting the EGFR deregulated signaling pathway in SCC has proven not efficient, so far (*Argiris,* 2013; *Martins,* 2013). Even more intriguing, are the evidences that loss, rather than overexpression, of ΔNp63α is associated with a more invasive phenotype, at least in some tissues (*Rocco,* 2006). For instance, inactivation of p63 functions was demonstrated to be critical to TGFβ-mediated metastatic potential, through a mechanism involving TGFβ signaling activation, Smad and p53 mutant proteins (*Adorno*, 2009). These observations imply that a gene-therapy based on ΔNp63α silencing must be carefully evaluated.
Therapeutic targeting of ΔNp63α molecular partners is an exciting, but still relatively underexplored area for potential therapeutic intervention in SCC.
By coimmunoprecipitation and mass spectrometry analysis, my research team has identified the Y box-binding protein 1 as a ΔNp63α interactor (*Amoresano*, 2010).
YB-1 is variably expressed in most normal human tissues and YB-1 knockout mice are embryonically lethal (*Uchiumi*, 2006). As previously described YB-1 protein is a stem cell marker with a well assessed oncogenic potential and it shows interesting features that makes it a valuable therapeutic target. Moreover, YB-1 should also be regarded as a useful biomarker of cancer progression.
Studies on targeting YB-1, using cell-permeable inhibitory peptides, YB-1 siRNAs or oligonucleotide decoys, are the current challenge and promise in experiments to therapeutically target this master regulator of cancer cell biology.

Given these considerations and interest in understanding how YB-1 functions in association with ΔNp63α in oncogenic pathways leading to SCC, my PhD project was aimed to advance in the characterization of the functional interplay between ΔNp63α and Y-box binding 1 oncoproteins using *in cell* approaches to finally focus on its therapeutic implications.

Starting from the mass spectrometry data about YB-1 and ΔNp63α interaction and on the basis of the expertise of my research group on the role of ΔNp63α in epithelial cell system, I focused my study on the following points:

- Validation of the YB-1/ΔNp63α molecular interaction in primary, immortalized and transformed keratinocytes.

- Study of the effects of ΔNp63α expression on YB-1 functions in cancer cells, in terms of localization, gene expression and cell function, in order to elucidate their potential cross-talk.

- Study of the effects of YB-1 expression in immortalized keratinocytes and squamous cancer cells in terms of gene expression and cell functions.

2.RESULTS

2.1. YB-1 interacts with ΔNp63α in vitro and in vivo

At beginning of my PhD project in the laboratory of Prof. Calabrò I was involved in a study aimed to gain insight into the functional cross-talk between p63 and YB-1 proteins. In fact, Calabro's team, using functional proteomics, had previously described that the Y-box binding protein 1 (YB-1, NSEP1 or YBX1) is a potential p63 interacting partner (*Amoresano*, 2010).

I first validated that endogenous YB-1 and ΔNp63α are abundantly co-expressed in human squamous carcinoma cells using immunoblots and immunofluorescence assays, confirming that A431, SCC022 and SCC011 cell lines showed intense signals for both proteins (Fig. 1A and B).

FIGURE 1

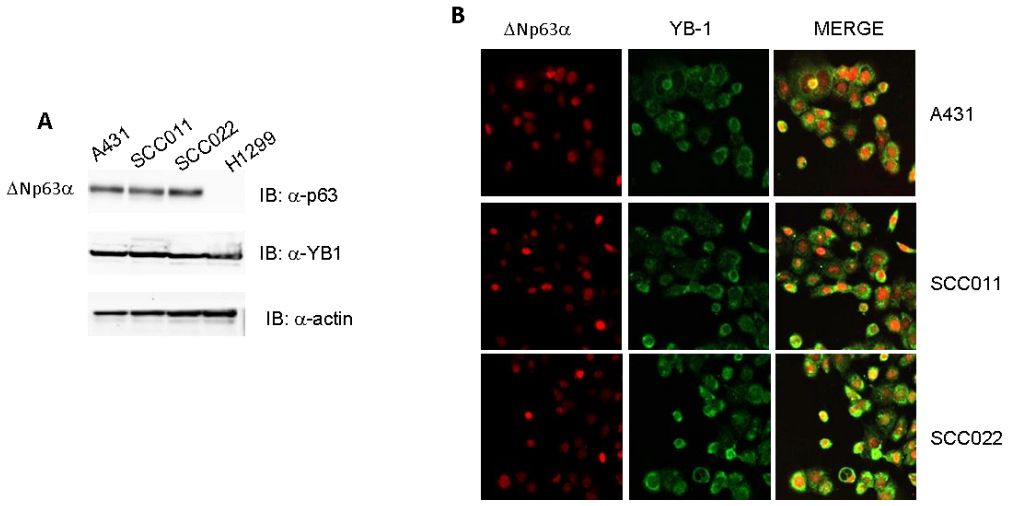

FIGURE 1. ΔNp63α and YB-1 are co-expressed in squamous carcinoma cell lines. (**A**) Whole cell lysates were obtained from H1299 (non-small cell lung carcinoma), A431 (epidermoid carcinoma cell line), SCC011 and SCC022 (keratinocytes-derived SCC) cells. 30μg of total protein extracts were separated by SDS PAGE and subjected to immunoblot. Proteins were detected with specific antibodies, as indicated. Images were acquired with CHEMIDOC (BIORAD) and analyzed with the Quantity-ONE software. (**B**) A431, SCC011, SCC022 cells were seeded (2.5 x 10^5) on 35 mm dish, grown on micro cover glasses (BDH). After 24 hours at seeding cells were fixed and subjected to double immunofluorescence using rabbit primary YB-1 antibody and Fitch-conjugated secondary antibodies (green). P63 protein was detected using mouse anti-p63 and Cy3-conjugated secondary antibodies (red). Images of merge (yellow) show the co-expression of two proteins.

Next, I decided to confirm the interaction between ΔNp63α and YB-1 in non transformed HaCaT keratinocytes and in squamous cell carcinoma (SCC011), by co-immunoprecipitation assay. Immunocomplexes containing ΔNp63α and YB-1 were isolated from total cell lysates, using either antibodies against YB-1 or antibodies against p63, thus confirming the interaction inferred by mass spectrometry (Figure 2A-2D).

Figure 2

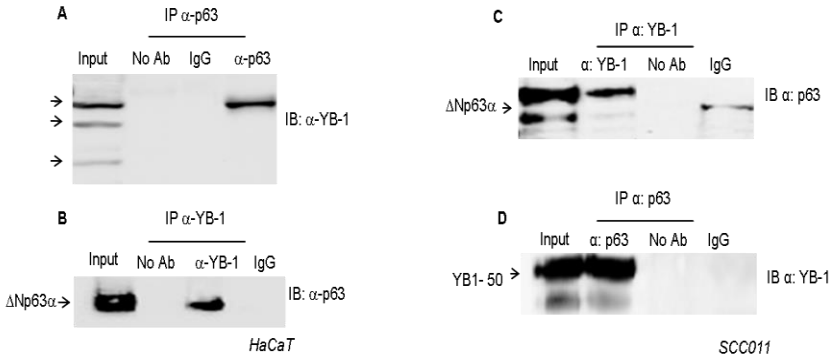

FIGURE 2. **ΔNp63α interacts with YB-1.** (**A**) Extracts from HaCaT cells were immunoprecipitated with anti-p63 antibodies and the immunocomplexes were blotted and probed with anti-YB-1, as indicated. (**B**) Extracts from HaCaT cells were immunoprecipitated with anti-YB-1 antibodies and the immunocomplexes were blotted and probed with anti-p63. (**C**) Extracts from SCC011 cells were immunoprecipitated with anti-YB1 antibodies and the immunocomplexes were blotted and probed with anti-p63, as indicated. (**D**) Extracts from SCC011 cells were immunoprecipitated with anti-p63 antibodies and the immunocomplexes were blotted and probed with anti-YB1. Samples with no antibody (no Ab) or irrelevant α-mouse and α-rabbit antibodies were included as controls.

Previous data showed that the C-terminal region of ΔNp63α isoform is involved in the association with YB-1 and the interaction between the two proteins requires no additional factors in breast cancer cell lines. To determine if YB-1 interacts specifically with the α isoform of ΔNp63, I transfected p63 null H1299 cells, with ΔNp63α or ΔNp63γ to perform co-immunoprecipitation assays. As shown in Fig.3, YB-1 associates with ΔNp63α but not with ΔNp63γ.

FIGURE 3

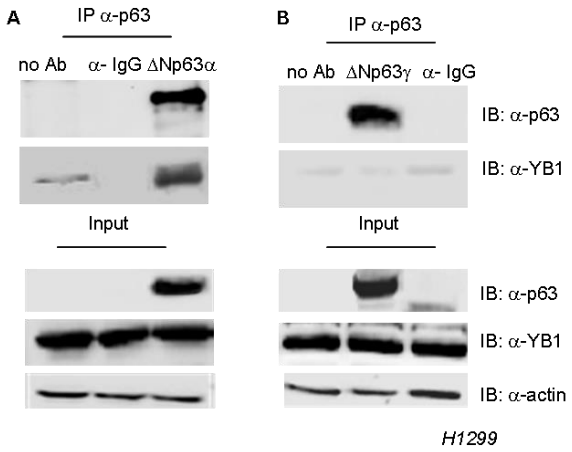

FIGURE 3. ΔNp63α but not ΔNp63γ interacts with YB-1. (**A**) H1299 cells were transiently transfected with 5 μg of ΔNp63α or (**B**) ΔNp63γ expression vectors. Equal amounts (1 mg) of extracts were immunoprecipitated with anti-p63 antibodies (4A4) or unrelated α-mouse IgG. The immunocomplexes were blotted and probed with anti-p63 and anti-YB-1 antibodies, as indicated.

2.2 ΔNp63α induces YB-1 nuclear accumulation

It has been reported that YB-1 is ubiquitously expressed and predominantly localized into the cytoplasm (*Homer*, 2005), while ΔNp63α is mainly expressed by basal and myoepithelial cells in skin and glands and is almost completely restricted to the nuclear compartment (*Di Como*, 2002). Since I noticed some overlapping between the p63 and YB-1 immunofluorescence signals into the nucleus of squamous carcinoma cell lines, I have investigated whether ΔNp63α had an effect on YB-1 subcellular localization. I transfected ΔNp63α in MDA-MB-231 cells, human metastatic breast carcinoma cells lacking p63, but expressing high level of endogenous YB-1. As shown in Fig.4, in cells with no detectable p63 signal, YB-1 exhibited a largely prevalent cytoplasmic localization (Fig. 4A, white arrows), while 95% of ΔNp63α expressing cells showed a strong YB-1 nuclear staining (Fig. 4A, yellow arrows).

FIGURE 4

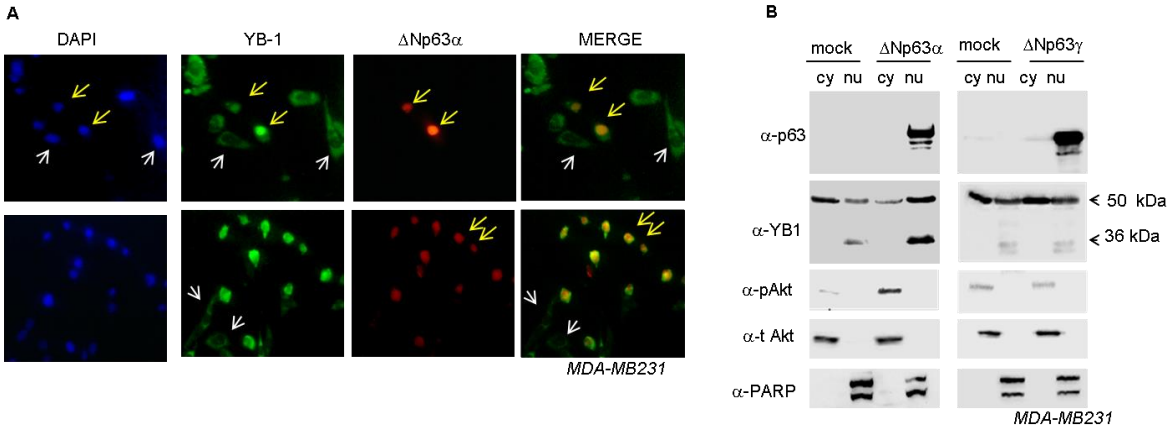

FIGURE 4. Endogenous YB-1 accumulates in the nucleus of breast cancer cells expressing ΔNp63α. (**A**) A representative image of a cell expressing ΔNp63α and showing nuclear endogenous YB-1 (yellow arrow). A representative image showing YB-1 cytoplasmic localization in cells bearing no detectable ΔNp63α expression (white arrows). MDA-MB-231 cells were seeded at 60% confluency (2.3×10^5) on 24 x 24 mm sterile coverglasses placed in 60 mm dishes and transiently transfected with 1 μg of of ΔNp63α expression vector. Cells were fixed and subjected to double indirect immunofluorescence using rabbit primary YB-1 antibody and Fitch-conjugated secondary antibodies (green). P63 protein was detected using mouse anti-p63 and Cy3-conjugated secondary antibodies (red). 4',6-Diamidino-2-phenylindole (DAPI) was used to stain nuclei (blue). (**B**) MB-MDA-231 cells were transiently transfected with a fixed amount (5 μg) of an empty vector (mock), ΔNp63α or ΔNp63γ expression vector in 100 mm dishes. 24h after transfection, cell lysates were fractionated to obtain cytoplasmic and nuclear fractions. 20μg of nuclear and cytoplasmic extracts were separated by SDS PAGE and subjected to immunoblot. Proteins were detected with specific antibodies, as indicated. PARP and total AKT were used as nuclear and cytoplasmic control respectively, to check for cross-contamination. Images were acquired with CHEMIDOC (BIORAD) and analyzed with the Quantity-ONE software.

I verified this observation by nuclear/cytoplasmic fractionation of MDA-MB-231 cells transfected with ΔNp63α or ΔNp63γ. Endogenous YB-1 protein, in MDA-MB-231 cells, was detectable as 50 and 36 kDa immunoreactive forms. Both forms of YB-1 appear to accumulate in the nuclear compartment of cells transfected with ΔNp63α, but not ΔNp63γ (Fig. 4B). Immunoblots with antibodies against PARP-1 (nuclear) and Akt (cytoplasmic) were performed to check for the quality of the fractionation. Interestingly, while the amount of total Akt was comparable, phosphorylated Akt, at

Serine 473, was enhanced in ΔNp63α, but not ΔNp63γ transfected cells (Fig. 4B). This observation was in line with previous data showing the specific ability of ΔNp63α isoform to promote PI3K/Akt pathway activation (*Barbieri*,2003).

I then evaluated the contribution of ΔNp63α to YB-1 subcellular distribution in SCC011 and in SCC022 cells expressing both proteins endogenously. To this aim, I analyzed YB-1 subcellular distribution, following p63 depletion, by immunoblot on nuclear/cytoplasmic fractions in SCC011 cells and by immunofluorescence in SCC022 cells. As shown in fig. 5A and B, following p63 knock-down, the YB-1 nuclear pool was dramatically reduced.

FIGURE 5

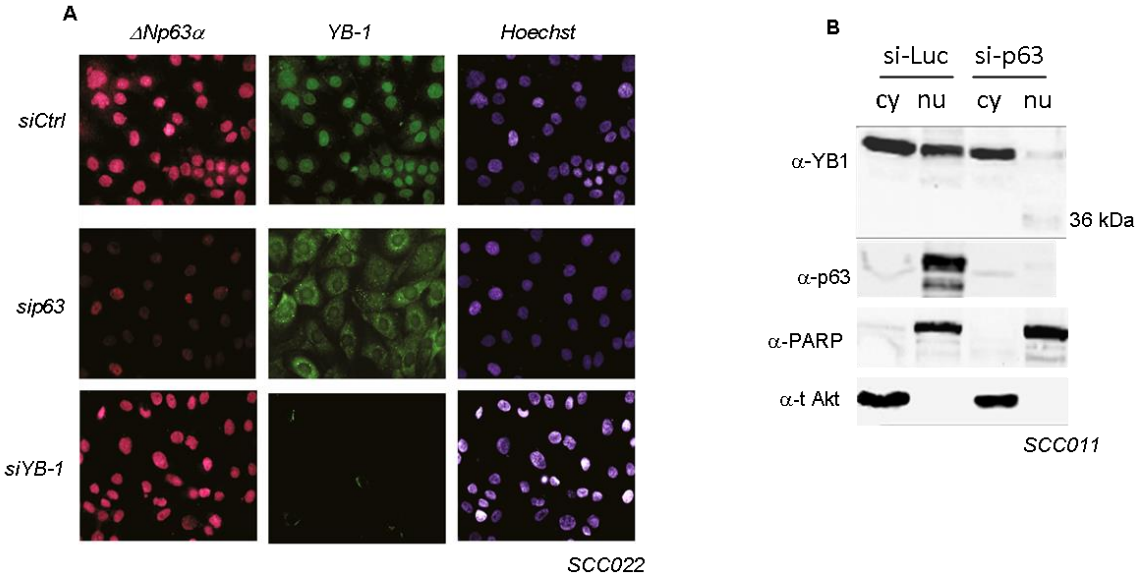

FIGURE 5. YB-1 and p63 knockdown in SCC022 cells. (A) Immunofluorescence assay in SCC022 cells transfected with scrambled, YB-1 or p63 siRNA oligos. YB1 was detected using anti-YB-1 and secondary anti-rabbit Cy5-conjugated (green) antibodies. p63 was detected using anti-p63 and secondary anti-mouse Cy3-conjugated (red) antibodies. Hoechst was used to stain nuclei**. (B)** SCC011 cells were seeded at 60% confluency (1.5×10^6) in 100mm dishes. 24h after seeding cells were transiently silenced with IBONI p63-siRNA pool (20nm final concentration). 48h after p63-silencing cell lysates were fractionated to obtain cytoplasmic and nuclear fractions. Nuclear and cytoplasmic extracts were separated by SDS PAGE and subjected to immunoblot. Proteins were detected with specific antibodies, as indicated. PARP and total AKT were used as nuclear and cytoplasmic control respectively, to check for cross-contamination. Images were acquired with CHEMIDOC (BIORAD) and analyzed with the Quantity-ONE software.

2.3 ΔNp63α affects YB-1 binding to Snail and YB-1 mRNAs

Nuclear accumulation of YB-1 induced by ΔNp63α causes consequently a reduction of its cytoplasmic pool, therefore, affecting YB-1 functions.
Cytoplasmic localization of YB-1 was associated with binding and translational activation of Snail1 mRNA (*Evodokimova*, 2009). Snail1 protein is a transcriptional repressor of ΔNp63α and E-cadherin and promotes the epithelial-mesenchimal transition in several epithelial-derived cancer cell lines (*Peirò*, 2006). My group had

previously observed that ΔNp63α overexpression in MB-MDA-231 caused a reduction of Snail1 protein level (Fig. 6A). Such reduction was not associated with a decrease of Snail1 mRNA level (Fig. 6B), thereby suggesting that Snail1 protein was down-regulated at translational level. They hypothesized that the specific association of ΔNp63α with YB-1 would reduce the amount of YB-1 bound to the Snail1 transcript. To test this hypothesis they performed RNA-Immunoprecipitation (RNA-IP) coupled with real time PCR to quantitate the amount of Snail1 mRNA bound to endogenous YB-1, in mock and ΔNp63α transfected MDA-MB-231 cells. The obtained results confirm that ΔNp63α reduces the amount of YB-1 bound to Snail1 transcript (Fig. 6C). A similar analysis performed on YB-1 transcript gave the same result (Fig. 6D).

FIGURE 6

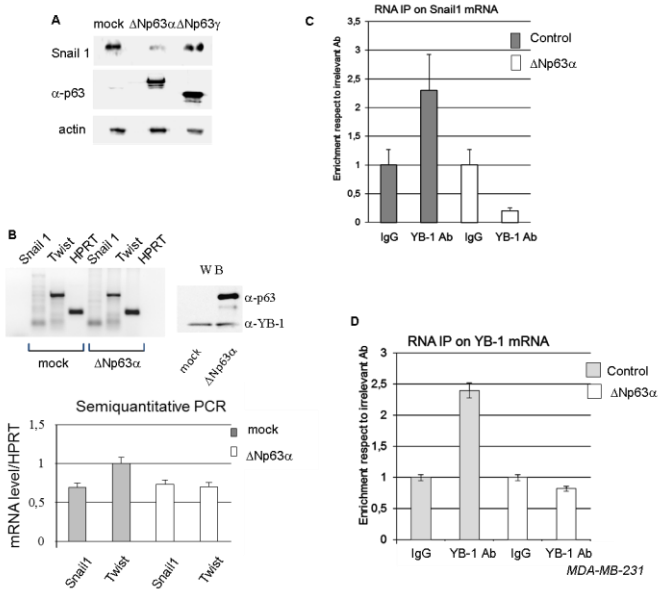

FIGURE 6. ΔNp63α affects Snail1 protein level and YB-1 binding to Snail1 and YB-1 mRNAs in MDA-MB-231 cells. (**A**) MDA-MB-231 cells were transfected with an empty vector (mock) or a fixed amount (1μg in 60mm dishes) of ΔNp63α or ΔNp63γ expression vector. 24 hr after transfection, cells were harvested and total extracts were prepared. 20μg of each extract were loaded on SDS-PAGE and subjected to immunoblot with the indicated antibodies. (**B**) MB-MDA-231 cells were transfected with an empty vector or ΔNp63α encoding plasmid. 24hr after transfection total RNA was purified and retrotranscribed as described in Materials and Methods. The expression level of ΔNp63α was checked by immunoblot (**right panel**). PCR was performed with primers designed to specifically amplify Snail1, Twist or HPRT transcripts and analyzed by agarose-gel electrophoresis (**left panel**). Plot showing the level of Snail1 and Twist transcripts was normalized respect to HPRT. Values are the mean of 3 independent experiments (**lower panel**).
Nuclear extracts from ΔNp63α transfected MB-MDA-231 cells were immunoprecipitated with anti-YB1 antibody. After reverse cross-linking the YB1-bound RNA was purified, retrotranscribed and subject to qRT-PCR analysis using oligonucleotides designed to specifically amplify Snail1 transcript (**C**) or YB-1 transcript (**D**). Plots represent the % of enrichment of Snail1/YB-1 transcript normalized as indicated in Materials and Methods. 1/50 of the input extract was loaded as control. The values are the mean ± S.D. of three biological replicates.

2.4 ΔNp63α and YB-1 binds to the PIK3CA gene promoter and cooperate in its transcriptional activation

Given the observed YB-1 behaviour in the cytoplasm in presence of ΔNp63α, I focused my attention on the potential role of two proteins in the regulation of nuclear targets. The *PIK3CA* gene encodes the p110α catalytic subunit of the phosphatidylinositol-3-kinase (PI3K) and is a well characterized YB-1 direct transcriptional target (*Astanehe*, 2009). I speculated that ΔNp63α should increase *PIK3CA* promoter activity because of its ability to cause YB-1 nuclear accumulation.

Previous luciferase assays, shown in Fig. 7A, revealed that ΔNp63α transfection in MDA-MB-231 cells caused a relevant increase of the PIK3CA promoter activity, consistently attenuated by YB-1 knock-down. Since my group had already observed that ΔNp63α was able to transactivate the PIK3CA promoter in a dose dependent manner, while ΔNp63γ was completely uneffective (Fig. 7B), we deeply investigated the role of ΔNp63α and YB-1 in PIK3CA promoter activation by Chromatin Immunoprecipitation (ChIP).

FIGURE 7

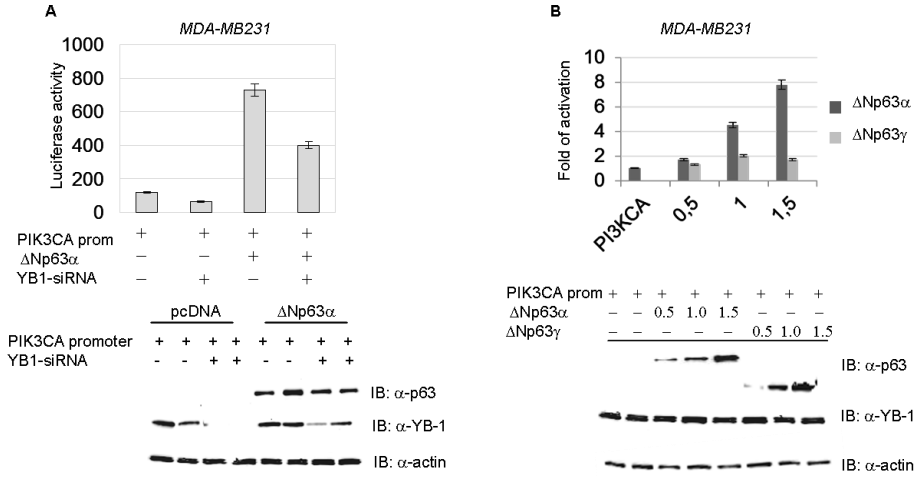

FIGURE 7. ΔNp63α and YB-1 activates the PIK3CA gene promoter. (**A**) MB-MDA- cells were transfected with 1μg of PIK3CA-promoter luciferase reporter plasmid. The luciferase activity upon siRNA-mediated knockdown of endogenous YB-1 was measured in presence or absence of ΔNp63α expression. Values are shown as mean ± SD of three biological replicates. The extent of YB-1 knock-down was documented by western blotting as shown in the lower panel. (**B**) MB-MDA-231 cells were seeded at 60% confluency (1.2×10^6) in 100mM dishes and transiently transfected with 1μg of PIK3CA-promoter luciferase reporter plasmid and the indicated amounts of ΔNp63α or ΔNp63γ plasmid. Values are the mean ± SD of three independent experimental points. Lower panel: immunoblotting with indicated antibodies to detect proteins in samples transfected with different amounts of ΔNp63α or ΔNp63γ.

We first performed ChIP assays in MDA-MB-231 cells transfected with ΔNp63α or ΔNp63γ, using anti-p63 antibodies and PIK3CA promoter specific primers. As shown in Fig. 8A, ΔNp63α, but not ΔNp63γ, binds to the genomic sequence of the PIK3CA promoter.

Then, we evaluated the effect of ΔNp63α expression on the binding of YB-1 to the PIK3CA promoter. Flag-YB-1 was transfected, in MB-MDA-231 cells, with or without ΔNp63α plasmid. Chromatin immunoprecipitations (ChIP) was carried out with anti-Flag antibodies and coupled with quantitative real-time PCR. As show in Fig. 8B, Flag-YB1 efficiently binds to the PIK3CA promoter and its binding was substantially increased by ΔNp63α.

Lastly, by using a sequential chromatin immunoprecipitation assay (Re-ChIP) in SCC011 cells, expressing endogenous ΔNp63α and YB-1, I found that both proteins are recruited to the PIK3CA proximal promoter suggesting that they cooperate in PIK3CA gene transactivation as a complex (Fig. 8C).

FIGURE 8

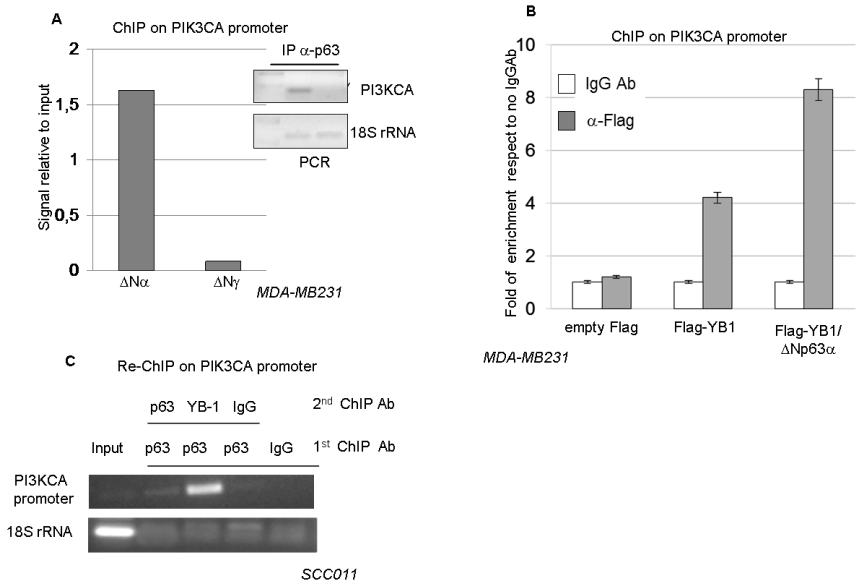

FIGURE 8. **ΔNp63α increases YB-1 binding to the PIK3CA gene promoter**. (**A**) MDA-MB-231 cells were seeded at 60% confluency (1.2 x 10^6) in 100mM dishes and transiently transfected with ΔNp63α or ΔNp63γ plasmid (5 μg). After formaldehyde cross-linking, the DNA/proteins complexes were immunoprecipitated with anti-p63 (4A4) antibody. Immunoprecipitated DNA was PCR amplified with PIK3CA promoter oligos and 18S rRNA oligos (right). The data obtained from the ChIP assay were measured by densitometry and are presented as signal relative to the input (left). (**B**) MDA-MB-231 cells were seeded at 60% confluency (1.2 x 10^6) in 100mM dishes and transiently transfected with 3XFlag empty vector or 3XFlag-YB-1 (5 μg) plasmid with or without ΔNp63α (2.5 μg) expression vector. The cells were cross-linked with formaldehyde and DNA/protein complexes were immunoprecipitated with anti-Flag antibody or irrelevant IgG antibody as negative control. The DNA immunoprecipates were analysed by qPCR using PIK3CA or GAPDH promoter oligos. qRT-PCR results were analized with the $\Delta\Delta C^T$ method and expressed as fold of enrichment respect to the IgGAb control samples. Values are represented as the mean of three independent experiments. (**C**) SCC011 cells at 85% confluency were fixed with formaldehyde, the DNA/proteins complexes were subjected to sequential-ChIP with anti-p63 (4A4), anti-YB1(Ab12148) or irrelevant IgG antibody as described in experimental procedure. Immunoprecipitated DNA was PCR amplified with PIK3CA promoter primers and 18S rRNA primers to check the quality of the input chromatin and the cleaning of the other samples.

2.5 ΔNp63α affects cell shape and motility

So far, little attention has been focused on the effects of ΔNp63α on epithelial cancer cell morphology and motility. I have unexpectedly noted a profound change in cell morphology when SCC011 cells were depleted of ΔNp63α by siRNA. SCC011 cells are round in shape and under high-density culture conditions appear orderly arranged with tight cell-cell contacts. Conversely, ΔNp63α-depleted cells tend to lose their contacts and exhibited an unusual extended phenotype that was distinct from that of the control cells cultured at the same density (Fig. 9A). The unusual change in morphology of ΔNp63α-depleted cells indicated possible alterations in actin cytoskeleton organization. Therefore, I examined the status of actin stress fibers at the level of individual cells, in control and ΔNp63α-depleted cells, with TRITC-phalloidin followed by fluorescence microscopy. As shown in Fig. 9B, the control cells exhibited a diffuse pattern of actin staining, while ΔNp63α-depleted cells displayed a

more substantial enhancement of actin stress fibers suggesting an inhibitory effect of ΔNp63α on cancer cell motility.
Remarkably, compared to the control cells, ΔNp63α-depleted SCC011 cells express higher level of N-cadherin and lower amount of E-cadherin suggesting that they were undergoing epithelial to mesenchimal trans-differentiation (EMT) (Fig. 9C).
I determined the influence of ΔNp63α on cell motility by time-lapse microscopy using siRNA-based silencing of endogenous ΔNp63α in SCC011 cells. Silencing efficiency was about 90% as determined by fluorescent staining for p63 protein (data not shown). SCC011 migration was characterized by oscillations of the cells around their initial adhesion site. These oscillations occurred at random directions in space, as reported in the windrose plots of the trajectories (Fig. 9D, inset). Conversely, ΔNp63α silenced cells display much wider oscillations (Fig. 9D). These observations were confirmed by the analysis of the migration parameters "Speed (S)" and "Persistence time (P)", that are computed from cell tracks and are a measure of the frequency of cell steps and of the minimum time that is necessary for a cell to significantly change direction. According to those parameters, SCC011 exhibit lower speed ($p<0.05$) and shorter persistence time (0.26 ± 0.03 μm/min and 6.5 ± 0.7 min), respect to ΔNp63α depleted cells (0.44 ± 0.05 μm/min and 8.2 ± 2.3 min). These data indicate a role of ΔNp63α in affecting cell motility. In particular, the absence of ΔNp63α causes the cells to migrate faster with less frequent direction changes, which enables the cells to explore larger areas, in a fixed time interval.

FIGURE 9

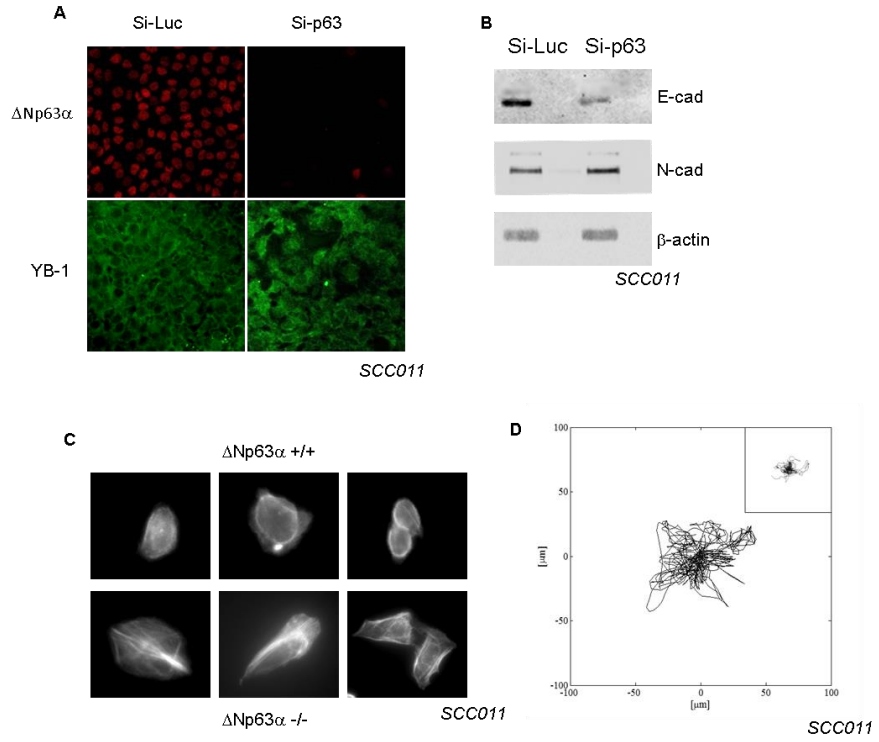

FIGURE 9. ΔNp63α affects cell shape and motility. (**A**) SCC011 cells were transiently silenced with IBONI p63-siRNA pool (20nm final concentration). Cell were fixed and subjected to double immunofluorescence 48 hrs after silencing. (**B**) Protein extracts from control and p63 depleted cells were separated by SDS PAGE and subjected to immunoblot. Proteins were detected with specific antibodies. (**C**) Actin staining with TRITC conjugated phalloidin of control and ΔNp63α-depleted SCC011 cells (see Materials and Methods). Cell expressing ΔNp63α displayed a round morphology. Conversely, ΔNp63α-depleted cells had a polarized morphology with more evident lamellipodia and trailing edge. (**D**) Windrose plot of trajectories described by ΔNp63α depleted SCC011 or SCC011 control cells (inset) in 12 hour time lapse video. Only fifteen cell trajectories were reported in each plot for graphical clarity.

Since previous observations had shown that the absence of ΔNp63α affects cell motility in YB-1 dependent manner (data not shown), I have investigated on the potenital effect of YB-1 silencing on SCC022 motility, by time-lapse microscopy. siRNA-based silencing of endogenous proteins, according to our observations in SCC011 cells, showed that ΔNp63α silenced cells display higher speeds ($p < 0.01$) than control cells. Conversely, SCC022 cell motility was unaffected by YB-1 depletion (Fig. 10A and 10B).

FIGURE 10

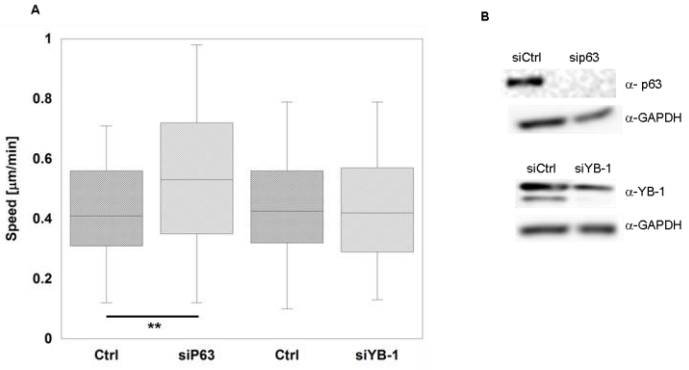

FIGURE 10. Effect of p63 and YB-1 silencing on SCC022 cells migration speed. (**A**) Motility assay on SCC022 cells after transient silencing of p63 and YB-1 performed by time-lapse microscopy. After 24 h of incubation with siRNA oligos, cell migration assay was performed. Averaged cell speeds after 16 h of observation are reported. Horizontal lines and boxes and whiskers represent the medians, 25th/75th, and 5th/95th percentile, respectively. P-value < 0.01 is represented by **. Only statistically different doubles are marked. (**B**) Immunoblot analysis of ΔNp63a and YB-1 proteins levels in SCC022 cells after 40 h of ΔNp63α or YB-1 silencing and used in cell migration assay. Cell extracts were blotted and probed with anti-p63 or anti-YB-1 antibodies. GAPDH was used as a loading control. ΔNp63α protein band was almost undetectable while YB-1 protein was reduced to 40%, as assed by densitometric scanning.

2.6 YB-1 knockdown in HaCaT cells

Since I have shown that ΔNp63α inhibits epithelial-to-mesenchimal transition and motility of squamous carcinoma cells, I decided to expand our knowledge on YB-1 and ΔNp63α functional cross-talk evaluating the role of YB-1 on survival of keratinocytes and squamous carcinoma cells.

FIGURE 11

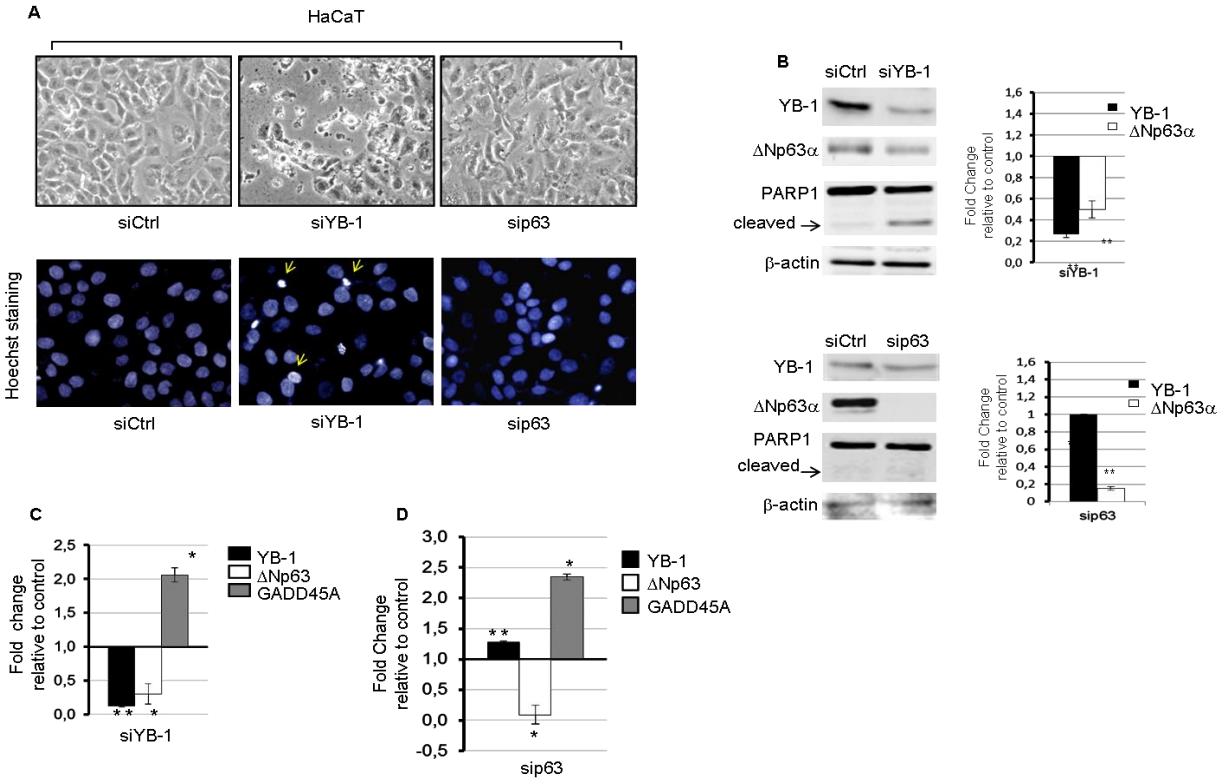

FIGURE 11. YB-1 knockdown affects HaCaT cell survival. (**A) upper panel,** Phase-Contrast imaging and Hoechst staining (**lower panel**) showing HaCaT keratinocyte cells transfected with scrambled, YB-1 or p63 siRNA oligos. (**B**) Immunoblot analysis of HaCaT keratinocytes transfected with scrambled and YB1 (**upper panel**) or p63 (**lower panel**) siRNA oligos, respectively. 48 hours after silencing whole cell extracts were immunoblotted with YB-1, p63 and PARP antibodies. Actin was used as a loading control. A representative immunoblot (**left panel**) and densitometric analysis (**right panel**) are shown from four independent experiments (n=4). The blots were normalized to actin and the fold-change protein level expression is reported in comparison to control (value set at 1.0). (**C**) Quantitative real-time PCR analysis of HaCaT keratinocytes transfected with scrambled or YB-1 siRNA oligos. GADD45A mRNA level was measured as a control. (**D**) Quantitative Real-time PCR analysis of HaCaT keratinocytes transfected with scrambled or p63 siRNA oligos. In both experiments data were analyzed according to the fold-changes compared to scrambled control (value set at 1.0) using the $2^{-\Delta\Delta Ct}$ method. P-value <0.05 is represented by *; P-value <0.01 is represented by **.

First, I examined the effect of YB-1 silencing in mitotically active HaCaT keratinocytes. Interestingly, at 48 hrs of silencing I observed massive cell detachment (Figure 11A, upper panel) associated with a high proportion of condensed and fragmented nuclei (Figure 11A, lower panel). Western blot analysis showed a significant reduction of ΔNp63α protein level and PARP1 proteolytic cleavage (Figure 11B, left panel) indicating that YB-1 is critical for keratinocyte survival.

ΔNp63α is known to sustain survival in squamous cell carcinoma (*Rocco*, 2006; *Hibi*, 2000) and up-regulate cell adhesion-associated genes (*Carrol*, 2006). To rule out the possibility that YB-1 silencing induces cell death by merely reducing the level of ΔNp63α, I knocked down ΔNp63α expression in HaCaT cells by RNA interference. According to previous studies (*Barbieri*, 2006), I observed neither cell detachment

(Figure 1A, upper panel) nor PARP1 activation (Figure 11B, right panel) clearly indicating that apoptosis, induced by YB-1 depletion, cannot be simply ascribed to the lack of ΔNp63α.
Next, I evaluated the level of ΔNp63α transcript following YB-1 knockdown by Real Time quantitative PCR (RT-qPCR) and I found that it was drastically reduced (Figure 11C). After p63 silencing, instead, YB-1 transcript level was slightly enhanced (Figure 11D) while the mRNA of GADD45A, a gene induced by stressful conditions and used as control, was enhanced in both experiments (Figure 11 C and D).

2.7 YB-1 knockdown in squamous carcinoma cells

Next, I used RNA interference to explore the function of YB-1 in squamous cell carcinoma (SCC). SCC022 are highly metastatic and, when subcutaneously injected in nude mice, form large tumors, while SCC011 cells, instead, generate only keratin pearls (C. Missero, personal communication).

FIGURE 12

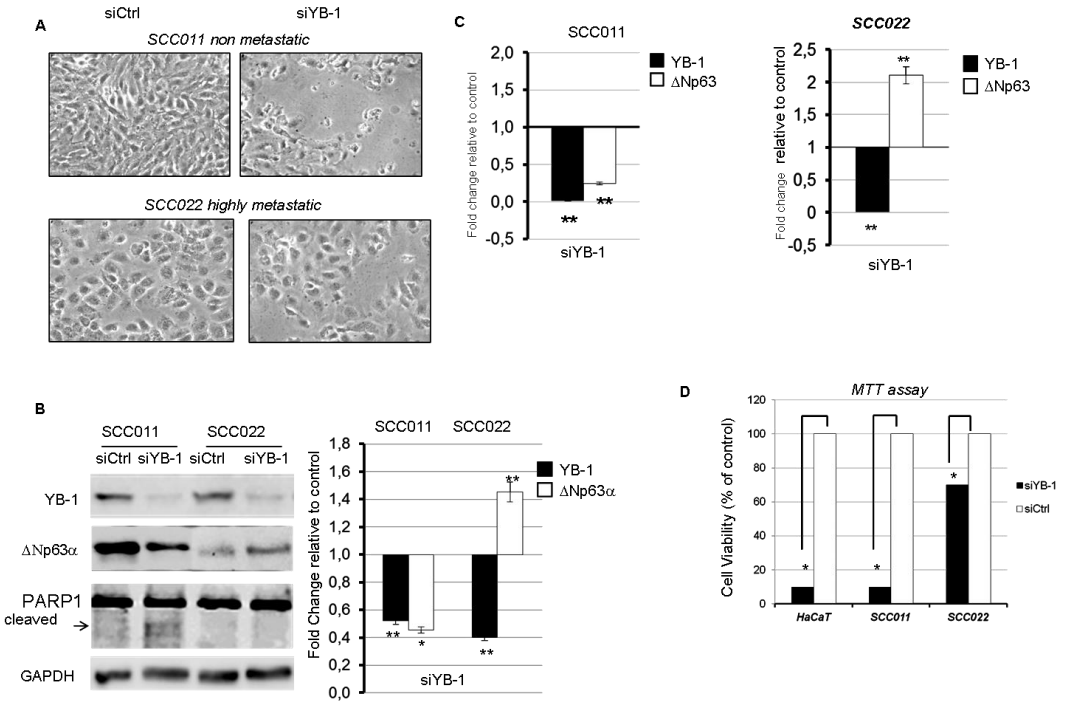

FIGURE 12. YB-1 knockdown in SCC011 and SCC022 squamous carcinoma cells. (A) Phase-contrast imaging showing SCC011 (**upper panel**) and SCC022 (**lower panel**) cells at 48 hours post-YB1 silencing. (**B**) Immunoblot analysis of SCC011 or SCC022 cells transfected with scrambled or YB-1 siRNA oligos. 48 hours after silencing whole cell lysates were immunoblotted with YB-1, p63 and PARP antibodies. GAPDH was used as a loading control. A representative immunoblot (**left panel**) and densitometric analysis (**right panel**) are shown from four independent experiments (n=4). The blots were normalized to GAPDH and the fold-change protein level expression is reported in comparison to control (value set at 1.0). (**C**) Quantitative Real-time PCR analysis of SCC011 (**left panel**) and SCC022 cells (**right panel**) transfected with scrambled or YB-1 siRNA oligos. Data were analyzed according to the fold-changes compared to scrambled control (value set at 1.0) using the $2^{-\Delta\Delta Ct}$ method. P-value <0.05 is represented by *; P-value <0.01 is represented by **. (**D**) Effect of YB1 silencing on the viability of HaCaT and SCC cells. Cell viability was assessed by MTT assay following 48 hours of YB-1 silencing. Data are represented as the mean +/- SD from three independent experiments. The asterisk indicates P-value<0.05.

Similarly to what observed in HaCaT cells, YB1-depleted SCC011 cells detached from the plate generating abundant cellular debris (Figure 12A, upper panel) and exhibited a reduced level of ΔNp63α protein (Figure 12B). PARP1 cleavage was barely detectable (Figure 12B).
According to our previous observations described above (see paraghraph 2.5, Figure 10), SCC022 cells looked healthy and tightly adherent to the plate after YB1 silencing (Figure 12A, lower panel). Surprisingly, as detected by immunoblot analysis, the expression level of ΔNp63α protein was significantly increased (Figure 12B). Interestingly, ΔNp63α transcript in SCC011 was reduced while in SCC022 it was 2.1-fold higher than control (Figure 12C).

Analysis of cell viability by the MTT assay showed that after 48 hrs of YB-1 knockdown the percentage of viability of SCC022 cells was 70% of the control, while it was reduced to 10% in HaCaT and SCC011 cells (Figure 12D).

2.8 YB-1 silencing hyper-activates the PI3K/AKT signaling pathway in SCC022 cells

ΔNp63α is a target of the phosphoinositide-3-kinase (PI3K) pathway downstream of the Epidermal Growth Factor Receptor (*Barbieri*, 2003). I hypothesized an involvement of the PI3K/AKT pathway in the upregulation of ΔNp63α observed in SCC022 cells following YB-1 silencing, and I looked for changes in the phosphorylation status of $AKT_{Ser473.}$ Interestingly, unlike HaCaT and SCC011, SCC022 cells exhibited constitutive phosphorylation of AKT_{Ser473} which was reproducibly potentiated following YB-1 depletion (Figure 13A and B), suggesting that YB-1 expression restrains AKT activation. To corroborate this result, I treated YB1-silenced SCC022 cells with Ly294002, a highly selective PI3K inhibitor. Remarkably, Ly294002 treatment counteracted AKT hyperphosphorylation and the increase of ΔNp63α protein level in response to YB-1 silencing (Figure 13B). Moreover, it resulted in cell death and detachment (data not shown). Importantly, Ly294002 treatment alone had no apparent effect on ΔNp63α level and SCC022 cell viability (Figure 13B and data not shown). Quantification of ΔNp63α transcript in YB-1 depleted SCC022 cells, treated or not with LY294002, showed that the increase of ΔNp63α transcription was strictly dependent on the PI3K/AKT pathway (Figure 13B). Moreover, inhibition of the proteasome activity with MG132 did not significantly enhance ΔNp63α protein level in YB1-silenced SCC022 cells, thereby confirming that ΔNp63α up-regulation was almost exclusively at transcriptional level (data not shown).
The PI3K/AKT signaling pathway is negatively regulated by the phosphatase and tensin homologue PTEN (*Song*, 2012). To further investigate on the ability of SCC022 cells to escape from death following YB-1 depletion, I compared the protein level of PTEN among HaCaT, SCC011 and SCC022 cell lines. Compared to HaCaT and SCC011 cells, the level of PTEN protein in SCC022 cells was very low, accounting for their high basal level of AKT_{Ser473} phosphorylation (Figure 13D). Furthermore, YB-1 silencing resulted in increased levels of cytoplasmic PTEN in HaCaT and SCC011 cells, while no effects on PTEN protein level was observed in YB-1 silenced SCC022 cells (Figure 13E).

FIGURE 13

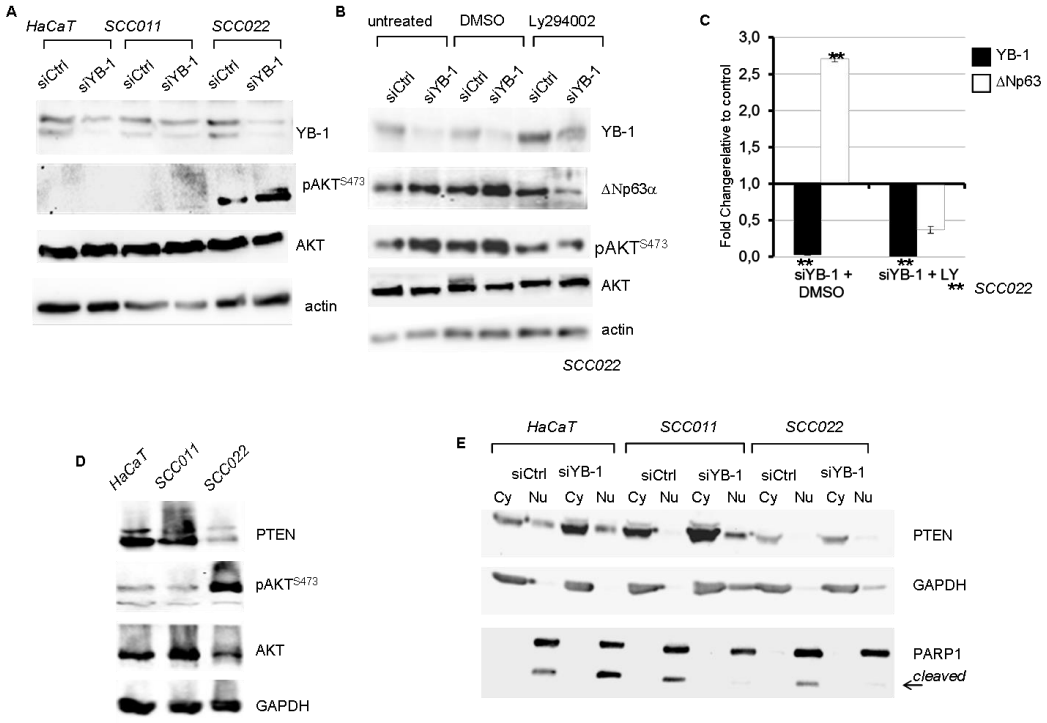

FIGURE 13. YB-1 knockdown enhances pAKT^{S473} in SCC022 squamous carcinoma. (**A**) Immunoblot analysis of HaCaT, SCC011 and SCC022 cells transfected with scrambled or YB1-siRNA oligos. 48 hours after silencing whole cell extracts were immunoblotted with YB-1, pAKT^{S473} and AKT antibodies. Actin was used as a loading control. (**B**) SCC022 cells were transfected with scrambled or YB-1 siRNA oligos transfection. After 42 hrs cells were treated with LY294002 for 6 hrs. Whole cell extracts were analyzed by immunoblotting with YB-1, pAKT^{S473}, p63 and AKT antibodies. Actin was used as loading control. (**C**) Quantitative Real-time PCR of ΔNp63 mRNA levels. ΔNp63 mRNA levels were analyzed according to the fold-changes compared to scrambled control (value set at 1.0) using the $2^{-\Delta\Delta Ct}$ method. P-value < 0.05 is represented by *; P-value < 0.01 is represented by **. DMSO was used as control (**D**) Immunoblot analysis of HaCaT, SCC011 and SCC022 cells. Whole cell extracts were immunoblotted with, PTEN, pAKT^{S47}, and AKT antibodies. GAPDH was used as loading control. (**E**) Nuclear and cytoplasmic fractionation of extracts from control or YB-1 silenced HaCaT, SCC011 and SCC022 cells are shown in Figure 5A. Fractions were analysed by immunoblotting with PTEN antibody. GAPDH and PARP were used as cytoplasmic and nuclear controls, respectively.

2.9 Cross-talk of ΔNp63α and YB-1 with EGFR/STAT3 and PI3K/AKT signaling pathways

In pancreatic cancer cells, ΔNp63α expression was shown to induce the Epidermal Growth Factor Receptor (EGFR) (*Danilov*, 2011). As I observed a PI3K-dependent increase of ΔNp63α in SCC022 cells upon YB-1 silencing, I decided to evaluate the level of EGFR and its direct downstream target STAT3 in SCC022 cells upon YB-1 or ΔNp63α silencing. As shown in Figure 14, along with ΔNp63α, YB-1 depletion up-regulates EGFR and STAT3 both at protein (Figure 14A) and RNA level (Figure 14B). Real Time PCR assay in SCC022 cells clearly shows that YB-1 silencing results in about 2 and 3.5 fold induction of EGFR and STAT3 transcripts, respectively (Figure 14B). Following ΔNp63α silencing, instead, the expression of both EGFR and STAT3 was switched off although the level of YB-1 protein remained unaltered (Figure 14A). These results suggest that ΔNp63α is a major activator of the

EGFR/STAT3 axis in squamous carcinoma cells. Accordingly, in SCC011 and HaCaT cells where YB-1 silencing reduces ΔNp63α, EGFR and STAT3 transcription was also reduced (Fig. 14C and D).

FIGURE 14

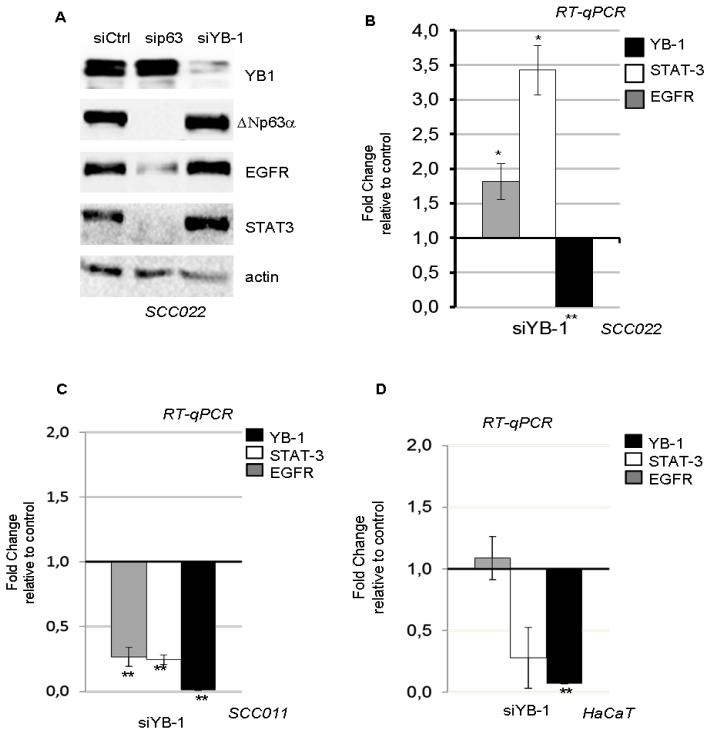

FIGURE 14. Cross-talk of ΔNp63α and YB-1 with EGFR/STAT3 pathway. (**A**) Immunoblot analysis of SCC022 cells transfected with scramble, YB-1 or p63 siRNA oligos. Whole cell extracts were immunoblotted with, YB-1, p63, EGFR, STAT3 antibodies. Actin was used as a loading control. (**B**) Quantitative Real-time PCR analysis of SCC022 cells transfected with scrambled or YB-1 siRNA oligos. YB-1, EGFR and STAT3 mRNA levels were analyzed according to the fold-changes compared to scrambled control (value set at 1.0) using the $2^{-\Delta\Delta Ct}$ method. P-value < 0.05 is represented by *; P-value < 0.01 is represented by **. Quantitative Real-time PCR analysis of (**C**) SCC011 cells and (**D**) HaCaT cells transfected with scrambled or YB-1 siRNA oligos. YB-1, EGFR and STAT3 mRNA levels were analyzed according to the fold-changes compared to scrambled control (value set at 1.0) using the $2^{-\Delta\Delta Ct}$ method. P-value < 0.05 is represented by *; P-value < 0.01 is represented by **.

To confirm the ability of ΔNp63α to regulate EGFR gene expression I performed transient transfection and luciferase reporter assays in MDA-MB231 breast cancer cells expressing no detectable p63. MDA-MB231 cells were transiently transfected with the EGFR promoter-luciferase vector and increasing amount of expression plasmid encoding wild type ΔNp63α or its mutant form bearing the F to L substitution at position 518 of the SAM domain. This mutant was previously described to be transactivation defective (*Radoja*, 2007).

FIGURE 15

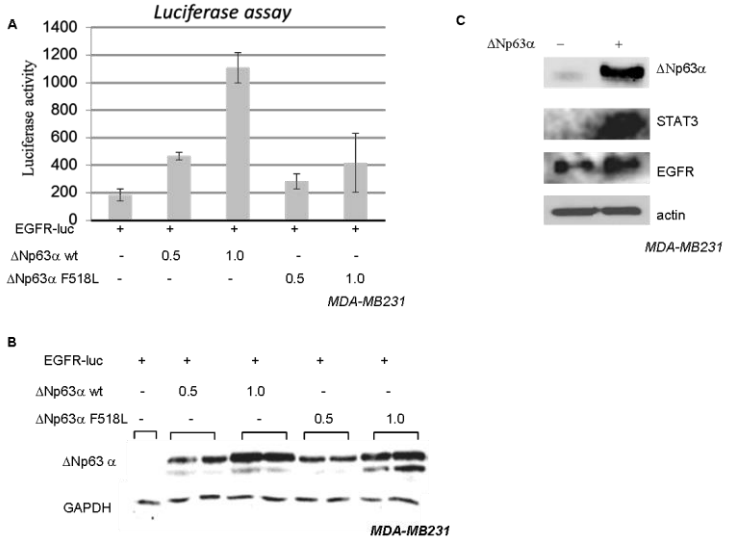

FIGURE 15. ΔNp63α regulates EGFR expression. (A) Luciferase assay of EGFR-promoter activity in MDA-MB231 cells. Cells were transiently transfected with 1μg of luciferase reporter plasmid and the indicated amounts of ΔNp63α or ΔNp63α F518L plasmids. Luciferase assay was performed at 48 hrs post-transfection. Values are the mean +/- SD of three independent experimental points. **(B**) Representative immunoblotting showing the level of ΔNp63α in transfected MDA-MB231 cell extracts used for the luciferase assay shown in 7C. GAPDH immunodetection was used as loading control. **(C**) MDA-MB231 cells were transfected with empty vector or ΔNp63α plasmids. At 24h post-transfection cells were harvested and whole cell extracts were analyzed by immunoblotting with p63, STAT3 and EGFR antibodies. Actin was used as a loading control.

Remarkably, wild type but not mutant ΔNp63α protein induced luciferase activity, in a dose-dependent manner (Figure 15A and B). Moreover, Western blot analysis of extracts from MDA-MB231 breast cancer cells transiently transfected with ΔNp63α showed induction of both EGFR and STAT3 endogenous proteins, confirming that EGFR and STAT3 expression are induced by ΔNp63α (Figure 15C).

2.10 YB-1 controls CD44 expression in keratinocytes

It was previously reported that YB-1 induces the expression of CD44 in breast cancer cells (*To*, 2010). Since CD44 is a cell surface adhesion molecule involved in the control of keratinocyte proliferation (*Tuhkanen*, 1999) I decided to evaluate its potential involvement in YB1 dependent HaCaT cell death. I first evaluated the effect of YB-1 depletion on CD44 expression. As expected, YB-1 knockdown in HaCaT cells reduced CD44 protein level (Figure 16A). Moreover, full length CD44 transcript and its epithelial isoforms CD44v4 and CD44v5 were all reduced upon YB-1 silencing (Figure 16B). Conversely, ΔNp63α silencing resulted in a slight increase of CD44 protein (Figure 16C) and transcript levels (Figure 16D).

FIGURE 16

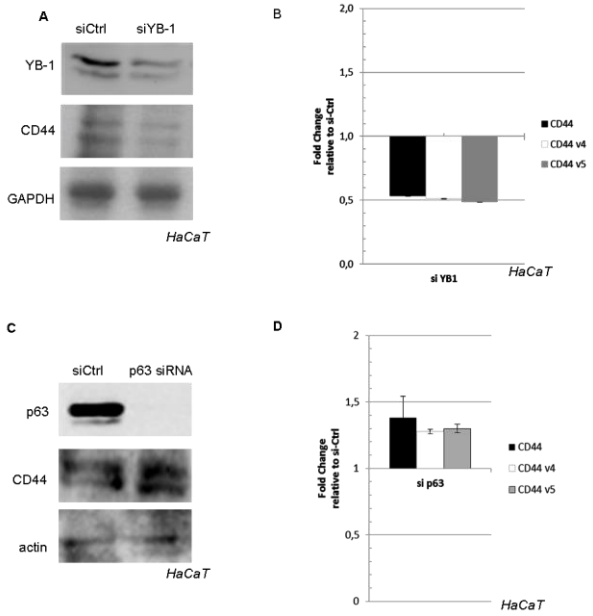

FIGURE 16. YB-1 knockdown in HaCaT cells induces CD44 downregulation. (**A**)(**C**) Immunoblot analysis of HaCaT keratinocytes transfected with scrambled and YB1 (**upper panel**) or p63 (**lower panel**) siRNA oligos, respectively. 48 hours after silencing whole cell extracts were immunoblotted with YB-1, p63 and CD44 antibodies. Actin and GAPDH were used as a loading control. (**B**) Quantitative real-time PCR analysis of HaCaT keratinocytes transfected with scrambled or YB-1 siRNA oligos. (**D**) Quantitative Real-time PCR analysis of HaCaT keratinocytes transfected with scrambled or p63 siRNA oligos. In both experiments data were analyzed according to the fold-changes compared to scrambled control (value set at 1.0) using the $2^{-\Delta\Delta Ct}$ method. P-value <0.05 is represented by *; P-value <0.01 is represented by **.

Similarly, in SCC011 cells, that are prone to detach, CD44 transcripts were reduced following YB-1 depletion (Figure 17A), while in SCC022, CD44 transcripts were significantly enhanced (Figure 17B). As shown for ΔNp63α expression (Figure 13B), LY294002 treatment of YB-1 silenced SCC022 showed that the increase of CD44 transcription was dependent on the PI3K/AKT pathway hyper-activation (Figure 17C).

FIGURE 17

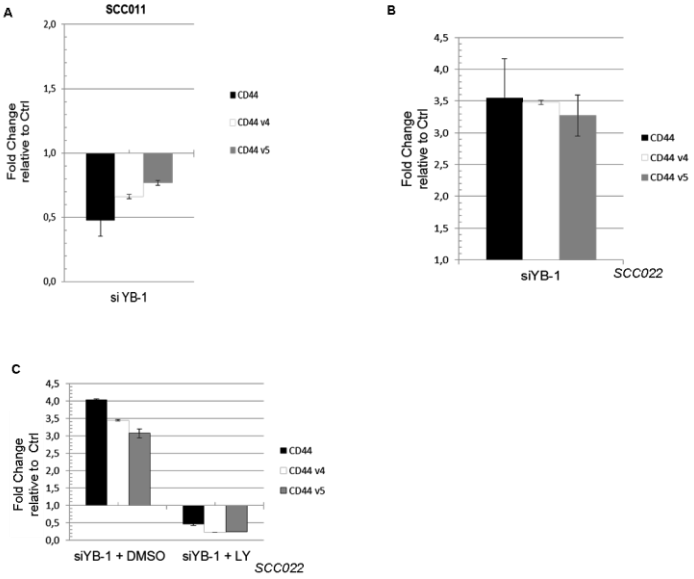

(**A**) (B) Quantitative real-time PCR analysis of SCC011 and SCC022 transfected with scrambled or YB-1 siRNA oligos, respectively. CD44 mRNA levels were analyzed according to the fold-changes compared to scrambled control (value set at 1.0) using the $2^{-\Delta\Delta Ct}$ method. P-value < 0.05 is represented by *; P-value < 0.01 is represented by **. DMSO was used as control (**C**) Quantitative Real-time PCR analysis of SCC022. transfected with scrambled or yb-1 siRNA oligos. After 42 hrs cells were treated with LY294002 for 6 hrs. In both experiments data were analyzed according to the fold-changes compared to scrambled control (value set at 1.0) using the $2^{-\Delta\Delta Ct}$ method. P-value <0.05 is represented by *; P-value <0.01 is represented by **.

Finally, we simultaneously depleted ΔNp63α and CD44 in HaCaT cells to check whether it was enough to mimic the effect of YB-1 silencing. However, although the

silencing at 48 hrs was highly efficient (Figure 18A), I observed neither cell detachment (Figure 18B) nor PARP1 proteolytic activation (Figure 18A). Moreover, as shown by the induction of cytokeratin-1 (CK1) (Figure 18A) and the change of cell morphology (Figure 18B), CD44 and ΔNp63α concomitant knockdown appears to induce keratinocyte differentiation rather than apoptosis

FIGURE 18

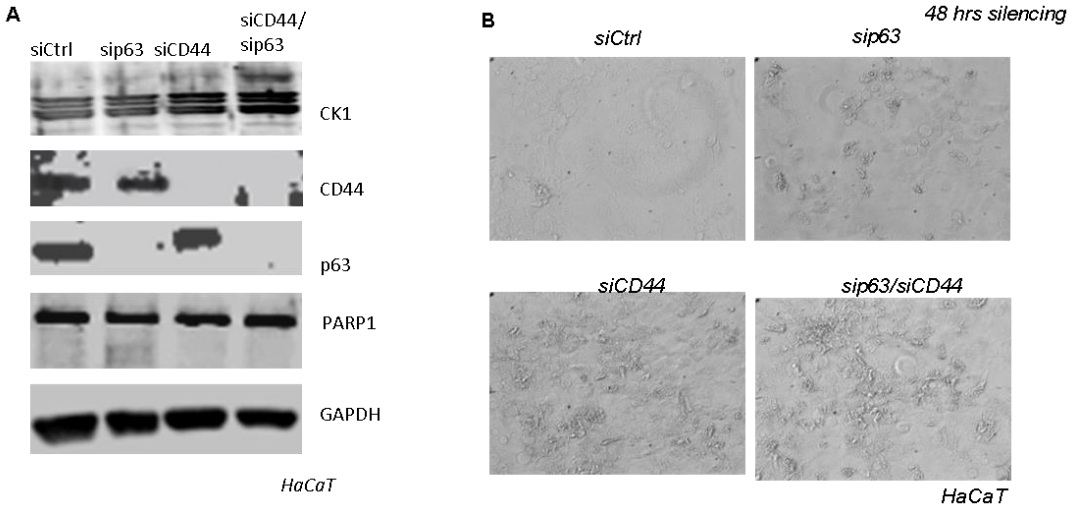

Figure 18. **p63/CD44 knockdown in HaCaT cells.** (**A**) Immunoblotting and (**B**) Phase-Contrast imaging of HaCaT keratinocytes cells transfected with scrambled, p63 and/or CD44 siRNA oligos. Whole cell extracts were immunoblotted with CK-1, p63, PARP and CD44 antibodies. GAPDH was used as loading control.

2.11 YB-1 and p63: crosstalk pathway in Melanoma

I have spent six months **(from May 13st to December 18st 2013)** of my PhD's 2nd year working at Blizard Institute - Queen Mary University of London to collaborate with Bergamaschi's team.

Recently, Bergamaschi's group showed for the first time there is the stabilization of endogenous TA and ΔN p63 isoforms in both nuclear and mitochondrial compartments of melanoma cells, in response to genotoxic stress. Moreover, depletion of p63 by RNA interference (RNAi) revealed that the expression of TA and/or ΔN p63 isoforms confers resistance to chemotherapy in melanoma cell lines and provides evidence for an oncogenic role of p63 in this tumor (*Matin*, 2013).

Malignant melanoma, a highly malignant tumor of the pigment-producing cells in the skin, is among the human cancers whose incidence has increased most rapidly in the last few decades. Cell for cell, probably no human cancer is as aggressive as melanoma. It is among a handful of cancers whose dimensions are reported in millimeters (*Chin*, 2006). Early-stage melanoma can be cured by surgical resection, but late-stage melanoma is difficult to treat with current therapies. To improve treatment for melanoma patients, large efforts have been put into the elucidation of cellular and molecular mechanisms underlying this disease. So far, the initiation and

progression of melanoma have been associated with a number of signaling pathways, including Ras/Raf/MEK/ERK signaling, WNT/β-catenin signaling, and PTEN/AKT signaling, and recently microRNAs (miRNAs) have been implicated as key regulators in these pathways (*Gray-Schopfer*, 2007; *Mueller*, 2009; *Mueller and Bosserhoff*, 2010; *Bell and Levy*, 2011). It has been also reported that YB-1 expression results upregulated in melanoma. YB-1 protein is translocated to the nucleus during melanoma progression and, in addition, that it is a critical factor in proliferation, survival, migration, invasion and chemosensitivity of this tumor (*Shittek*, 2007).
Our collaboration was aimed to explore the possibility of p63 and YB-1 cross-talk pathways, involved in melanoma development as in our SCC model system.

Among available melanoma cell lines I have choosen to perform my experiments in two metastatic cell lines, WM1158 and A375M, which express TAp63 and ΔNp63 isoforms, respectively. In addition, I have used MEL-224 cells, derived from a typical VGP melanoma tumor devoid of p63 expression.
I have detected in all melanoma cells, for the first time, a typical pattern of YB-1 including bands between 10 KDa and full length 50KDa.
MG132-treatment on melanoma cells, trasfected or not with TAp63α and ΔNp63α, reaveled that the small molecular weight YB-1 bands are partially derived from proteasome activity and their abundance and localization depends on p63 expression (Figure 19A).

FIGURE 19

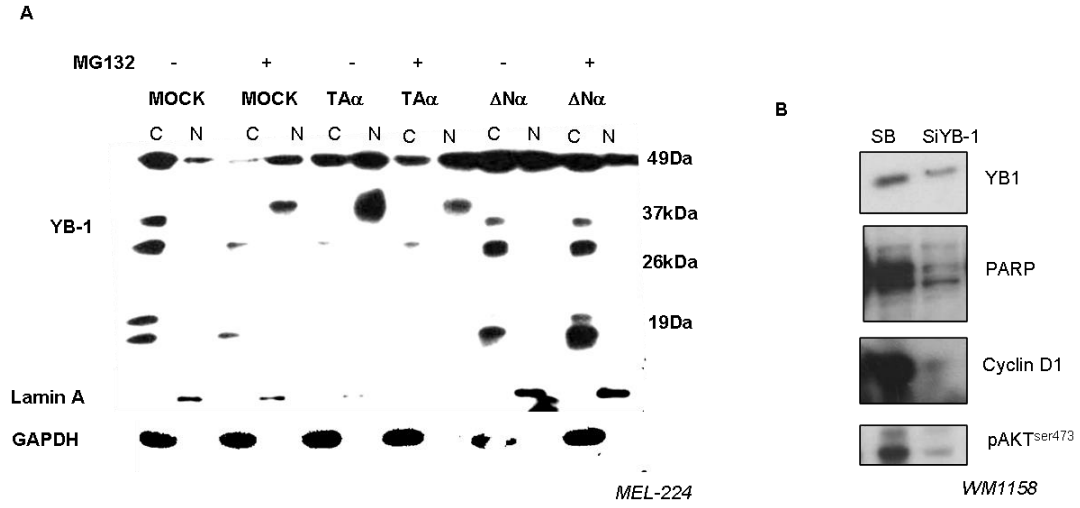

FIGURE 19. YB-1 Expression in MEL-224 and WM1158 melanoma cells. (**A**) Immunoblot analysis of MEL-224 cells transfected with scrambled plasmid or ΔNp63α/TAp63α treated or not with MG132 for six hours, after 18hrs of transfection. Cytoplasmic and nuclear fractions were immunoblotted with YB-1 antibodies. GAPDH and LaminaA were used as a loading and quality control. (**B**) WM1158 cells were transfected with scrambled or YB-1 siRNA oligos transfection. After 48 hrs of silencing whole cell extracts were immunoblotted with YB-1, PARP, Cyclin D1 and pAKT^{ser473}

Since YB-1 silencing affects keratinocyte adhesion, I have investigated the effects of YB-1 knock-down on melanoma cell lines. Interestingly, I have found that, in WM1158 cells, expressing TAp63α isoform, YB-1 depletion induces apoptosis and

cell detachment (Figure 19B). Moreover, I have observed that TAp63α isoform induces nuclear accumulation of YB-1, as shown in figure 20A and B.

FIGURE 20

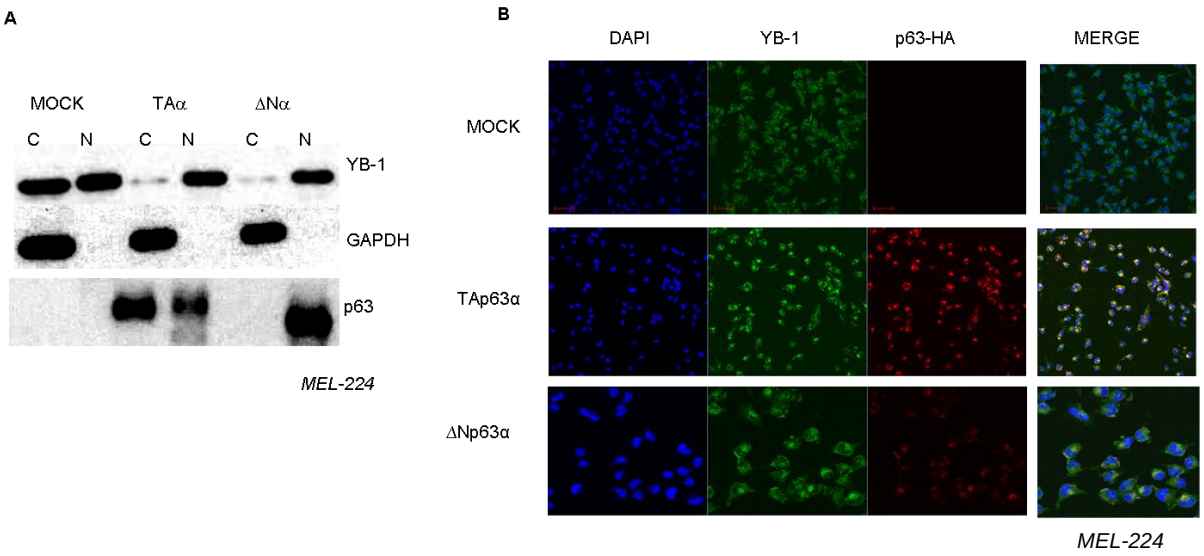

FIGURE 20. p63-dependent YB-1 localization in MEL-224 cells. (**A**) Immunoblot analysis of MEL-224 cells transfected with scrambled plasmid or ΔNp63α/TAp63α. 24 after transfection cytoplasmic and nuclear fractions were immunoblotted with YB-1 and p63 antibodies. GAPDH was used as a loading control. (**B**) Immunofluorescence assay on MEL-224 cells transfected with scrambled plasmid or ΔNp63α/TAp63α–HA tagged. At 24 hours after transfection, cells were fixed and subjected to double immunofluorescence using rabbit primary YB-1 antibody and Fitch-conjugated secondary antibodies (green). p63-HA protein was detected using mouse anti-HA and Cy3-conjugated secondary antibodies (red). Images of merge (yellow) show the co-expression of two proteins.

Our preliminary data indicate that ΔNp63α controls YB-1 protein integrity and nuclear localization both in keratinocytes, SCC cell lines and melanoma model. Moreover, I have observed that the cross-talk between p63 and YB-1 is expected to be functionally significant in proliferating keratinocytes as well as in melanoma system.

3.DISCUSSION

A significant proportion of the human population suffers from some form of skin disorder, whether it be from burn, injury or inherited skin anomalies. The ideal treatment would be to regrow skin tissue from autologous stem cells. Elucidating the molecules involved in orchestrating the production of new skin cells are important steps in devising more efficient methods to produce bio-epidermal substitutes. ΔNp63α and YB-1 are highly expressed in the proliferating basal layer of stratified epithelia of skin, breast and prostate.

During my PhD a number of evidences have been collected clearly indicating that ΔNp63α and YB-1 expression must be switched off to allow skin terminal differentiation (*di Martino,* 2015 submitted). In primary keratinocytes, transient overexpression of ΔNp63α causes skin hyperplasia and abnormal differentiation thereby predisposing to malignant transformation (*Moll*, 2004).

My work contributed to a deeper knowledge of ΔNp63α-YB-1 functional crosstalk in highly proliferative immortalized or transformed keratinocytes (SCC011/22).

First, I have validated ΔNp63α/YB-1 interaction in distinct cell contexts and demonstrated that this interaction causes accumulation of YB-1 into the nuclear compartment, thereby influencing its localization-dependent functions. In fact, YB-1 into the nucleus is expected to induce pro-proliferative genes while in the cytoplasm regulates translation.

A clear evidence of ΔNp63α/YB-1 cooperation in regulation of gene expression is shown by my experiments on the PI3KCA gene promoter. In fact, using Chromatin IP and reporter assays I have demonstrated that ΔNp63α and YB-1 are both recruited to the PIK3CA proximal promoter and transactivate PIK3CA gene promoter, thereby supporting the hypothesis that this molecular association can act as a pro-survival mechanism.

Moreover, although preliminary, in melanoma cells I have shown that a potential interaction between TAp63α and YB-1 might exist. In fact, this p63 isoform is able to accumulate YB-1 in the nucleus of MEL-224 cells, as shown by immunofluorescence and immunoblot assays.

Into the cytoplasm, YB-1 functions as a positive regulator of EMT, by enhancing Snail1 translation, which reduces cell-cell adhesion (*Evdokimova*, 2009). Accordingly, I have shown that ΔNp63α enforced expression reduces the activating binding of YB-1 to the Snail1 transcript and, remarkably, depletion of endogenous ΔNp63α in SCCs results in E-cadherin repression and increased cell motility.

Moreover, YB-1 plays, also, an important role in cytoskeleton organization by binding to F-actin and microtubules (*Uchiumi*, 2006). I have shown, by phalloidin staining, that ΔNp63α depletion in SCC cells promotes morphological changes and causes a profound cytoskeleton reorganization. Interestingly, ΔNp63α depleted cells had a polarized morphology, with more evident lamellipodia and trailing edge and exhibited mature stress fibers, suggesting a pro-migratory behavior. I can speculate that the absence of ΔNp63α can promote F-actin polymerization by YB-1, thereby inducing the formation of stress fibers.

All together, these data indicate that ΔNp63α/YB1 association into the nucleus can act as a pro-proliferative/survival mechanism and that, probably, the balance

between ΔNp63α and YB-1 protein levels could be critical for the transition to a mesenchimal-like phenotype explaining, at least in part, why ΔNp63α depletion promotes cancer cell invasion and spread. Moreover, the oncongenic potential of YB-1 itself is well-assessed, but because of its multifunctional character, its specific role remains elusive.
Given all these considerations, the last part of my work was aimed to extend our knowledge on the YB-1 and ΔNp63α functional interplay.
First, I studied the effects of YB-1 silencing on cancer cell vitality. Remarkably, I found that YB-1 depletion caused HaCaT and SCC011 cell death. Moreover, YB-1 knockdown strongly reduced ΔNp63α transcripts and protein levels, showing the existence of a reciprocal regulation between p63 and YB-1 (*Yang*, 1999). Furthermore, following YB-1 depletion I also found downregulation of CD44, the principal receptor for hyaluronate, that is also known to maintain the proliferative state of basal keratinocytes (*Tuhkanen*, 1999; *Westfall*, 2003). However, my results showed that ΔNp63α knockdown is not sufficient to trigger cell death, indicating that YB-1, in keratinocytes, plays additional p63-independent pro-survival functions.
Unexpectedly, in highly metastatic SCC022 cells, YB-1 silencing induced ΔNp63α transcription and potentiated AKT activation rather than promote cell death. This phenomenon suggest that YB-1 can act as a negative AKT regulator.
ΔNp63α induction is a consequence of AKT hyperactivation as previously described by Barbieri (*Barbieri*, 2003). But how can I explain this negative modulation of PI3K/AKT pathway by YB-1 from a molecular and mechanistic point of view?
It could be useful to remind that YB-1 interacts with AKT kinase which induces its phosphorylation (*Bader*, 2008). A possible explanation might be that YB-1/AKT interaction impairs AKT phosphorylation. Future studies on structural aspects of YB-1 and pAKT interaction might clarify this point. Moreover, this would allow us to create mutants that specifically lack this interaction to assess if it is amenable to pharmacological intervention.
Remarkably, I did not observe AKT activation in YB-1 depleted HaCaT and SCC011 cells. How can I describe the different outcomes of the cell lines in response to YB-1 silencing?
I have hypotesized the involvement of PTEN (phosphatase and tensin homolog), that functions as tumour suppressor by negatively regulating AKT signaling pathway. On the other hand, ΔNp63α is known to repress the expression of PTEN (*Leonard*, 2011).
Accordingly, in PTEN-proficient HaCaT and SCC011 cells, where YB-1 silencing caused a decrease of ΔNp63a, I observed an increase of PTEN protein level. Instead, in SCC022 cells PTEN was defective and non-responsive to YB-1 silencing.
These findings indicate that YB-1 not only inhibits AKT, but also controls PTEN levels. Moreover, the revelance of these data is also supported by interesting results of cytoplasmic PTEN modulation following YB-1 depletion in MDA-MB231 and A431 cells (data not shown). In fact, YB-1 silencing down-regulates PTEN in the cytoplasm of A431 squamous carcinoma cells, while causes its increase in MDA-MB231 breast cancer cells, suggesting that YB-1/PTEN regulation is a wide and general mechanism in the oncogenesis.

In summary, our results indicate that, being able to sustain ΔNp63α gene expression, YB-1 is part of a complex molecular network linking ΔNp63α to the PI3K/AKT/PTEN pathway and that establishment of a positive feedback loop coupling induction of

ΔNp63α expression with PI3K/AKT activation may be a relevant step in progression of squamous carcinogenesis.
An important finding of my work is the observation that ΔNp63α controls the expression of the Epidermal Growth Factor Receptor switching-on the entire EGFR/STAT3 axis. Accordingly, in normal adult epidermis, the EGFR is predominantly expressed in basal keratinocytes and signaling events elicited by it are known to affect their proliferation and migration (*Bito*, 2011). ΔNp63α therefore, represents an important molecular connection between YB-1, the PI3K/AKT and the EGFR/STAT3 signaling pathways. I can postulate that constitutive activation of PI3K/AKT, such as in PTEN-deficient cells, may likely cause persistence of ΔNp63α which can induce keratinocyte hyper-proliferation by impinging on the EGFR/STAT3 pathway. Interestingly, in physiological conditions EGF-dependent and PI3K/AKT pathways are both required for efficient skin wound re-epithelialization (*Chen*, 2014). Moreover, EGFR/STAT3 inhibition was shown to be unable to induce apoptosis (*Bito*, 2003), thereby providing a plausible explanation of why ΔNp63α silencing alone was not sufficient to induce cell death in our experimental settings.
In summary, I have presented clear evidences suggesting that YB-1 can play a role in skin carcinogenesis. However, the emerging picture is that the molecular basis of squamous cancerogenesis is quite heterogenous. Therefore, a careful evaluation of the signaling pathways activated in each particular tumour is mandatory.
Association of YB1-targeting with drugs that inhibits the PI3K and/or EGFR pathway could be valuable strategies to treat squamous carcinoma. *In vivo* experiments will help to clarify this relevant point.

Finally, small YB-1 derived peptides were recently isolated from human body fluids (urine, plasma). Such peptides have been shown to be produced and secreted by mesangial and tumour cells (*Frye*, 2009); in addition, they have pro-proliferative and pro-inflammatory functions.
During my work, I have observed in melanoma cells small YB-1 derived peptides whose abundance is regulated by p63. I can hypothesize that YB-1 secretion pathway is a more general mechanism involving a wide number of tumour cells. Further experiments are needed to shed light on this molecular mechanism.
The most relevant aspect of this finding is its potential application as prognostic and diagnostic marker of cancer progression and potential therapeutic target.

SECOND PART

4.INTRODUCTION

Thanks to the collaboration with Prof. Piera Quesada's team I had the opportunity to perform experiments aimed to investigate the role of p53 family members in the response of cancer cells to Topoisomerase I and poly(ADP-ribose)polymerase (PARP1) inhibitors. Prof. Piera Quesada, has a long-term experience on poly(ADP-ribose)polymerase enzymes and the role of PARP1 in the DNA damage signaling network.

4.1 Poly(ADP-ribose) polymerase (PARP) - 1

PARP-1 is the founding and the most fully studied members of a large family of 18 multifunctional enzymes, encoded by different genes and displaying a conserved catalytic domain, that catalyze the poly(ADP-ribosyl)ation (PARylation) of target proteins.
PARylation is an immediate DNA-damage-dependent post-translational modification of nuclear proteins, that contributes to the survival of injured cells (*Burkle*, 2013).

PARP-1 has four important domains:
1) a 46-kDa N-terminal DNA binding domain (DBD), containing 2 zinc finger motifs, and responsible for the interactions with DNA breaks;
2) a 54-kDa catalytic domain (CD) at the carboxyl terminus that polymerizes linear or branched poly-ADP ribose units;
3) a caspase-cleaved domain, containing a bipartite nuclear localization signal (NLS) and a caspase-3 cleavage site;
4) a 22-kDa central auto-modification domain, containing a BRCT (BRCA1 carboxy-terminal) motif, involved in protein-protein interactions, which promotes the recruitment of DNA repair enzymes to the site of DNA damage (*de Lartigue*, 2013).
PARP-1 is immediately stimulated by DNA strand breaks and it sequentially transfers ADP-ribose units from β-NAD^+ to various nuclear proteins acceptors, or itself in an automodification reaction, thereby synthesizing PAR, a linear or multi-branched polymer of ADP ribose (*Davar*, 2012).

4.2 Role of PARP in DNA Repair

DNA can be damaged as a result of constant barrage of environmental insults, toxic products of metabolism and erroneous DNA replication. These alterations can be

divided into: 1) base modifications; 2) single strand breaks (SSB); 3) double strand breaks (DSB); and 4) intrastrand or interstrand cross-links. Several DNA repair mechanisms have evolved to repair these lesions and maintain genomic integrity. Given the large array of potential lesions and the importance of high-fidelity repair, DNA repair mechanisms are generally complex, highly redundant and conserved across phylogenetic classes (*O'Brien*, 2006).
DNA repair mechanisms include: 1) base excision repair (BER); 2) nucleotide excision repair (NER); 3) mismatch repair (MMR); 4) direct repair mechanisms; 5) homologous recombination (HR) and non-homologous end-joining (NHEJ) (*Jackson*, 2009).
PARP-1 enzyme has a critical role in the BER pathway, the predominant mechanism of SSB repair, in fact it binds to single-strand breaks (SSBs) in DNA, modifies proteins in the proximity and, ultimately, leads to the recruitment of DNA repair proteins to the sites of the damage. Actually, PARP-1 acts as a "molecular sensor" to identify DNA SSBs; it is recruited and activated by SSBs as homodimer in a fast reaction, which is amplified from 10 to 500-fold with formation of PAR-polymers within 15 to 30 seconds. Upon binding to a damaged strand *via* its zinc finger DNA-binding domain, PARP-1 undergoes a conformational change, inducing the catalytic monomer/subunit to transfer ADP-ribose moieties from βNAD+ (Nicotinamide-Adenine-Dinucleotide) substrate to the auto-modification domain of acceptor monomer/subunit (*Davar*, 2012).
The lengthening PAR chain builds up a large negatively charged structure at the SSB which recruits other DNA repairing enzymes. These include DNA ligase III (LigIII), DNA polymerase beta (polβ), and scaffolding proteins such as x-ray cross complementing gene 1 (XRCC1), that collectively form the base excision repair (BER) multi-protein complex.
Furthermore, PARylated PARP-1 can modulate DNA-topoisomerase 1 by not covalent but specific interaction of PAR with some TOP I sites, resulting in DNA cleavage inhibition and stimulation of the re-ligation reaction (*see also later*).
As it dissociates from DNA, PARylated PARP-1 becomes a target of the poly(ADPR) glycohydrolase enzyme that catalyze the degradation of PAR polymers, thereby assuring the restoration of its native and active form (*Burkle*, 2013).

In response to DNA damage cell cycle checkpoint activation and growth arrest rely on the ATM/ATR kinases and their downstream targets, like p53 (*Nguyen*, 2011). It has been shown that p53 can be a target of PARP-1, as well as other transcription factors (i.e. p21) which binds PARP-1 during base excision repair.
Moreover, PARP-1 is one of several known cellular substrates of caspases and its cleavage by caspases is considered to be a hallmark of apoptosis (*Daniel*, 2010).
The cleavage of PARP-1 by caspases 3 and/or 7 results in the formation of 2 specific fragments: a 89-kDa catalytic fragment and a 24-kDa DBD (*Hunter*, 2011). The 89-kDa fragment, containing the auto-modification domain and the catalytic domain of the enzyme, have a greatly reduced DNA binding capacity.
The 24-kDa cleaved fragment with 2 zinc-finger motifs is retained in the nucleus, irreversibly bound to nicked DNA, where it acts as a trans-dominant inhibitor of active PARP-1. Importantly, irreversible binding of the 24-kDa PARP-1 fragment to DNA strand breaks inhibits DNA repair enzymes (including PARP-1) and attenuates DNA repair (also preserving the cellular ATP pools) (*Ferraris*, 2010).
Apoptosis, the process of programmed cell death, is an essential part of the maintenance of cellular homeostasis and survival of multi-cellular organisms.

Physiological apoptosis controls cell numbers, tissue and organ morphology and patterning, and removes injured or mutated cells (*Audeh*, 2010). Dysregulated apoptosis results in elevated or decreased cell death often leading to neurodegenerative disorders, cancer and other hyper-proliferative disorders (*Ledermann*, 2011).

4.3 PARP Inhibitors

PARP-1 knockout mice are viable, but they appear to be highly sensitive to genomic instability caused by DNA-alkylating agents or γ-irradiation (*Sugo*, 2007). This is not surprising given the multiple redundant DNA repair mechanisms present in eukaryotic cells; unrepaired SSBs can possibly be converted into DSBs at replication forks, allowing subsequent repair by unaffected HR mechanisms. However, if cells have a deficient HR repair mechanism, PARP-1 inhibition can be expected to result in unsalvageable DNA damage and consequent lethality (*Davar*, 2012). Bryant *et al*. showed that BRCA2-deficient cells - in which the homologous recombination mechanism is defective - were exquisitely sensitive to PARP-1 inhibition (*Bryant*, 2005). Subsequently, Farmer and colleagues demonstrated that PARP-1 inhibition in embryonic stem cells, lacking wild-type BRCA1 and BRCA2, resulted in early cell death (*Farmer*, 2005).
Given these considerations, an anti-tumor strategy based on this approach would specifically target cells with the primary defect and spare healthy cells. Hence, it stands to reason that PARP inhibition will be similarly effective in cells in which HR is deficient or impaired – i.e. cells that share a “BRCA phenotype” or “BRCAness” (*Davar*, 2012).

PARP inhibitors block the activity of the PARP enzymes by mimicking the nicotinamide moiety of nicotinamide adenine dinucleotide (NAD) and binding to the PARP catalytic site, which either directly blocks PARP enzymatic activity or causes PARP to accumulate on DNA (known as *PARP trapping*).

PARP inhibitors are the poster child for the therapeutic paradigm of synthetic lethality in cancer drug development, the theory that two defects, which alone are benign in cancer cells, can be lethal when combined. If SSBs are left unrepaired, they have the potential to develop into lethal double-strand breaks (DSBs), which would lead to cell death. Suppressing PARP activity prevents SSB repair via the BER pathway, but other DNA repair pathways such as HR and NHEJ simply take over. However, if PARP inhibitors are used against tumors in which there is already a DNA repair defect, the combination drives synthetic lethality (*Davar*, 2012).
There are two routes to synthetic lethality with PARP inhibitors. They can be used as monotherapy in patients with known mutations in DNA repair proteins, the most renowned being the breast cancer type 1 and 2 susceptibility proteins (BRCA1 and BRCA2), or they can be used as combination therapy with DNA-damaging chemotherapeutic agents or radiotherapy.

In particular, PARP inhibitors increase the cytotoxic effects of some chemotherapeutic agents as camptothecin (CPT), the prototype of TOP1 (DNA Topoisomerase 1) inhibitors, or its derivative Topotecan (TPT).
Top1 enzymes are the only topoisomerases that form a covalent link with the 3′-end of the broken DNA, while generating a 5′-hydroxyl end at the other end of the break. Another unique feature of the Top1 enzymes is their DNA relaxation mechanism by "controlled rotation" rather than by "strand passage". In other words, Top1 enzymes relax DNA by letting the 5′-hydroxyl end swivel around the intact strand. This mode of catalysis involves an intermediate known as the cleavage complex, which comprises the Topoisomerase enzyme attached to the cleaved DNA by a covalent phosphotyrosyl bond (*Alagoz*, 2012).
Camptothecin (CPT), an alkaloid plant identified from the Camptotheca acuminate, and its water–soluble derivative TPT act as TOP 1 inhibitors. In fact, they are able to stabilize the cleavage complex in the abortive complex and abolish the DNA relegation activity of the enzyme, generating an accumulation of SSBs to which the protein is covalently linked. Double strand breaks arise when replication forks collide with the SSBs and run off. The cytotoxic mechanism of CPT/TPT is largely S-phase-dependent and is usually repaired by the HR pathway (*Davar*, 2012).
Quesada and collaborators have demonstrated that PARylated PARP-1 counteract CPT through non covalent but specific interaction of PAR with some TOP 1 sites, which results in inhibition of DNA cleavage and stimulation of the relegation reaction (*Malanga*, 2004). Moreover, they have shown that PJ34, a PARP inhibitor, can positively or negatively modulate p53 and its target p21WAF depending on the cell genetic background or DNA damage stimulus (i.e. cisplatin or TPT) (*Cimmino*, 2007; *Gambi*, 2008; *D'Onofrio*, 2011).
Remarkably, regulating p21WAF expression is one model whereby PARP inhibitors, following the activation of different checkpoint pathways, can cause cell cycle arrest. In addition, it has recently been reported that in breast carcinoma MCF7 cells, PJ34 causes a p21WAF-dependent mitotic arrest and neither PARP-1 nor p53 is required for this mechanism (*Madison*, 2011). Furthermore, in triple negative breast cancer cell lines, PJ34 synergizes with cisplatin by reducing the levels of ΔNp63α with a concomitant increase of p21WAF (*Hastak*, 2010).

In this scenario, chemotherapy protocols based on PARP inhibitors can be useful to restore apoptotic cell death and they can be used as adjuvant of TOP I inhibitors.

The aim of my work was to investigate the effects of PJ34 used as a single agent or in association with CPT or TPT in the DNA damage response of mammary breast cancer cells (MCF7^{p53wt} and MDA-MB231^{p53mut}) and squamous carcinoma cells (SCC022 ^{p53null}). I was particular interested at the involvement of p63 in the sensitivity to these agents. The other relevant point was to look at the expression levels of pro-arrest or proapoptotic proteins implicated in the p53/p63-dependent pathway (i.e. p21WAF, MDM2, BAX).

5.RESULTS

Prof. Quesada and collaborators have demonstrated that p53 proficient MCF7 cells show high sensitivity to PJ34 in combination with 1μM CPT or 5μM TPT. p53-null MDA-MB231 and SCC022 squamous carcinoma cells, instead, were more resistant. In MCF7 cells, TPT, known to be S-phase specific, caused a G2/M cell cycle arrest when used at lower concentration (1 μM). In addition, the TPT-dependent G2/M cell cycle arrest was enhanced by TPT±PJ34 combined treatment and resulted in a remarkable increase of cells with sub-diploid DNA, confirming a synergic cytotoxic effect of TOP I and PARP-1 inhibitors. Given the similarity between p53 and p63 it was our interest to look at the expression of p63 protein isoforms and its down-stream target genes upon combined treatment with TOP I and PARP-1 inhibitors.

5.1 Involvement of p63 in the cell response to TPT ± PJ34 treatment

I first analyzed the response of MCF7 cells to TPT ± PJ34 treatment by looking at the expression level of p53 and p63 by western blot analysis. I also monitored the expression of some of p53/p63 target genes, such as p21WAF and cyclin B1, known to be involved in the regulation of the cell cycle.
I found that compared to TPT alone, combined treatment up-regulated p53 expression more efficiently. On the other hand, I observed down-regulation of MDM2, the most important p53 negative regulator (Figure 21A).

FIGURE 21

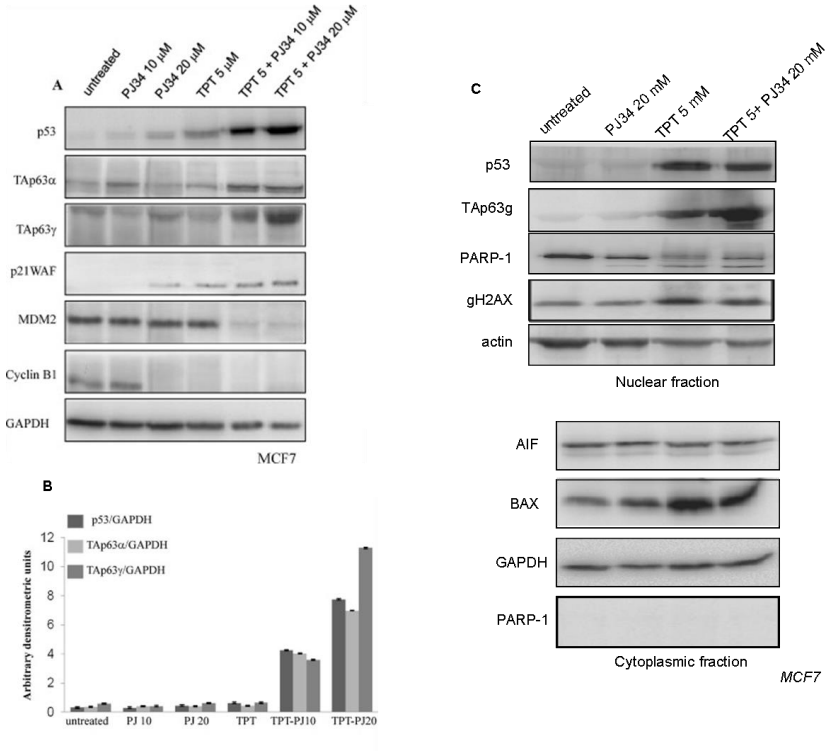

FIGURE 21 PJ±PJ34 treatment in MCF7 cells. (**A**) Western blot analysis of p53, p63, p21WAF and cyclin B1 expression in MCF7 cells untreated or 48 hrs treated with the indicated drugs. GAPDH was used as loading control. (**B**) p53 and TAp63γ band intensities were quantified by densitometric scanning. Data expressed as Arbitrary Densitometric Units (ADU) were normalized to the internal control GAPDH. (**C**) Immunodetection of p53 and γ-H2AX or AIF and Bcl2 respectively in the nuclear or postnuclear fraction of MCF7 cells treated with CPT and PJ34 alone and in combination.

Interestingly, p63 immunoreactive bands, corresponding to the molecular weight of the pro-apoptotic TAp63α and γ isoforms was also up-regulated by S.E.combined treatments.
Densitometric analysis revealed a 19 to 20 fold induction of both p53 and p63 protein expression after TPT ± PJ34 20μM treatment (Figure 21B). The CDK inhibitors p21WAF was also increased while cyclin B1 level was reduced. These data were in line with the G2/M block previously observed by cytofluorimetric analyses (data not shown).
To verify the subcellular localization of induced p53 and TAp63 proteins, I have fractionated nuclear and cytoplasmic extracts of MCF7 cells to perform immunoblot analysis. As shown in figure 21 C, following TPT-PJ34 20μM treatment p53 and TAp63γ accumulated in the nucleus were they functions as transcription factors. Nuclear γH2AX expression and PARP-1 specific cleavage were also monitored as markers of dsDNA damage and caspase-dependent apoptosis, respectively (upper panel).
Furthermore, the expression level of the pro-apoptotic BAX protein, whose gene is transcriptionally activated by p53 and TAp63, increased in the cytoplasmic fraction by either TPT alone or TPT-PJ34 combined treatment. The level of the mitochondrial apoptosis inducing factor AIF was unaffected (Figure 21C lower panel).

5.2 Analysis of the effects of TPT+/-PJ34 treatments on SCC022 squamous carcinoma cells.

SCC022 carcinoma cells are devoid of p53, but express high level of the anti-apoptotic ΔNp63α isoform. Interestingly, ΔNp63α was dramatically reduced by CPT/TPT treatment with or without PJ34. Immunoblot analysis also showed a concomitant reduction of Cyclin B1 suggesting that cells were undergoing a G2/M cell cycle arrest. Importantly, by western blot I was unable to detect p63 isoforms other than ΔNp63α both in untreated and TPT ± PJ34 treated SCC022 cells, although the 4A4 antibody used was able to detect all p63 isoforms (data not shown).
However, ΔNp63α depletion following CPT/TPT ± PJ34 treatments was not sufficient to induce apoptosis suggesting that p53 or TAp63 expression are necessary to induce the apoptotic response (Figure 22 A). To prove this hypothesis we transfected p53 and TAp63 in SCC022 cells. After 24 hours the cells were incubated with the drugs for further 24 hours.
Immunoblot analysis confirmed that SCC022 cells respond to TPT+PJ34 treatment by reducing ΔNp63α protein level. However, caspase-dependent cleavage of PARP-1 was observed only in p53 or TAp63 transfected cells (Figure 22B)**.**
By RT-PCR analysis I measured the level of ΔNp63α mRNA in untreated (CTR) and TPT+PJ34 treated SCC022 cells and I found that it was comparable thus suggesting that ΔNp63α down-regulation was exclusively at protein level (Figure 22C).
In MDA-MB231 cells, no p63 immunoreactive bands were seen in all experimental conditions (data not shown), thereby excluding a possible role for p63 in TPT ± PJ34 – induced cytotoxicity in this cellular context.

FIGURE 22

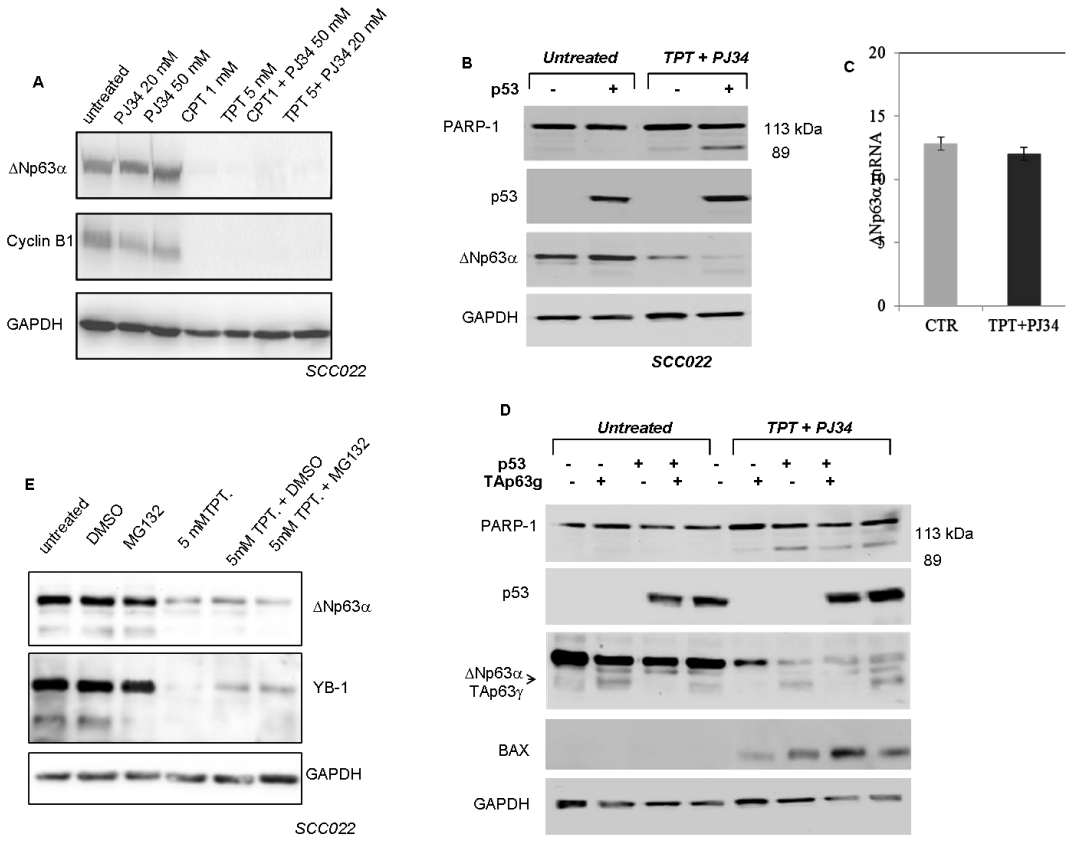

FIGURE 22. Analyses of the effects of TPT+PJ34 treatment in SCC022p53null cells p53+/-TAp63γ transfected. (**A**) Western blot analysis of p63 and Cyclin B1 expression in MCF7 cells untreated or 48 hrs treated with the indicated drugs. GAPDH was used as loading control. (**B**) Western blot analysis of p63, PARP-1 and p53 expression in SCC022 cells p53+/- transfected**.** (**C**) Analysis by RT-PCR of mRNA levels of ΔNp63α in untreated and 24 hrs treated cells with the indicated drugs. (**D**) Immunodetection with anti-PARP-1, anti-p53, anti-panp63, anti-BAX antibodies. GAPDH was used as loading control. (**E**) Immunoblot on SCC022 extract treated with TPT and MG132 using YB-1 and p63 antibodies. GAPDH was used as loading control.

Figure 22C and D show the appearance of the PARP-1 89 KDa proteolytic fragment (Figure 22C and D), in p53 or TAp63γ expressing cells. Moreover, endogenous ΔNp63α protein was further reduced after TPT+PJ34 treatment (Figure 22D). Immunoblot analysis with a pan-p63 antibody was used to reveal both endogenous ΔNp63α and transfected TAp63γ proteins (Figure 22D).

These results indicates that reduction of ΔNp63α, induced by TPT+PJ34 in SCC022 cells, *per se* is not sufficient to induce apoptosis, but it seems to cooperate with exogenous p53 or TAp63γ in the restoration of apoptosis upon TPT+PJ34 treatment.

To test a possible involvement of the ubiquitin/proteasome pathway in ΔNp63α degradation we repeated the experiment in presence of the proteasome inhibitor MG132. As shown in Figure 22E MG132 treatment did not rescue the level of ΔNp63α protein. Based on this result we can speculate that ΔNp63α degradation upon TPT+PJ34 treatment might dependent on caspase activity. Further experiments with caspase-specific inhibitors can clarify this point.

5.3 Analysis of the effects of TPT+/-PJ34 treatments on p53 post-translational modifications.

Activation of p53 transcriptional function by genotoxic stimuli imposes a variety of p53 posttranslational modifications; one of the best characterized is phosphorylation at Serine 15 by ATM (Dumaz, 1999). We analyzed the effect of TPT alone and in combination with PJ34 on p53 protein phosphorylation by using a phospho-specific antibody that recognizes ^{15ser}p-p53 (Figure 23A). In MCF7 cells, after 6 hours of treatment with TPT+/-PJ34, the steady state level of endogenous p53 protein increased along with its phosphorylated form at serine 15. Densitometric analyses indicated a 10 to 12 fold increase of p53 amount in TPT and TPT+PJ34 samples starting from 6 hours of treatment (Figure 23B). Remarkably, immunoblot analysis showed that stabilized and phosphorylated ^{ser15}p53 was located in the nucleus where it can play its transcriptional functions (Figure 23C and D).

FIGURE 23

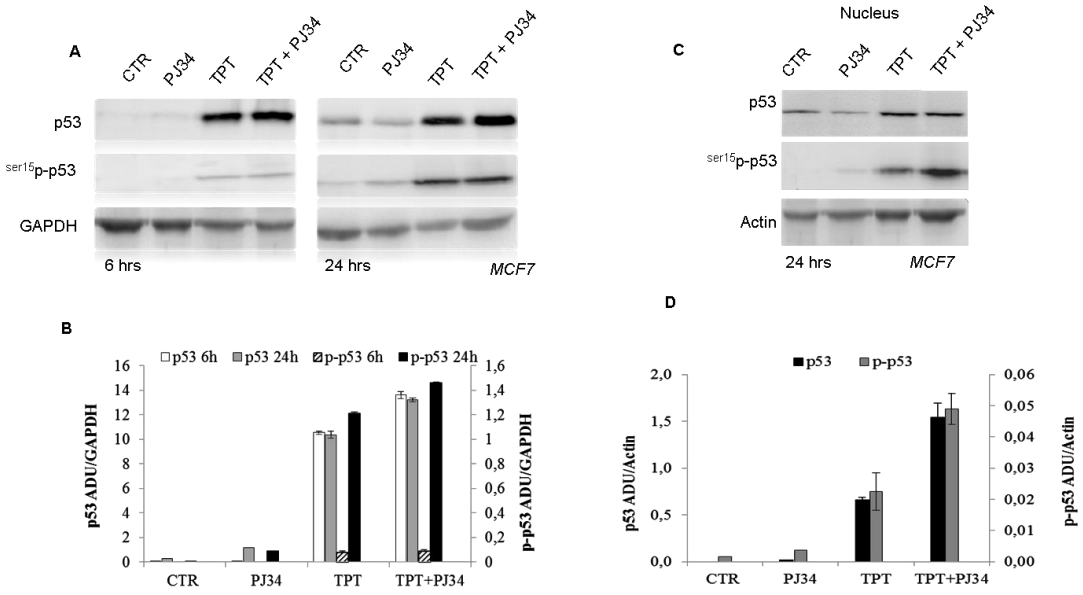

FIGURE 23. Analyses of TPT+/-PJ34 dependent p53 phosphorylation in MCF7 cells. (**A**) Western blot analysis of MCF7 cells and (**B**) isolated nuclei untreated or 6 and 24 hrs treated with the indicated drugs. Immunodetection of ser15-p-p53 and p53 band intensities were quantified by densitometric scanning (**C**) (**D**). Data are the mean ± S.E.M. of three independent experiments on three biological samples, expressed as Arbitrary Densitometric Units (ADU) and normalized to internal controls GAPDH and Actin.

5.4 Analysis of the effects of TPT+/-PJ34 treatments on mRNA levels of p21WAF and BAX genes.

Next, using qRT-PCR, we quantified the level of p21 and BAX transcript, upon treatment of MCF7 cells with TPT+/-PJ34 for 6 or 24 hours. p21 and BAX are activated by p53 upon DNA damage. These experiments were performed on cells that showed comparable levels of p53 and ser15p-p53 protein (Figure 23). Total RNA was purified from cells treated with the indicated drugs. RNA was subjected to qRT-

PCR assays to quantify p21WAF and BAX mRNA levels. As shown in Figure 24A, we found a 4.5 fold increase in p21WAF mRNA level in cells subjected to TPT treatment that was strongly reduced by PJ34 addition. Concerning BAX we found only slight differences suggesting a PJ34-dependent increase of BAX mRNA after 24 hours of treatment (Figure 24B).

FIGURE 24

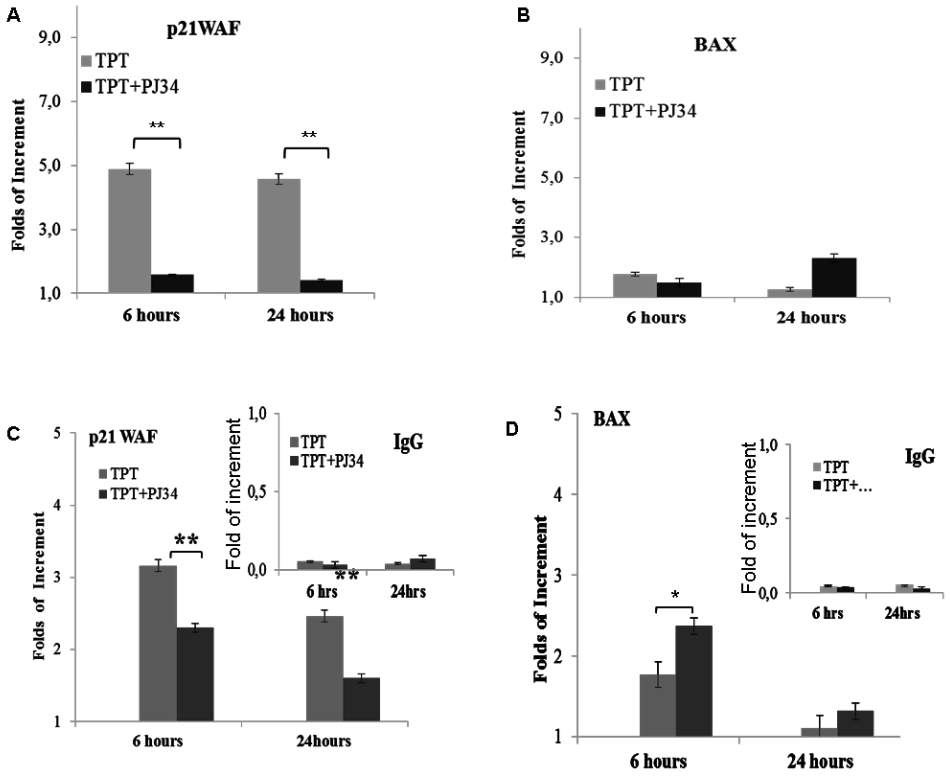

Figure 24. Analyses of TPT+/-PJ34 dependent expression of p21WAF and BAX genes. (**A**)(**B**) Real-time-PCR analysis of mRNA levels of p21WAFand BAX genes in MCF7 cells 6-24 hours treated with the indicated drugs. Data normalized respect to 18S are reported as increment's fold of controls and represent the mean ± S.E.M. of three independent experiments on three biological samples. Unpaired Student's *t*-test was conducted to determine whether mRNA level was higher in cells induced with TPT compared with TPT+PJ34 at the same time points. **P <0.01.
(**C**)(**D**) ChIP experiments were performed in MCF7 cells 6-24 hours treated with the indicated drugs with p53 or control immunoglobulin G (IgG) antibodies and quantified by PCR on p21WAF or BAX promoter. Data normalized respect to control samples are reported as increment's fold and represent the mean ± S.E.M. of three independent experiments on three biological samples. Unpaired Student's *t*-test was conducted to determine whether promoter occupancy was higher in cells treated with TPT compared with TPT+PJ34 at the same time points. *P <0.05 and **P <0.01.

5.5 Analysis of the effects of TPT+/-PJ34 treatments on p53 binding to promoters of p21WAF and BAX genes.

Finally, we used the Chromatin Immunoprecipitation (ChIP) to measure occupancy of p21WAF and BAX gene promoters by p53 protein, in cells treated with TPT or TPT+PJ34. Since it was previously shown that standard ChIP is flawed by PAR that

may cause changes in promoter-occupancy dependent on artificial formation of polymers (*Beneke*, 2015), we modified the standard protocol, as described in Materials and Methods, to prevent artificial polymer synthesis. Interestingly, according to the observed increase of p21WAF transcript (Figure 24A), p53 occupancy of p21WAF promoter was strongly increased in TPT treated cells compared to control cells and significantly reduced by addition of PJ34 (Figure 24C). Occupancy of BAX promoter by p53, instead, was significantly increased by TPT+PJ34 combined treatment after 6 hours of treatment, while at 24 hours of treatment we could not detect significant changes (Figure 24D).

6.DISCUSSION

We reported that TPT+PJ34 treatment in MCF7 cells causes a remarkably increase of TAp63 α and γ protein levels. In particular, TAp63γ is a potent apoptosis inducer and like p53 accumulates in the nucleus, where it can functionally interact with p53 in the control of transcription. My work describe the response of p53 proficient MCF7 cells to TOP I or TOP I and PARP-1 inhibitors. Such treatment increases p53 level and its phosphorylation status at serine 15. Transcriptionally activated p53 can induce p53-dependent transcription leading to increase of p21WAF and BAX transcript and protein levels.
In fact, in p53 proficient cells such as MCF7, as a consequence of TPT-dependent DNA damage, the pro-arrest p21WAF protein is rapidly up-regulated. Indeed, both p53 binding to p21WAF promoter and p21WAF mRNA appeared to be enhanced after 6 hours of TPT treatment. Concomitant PARP-1 auto-modification was indicative of a DNA repair attempt.
Under more severe DNA damage conditions, the p53 binding at the p21WAF promoter was reduced while occupancy of BAX promoter was enhanced. However, the increase of BAX transcript was delayed and the protein level was clearly detectable only after 24 hours. Under this condition, PARP-1 undergoes caspase dependent cleavage.
These observations underline the role of PAR and PARP-1 in the differential recruitment of p53 on its target promoters upon DNA damage. Indeed, while TPT treatment induces p53 recruitment on p21/WAF gene promoter with its consequent up-regulation, TPT+PJ34 treatment acts as a switch in the cell fate decision by inducing the pro-apoptotic BAX gene expression. A selective binding and control of pro-arrest or pro-apoptotic gene promoters by p53 occurring under specific stimuli, may likely reflect the severity of DNA damage.

Finally, my results point to a role for p63 in the cell response to treatment with TOP I and PARP-1 inhibitors. In, MCF7^{p53WT} cells the endogenously expressed TAp63γ isoform, which closely mimics p53, is up-regulated upon TPT+PJ34 treatment. Moreover, we found that transfected TAp63γ is sufficient to trigger caspase-dependent apoptosis in apoptosis-resistant SCC022 cells by inducing BAX expression and degradation of the endogenous anti-apoptotic ΔNp63α protein.
The restoration of apoptosis is considered a chemotherapic strategy that can be based on PARP-1 and p53 joint tumor suppressor functions. Our results indicate that modulation of other components of the p53 family (i.e. TAp63γ and/or ΔNp63α) can be involved and significantly contribute to the cell response to DNA damage stimuli thus adding further complexity to this phenomenon (*Costanzo*, 2014).
Our studies highlighting the different outcome (i.e cell cycle arrest *vs* apoptosis) of PARP-1 activation/inhibition and give right of the use of PARP inhibitor as chemotherapic adjuvant and/or in monotherapy also in TAp63/ΔNp63α proficient cancer cells .
Finally, even if preliminary, concomitant YB-1 and ΔNp63α down-regulation in TPT treated SCC022 cells suggest a new potential approach to sensitize these cancer cells to chemotherapy. Further experiments are needed to gain insight into this mechanism.

7.MATERIALS AND METHODS

Plasmids - *PIK3CA* promoter luciferase plasmid was provided by Dr Arezoo Astanehe (Research Institute for Children's and Women's Health, Vancouver, British Columbia, Canada).
The 1.1 Kb EGFR promoter luciferase plasmid was provided by Dr. A.C. Johnson (US National Cancer Institute, Massachusetts, USA). The cDNA encoding human ΔNp63α and ΔNp63α F518L were previously described (*Lo Iacono*, 2006).

Cell lines and transfection – Squamous carcinoma cells (SCC011 and SCC022) were provided by Dr. C. Missero. These cell lines were maintained in RPMI supplemented with 10% fetal bovine serum at 37°C and 5% CO_2. A431 and H1299 cells were obtained from ATCC and maintained in DMEM supplemented with 10% fetal bovine serum at 37°C and 5% CO_2.
HaCaT, MCF7 and MDA-MB231 cells were purchased from Cell Line Service (CLS, Germany) and cultured at 37°C and 5% CO_2.
MEL-224 and WM1158 melanoma cells were provided by Dr. D. Bergamaschi.
HaCaT, MCF7, MEL-224 and WM1158 cells were maintained in DMEM supplemented with 10% FBS. MDA-MB231 cells were maintained in DMEM supplemented with 5% FBS.

Lipofections were performed with Lipofectammine 2000 (Life Technologies, CA, USA), according to the manufacturer's recommendations.
YB1 transient silencing was carried out with IBONI YB-1siRNA pool (RIBOXX GmbH, Germany) and RNAiMAX reagent (Life Technologies, CA, USA), according to the manufacturer's recommendations. Briefly, cells were seeded at 60% confluence (1.5×10^6) in 100-mm dishes and transiently silenced with IBONI YB1-siRNA at 20 nM final concentration.
YB-1 guide sequences:
UUUAUCUUCUUCAUUGCCGCCCCC;
UUAUUCUUCUUAUGGCAGCCCCC;
UUCAACAACAUCAAACUCCCCC;
UCAUAUUUCUUCUUGUUGGCCCCC.

ΔNp63α transient silencing was carried out with IBONI p63-siRNA pool (RIBOXX GmbH, Germany) at 20 nM final concentration and RNAiMAX reagent (Life Technologies, CA, USA).
p63 guide sequences:
UUAAACAAUACUCAAUGCCCCC;
UUAACAUUCAAUAUCCCACCCCC;
AUCAAUAACACGCUCACCCCC;
AUGAUUCCUAUUUACCCUGCCCCC.

"All Star Negative Control siRNA", provided by Quiagen (Hilden, Germany), was used as negative control.

Antibodies and chemical reagents - p63 (4A4) , anti-actin (1-19), anti-cytokeratin 1 (4D12B3), anti-GAPDH (6C5), were from Santa Cruz (Biotechnology Inc.), PARP,

EGFR, STAT3 AKT, pAKT (Ser473) and rabbit polyclonal YB1 antibody (Ab12148) were from Cell Signaling Technology (Beverly, Massachussets). Mouse monoclonal E-CADHERIN (ab1416) and SNAIL1 antibodies were from Abcam (Cambridge, UK). Mouse monoclonal N-CADHERIN (610921) was from BD Transduction Laboratories. Cy3-conjugated anti-mouse IgG and Cy5-conjugated anti-rabbit IgG were from Jackson (ImmunoResearch Laboratory, Inc, Pennsylvania). Antiphospho-p53(ser15) (9284), anti-BAX (D2E11) and anti-CD44 rabbit polyclonal antibodies were from Cell Signaling (Invitrogen, Milano, Italy). Anti-MDM2 (Ab-2) mouse monoclonal antibody was from Oncogene Research Products (Boston, USA).

Proteasome inhibitor MG132 were purchased from Sigma-Aldrich (St Louis, MO) and used at 10 μM final concentration in DMSO (Sigma-Aldrich, St Louis, MO). LY294002 was purchased from Calbiochem (CA, USA) and used at 50 μM final concentration in DMSO. TPT was from Glaxo Smith-Kline (Verona, Italy) and PJ34 [N-(6-oxo-5,6,-dihydrophenanthridin-2-
yl)-(N,N-dimethylamino) Acetamide] from Alexis Biochemicals (Vinci-Biochem, Firenze, Italy).
The cocktail of protease inhibitors was from ROCHE-Diagnostic (Milano, Italy).

Chromatin immunoprecipitation (ChIP) assay - ChIP was performed with chromatin from human MDA-MB-231 cells transfected with ΔNp63γ, ΔNp63α and/or FlagYB1. Chromatin samples were subjected to pre-clearing with 80 µl of Salmon Sperm DNA-satured agarose A beads, 2 hrs at 4°C with rotation. The immunoprecipitation step was obtained with YB-1 antibodies (ab12148).
Real Time PCR was performed with the 7500 Applied Biosystems apparatus and Syber Green MasterMix (Applied Biosystems) using the following oligonucleotides:
PIK3CA-Forw CCCCCGAACTAATCTCGTTT
PIK3CA-Rev TGAGGGTGTTGTGTCATCCT
Sequential Chromatin Immunoprecipitation was performed with chromatin from SCC011.
Chromatin samples were subjected to pre-clearing with 80 µl of Salmon Sperm DNA-satured agarose A beads, 2 hrs at 4°C with rotation. The first immunoprecipitation step was obtained with p63 antibodies (4A4). After several washes immunocomplexes were extracted from beads with 100 µl of TE-SDS 2% . The second immunoprecipitation step was obtained with YB1 (Ab12148) antibodies after a 30 fold dilution in DB buffer. (Tris-HCl 50 mM, EDTA 5 mM, NaCl 200 mM, NP40 0.5%, 15 mM DTT). Samples were incubated overnight at 4°C with rotation. Immunocomplexes were extracted from beads as above described. Immunoprecipitated protein-DNA complexes were subjected to reverse cross-linking and Proteinase K treatment. DNA was purified by phenol/chloroform extraction and resuspended in 40 µl of TE. 2 µl were used for PCR reaction performed with the following primers:
PIK3CA promoter-For
ACAAACCCCTGGAATGTGAG
PI3KCA promoter-Rev
TGGAAAAGCGTAGGAGCAGT

Coimmunoprecipitation - To detect p63/YB-1 interaction in SCC011 cells, 5.0 $\times 10^5$ cells were plated in 60 mm dishes. For coimmuprecipitations, whole cell extracts, precleared with 30 µl of protein A-agarose (50% slurry; Roche, Manheim, Germany),

were incubated overnight at 4°C with anti-YB-1(3 µg) or α-rabbit IgG (3 µg). The reciprocal experiment was performed with anti-p63 (2 µg) or α-mouse IgG.

Luciferase reporter assay - MDA-MB-231 cells were cotransfected with ΔNp63α, *PIK3CA* luc-promoter/EGFR-luc promoter and pRL-TK. YB-1 gene silencing was carried out 24 hrs before plasmid transfection. At 24h after transfection, cells were harvested in 1x PLB buffer (Promega) and luciferase activity was measured using Dual Luciferase Reporter system (Promega) using pRL-TK activity as internal control. FireFly-derived luciferase activity was normalized for transfection efficiency. Successful transfection of p63 and silencing of YB-1 was confirmed by immunoblotting.

RNA Immunoprecipitation - 1 x 10^6 MDA-MB-231 cells were seeded in 100mm plates and transfected with pcDNA3.1 or ΔNp63α expression plasmids. 24h after transfection, cells were fixed with 1% formaldehyde for 10 min and washed twice in ice-cold PBS. Cell extracts were prepared in RNA-immunoprecipitation buffer (0.1% SDS, 1% Triton, 1mM EDTA, 10mM Tris pH 7.5, 0.5mM EGTA, 150mM NaCL) supplemented with complete protease inhibitor mixture (Sigma Chemical Co., St. Louis, MO, USA) and sonication was carried out with BANDELINE SONOPULSE HD2200 instrument under following conditions: 8 pulses of 4 sec at 0.250% of intensity. Cell extracts were incubated with anti-YB-1 (3µg) at 4°C overnight. The RNA-protein immunocomplexes were precipitated with protein A beads (Roche Applied Science, IN) satured with tRNA and, after reverse cross-link, subjected to RealTime PCR.

Immunofluorescence – A431, SCC011 and SCC022 cells (2.5 x 10^5) were plated in 35 mm dish, grown on micro cover glasses (BDH). At 24 hours after seeding, cells were washed with cold phosphate-buffered saline (PBS) and fixed with 4% paraformaldehyde (PFA) (Sigma-Aldrich, Germany) for 15 min at 4°C. Cells were permeabilized with ice-cold 0.1% Triton X-100 for 10 min and then washed with PBS. p63 was detected using a 1:200 dilution of the monoclonal antibody 4A4. YB-1 was detected using 1:100 dilution of the YB1 antibody (Ab12148).
After extensive washing in PBS, the samples were incubated with Cy3-conjugated anti-mouse IgGs and Cy5-conjugated anti-rabbit IgGs at room temperature for 30 min. After PBS washing, the cells were incubated with DAPI (4′,6′-diamidino-2-phenylindole; 10 mg/ml (Sigma-Aldrich, Germany) for 3 min. The glasses were mounted with Moviol (Sigma-Aldrich, Germany) and examined under a fluorescence microscope (Nikon). Images were digitally acquired and processed using Adobe Photoshop software CS.

Cytoskeleton analysis – Actin bundles were stained with TRITC conjugated phalloidin. Cell fixation was performed with 4% paraformaldehyde for 20 min and then permeabilized with 0.1% Triton X-100 (Sigma, St. Louis, MO, USA) in PBS 1x for 10 min. Actin staining was done by incubating sample with TRITC phalloidin (Sigma) in PBS for 30 min at room temperature. Images of fluorescent cells were collected with a fluorescent inverted microscope (IX81, Olympus, Tokyo, Japan) equipped with an ORCA 2.8 digital camera (Hamamatsu Photonics, Japan).

Time-lapse microscopy – SCC011 cells were cultured on 35 mm dishes (Corning, NY) at 2x10^4 cells/dish density. ΔNp63α transient silencing was performed as

described in the Experimental procedure. At 48 hours from the addition of ΔNp63α si-RNA, the culture dishes were placed in a mini-incubator connected to an automated stage of an optical microscope (Olympus Co., Japan). Images of selected positions of the cell culture were collected in brightfield (BF) every 10 minutes for 12h. The BF images were mounted to obtain 72 frames time lapse video per each position. Cell trajectories were reconstructed from time lapse video using Metamorph software (Molecular Device, CA). Root mean square speed (*S*) and persistence time (*P*) were chosen as relevant parameters in order to describe the macroscopic features of cell migration in the different experimental conditions. These parameters were calculated according to the procedure reported by Dunn G.A. (*Dunn*, 1983) Briefly, mean-squared displacement (MSD) of each cell, is calculated according to overlapping time intervals method (*Dickinson*, 1993). Subsequently, *S* and *P* are estimated by fitting the experimental data of the MSD to a linear approximation of the persistent random walk model. The upper limit for the data fitting was set approximately at 200 min per each cell owing to the deviation from linearity that is observed at higher time points. The fitting procedure provided (*S*, *P*) pairs per each cells and Statistical significance between *S* and *P* values of the different experimental setups was assessed by performing a non-parametric Kruskal-Wallis test in Matlab (MathWorks, MA). *p* values < 0.05 were considered significant.
Cell migration in H1299 cells was evaluated with a similar approach. Briefly, cells were cultured on 35 mm dishes (Corning, NY) at a density of 2×10^4 cells/dish. ΔNp63α expression was induced with 2 μg/ml doxycycline for 48 hr. 16 hr after transfection, cell dishes were placed in a mini-incubator connected to an automated stage of an optical microscope (Cell^R, Olympus Co., Japan). Time zero images of selected position were collected in fluorescence in order to localize transfected cells. Then, at the same positions, images were recorded in brightfield (BF) every 10 minutes for 12 hours. Data analysis was performed as described above.

Cell Viability assay - Cell viability was determined by the MTT 3-(4,5-dimethylthiazol-2-yl)-2,5-diphenyl tetrazolium bromide assay (Sigma-Aldrich, St Louis, MO). Briefly, cells were seeded in 96-well plates at 2×10^3 and transfected with scrambled or YB-1 siRNA oligos, 48h after silencing MTT solution (5mg/ml in PBS, 20 μl/well) was added to cells to produce formazan crystals. MTT solution was substituted by 150 μl DMSO 30 minutes later to solubilize the formazan crystals. The optical absorbance was determined at 570 nm using an iMark microplate reader (Bio-Rad, USA). The experiments were carried out in triplicate for each knockdown and compared to scrambled control.

Quantitative Real Time-PCR-For PCR analysis total RNA was isolated using the RNA Extraction Kit from Qiagen (Hilden, Germany) according to the manufacturer's instructions. RNA (2-5μg) was treated with DNAse I (Promega, Madison USA) and used to generate reverse transcribed cDNA using SuperScript III (Life Technologies, CA, USA), according to the manufacturer's instructions. All samples in each experiment were reverse transcribed at the same time, the resulting cDNA diluted 1:5 in nuclease-free water and stored in aliquots at –80°C until used.
Real Time PCR with SYBR green detection was performed with a 7500 RT-PCR Thermo Cycler (Applied Biosystem, Foster City, USA). The thermal cycling conditions were composed of 50ºC for 2 min followed by an initial denaturation step at 95ºC for 10 min, 45 cycles at 95ºC for 30s, 60ºC for 30s and 72ºC for 30s. Experiments were carried out in triplicate. The relative quantification in gene expression was determined

using the $2^{-\Delta\Delta Ct}$ method (Livak and Schmittgen, 2011). Using this method, we obtained the fold changes in gene expression normalized to an internal control gene and relative to one control sample (calibrator). 18S was used as an internal control to normalize all data and the siCtrl was chosen as the calibrator.
Appropriate no-RT and non-template controls were included in each 96-well PCR reaction and dissociation analysis was performed at the end of each run to confirm the specificity of the reaction.
TWIST (F): 5' AGAAGTCTGCGGGCTGTG
TWIST (R):5'TCTGCAGCTCCTCGTAAGACT
HPRT (F):5'CCTGCTGGATTACATTAAAGC
HPRT (R) : 5' CTTCGTGGGGTCCTTTTC
YB1 (F):5'CGCAGTGTAGGAGATGGAGAG
YB1 (R):5'GAACACCACCAGGACCTGTAA
∆Np63 (F):5'GGTTGGCAAAATCCTGGAG
∆Np63 (R):5'GGTTCGTGTACTGTGGCTCA
EGFR (F) :5'TTCCTCCCAGTGCCTGAA
EGFR (R):5'GGGTTCAGAGGCTGATTGTG
STAT3 (F) :5'CCTCTGCCGGAGAAACAG
STAT3 (R):5'CTGTCACTGTAGAGCTGATGGAG
GADD45A (F): 5' TTTGCAATATGACTTTGGAGGA
GADD45A (R): 5' CATCCCCCACCTTATCCAT
18S (F):5'TCGAGGCCCTGTAATTGGAA
18S (R):5'CTTTAATATACGCTATTGGAGCTG

Chromatin Immunoprecipitation (ChIP) assay in MCF7 cells **-** According with *Beneke*, 2015 cells were cross-linked for 10 min at room temperature with 4% formaldehyde into the medium and neutralized by the addition of 1.25 M glycine/PBS for 2 min. After removing of the solution, plates were washed twice with PBS (2 min each). To yield chromatin suspension, cells were scraped in 0.5 ml SDS lysis buffer (1% SDS, 10 mM EDTA (pH8.0), 50 mM Tris-HCl (pH 8.0) supplemented with protease inhibitors (ROCHE-Diagnostic) after incubation for 5 min at 4°C. Suspensions were sonicated using Bioruptor (Diagenode) on high setting (30 sec on and 30 sec off) for 50 cycles. Concentration was adjusted to 1 µg/µl with lysis buffer and stored at 4°C.
For ChIP, suspensions were brought to room temperature and 160 µl were spun down for 5 min at maximum speed. 150 µl supernatant was mixed with 1.35 ml ChIP dilution buffer (20 mM Tris-HCl (pH 8.0), 2 mM EDTA (pH 8.0), 150 mM NaCl, 1% Triton-X-100) supplemented with protease inhibitors (ROCHE-Diagnostic) and incubated with 1.5 µg of p53 (DO-1) monoclonal antibody or 1.5 µg of normal IgG (Santa Cruz Biotechnology). Samples were rotated overnight at 4°C. 100 µl of on agarose-beads immobilized Protein G (Thermo Scientific, Rockford/IL, USA) were resuspended in 1 ml 9:1 dilution buffer:lysis buffer mix (DB:LB) and pre-absorbed with 100 µg/ml BSA and 500 µg/ml sheared salmon sperm DNA overnight at 4°C on a rotator.
On the next day, beads were washed twice with DB:LB and resuspended in 1 ml DB:LB. 50 µl of the beads suspension was added to each cell lysate and incubated for at least 2 h at 4°C on a rotator.
Suspensions were spun down 10 min at 1000 *x g* and supernatant was aspirated. Beads were washed 3 times in 0.5 ml wash buffer (150 mM NaCl, 20 mM Tris-HCl (pH 8.0), 2 mM EDTA (pH 8.0), 1% Triton-X-100, 0.1 % SDS) supplemented with protease inhibitors (ROCHE-Diagnostic) and centrifuged as above; Beads were

washed in 0.5 ml final wash (500 mM NaCl, 20 mM Tris-HCl (pH 8.0), 2 mM EDTA (pH 8.0), 1% Triton-X-100, 0.1% SDS) supplemented with protease inhibitors (ROCHE-Diagnostic) and immune-complexes were eluted by addition of 160 µl elution buffer (100 mM NaHCO3, 1% SDS) 5 min at room temperature. 500 µg/ml of Proteinase K and RNAse A were added to each sample and incubated for 30 min at 37°C and for 1 h at 56°C. DNA-protein crosslinks were reversed by adding NaCl to a final concentration of 200 mM and incubation overnight at 65°C. DNA was isolated by Phenol/Chloroform procedure and subsequent ethanol precipitation.
DNA fractions were subjected to PCR with primers specific for p21WAF and BAX promoter regions and with KOD Hot Start polymerase according to manufacturer's instructions (Novagen/Merck, Darmstadt, Germany).
PCR was performed in 32 cycles (20 sec 95°C/10 sec annealing temperature/5 sec 70°C) and products were resolved by 2.5% agarose gel electrophoresis. Primer sequences and respective annealing temperatures are listed:
Primer sequence fwd / rev (5'-3');
p21WAF GTGGCTCTGATTGGCTTTCTG/GCTAAGGTTTACCTGGGGTCTTTA
BAX ATAACGTCCTGCCTGGAAGC/CCCCAGCGCAGAAGGAATTA
ChIP experiments were performed as three independent biological replicates and each experiment was performed in triplicate. Promoter occupancy was calculated with the percent input method by using the Image J software.

Statistics - Statistical Analysis was performed by using the Graph Pad software and the unpaired Student's t test.P-value of <0.05 were considered statistically significant (*); P-value of <0.01 were considered extremely statistically significant (**).

8. REFERENCES

1. Adorno M, Cordenonsi M, Montagner M, Dupont S, Wong C, Hann B, Solari A, Bobisse S, Rondina MB, Guzzardo V, Parenti AR, Rosato A, Bicciato S, Balmain A, Piccolo S. **A Mutant-p53/Smad complex opposes p63 to empower TGFbeta-induced metastasis**. Cell. 2009 Apr 3;137(1):87-98. doi: 10.1016/j.cell.2009.01.039.PubMed PMID: 19345189.
2. Alagoz M, Gilbert DC, El-Khamisy S, Chalmers AJ. **DNA repair and resistance to topoisomerase I inhibitors: mechanisms, biomarkers and therapeutic targets**. Curr Med Chem. 2012;19(23):3874-85. Review. PubMed PMID: 22788763
3. Amoresano A, Di Costanzo A, Leo G, Di Cunto F, La Mantia G, Guerrini L, Calabrò V. **Identification of ΔNp63α protein interactions by mass spectrometry.** J Proteome Res. 2010 Apr 5;9(4):2042-8. doi: 10.1021/pr9011156.
4. Argiris A, Kotsakis AP, Hoang T, Worden FP, Savvides P, Gibson MK, Gyanchandani R, Blumenschein GR Jr, Chen HX, Grandis JR, Harari PM, Kies MS, Kim S. **Cetuximab and bevacizumab: preclinical data and phase II trial in recurrent or metastatic squamous cell carcinoma of the head and neck.** Ann Oncol. 2013 Jan;24(1):220-5. doi: 10.1093/annonc/mds245. Epub 2012 Aug 16. PubMed PMID: 22898037; PubMed Central PMCID: PMC3525135.
5. Audeh MW, Carmichael J, Penson RT, et al. **Oral poly(ADP-ribose) polymerase inhibitor olaparib in patients with BRCA1 or BRCA2 mutations and recurrent ovarian cancer: a proof-of-concept trial**. Lancet. 2010 Jul 24;376(9737):245–251
6. Bader AG, Vogt PK. **Phosphorylation by Akt disables the anti-oncogenic activity of YB-1**. Oncogene. 2008 Feb 14;27(8):1179-82. Epub 2007 Aug 20. PubMed PMID: 17704806.
7. Baker SJ, Preisinger AC, Jessup JM, Paraskeva C, Markowitz S, Willson JK, Hamilton S, Vogelstein B. **p53 gene mutations occur in combination with 17p allelic deletions as late events in colorectal tumorigenesis**. Cancer Res. 1990 Dec 1;50(23):7717-22. PubMed PMID: 2253215.
8. Baker SJ, Preisinger AC, Jessup JM, Paraskeva C, Markowitz S, Willson JK, Hamilton S, Vogelstein B. **p53 gene mutations occur in combination with 17p allelic deletions as late events in colorectal tumorigenesis**. Cancer Res. 1990 Dec 1;50(23):7717-22. PubMed PMID: 2253215.
9. Barbareschi, M., Pecciarini, L., Cangi, M.G., Macrì, E., Rizzo, A., Viale, G., Dogliosi, C., (2001) **p63, a p53 homologue, is a selective nuclear marker of myoepithelial cells of the human breast** Am J Surg Pathol **25**(8) 1054-60.
10. Barbieri CE, Barton CE, Pietenpol JA. **ΔNp63α expression is regulated by the phosphoinositide 3-kinase pathway**. *J Biol Chem. 2003 Dec 19;278(51):51408-14. Epub 2003 Oct 10.*

11. Barbieri CE, Pietenpol JA. **p63 and epithelial biology**. Exp Cell Res. 2006 Apr 1;312(6):695-706. Epub 2006 Jan 9. Review. PubMed PMID: 16406339. p63 and epithelial biology Christopher E. Barbieri, Jennifer A. Pietenpol.)
12. Barbieri, C.E., Tang, L.J., Brown, K.A., Pietenpol, J.A., (2006) **Loss of p63 leads to increased cell migration and up-regulation of genes involved in invasion and metastasis.** Cancer Res **66**(15) 7589-7597.
13. Bargou RC, Jürchott K, Wagener C, Bergmann S, Metzner S, Bommert K, Mapara MY, Winzer KJ, Dietel M, Dörken B, Royer HD. **Nuclear localization and increased levels of transcription factor YB-1 in primary human breast cancers are associated with intrinsic MDR1 gene expression.** Nat Med. 1997 Apr;3(4):447-50. PubMed PMID: 9095180.
14. Basaki Y, Hosoi F, Oda Y, Fotovati A, Maruyama Y, Oie S, Ono M, Izumi H, Kohno K, Sakai K, Shimoyama T, Nishio K, Kuwano M. **Akt-dependent nuclear localization of Y-box-binding protein 1 in acquisition of malignant characteristics by human ovarian cancer cells**. Oncogene. 2007 Apr 26;26(19):2736-46. Epub 2006 Oct 30.
15. Bell RE, Levy C. **The three M's: melanoma, microphthalmia-associated transcription factor and microRNA**. Pigment Cell Melanoma Res. 2011 Dec;24(6):1088-106. doi: 10.1111/j.1755-148X.2011.00931.x. Review. PubMed PMID:22004179
16. Beneke S. **Improving Chromatin Immunoprecipitation (ChIP) by Suppression of Method-Induced DNA-Damage Signaling** In: Hancock R. editor. The Nucleus, Methods in Molecular Biology. Springer Science+Business Media New York, 2015 vol. 1228 pp 67-81.
17. Bensouillah J (2012) **Skin structure and function**. www.courses.washington.edu/bioen327/labs/lit_skinstruct_bensouillah_ch01.pdf
18. Bergmann S, Royer-Pokora B, Fietze E, Jürchott K, Hildebrandt B, Trost D, Leenders F, Claude JC, Theuring F, Bargou R, Dietel M, Royer HD. **YB-1 provokes breast cancer through the induction of chromosomal instability that emerges from mitotic failure and centrosome amplification.** Cancer Res. 2005 May 15;65(10):4078-87. PubMed PMID: 15899797.
19. Bito T, Sumita N, Ashida M, Budiyanto A, Ueda M, Ichihashi M, Tokura Y, Nishigori C. **Inhibition of Epidermal Growth Factor Receptor and PI3K/Akt Signaling Suppresses Cell Proliferation and Survival through Regulation of Stat3 Activation in Human Cutaneous Squamous Cell Carcinoma**. J Skin Cancer. 2011;2011:874571. doi: 10.1155/2011/874571. Epub 2010 Dec 8. PubMed PMID:21197106; PubMed Central PMCID: PMC3005828
20. Blanpain C, Fuchs E. **p63: revving up epithelial stem-cell potential**. Nat Cell Biol. 2007 Jul;9(7):731-3. PubMed PMID: 17603506.
21. Brunner HG, Hamel BC, Van Bokhoven H. **The p63 gene in EEC and other syndromes.** J Med Genet. 2002 Jun;39(6):377-81. Review. PubMed PMID: 12070241; PubMed Central PMCID: PMC1735150.
22. Bryant HE, Schultz N, Thomas HD, et al. **Specific killing of BRCA2-deficient tumours with inhibitors of poly(ADP-ribose) polymerase**. Nature. 2005 Apr 14;434(7035):913–917

23. Bürkle A, Virág L. **Poly(ADP-ribose): PARadigms and PARadoxes**. Mol Aspects Med. 2013 Dec;34(6):1046-65. doi: 10.1016/j.mam.2012.12.010. Epub 2013 Jan 2. Review.PubMed PMID: 23290998.

24. Buzzell R A. **Effects of solar radiation on the skin.** Otolaryngol Clin North Am.1993;26:1–11

25. C.D. Thanos, J.U. Bowie**, p53 Family members p63 and p73 are SAM domain-containing proteins**, Protein Sci. 8 (1999) 1708–1710.

26. Carroll DK, Carroll JS, Leong CO, Cheng F, Brown M, Mills AA, Brugge JS, Ellisen LW. **p63 regulates an adhesion programme and cell survival in epithelial cells**. Nat Cell Biol. 2006 Jun;8(6):551-61. Epub 2006 May 21. PubMed PMID: 16715076.

27. Castillo-Martin M, Domingo-Domenech J, Karni-Schmidt O, Matos T, Cordon-Cardo C. **Molecular pathways of urothelial development and bladder tumorigenesis**. Urol Oncol. 2010 Jul-Aug;28(4):401-8. doi: 10.1016/j.urolonc.2009.04.019. Review. PubMed PMID: 20610278.

28. Celli J, Duijf P, Hamel BC, Bamshad M, Kramer B, Smits AP, Newbury-Ecob R, Hennekam RC, Van Buggenhout G, van Haeringen A, Woods CG, van Essen AJ, de Waal R, Vriend G, Haber DA, Yang A, McKeon F, Brunner HG, van Bokhoven H. **Heterozygous germline mutations in the p53 homolog p63 are the cause of EEC syndrome.** Cell. 1999 Oct 15;99(2):143-53. PubMed PMID: 10535733.

29. Chen JC, Lin BB, Hu HW, Lin C, Jin WY, Zhang FB, Zhu YA, Lu CJ, Wei XJ, Chen RJ. **NGF accelerates cutaneous wound healing by promoting the migration of dermal fibroblasts via the PI3K/Akt-Rac1-JNK and ERK pathways.** Biomed Res Int. 2014;2014:547187. doi: 10.1155/2014/547187. Epub 2014 May 21. PubMed PMID:25006578; PubMed Central PMCID: PMC4055427.

30. Chin L, Garraway LA, Fisher DE. **Malignant melanoma: genetics and therapeutics in the genomic era.** Genes Dev. 2006 Aug 15;20(16):2149-82. Review. PubMed PMID:16912270.

31. Cimmino G, Pepe S, Laus G, Chianese M, Prece D, Penitente R, Quesada P. **Poly(ADPR)polymerase-1 signalling of the DNA damage induced by DNA topoisomerase I poison in D54(p53wt) and U251(p53mut) glioblastoma cell lines.** Pharmacol Res.2007 Jan;55(1):49-56. Epub 2006 Oct 20. PubMed PMID: 17127074

32. Compérat E, Bièche I, Dargère D, Ferlicot S, Laurendeau I, Benoît G, Vieillefond A, Verret C, Vidaud M, Capron F, Bedossa P, Paradis V. **p63 gene expression study and early bladder carcinogenesis.** Urology. 2007 Sep;70(3):459-62. PubMed PMID: 17905096.

33. Costanzo A, Pediconi N, Narcisi A, Guerrieri F, Belloni L Fausti F,,Botti E, Levrero M..TP63 and TP73 in cancer, an unresolved "family" puzzle of complexity, redundancy and hierarchy FEBS Lett. 2014;588(16):2590-99.

34. Daniel RA, Rozanska AL, Mulligan EA, et al. **Central nervous system penetration and enhancement of temozolomide activity in childhood medulloblastoma models by poly(ADP-ribose) polymerase inhibitor AG-014699**. Br J Cancer. 2010 Nov

35. Danilov AV, Neupane D, Nagaraja AS, Feofanova EV, Humphries LA, DiRenzo J,Korc M. **DeltaNp63alpha-mediated induction of epidermal growth factor receptor promotes pancreatic cancer cell growth and chemoresistance**. PLoS One. 2011;6(10):e26815. doi: 10.1371/journal.pone.0026815. Epub 2011 Oct 28. PubMed PMID: 22053213; PubMed Central PMCID: PMC3203907.

36. Davar D, Beumer JH, Hamieh L, Tawbi H**. Role of PARP inhibitors in cancer biology and therapy.** Curr Med Chem. 2012;19(23):3907-21. Review. PubMed PMID:22788767; PubMed Central PMCID: PMC3421454

37. Dazert E, Hall MN. **mTOR signaling in disease**. Curr Opin Cell Biol. 2011 Dec;23(6):744-55. doi: 10.1016/j.ceb.2011.09.003. Epub 2011 Sep 29. Review. PubMed PMID: 21963299.

38. de Lartigue, Jane **New Life for PARP Inhibitors: Emerging Agents Leave Mark at ASCO** Published Online: Friday, August 30, 201 - See more at: http://www.onclive.com/publications/Oncology-live/2013/August-2013/New-Life-for-PARP-Inhibitors-Emerging-Agents-Leave-Mark-at-ASCO#sthash.sksjvoNJ.dpuf

39. Di Como CJ, Urist MJ, Babayan I, Drobnjak M, Hedvat CV, Teruya-Feldstein J, Pohar K, Hoos A, Cordon-Cardo C. **p63 expression profiles in human normal and tumor tissues**. Clin Cancer Res. 2002 Feb;8(2):494-501. PubMed PMID: 11839669.

40. Di Costanzo A, Festa L, Roscigno G, Vivo M, Pollice A, Morasso M, La Mantia G, Calabrò V. **A dominant mutation etiologic for human tricho-dento-osseous syndrome impairs the ability of DLX3 to downregulate ΔNp63α**. J Cell Physiol. 2011 Aug;226(8):2189-97. doi: 10.1002/jcp.22553. PubMed PMID: 21520071.

41. Di Costanzo A, Troiano A, di Martino O, Cacace A, Natale CF, Ventre M, Netti P, Caserta S, Pollice A, La Mantia G, Calabrò V. **The p63 protein isoform ΔNp63α modulates Y-box binding protein 1 in its subcellular distribution and regulation of cell survival and motility genes.** J Biol Chem. 2012 Aug 31;287(36):30170-80. doi: 10.1074/jbc.M112.349951. Epub 2012 Jul 11. PubMed PMID: 22787154; PubMed Central PMCID: PMC3436271.

42. Di Iorio E, Barbaro V, Ruzza A, Ponzin D, Pellegrini G, De Luca M. **Isoforms of ΔNp63 and the migration of ocular limbal cells in human corneal regeneration**. Proc Natl Acad Sci U S A. 2005; 102(27):9523-8.

43. di Martino O, Troiano A, Guarino AM, Pollice A, Vivo A, La Mantia G, Calabrò V **"ΔNp63α protects YB-1 oncoprotein from proteasome-dependent proteolysis"** Febs Letters submitted 2015

44. Dickinson R. B., Tranquillo R. T. (1993) **Optimal estimation of cell movement indices from the statistical analysis of cell tracking data**. AIChE J. 39, 1995–2010

45. Didier DK, Schiffenbauer J, Woulfe SL, Zacheis M, Schwartz BD. **Characterization of the cDNA encoding a protein binding to the major histocompatibility complex class II Y box**. Proc Natl Acad Sci U S A. 1988 Oct;85(19):7322-6. PubMed PMID: 3174636; PubMed Central PMCID: PMC282178.

46. Dolfini D, Mantovani R. **Targeting the Y/CCAAT box in cancer: YB-1 (YBX1) or NF-Y?** Cell Death Differ. 2013 May;20(5):676-85. doi: 10.1038/cdd.2013.13. Epub 2013 Mar 1. Review. PubMed PMID: 23449390; PubMed Central PMCID: PMC3619239.

47. D'Onofrio G, Tramontano F, Dorio AS, Muzi A, Maselli V, Fulgione D, Graziani G, Malanga M, Quesada P. **Poly(ADP-ribose) polymerase signaling of topoisomerase 1-dependent DNA damage in carcinoma cells. Biochem Pharmacol.** 2011 Jan15;81(2):194-202. doi: 10.1016/j.bcp.2010.09.019. Epub 2010 Sep 25. PubMed PMID: 20875401.

48. Dumaz N, Milne DM, Meek DW. **Protein kinase CK1 is a p53-threonine 18 kinase which requires prior phosphorylation of serine 15**. FEBS Lett. 1999 Dec 17;463(3):312-6. PubMed PMID: 10606744.

49. Dunn GA. **Characterising a kinesis response: time averaged measures of cell speed and directional persistence.** Agents Actions Suppl. 1983;12:14-33. PubMed PMID: 6573115.

50. E.R. Flores, K.Y. Tsai, D. Crowley, S. Sengupta, A. Yang, F. McKeon, T. Jacks, **p63 and p73 are required for p53-dependent apoptosis in response to DNA damage**, Nature 416 (2002) 560–564.

51. Evdokimova V, Tognon C, Ng T, Ruzanov P, Melnyk N, Fink D, Sorokin A, Ovchinnikov LP, Davicioni E, Triche TJ, Sorensen PH. **Translational activation of snail1 and other developmentally regulated transcription factors by YB-1 promotes an epithelial-mesenchymal transition.** Cancer Cell. 2009 May 5;15(5):402-15. doi:10.1016/j.ccr.2009.03.017. PubMed PMID: 19411069.

52. Farmer H, McCabe N, Lord CJ, et al. **Targeting the DNA repair defect in BRCA mutant cells as a therapeutic strategy**. Nature. 2005 Apr 14;434(7035):917–921.

53. Faury D, Nantel A, Dunn SE, Guiot MC, Haque T, Hauser P, Garami M, Bognár L, Hanzély Z, Liberski PP, Lopez-Aguilar E, Valera ET, Tone LG, Carret AS, Del Maestro RF, Gleave M, Montes JL, Pietsch T, Albrecht S, Jabado N. **Molecular profiling identifies prognostic subgroups of pediatric glioblastoma and shows increased YB-1 expression in tumors**. J Clin Oncol. 2007 Apr 1;25(10):1196-208.PubMed PMID: 17401009.

54. Ferraris DV. **Evolution of poly(ADP-ribose) polymerase-1 (PARP-1) inhibitors. From concept to clinic.** J Med Chem. 2010;53(12):4561–4584

55. Fillmore CM, Kuperwasser C. **Human breast cancer cell lines contain stem-like cells that self-renew, give rise to phenotypically diverse progeny and survive chemotherapy.** Breast Cancer Res. 2008;10(2):R25. doi: 10.1186/bcr1982. Epub 2008 Mar 26. PubMed PMID: 18366788; PubMed Central PMCID: PMC2397524.

56. Flores ER, Tsai KY, Crowley D, Sengupta S, Yang A, McKeon F, Jacks T. **p63 and p73 are required for p53-dependent apoptosis in response to DNA damage.** Nature.2002 Apr 4;416(6880):560-4. PubMed PMID: 11932750.

57. Fraser, D. J., Phillips, A. O., Zhang, X., van Roeyen, C. R., Muehlenberg, P., En-Nia, A. and Mertens, P. R. (2008) **Y-box protein-1 controls transforming**

growth factor-beta1 translation in proximal tubular cells. Kidney Int. **73**, 724-732

58. Frye BC, Halfter S, Djudjaj S, Muehlenberg P, Weber S, Raffetseder U, En-Nia A, Knott H, Baron JM, Dooley S, Bernhagen J, Mertens PR. **Y-box protein-1 is actively secreted through a non-classical pathway and acts as an extracellular mitogen.** EMBO Rep. 2009 Jul;10(7):783-9. doi: 10.1038/embor.2009.81. Epub 2009 May 29. PubMed PMID: 19483673; PubMed Central PMCID: PMC2690452.

59. Fujita T, Ito K, Izumi H, Kimura M, Sano M, Nakagomi H, Maeno K, Hama Y,Shingu K, Tsuchiya S, Kohno K, Fujimori M. **Increased nuclear localization of transcription factor Y-box binding protein 1 accompanied by up-regulation of P-glycoprotein in breast cancer pretreated with paclitaxel.** Clin Cancer Res. 2005 Dec 15;11(24 Pt 1):8837-44. PubMed PMID: 16361573.

60. Galli F, Rossi M, D'Alessandra Y, De Simone M, Lopardo T, Haupt Y, Alsheich-Bartok O, Anzi S, Shaulian E, Calabrò V, La Mantia G, Guerrini L. **MDM2 and Fbw7 cooperate to induce p63 protein degradation following DNA damage and cell differentiation**. J Cell Sci. 2010 Jul 15;123(Pt 14):2423-33. doi:10.1242/jcs.061010. Epub 2010 Jun 22. PubMed PMID: 20571051.

61. Gambi N, Tramontano F, Quesada P. **Poly(ADPR)polymerase inhibition and apoptosis induction in cDDP-treated human carcinoma cell lines. Biochem Pharmacol.** 2008 Jun 15;75(12):2356-63. doi: 10.1016/j.bcp.2008.03.015. Epub 2008 Mar 30. PubMed PMID: 18468580.

62. Gao, Y., Fotovati, A., Lee, C., Wang, M., Cote, G., Guns, E., Toyota, B., Faury, D., Jabado, N. and Dunn, S. E. (2009) **Inhibition of Y-box binding protein-1 slows the growth of glioblastoma multiforme and sensitizes to temozolomide independent O6-methylguanine-DNA methyltransferase**. Mol. Cancer Ther. **8**, 3276-3284

63. Ghioni P, Bolognese F, Duijf PH, Van Bokhoven H, Mantovani R, Guerrini L. **Complex transcriptional effects of p63 isoforms: identification of novel activation and repression domains.** Mol Cell Biol. 2002 Dec;22(24):8659-68. PubMed PMID: 12446784; PubMed Central PMCID: PMC139859.

64. Giménez-Bonafé P, Fedoruk MN, Whitmore TG, Akbari M, Ralph JL, Ettinger S, Gleave ME, Nelson CC. **YB-1 is upregulated during prostate cancer tumor progression and increases P-glycoprotein activity**. Prostate. 2004 May 15;59(3):337-49. PubMed PMID: 15042610.

65. Gray-Schopfer V, Wellbrock C, Marais R**. Melanoma biology and new targeted therapy.** Nature. 2007 Feb 22;445(7130):851-7. Review. PubMed PMID: 17314971.

66. Guryanov SG, Filimonov VV, Timchenko AA, Melnik BS, Kihara H, Kutyshenko VP, Ovchinnikov LP, Semisotnov GV. **The major mRNP protein YB-1: structural and association properties in solution.** Biochim Biophys Acta. 2013 Feb;1834(2):559-67. doi: 10.1016/j.bbapap.2012.11.007. Epub 2012 Dec 5. PubMed PMID: 23220387

67. Guryanov SG, Selivanova OM, Nikulin AD, Enin GA, Melnik BS, Kretov DA, Serdyuk IN, Ovchinnikov LP**. Formation of amyloid-like fibrils by Y-box**

binding protein 1 (YB-1) is mediated by its cold shock domain and modulated by disordered terminal domains. PLoS One. 2012;7(5):e36969. doi: 10.1371/journal.pone.0036969. Epub 2012 May 8. PubMed PMID: 22590640; PubMed Central PMCID: PMC3348147.

68. H. Lee, D. Kimelman, **A dominant-negative form of p63 is required for epidermal proliferation in zebrafish**, Dev. Cell 2 (2002) 607–616.

69. Hanssen L, Alidousty C, Djudjaj S, Frye BC, Rauen T, Boor P, Mertens PR, van Roeyen CR, Tacke F, Heymann F, Tittel AP, Koch A, Floege J, Ostendorf T, Raffetseder U. **YB-1 is an early and central mediator of bacterial and sterile inflammation in vivo**. J Immunol. 2013 Sep 1;191(5):2604-13. doi:10.4049/jimmunol.1300416. Epub 2013 Jul 19. PubMed PMID: 23872051.

70. Hastak K, Alli E, Ford JM. **Synergistic chemosensitivity of triple-negative breast cancer cell lines to poly(ADP-Ribose) polymerase inhibition, gemcitabine, and cisplatin**. Cancer Res. 2010 Oct 15;70(20):7970-80. doi:10.1158/0008-5472.CAN-09-4521. Epub 2010 Aug 26. PubMed PMID: 20798217; PubMedCentral PMCID: PMC2955854.

71. Hedvat CV, Teruya-Feldstein J, Puig P, Capodieci P, Dudas M, Pica N, Qin J, Cordon-Cardo C, Di Como CJ. **Expression of p63 in diffuse large B-cell lymphoma.** Appl Immunohistochem Mol Morphol. 2005 Sep;13(3):237-42. PubMed PMID: 16082248

72. Hibi K, Trink B, Patturajan M **AIS is an oncogene amplified in squamous cell carcinoma**. Proc Natl Acad Sci U S A. 2000 May 9;97(10):5462-7.

73. Homer C., Knight D.A., Hananeia L., Sheard P.M., Risk J., Lasham A. et al. **Y-box factor YB1 controls p53 apoptotic function**. Oncogene 2005; 24, 8314-8325.

74. Homer, C., Knight, D. A., Hananeia, L., Sheard, P., Risk, J., Lasham, A., Royds, J. A. and Braithwaite, A. W. (2005) **Y-box factor YB1 controls p53 apoptotic function**. Oncogene **24**, 8314-8325

75. Hunter JE, Willmore E, Irving JA, et al. **NF-κB mediates radio-sensitization by the PARP-1 inhibitor, AG-014699**. Oncogene. 2011 Jun 27

76. Inoue I, Matsumoto K, Yu Y, Bay BH. **Surmounting chemoresistance by targeting the Y-box binding protein-1**. Anat Rec (Hoboken). 2012 Feb;295(2):215-22. doi:10.1002/ar.22401. Epub 2011 Dec 20. Review. PubMed PMID: 22190445

77. J. Bakkers, M. Hild, C. Kramer, M. Furutani-Seiki, M. Hammerschmidt, **Zebrafish DeltaNp63 is a direct target of Bmp signaling and encodes a transcriptional repressor blocking neural specification in the ventral ectoderm**, Dev.Cell 2 (2002) 617–627.

78. J. Schultz, C.P. Ponting, K. Hofmann, P. Bork, **SAM as a protein interaction domain involved in developmental regulation,** Protein Sci. 6 (1997) 249–253.

79. Jackson SP, Bartek J. **The DNA-damage response in human biology and disease.**Nature. 2009 Oct 22;461(7267):1071–1078.

80. Jamora, C., DasGupta, R., Kocieniewski, P. and Fuchs, E. (2003) **Links between signal transduction, transcription and adhesion in epithelial bud development**. Nature 422, 317-322

81. Johnson T M, Rowe D E, Nelson B R, Swanson N A. **Squamous cell carcinoma of the skin (excluding lip and oral mucosa)** J Am Acad Dermatol. 1992;26 (3 Pt 2):467–484)

82. Kanitakis J, Chouvet B. **Expression of p63 in cutaneous metastases**. Am J ClinPathol. 2007 Nov;128(5):753-8. PubMed PMID: 17951196.

83. Khan MI, Adhami VM, Lall RK, Sechi M, Joshi DC, Haidar OM, Syed DN, Siddiqui IA, Chiu SY, Mukhtar H. **YB-1 expression promotes epithelial-to-mesenchymal transition in prostate cancer that is inhibited by a small molecule fisetin.** Oncotarget. 2014 May 15;5(9):2462-74. PubMed PMID: 24770864; PubMed Central PMCID: PMC4058019.

84. Kim ER, Selyutina AA, Buldakov IA, Evdokimova V, Ovchinnikov LP, Sorokin AV. **The proteolytic YB-1 fragment interacts with DNA repair machinery and enhances survival during DNA damaging stress**. Cell Cycle. 2013 Dec 15;12(24):3791-803. doi: 10.4161/cc.26670. Epub 2013 Oct 7. PubMed PMID: 24107631; PubMed Central PMCID: PMC3905071

85. Kirkuam N. **Tumors and cysts of the epidermis**.In: Elder DE, Elenitsas R, Murphy GF, et al., editor. Lever's Histopathology of the Skin. 9th ed. Baltimore, MD: Lippincott Williams & Wilkins; 2005. pp. 805–866.

86. Kohno K, Izumi H, Uchiumi T, Ashizuka M, Kuwano M. **The pleiotropic functions of the Y-box-binding protein, YB-1.** Bioessays. 2003 Jul;25(7):691-8. Review. PubMed PMID: 12815724.

87. Koike K, Uchiumi T, Ohga T, Toh S, Wada M, Kohno K, Kuwano M. **Nuclear translocation of the Y-box binding protein by ultraviolet irradiation**. FEBS Lett.1997 Nov 17;417(3):390-4. PubMed PMID: 9409758.

88. Kuwano M, Oda Y, Izumi H, Yang SJ, Uchiumi T, Iwamoto Y, Toi M, Fujii T, Yamana H, Kinoshita H, Kamura T, Tsuneyoshi M, Yasumoto K, Kohno K. **The role of nuclear Y-box binding protein 1 as a global marker in drug resistance**. Mol Cancer Ther. 2004 Nov;3(11):1485-92. Review. PubMed PMID: 15542787.

89. Lasham A, Print CG, Woolley AG, Dunn SE, Braithwaite AW **YB-1: oncoprotein, prognostic marker and therapeutic target?** *Biochem J. 2013 Jan 1;449(1):11-23. doi: 10.1042/BJ20121323.*

90. Lasham A, Samuel W, Cao H, Patel R, Mehta R, Stern JL, Reid G, Woolley AG, Miller LD, Black MA, Shelling AN, Print CG, Braithwaite AW. **YB-1, the E2F pathway, and regulation of tumor cell growth.** J Natl Cancer Inst. 2012 Jan18;104(2):133-46. doi: 10.1093/jnci/djr512. Epub 2011 Dec 28. PubMed PMID:22205655.

91. Lasham, A., Moloney, S., Hale, T., Homer, C., Zhang, Y. F., Murison, J. G., Braithwaite, A. W. and Watson, J. (2003) **The Y-box-binding protein, YB1, is a potential negative regulator of the p53 tumor suppressor**. J. Biol. Chem.**278**, 35516-35523

92. Law, J. H., Li, Y., To, K., Wang, M., Astanehe, A., Lambie, K., Dhillon, J., Jones, S. J., Gleave, M. E., Eaves, C. J. and Dunn, S. E. (2010) **Molecular decoy to the Y-box binding protein-1 suppresses the growth of breast and prostate cancer cells whilst sparing normal cell viability.** PLoS ONE **5**

93. Ledermann JA, Harter P, Gourley C, et al. **Phase II randomized placebo-controlled study of olaparib (AZD2281) in patients with platinum-sensitive relapsed serous ovarian cancer** (PSR SOC) J Clin Oncol. 2011;29

94. Lee H, Kimelman D. **A dominant-negative form of p63 is required for epidermal proliferation in zebrafish**. Dev Cell. 2002 May;2(5):607-16. PubMed PMID:12015968.

95. Leonard MK, Hill NT, Grant ED, Kadakia MP. **ΔNp63α represses nuclear translocation of PTEN by inhibition of NEDD4-1 in keratinocytes**. Arch Dermatol Res. 2013 Oct;305(8):733-9. doi: 10.1007/s00403-013-1352-7. Epub 2013 Apr 16 PubMed PMID: 23589096; PubMed Central PMCID: PMC3779491.

96. Litman T, Druley TE, Stein WD, Bates SE. **From MDR to MXR: new understanding of multidrug resistance systems, their properties and clinical significance.** Cell Mol Life Sci. 2001 Jun;58(7):931-59. Review. PubMed PMID: 11497241.

97. Lo Iacono M, Di Costanzo A, Calogero RA, Mansueto G, Saviozzi S, Crispi S, Pollice A, La Mantia G, Calabrò V. **The Hay Wells syndrome-derived TAp63alphaQ540L mutant has impaired transcriptional and cell growth regulatory activity.** Cell Cycle. 2006 Jan;5(1):78-87. Epub 2006 Jan 21. PubMed PMID: 16319531.

98. Lovett, D. H., Cheng, S., Cape, L., Pollock, A. S. and Mertens, P. R. (2010) **YB-1 alters MT1-MMP trafficking and stimulates MCF-7 breast tumor invasion and metastasis.** Biochem. Biophys. Res. Commun. **398**, 482-488

99. Loyo M, Li RJ, Bettegowda C, Pickering CR, Frederick MJ, Myers JN, Agrawal N. **Lessons learned from next-generation sequencing in head and neck cancer**. Head Neck. 2013 Mar;35(3):454-63. doi: 10.1002/hed.23100. Epub 2012 Aug 21.

100. Lu ZH, Books JT, Ley TJ. **YB-1 is important for late-stage embryonic development, optimal cellular stress responses, and the prevention of premature senescence**. Mol Cell Biol. 2005 Jun;25(11):4625-37. PubMed PMID: 15899865; PubMed Central PMCID: PMC1140647.

101. Lyabin DN, Eliseeva IA, Ovchinnikov LP. **YB-1 protein: functions and regulation.** Wiley Interdiscip Rev RNA. 2014 Jan-Feb;5(1):95-110. doi: 10.1002/wrna.1200. Epub 2013 Nov 11. Review. PubMed PMID: 24217978

102. M.D. Westfall, D.J. Mays, J.C. Sniezek, J.A. Pietenpol, **The ΔNp63 alpha phosphoprotein binds the p21 and 14-3-3s promoters in vivo and has transcriptional repressor activity that is reduced by Hay–Wells syndrome-derived mutations,** Mol. Cell. Biol. 23 (2003) 2264–2276.

103. Madison DL, Stauffer D, Lundblad JR. **The PARP inhibitor PJ34 causes a PARP1-independent, p21 dependent mitotic arrest**. DNA Repair (Amst). 2011 Oct 10;10(10):1003-13. doi: 10.1016/j.dnarep.2011.07.006. Epub 2011 Aug 12. PubMed PMID: 21840268; PubMed Central PMCID: PMC3185120

104. Malanga M, Althaus FR. **Poly(ADP-ribose) reactivates stalled DNA topoisomerase I and Induces DNA strand break resealing**. J Biol Chem. 2004 Feb 13;279(7):5244-8 Epub 2003 Dec 29. PubMed PMID: 14699148

105. Marks R. **An overview of skin cancers. Incidence and causation**. Cancer.1995; 75(2 Suppl):607–612

106. Martins RG, Parvathaneni U, Bauman JE, Sharma AK, Raez LE, Papagikos MA, Yunus F, Kurland BF, Eaton KD, Liao JJ, Mendez E, Futran N, Wang DX, Chai X, Wallace SG, Austin M, Schmidt R, Hayes DN. **Cisplatin and radiotherapy with or without erlotinib in locally advanced squamous cell carcinoma of the head and neck: a randomized phase II trial**. J Clin Oncol. 2013 Apr 10;31(11):1415-21. doi:10.1200/JCO.2012.46.3299. Epub 2013 Mar 4. PubMed PMID: 23460709.

107. Massion PP, Taflan PM, Jamshedur Rahman SM, Yildiz P, Shyr Y, Edgerton ME,Westfall MD, Roberts JR, Pietenpol JA, Carbone DP, Gonzalez AL. **Significance of p63 amplification and overexpression in lung cancer development and prognosis**.Cancer Res. 2003 Nov 1;63(21):7113-21. PubMed PMID: 14612504.

108. Matin R, Chick A, Sanzà P, **p63 is an alternative p53 repressor in melanoma that confers chemoresistance and a poor prognosis** J. Exp. Med. 2013 Vol. 210 No. 3 581-603

109. McDade SS, McCance DJ. **The role of p63 in epidermal morphogenesis and neoplasia**. Biochem Soc Trans. 2010 Feb;38(Pt 1):223-8. doi: 10.1042/BST0380223.PubMed PMID: 20074064.

110. McGrath JA, Duijf PH, Doetsch V, Irvine AD, de Waal R, Vanmolkot KR, Wessagowit V, Kelly A, Atherton DJ, Griffiths WA, Orlow SJ, van Haeringen A, Ausems MG, Yang A, McKeon F, Bamshad MA, Brunner HG, Hamel BC, van Bokhoven **H.Hay-Wells syndrome is caused by heterozygous missense mutations in the SAM domain of p63**. Hum Mol Genet. 2001 Feb 1;10(3):221-9. PubMed PMID: 11159940.

111. Melino G, Knight RA, Cesareni G. **Degradation of p63 by Itch**. Cell Cycle. 2006 Aug;5(16):1735-9. Epub 2006 Aug 15. PubMed PMID: 16931910.

112. Mills AA, Zheng B, Wang XJ, Vogel H, Roop DR, Bradley A. **p63 is a p53 homologue required for limb and epidermal morphogenesis.** Nature. 1999 Apr 22;398(6729):708-13.

113. Moll UM, Slade N. **p63 and p73: roles in development and tumor formation**. MolCancer Res. 2004 Jul;2(7):371-86. Review. PubMed PMID: 15280445.

114. Montariello D, Troiano A, Di Girolamo D, Beneke S, Calabrò V, Quesada P. **Effect of poly(ADP-ribose)polymerase and DNA topoisomerase I inhibitors on the p53/p63-dependent survival of carcinoma cells.** Biochem Pharmacol. 2015 Feb 7.pii: S0006-2952(15)00081-7. doi: 10.1016/j.bcp.2015.01.012. [Epub ahead of print]PubMed PMID: 25667043

115. Montariello D, Troiano A, Malanga M, Calabrò V, Quesada P. **p63 involvement in Poly(ADP-ribose) polymerase 1 signaling of topoisomerase I-dependent DNA damage in carcinoma cells.** Biochem Pharmacol. 2013 Apr

1;85(7):999-1006. doi:10.1016/j.bcp.2013.01.019. Epub 2013 Jan 29. PubMed PMID: 23376119

116. Mueller DW, Bosserhoff AK. **Role of miRNAs in the progression of malignant melanoma.** Br J Cancer. 2009 Aug 18;101(4):551-6. doi: 10.1038/sj.bjc.6605204.Epub 2009 Jul 28. Review. PubMed PMID: 19638982; PubMed Central PMCID:PMC2736818.

117. Mueller DW, Bosserhoff AK. **The evolving concept of 'melano-miRs'-microRNAs in melanomagenesis**. Pigment Cell Melanoma Res. 2010 Oct;23(5):620-6. doi: 10.1111/j.1755-148X.2010.00734.x. Epub 2010 Jul 12. Review. PubMed PMID:20557479.

118. Nguyen D, Zajac-Kaye M, Rubinstein L, Voeller D, Tomaszewski JE, Kummar S, Chen AP, Pommier Y, Doroshow JH, Yang SX**. Poly(ADP-ribose) polymerase inhibition enhances p53-dependent and -independent DNA damage responses induced by DNA damaging agent.** Cell Cycle. 2011 Dec 1;10(23):4074-82. doi:10.4161/cc.10.23.18170. Epub 2011 Dec 1. PubMed PMID: 22101337; PubMed Central PMCID: PMC3272289.

119. Nylander K, Vojtesek B, Nenutil R, Lindgren B, Roos G, Zhanxiang W, Sjöström B, Dahlqvist A, Coates PJ. **Differential expression of p63 isoforms in normal tissues and neoplastic cells**. J Pathol. 2002 Dec;198(4):417-27. PubMed PMID: 12434410.

120. O'Brien PJ. **Catalytic Promiscuity and the Divergent Evolution of DNA Repair Enzymes**. Chem Rev. 2006;106:720–752

121. Ohga T, Koike K, Ono M, Makino Y, Itagaki Y, Tanimoto M, Kuwano M, Kohno K. **Role of the human Y box-binding protein YB-1 in cellular sensitivity to the DNA-damaging agents cisplatin, mitomycin C, and ultraviolet light**. Cancer Res. 1996 Sep 15;56(18):4224-8. PubMed PMID: 8797596

122. Ohga T, Uchiumi T, Makino Y, Koike K, Wada M, Kuwano M, Kohno K. **Direct involvement of the Y-box binding protein YB-1 in genotoxic stress-induced activation of the human multidrug resistance 1 gene.** J Biol Chem. 1998 Mar 13;273(11):5997-6000. PubMed PMID: 9497311.

123. Padgett J K, Hendrix J D., Jr **Cutaneous malignancies and their management**. Otolaryngol Clin North Am. 2001;34:523–553

124. Panupinthu N, Yu S, Zhang D, Zhang F, Gagea M, Lu Y, Grandis JR, Dunn SE, Lee HY, Mills GB. **Self-reinforcing loop of amphiregulin and Y-box binding protein-1contributes to poor outcomes in ovarian cancer**. Oncogene. 2014 May 29;33(22):2846-56. doi: 10.1038/onc.2013.259. Epub 2013 Jul 15. PubMed PMID: 23851501; PubMed Central PMCID: PMC4115609.

125. Radoja N, Guerrini L, Lo Iacono N, Merlo GR, Costanzo A, Weinberg WC, La Mantia G, Calabrò V, Morasso MI. **Homeobox gene Dlx3 is regulated by p63 during ectoderm development: relevance in the pathogenesis of ectodermal dysplasias**. Development. 2007 Jan;134(1):13-8. PubMed PMID: 17164413.

126. Ramsey MR, Wilson C, Ory B, Rothenberg SM, Faquin W, Mills AA, Ellisen LW. **FGFR2 signaling underlies p63 oncogenic function in squamous cell carcinoma**. J Clin Invest. 2013 Aug 1;123(8):3525-38. doi: 10.1172/JCI68899. Epub 2013 Jul 8.

127. Randall Wickett R. and Visscher Marty O. **Structure and function of the epidermal barrier** American Journal of Infection Control *(2006)* Volume 34, Issue 10, Supplement, December S98–S110 doi:10.1016/j.ajic.2006.05.295

128. Rath A, Davidson AR, Deber CM. **The structure of "unstructured" regions in peptides and proteins: role of the polyproline II helix in protein folding and recognition.** Biopolymers. 2005;80(2-3):179-85. Review. PubMed PMID: 15700296.

129. Ratko TA, Douglas GW, de Souza JA, Belinson SE, Aronson N. **Radiotherapy Treatments for Head and Neck Cancer Update** [Internet]. Rockville (MD): Agency for Healthcare Research and Quality (US); 2014 Dec. Available from http://www.ncbi.nlm.nih.gov/books/NBK269018/ PubMed PMID: 25590120

130. Ratushny V, Gober MD, Hick R, Ridky TW, Seykora JT. **From keratinocyte to cancer: the pathogenesis and modeling of cutaneous squamous cell carcinoma.** J Clin Invest. 2012 Feb;122(2):464-72. doi: 10.1172/JCI57415. Epub 2012 Feb 1. Review. PubMed PMID: 22293185; PubMed Central PMCID: PMC3266779.

131. Rauen T, Raffetseder U, Frye BC, Djudjaj S, Mühlenberg PJ, Eitner F, Lendahl U, Bernhagen J, Dooley S, Mertens PR. **YB-1 acts as a ligand for Notch-3 receptors and modulates receptor activation**. J Biol Chem. 2009 Sep 25;284(39):26928-40.doi: 10.1074/jbc.M109.046599. Epub 2009 Jul 29. PubMed PMID: 19640841; PubMed Central PMCID: PMC2785380

132. Reis-Filho JS, Torio B, Albergarie A., Schmitt FC. **P63 expression in normal skin and usual carcinomas** J. Cutan. Pathol. 2002 29(9): 517-523.

133. Ripamonti F, Albano L, Rossini A, Borrelli S, Fabris S, Mantovani R, Neri A, Balsari A, Magnifico A, Tagliabue E. **EGFR through STAT3 modulates ΔN63α expression to sustain tumor-initiating cell proliferation in squamous cell carcinomas**. J Cell Physiol. 2013 Apr;228(4):871-8. doi: 10.1002/jcp.24238. PubMedPMID: 23018838

134. Rocco JW, Leong CO, Kuperwasser N, DeYoung MP, Ellisen LW **p63 mediates survival in squamous cell carcinoma by suppression of p73-dependent apoptosis**. Cancer Cell. 2006 Jan;9(1):45-56.

135. Romani N, Brunner PM, Stingl G. **Changing views of the role of Langerhans** cells. J Invest Dermatol. 2012 Mar; 132(3Pt2):872-81. doi: 10.1038/jid.2011.437.Epub 2012 Jan 5. Review. PubMed PMID: 22217741.

136. Rosati P. and Colombo R. **I tessuti** edi-ermes (2003) 1,16-34

137. Rossi M, De Simone M, Pollice A, Santoro R, La Mantia G, Guerrini L, Calabrò V. **Itch/AIP4 associates with and promotes p63 protein degradation.** Cell Cycle. 2006 Aug;5(16):1816-22. Epub 2006 Aug 15. PubMed PMID: 16861923.

138. Sakura H, Maekawa T, Imamoto F, Yasuda K, Ishii S. **Two human genes isolated by a novel method encode DNA-binding proteins containing a common region of homology**. Gene. 1988 Dec 20;73(2):499-507. PubMed PMID: 2977358.

139. Samuel, S., Beifuss, K. K. and Bernstein, L. R. (2007) **YB-1 binds to the MMP-13 promoter sequence and represses MMP-13 transactivation via the AP-1 site.** Biochim. Biophys. Acta **1769**, 525-531

140. Schittek B, Psenner K, Sauer B, Meier F, Iftner T, Garbe C. **The increased expression of Y box-binding protein 1 in melanoma stimulates proliferation and tumor invasion, antagonizes apoptosis and enhances chemoresistance**. Int J Cancer. 2007 May 15;120(10):2110-8

141. Selivanova OM, Guryanov SG, Enin GA, Skabkin MA, Ovchinnikov LP, Serdyuk IN. **YB-1 is capable of forming extended nanofibrils**. Biochemistry (Mosc). 2010 Jan;75(1):115-20. PubMed PMID: 20331432.

142. Seton-Rogers, S. (2012) **Therapeutics: siRNAs jump the hurdle**. Nat. Rev. Cancer **12**, 376-377

143. Shen, H., Xu, W., Luo, W., Zhou, L., Yong, W., Chen, F., Wu, C., Chen, Q. and Han, X. (2011) **Upregulation of mdr1 gene is related to activation of the MAPK/ERK signal transduction pathway and YB-1 nuclear translocation in B-cell lymphoma.** Exp. Hematol. **39**, 558-569

144. Shibahara K, Uchiumi T, Fukuda T, Kura S, Tominaga Y, Maehara Y, Kohno K, Nakabeppu Y, Tsuzuki T, Kuwano M. **Targeted disruption of one allele of the Y-box binding protein-1 (YB-1) gene in mouse embryonic stem cells and increased sensitivity to cisplatin and mitomycin C.** Cancer Sci. 2004 Apr;95(4):348-53. PubMed PMID: 15072594.

145. Shumrick K A, Coldiron B. **Genetic syndromes associated with skin cancer.** Otolaryngol Clin North Am. 1993;26:117–137

146. Sinnberg T, Sauer B, Holm P, Spangler B, Kuphal S, Bosserhoff A, Schittek B. **MAPK and PI3K/AKT mediated YB-1 activation promotes melanoma cell proliferation which is counteracted by an autoregulatory loop**. Exp Dermatol. 2012 Apr;21(4):265-70. doi: 10.1111/j.1600-0625.2012.01448.x. PubMed PMID: 22417301.

147. Skabkin MA, Kiselyova OI, Chernov KG, Sorokin AV, Dubrovin EV, Yaminsky IV, Vasiliev VD, Ovchinnikov LP. **Structural organization of mRNA complexes with major core mRNP protein YB-1**. Nucleic Acids Res. 2004 Oct 19;32(18):5621-35. Print 2004. PubMed PMID: 15494450; PubMed Central PMCID: PMC524299.

148. Song MS, Salmena L, Pandolfi PP. **The functions and regulation of the PTEN tumour suppressor.** Nat Rev Mol Cell Biol. 2012 Apr 4;13(5):283-96. doi:10.1038/nrm3330. Review. PubMed PMID: 22473468.

149. Stein U, Jürchott K, Walther W, Bergmann S, Schlag PM, Royer HD. **Hyperthermia-induced nuclear translocation of transcription factor YB-1 leads to enhanced expression of multidrug resistance-related ABC transporters**. J Biol Chem. 2001 Jul 27;276(30):28562-9. Epub 2001 May 21. PubMed PMID: 11369762

150. Steinert PM **Structure, function and dynamics of keratin intermediate filamaments** J Invest Dermatol, 100 (1993), pp. 729–734

151. Stratford, A. L., Fry, C. J., Desilets, C., Davies, A. H., Cho, Y. Y., Li, Y., Dong, Z., Berquin, I. M., Roux, P. P. and Dunn, S. E. (2008) **Y-box binding protein-1**

serine 102 is a downstream target of p90 ribosomal S6 kinase in basal-like breast cancer cells. Breast Cancer Res. **10**, R99

152. Sugo N, Niimi N, Aratani Y, et al. **Decreased PARP-1 levels accelerate embryonic lethality but attenuate neuronal apoptosis in DNA polymerase β-deficient mice**.BiochemBiophys Res Commun. 2007 Mar 16;354(3):656–661.

153. Sutherland BW1, Kucab J, Wu J, Lee C, Cheang MC, Yorida E, Turbin D, Dedhar S, Nelson C, Pollak M, Leighton Grimes H, Miller K, Badve S, Huntsman D, Blake-Gilks C, Chen M, Pallen CJ, Dunn SE**. Akt phosphorylates the Y-box binding protein 1 at Ser102 located in the cold shock domain and affects the anchorage-independent growth of breast cancer cells**. *Oncogene. 2005 Jun 16;24(26):4281-92***.**

154. Thanos CD, Bowie JU. **p53 Family members p63 and p73 are SAM domain-containing proteins**.Protein Sci. 1999 Aug;8(8):1708-10. PubMed PMID: 10452616; PubMed Central PMCID: PMC2144426.

155. To K, Fotovati A, Reipas KM,. Law JH, Hu K, Wang J, Astanehe A, Davies AH, Lee L, Stratford A L, Raouf A, Johnson P, Berquin IM, Royer HD, Eaves CJ, Dunn SE,**YB-1 induces expression of CD44 and CD49f leading to enhanced self-renewal, mammosphere growth, and drug resistance** *Cancer Res. 2010 April 1; 70(7): 2840–2851. doi:10.1158/0008-5472.CAN-09-3155*

156. Toh S, Nakamura T, Ohga T, Koike K, Uchiumi T, Wada M, Kuwano M, Kohno K. **Genomic organization of the human Y-box protein (YB-1) gene**. Gene. 1998 Jan 5;206(1):93-7. PubMed PMID: 9461420*.*

157. Troiano A, Lomoriello IS, di Martino O, Fusco S, Pollice A, Vivo M, La Mantia G, Calabrò V. **Y-Box binding protein-1 is part of a complex molecular network linking ΔNp63α to the PI3K/AKT pathway in cutaneous squamous cell carcinoma.** J Cell Physiol. 2015 Jan 29. doi: 10.1002/jcp.24934. [Epub ahead of print] PubMed PMID: 25639555.

158. Truong AB, Kretz M, Ridky TW, Kimmel R, Khavari PA. **p63 regulates proliferation and differentiation of developmentally mature keratinocytes**. Genes Dev. 2006 Nov 15;20(22):3185-97. PubMed PMID: 17114587; PubMed Central PMCID:PMC1635152.

159. Tuhkanen AL, Agren UM, Tammi MI, Tammi RH. **CD44 expression marks the onset of keratinocyte stratification and mesenchymal maturation into fibrous dermis in fetal human skin.** J Histochem Cytochem. 1999 Dec;47(12):1617-24. PubMed PMID: 10567445.

160. Uchiumi T, Fotovati A, Sasaguri T, Shibahara K, Shimada T, Fukuda T, Nakamura T, Izumi H, Tsuzuki T, Kuwano M, Kohno K. **YB-1 is important for an early stage embryonic development: neural tube formation and cell proliferation.** J Biol Chem. 2006 Dec 29;281(52):40440-9. Epub 2006 Nov 2. PubMed PMID: 17082189

161. van Bokhoven H, Hamel BC, Bamshad M, Sangiorgi E, Gurrieri F, Duijf PH, Vanmolkot KR, van Beusekom E, van Beersum SE, Celli J, Merkx GF, Tenconi R, Fryns JP, Verloes A, Newbury-Ecob RA, Raas-Rotschild A, Majewski F, Beemer FA, Janecke A, Chitayat D, Crisponi G, Kayserili H, Yates JR, Neri G, Brunner HG. **p63 Gene mutations in eec syndrome, limb-mammary syndrome, and isolated split hand-split foot malformation suggest a genotype-phenotype**

correlation. Am J Hum Genet. 2001 Sep;69(3):481-92. Epub 2001 Jul 17. PubMed PMID: 11462173; PubMed Central PMCID: PMC1235479.

162. Vivanco I, Sawyers CL. **The phosphatidylinositol 3-Kinase AKT pathway in human cancer**. Nat Rev Cancer. 2002 Jul;2(7):489-501. Review. PubMed PMID: 12094235.

163. Wachowiak R, Thieltges S, Rawnaq T, Kaifi JT, Fiegel H, Metzger R, Quaas A, Mertens PR, Till H, Izbicki JR. **Y-box-binding protein-1 is a potential novel tumour marker for neuroblastoma**. Anticancer Res. 2010 Apr;30(4):1239-42. PubMed PMID: 20530434.

164. Weinberg WC, Denning MF. **P21Waf1 control of epithelial cell cycle and cell fate.** Crit Rev Oral Biol Med. 2002;13(6):453-64.Review. PubMed PMID: 12499239.

165. Weinstein MH, Signoretti S, Loda M. **Diagnostic utility of immunohistochemical staining for p63, a sensitive marker of prostatic basal cells**. Mod Pathol. 2002Dec;15(12):1302-8. PubMed PMID: 12481011.

166. Westfall MD, Mays DJ, Sniezek JC, Pietenpol JA. **The Delta Np63 alpha phosphoprotein binds the p21 and 14-3-3 sigma promoters in vivo and has transcriptional repressor activity that is reduced by Hay-Wells syndrome-derived mutations.** Mol Cell Biol. 2003 Apr;23(7):2264-76. PubMed PMID:12640112; PubMedCentral PMCID: PMC150720.

167. Yahata H, Kobayashi H, Kamura T, Amada S, Hirakawa T, Kohno K, Kuwano M, Nakano H. **Increased nuclear localization of transcription factor YB-1 in acquired cisplatin-resistant ovarian cancer**. J Cancer Res Clin Oncol. 2002 Nov;128(11):621-6. Epub 2002 Oct 22. PubMed PMID: 12458343.

168. Yang A, Kaghad M, Wang Y, Gillett E, Fleming MD, Dötsch V, Andrews NC, Caput D, McKeon F. **p63, a p53 homolog at 3q27-29, encodes multiple products with transactivating, death-inducing, and dominant-negative activities.** Mol Cell. 1998 Sep;2(3):305-16

169. Yang A., Schweitzer R., Sun D., Kaghad M., Walker N., Bronson et al. **p63 is essential for regenerative proliferation in limb, craniofacial and epithelial development**. Nature 1999; 398: 714-718

170. Yi R, Poy MN, Stoffel M, Fuchs E. **A skin microRNA promotes differentiation by repressing 'stemness'.** Nature. 2008 Mar 13;452(7184):225-9. doi:10.1038/nature06642. Epub 2008 Mar 2. PubMed PMID: 18311128; PubMed Central PMCID: PMC4346711.

171. Yun-Hsuan Ouyang, M.D. **Skin Cancer of the Head and Neck** Seminars In Plastic Surgery Volume 24, Number 2 2010

172. Zasedateleva OA, Krylov AS, Prokopenko DV, Skabkin MA, Ovchinnikov LP, Kolchinsky A, Mirzabekov AD. **Specificity of mammalian Y-box binding protein p50 in interaction with ss and ds DNA analyzed with generic oligonucleotide microchip.** J Mol Biol. 2002 Nov 15;324(1):73-87. PubMed PMID: 12421560.

LIST OF PUBLICATIONS

1. O. di Martino, **A. Troiano**, L. Addi, A. Guarino, S. Calabrò, R. Tudisco, N. Murru, M.I.Cutrignelli, F. Infascelli and V. Calabrò. "Regulation of Stearoyl Coenzyme A Desaturase 1 gene promoter in bovine mammary cells ***Animal Biotechnology 2015 in press.***
2. O. di Martino*, **A. Troiano***, A.M. Guarino, Alessandra Pollice, Maria Vivo, Girolama La Mantia, Viola Calabrò **"ΔNp63α protects YB-1 oncoprotein from proteasome-dependent proteolysis" Febs Letters** submitted January 2015.
3. Montariello D., **Troiano A.,** Di Girolamo D., Beneke S., Calabrò V., Quesada P. "Effect of poly(ADP-ribose) polymerase and DNA topoisomerase I inhibitors on the p53/p63-dependent survival of carcinoma cells". ***Biochem. Pharmacol. 2015*** Feb.6 DOI: 10.1016/j.bcp.2015.01.012. PMID: 25667043
4. **Troiano A**., Lomoriello IS., di Martino O., Fusco S., Pollice A., Vivo M., La Mantia G., Calabrò V. "Y-box binding protein-1 is part of a complex molecular network linking ΔNp63α to the PI3K/AKT pathway in cutaneous squamous cell carcinoma". ***J. Cell Physiol. 2015*** J Cell Physiol. 2015 Jan 29. doi: 10.1002/jcp.24934
5. Montariello D., **Troiano A**., Malanga M., Calabrò V., Quesada P. (2013) p63 involvement in poly(ADP-ribose) polymerase 1 signaling of topoisomerase I-dependent DNA damage in carcinoma cells. ***Biochem Pharmacol. 2013***; 85(7): 999-1006. doi: 10.1016/j.bcp.2013.01.019. Epub 2013 Jan 29.
6. Di Costanzo A, **Troiano A**, di Martino O, Cacace A, Natale CF, Ventre M, Netti P, Caserta S, Pollice A, La Mantia G, Calabrò V. The p63 protein isoform ΔNp63α modulates Y-box binding protein 1 in its subcellular distribution and regulation of cell survival and motility genes. **J Biol Chem. 2012** Aug 31;287(36):30170-80. doi: 10.1074/jbc.M112.349951. Epub 2012 Jul 11.

COMMUNICATIONS

- **A.Troiano**, O.di Martino, I. Schiano Lomoriello, M.Vivo, A. Pollice, G. La Mantia, V.Calabrò *YB-1 and ΔNp63α cross-talk in the control of squamous carcinoma cell adhesion and survival.* Oral Presentation at XIII FISV Congress – Pisa, Italy September 24-27, 2014
- Viola Calabro', Orsola di Martino, **Annaelena Troiano**, Irene Schiano Lomoriello, Maria Vivo, Alessandra Pollice, Girolama La Mantia. *Cooperation between YB-1 and deltaNp63alpha in the control of cell proliferation and survival*. abcd Congress Ravenna, Italy, September 2-14, 2013.
- Orsola di Martino, **Annaelena Troiano**, Irene Schiano Lomoriello, Daniela di Girolamo, Girolama La Mantia and Viola Calabrò. *DeltaNp63alpha and YB-1 functional interaction regulates proliferation and survival of normal and transformed keratinocytes*. AGI Congress - Cortona, Italy, September 25-27, 2013.
- **Troiano**, O.di Martino, A. Pollice, M.Ventre, C.Natale, G. La Mantia, V.Calabrò *The p63 protein as regulator of Y-box binding protein 1 subcellular distribution and functions.* XI FISV Congress - Roma, Italy, September 24-27, 2012
- O. di Martino, **A. Troiano**, A. Pollice, G. La Mantia, V. Calabrò *The ΔNp63α protein interacts with Y-box binding protein 1 and promotes its ubiquitination* XI FISV Congress - Roma, Italy, September 24-27, 2012

Queen Mary, University of London
Mile End Road, London, E1 4NS
T: +44 (0)20 7882 3697
F: +44 (0)20 7882 7033
www.qmul.ac.uk

Human Resources
www.hr.qmul.ac.uk

School of Medicine & Dentistry
www.smd.qmul.ac.uk

Mr Zubair Chopdat
HR Administrator
Email: z.chopdat@qmul.ac.uk

Ref: ZC/CE

18 June 2013

PRIVATE & CONFIDENTIAL
Dr Annaelena Troiano
Centre for Cutaneous Research
Blizard Institute
4 Newark Street
London
E1 2AT

Dear Dr Troiano,

RE: Application for Honorary Title

I am pleased to inform you that the recommendation that your application to be offered the title of Visiting Research Fellow in the Centre for Cutaneous Research within the Blizard Institute (within Barts & The London School of Medicine & Dentistry) Queen Mary University of London; has been approved.

You will hold this title with effect from 16 May 2013 until 13 December 2013. This is a non-stipendiary post. Further information about this honorary status is contained in the attached guidelines.

The title will remain effective whilst you are actively associated with the Blizard Institute and I should be grateful if you would inform me when this association ceases.

I should like to take this opportunity to thank you for the contribution you are making to the work of Queen Mary University of London.

Yours Sincerely,

Zubair Chopdat
HR Administrator

cc Kerry Newbury
Personal File

Gene Regulation:

The p63 Protein Isoform ΔNp63α Modulates Y-box Binding Protein 1 in Its Subcellular Distribution and Regulation of Cell Survival and Motility Genes

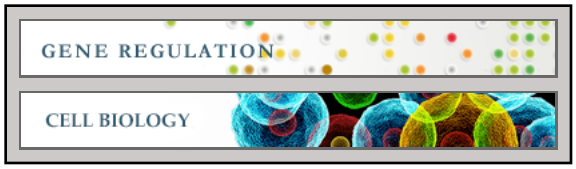

Antonella Di Costanzo, Annaelena Troiano, Orsola di Martino, Andrea Cacace, Carlo F. Natale, Maurizio Ventre, Paolo Netti, Sergio Caserta, Alessandra Pollice, Girolama La Mantia and Viola Calabrò

J. Biol. Chem. 2012, 287:30170-30180.
doi: 10.1074/jbc.M112.349951 originally published online July 11, 2012

THE JOURNAL OF BIOLOGICAL CHEMISTRY VOL. 287, NO. 36, pp. 30170–30180, August 31, 2012

The p63 Protein Isoform ΔNp63α Modulates Y-box Binding Protein 1 in Its Subcellular Distribution and Regulation of Cell Survival and Motility Genes*

Received for publication, February 5, 2012, and in revised form, July 9, 2012 Published, JBC Papers in Press, July 11, 2012, DOI 10.1074/jbc.M112.349951

Antonella Di Costanzo[‡], Annaelena Troiano[‡], Orsola di Martino[‡], Andrea Cacace[‡], Carlo F. Natale[§], Maurizio Ventre[§], Paolo Netti[§], Sergio Caserta[¶], Alessandra Pollice[‡], Girolama La Mantia[‡], and Viola Calabrò[‡1]

From the [‡]Department of Structural and Molecular Biology and [§]Center for Advanced Biomaterials for Health Care, Istituto Italiano di Tecnologia and Interdisciplinary Research Centre on Biomaterials, University of Naples "Federico II", Naples 80126 and the [¶]Department of Chemical Engineering, University of Naples "Federico II", Naples 80125, Italy

Background: YB-1 is a multifunctional protein that affects transcription, splicing, and translation.
Results: ΔNp63α, the main p63 protein isoform, interacts with YB-1 and affects YB-1 subcellular localization and regulation of cell survival and motility genes.
Conclusion: ΔNp63α and YB-1 interaction inhibits epithelial to mesenchymal transition and tumor cell motility.
Significance: This is the first demonstration of a physical and functional interaction between YB-1 and ΔNp63α oncoproteins.

The Y-box binding protein 1 (YB-1) belongs to the cold-shock domain protein superfamily, one of the most evolutionarily conserved nucleic acid-binding proteins currently known. YB-1 performs a wide variety of cellular functions, including transcriptional and translational regulation, DNA repair, drug resistance, and stress responses to extracellular signals. Inasmuch as the level of YB-1 drastically increases in tumor cells, this protein is considered to be one of the most indicative markers of malignant tumors. Here, we present evidence that ΔNp63α, the predominant p63 protein isoform in squamous epithelia and YB-1, can physically interact. Into the nucleus, ΔNp63α and YB-1 cooperate in *PI3KCA* gene promoter activation. Moreover, ΔNp63α promotes YB-1 nuclear accumulation thereby reducing the amount of YB-1 bound to its target transcripts such as that encoding the SNAIL1 protein. Accordingly, ΔNp63α enforced expression was associated with a reduction of the level of SNAIL1, a potent inducer of epithelial to mesenchymal transition. Furthermore, ΔNp63α depletion causes morphological change and enhanced formation of actin stress fibers in squamous cancer cells. Mechanistic studies indicate that ΔNp63α affects cell movement and can reverse the increase of cell motility induced by YB-1 overexpression. These data thus suggest that ΔNp63α provides inhibitory signals for cell motility. Deficiency of ΔNp63α gene expression promotes cell mobilization, at least partially, through a YB-1-dependent mechanism.

The Y-box binding protein 1 (YB-1), also known as NSEP1, CSBD, and MDR-NF1, is a member of the highly conserved Y-box family of proteins that regulate gene transcription by binding to the TAACC element (the Y-box) contained within many eukaryotic promoters (1). Transcriptional targets of YB-1 include genes associated with cell death, cell proliferation, and multidrug resistance (1, 2). YB-1 protein can also regulate gene transcription by binding to other transcription factors such as p53, AP1, and SMAD3 (2).

YB-1 is an important marker of tumorigenesis and is overexpressed in many malignant tissues, including breast cancer, non-small cell lung carcinoma, ovarian adenocarcinoma, human osteosarcomas, colorectal carcinomas, and malignant melanomas (1). Mostly cytosolic, YB-1 protein shuttles between the nucleus and cytoplasm. Cytoplasmic YB-1 acts as a translation factor of oncogenic/pro-metastatic genes (3). It binds to the mRNA cap structure and displaces the eukaryotic translation initiation factors eIF4E and eIF4G, thereby causing mRNA translational silencing (4). However, cytoplasmic YB-1 activates cap-independent translation of mRNA encoding SNAIL1, a transcription factor that promotes epithelial-mesenchymal transition by suppressing E-cadherin (5). According to those observations, the YB-1 protein level, in breast carcinoma, is positively correlated to the increase of SNAIL1 protein level and reduced expression of E-cadherin (6).

In normal conditions, YB-1 is located in the cytoplasm and transiently translocates to the nucleus at the G_1/S transition of the cell cycle (7). Moreover, nuclear translocation of YB-1 was shown to occur in response to DNA-damaging agents, phosphorylation at Ser-102 by AKT kinase, UV irradiation, TGFβ stimulation, virus infection, hypothermia, and pharmacological compounds (1, 8, 9). Under stress stimuli, YB-1 nuclear translocation requires a physical interaction with wild type p53 (10).

Herein, we report that YB-1 directly interacts with ΔNp63α and accumulates in the nuclear compartment. ΔNp63α is encoded by the *TP63* locus, a homologue of the p53 tumor suppressor gene and the most ancient member of the p53 family (11). Because of the presence of two promoters, the *TP63* gene encodes two major classes of proteins as follows: those containing a transactivating domain homologous to the one present in p53 (*i.e.* TAp63), and those lacking it (*i.e.* ΔNp63) (12). In addition, alternate splicing at the C terminus generates at least three p63 variants (α, β, and γ) in each class. The TAp63γ isoform

* This work was supported by MIUR Grant PRIN 2009KFS94X_003 (to V. C.).
[1] To whom correspondence should be addressed: Dept. Biologia Strutturale e Funzionale, Università Federico II, Via Cinzia Monte S Angelo, 80126 Napoli, Italy. Tel.: 39-081-679069; Fax: 39-081-679033; E-mail: vcalabro@unina.it.

resembles most p53, whereas the α-isoforms include a conserved protein-protein interaction domain named the sterile α motif.

Gene knock-out mice demonstrated that p63 plays a critical role in the morphogenesis of organs/tissues developed by epithelial-mesenchymal interactions such as the epidermis, teeth, hair, and glands (13). In adults, ΔNp63α expression occurs in the basal cells of stratified epithelia. High expression of ΔNp63α is associated with the proliferative potential of epithelial cells (14) and is enhanced at the early stages of squamous cell carcinomas (SCCs)[2] (15). Down-regulation of ΔNp63α by SNAIL transcription factor instead was found to reduce cell-cell adhesion and increase the migratory properties of squamous carcinoma cells (16). Moreover, a partial or complete loss of ΔNp63α expression was associated with tumor metastasis supporting the idea that ΔNp63α plays a relevant role in metastasis suppression (17, 18). Here, we provide experimental evidence that the YB-1 protein associates with ΔNp63α and such interaction plays a critical role in the control of genes involved in cell survival and motility.

EXPERIMENTAL PROCEDURES

Plasmids—cDNAs encoding human FLAG-tagged YB-1 were provided by Dr. Sandra Dunn (Research Institute for Children's and Women's Health, Vancouver, British Columbia, Canada). *PIK3CA* promoter luciferase plasmid was provided by Dr. Arezoo Astanehe (Research Institute for Children's and Women's Health, Vancouver, British Columbia, Canada). cDNA encoding human ΔNp63α and ΔNp63γ were previously described (19). For bacterial expression, ΔNp63γ and ΔNp63α cDNAs were inserted in pRSETA vector in XhoI/ClaI and XhoI/XbaI (filled) sites, respectively. GFP and YB-1-GFP vectors were provided by Dr. Paul R. Mertens (University Hospital Aachen, Germany). PET-YB-1 was from Dr. Jill Gershan (Medical College of Wisconsin, Milwaukee, WI).

Cell Lines, Transfection, and Antibodies—Squamous carcinoma cells (SCC011 and SCC022) were described previously and provided to us by Dr. C. Missero (20).

These cell lines were maintained in RPMI medium supplemented with 10% fetal bovine serum at 37 °C and 5% CO_2. A431, H1299, and MDA-MB-231 cells were obtained from ATCC and maintained in DMEM supplemented with 10% fetal bovine serum at 37 °C and 5% CO_2. Dox-inducible Tet-On H1299/ΔNp63α cells were described previously (21).

Lipofections were performed with Lipofectamine (Invitrogen), according to the manufacturer's recommendations. *YB-1* transient silencing was carried out with ON-TARGET plus SMART pool *YB-1*-siRNA (Dharmacon) and RNAiMAX reagent (Invitrogen). ΔNp63α transient silencing in SCC011 cells was carried out with RIBOXX (IBONI *p63*-siRNA pool) and RNAiMAX reagent (Invitrogen), according to the manufacturer's recommendation. An si-RNA against luciferase (si-Luc) was used as a negative control. Anti-p63 (4A4) and anti-actin(1–19) were from Santa Cruz Biotechnology Inc., and anti-FLAG M2 was from Sigma. PARP, AKT, pAKT (Ser-473) and rabbit polyclonal YB-1 antibody (Ab12148) were from Cell Signaling Technology (Beverly, MA). Mouse monoclonal E-cadherin (ab1416) and SNAIL1 antibodies were from Abcam (Cambridge, UK). Mouse monoclonal N-cadherin (610921) was from BD Transduction Laboratories. Cy3-conjugated anti-mouse IgG and Cy5-conjugated anti-rabbit IgG were from Jackson ImmunoResearch. Doxycycline was from Clontech.

Chromatin Immunoprecipitation (ChIP) Assay—ChIP was performed with chromatin from human MDA-MB-231 cells transfected with ΔNp63γ, ΔNp63α, and/or FLAG YB-1, as described previously (22). Real time PCR was performed with the 7500 Applied Biosystems apparatus and SYBR Green MasterMix (Applied Biosystems) using the following oligonucleotides: *PIK3CA*-For, CCCCCGAACTAATCTCGTTT, and *PIK3CA*-Rev, TGAGGGTGTTGTGTCATCCT.

Sequential ChIP was performed with chromatin from SCC011 cells. Method of chromatin extraction and controls used were previously described (22).

Chromatin samples were subjected to pre-clearing with 80 μl of salmon sperm DNA-saturated agarose A beads for 2 h at 4 °C with rotation. The first immunoprecipitation step was obtained with p63 antibodies (4A4). After several washes, the immunocomplexes were extracted from beads with 100 μl of 2% TE/SDS. The second immunoprecipitation step was obtained with YB-1 (Ab12148) antibodies after a 30-fold dilution in DB buffer (50 mM Tris-HCl, 5 mM EDTA, 200 mM NaCl, 0.5% Nonidet P-40, 15 mM DTT). Samples were incubated overnight at 4 °C with rotation. Immunocomplexes were extracted from beads as described above. Immunoprecipitated protein-DNA complexes were subjected to reverse cross-linking and proteinase K treatment. DNA was purified by phenol/chloroform extraction and resuspended in 40 μl of TE. 2 μl were used for PCR performed with the following primers: *PIK3CA* promoter For, ACAAACCCCTGGAATGTGAG, and *PI3KCA* promoter Rev, TGGAAAAGCGTAGGAGCAGT.

Immunoblot Analyses and Co-immunoprecipitation—Immunoblots and co-immunoprecipitations were performed as described previously (19). To detect p63/YB-1 interaction in SCC011 cells, 5.0×10^5 cells were plated in 60-mm dishes. For co-immunoprecipitations, whole cell extracts, precleared with 30 μl of protein A-agarose (50% slurry; Roche Applied Science), were incubated overnight at 4 °C with anti-YB-1(3 μg) or α-rabbit IgG (3 μg). The reciprocal experiment was performed with anti-p63 (2 μg) or α-mouse IgG.

Far Western Assays—Far Western assays were conducted according to the protocol described by Cui *et al.* (23). Increasing amounts (0.2, 0.5, and 1.5 μg) of ΔNp63α or ΔNp63γ recombinant proteins were subjected to SDS-PAGE and transferred to PVDF membrane (IPVH00010 Immobilon Millipore, Milan, Italy). Bovine serum albumin (0.5 and 1.5 μg; BSA) was used as control of unspecific binding and equal loading of BSA, and recombinant YB-1 or p63 proteins in far Western blotting was verified by Coomassie staining (data not shown).

Luciferase Reporter Assay—MDA-MB-231 cells were co-transfected with ΔNp63α, *PIK3CA* luc promoter, and pRL-TK. *YB-1* gene silencing was carried out 24 h before plasmid

[2] The abbreviations used are: SCC, squamous cell carcinoma; For, forward; Rev, reverse; PARP, poly(ADP-ribose) polymerase; Dox, doxycycline; TRITC, tetramethylrhodamine isothiocyanate; *S*, speed; *P*, persistence time; Ab, antibody; HPRT, hypoxanthine-guanine phosphoribosyltransferase.

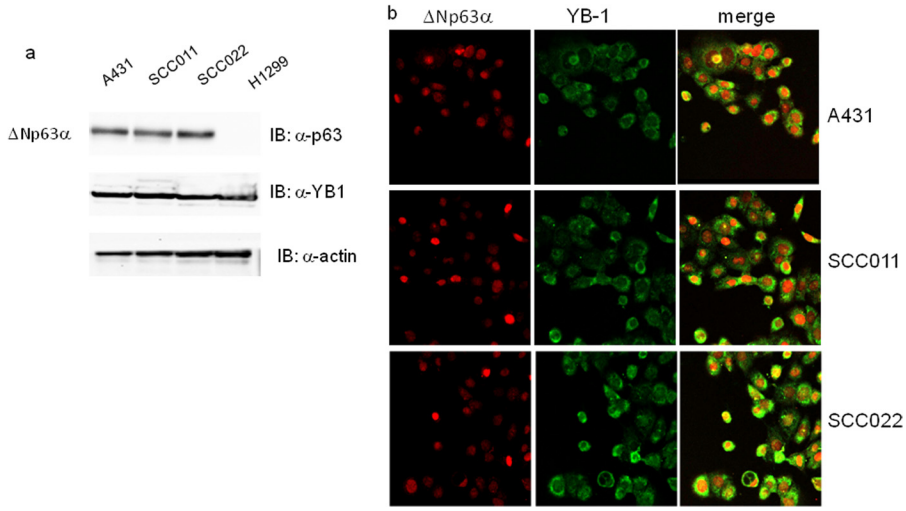

FIGURE 1. **ΔNp63α and YB-1 are co-expressed in squamous carcinoma cell lines.** *a,* whole cell lysates were obtained from H1299 (non-small cell lung carcinoma), A431 (epidermoid carcinoma cell line), and SCC011 and SCC022 (keratinocyte-derived SCC) cells. 30 μg of total protein extracts were separated by SDS-PAGE and subjected to immunoblot (*IB*). Proteins were detected with specific antibodies as indicated. Images were acquired with CHEMIDOC (Bio-Rad) and analyzed with the Quantity-ONE software. *b,* A431, SCC011, and SCC022 cells were seeded (2.5×10^5) on a 35-mm dish and grown on micro cover glasses (BDH). After 24 h at seeding, cells were fixed and subjected to double immunofluorescence using rabbit primary YB-1 antibody and Fitch-conjugated secondary antibodies (*green*). p63 protein was detected using mouse anti-p63 and Cy3-conjugated secondary antibodies (*red*). Images of merge (*yellow*) show the co-expression of two proteins.

transfection. At 24 h after transfection, cells were harvested in 1× PLB buffer (Promega), and luciferase activity was measured using the Dual-Luciferase Reporter system (Promega) using pRL-TK activity as internal control. Firefly-derived luciferase activity was normalized for transfection efficiency. Successful transfection of p63 and silencing of YB-1 was confirmed by immunoblotting.

RNA Immunoprecipitation—1×10^6 MDA-MB-231 cells were seeded in 100-mm plates and transfected with pcDNA3.1 or ΔNp63α expression plasmids. 24 h after transfection, cells were fixed with 1% formaldehyde for 10 min and washed twice in ice-cold PBS. Cell extracts were prepared in RNA immunoprecipitation buffer (0.1% SDS, 1% Triton, 1 mM EDTA, 10 mM Tris, pH 7.5, 0.5 mM EGTA, 150 mM NaCl) supplemented with complete protease inhibitor mixture (Sigma), and sonication was carried out with BANDELINE SONOPULSE HD2200 instrument under the following conditions: 8 pulses of 4 s at 0.250% of intensity. Cell extracts were incubated with anti-YB-1 (3 μg) at 4 °C overnight. The RNA-protein immunocomplexes were precipitated with protein A beads (Roche Applied Science) saturated with tRNA and, after reverse cross-link, subjected to real time PCR.

Semi-quantitative and Real Time PCR—For PCR analysis, total RNA was isolated using the RNA mini extraction kit (Qiagen, GmbH, Hilden, Germany) according to the manufacturer's instructions. Total RNA (1 μg) was used to generate reverse-transcribed cDNA using SuperScript III (Invitrogen). PCR analysis was performed with the following primers: *Twist* (For), 5′-AGAAGTCTGCGGGCTGTG, and *Twist* (Rev), ′-TCTGCAGCTCCTCGTAAGACT; *YB* (For), 5′-CGCAGTG-TAGGAGATGGAGAG, and *YB* (Rev), 5′-GAACACCACCA-GGACCTGTAA; and *HPRT* (For), 5′-CCT GCT GGA TTA CAT TAA AGC, and *HPRT* (Rev), 5′ CTT CGT GGG GTC CTT TTC.

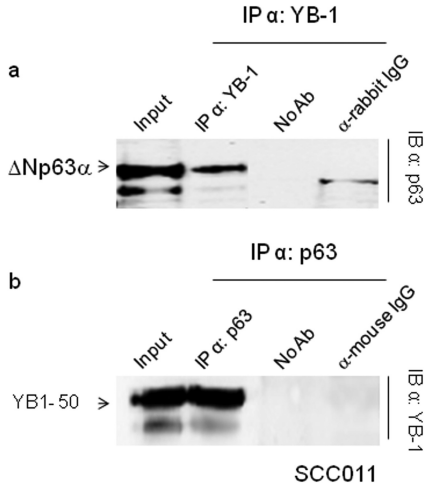

FIGURE 2. **ΔNp63α interacts with YB-1.** *a,* extracts from SCC011 cells were immunoprecipitated (*IP*) with anti-YB-1 antibodies, and the immunocomplexes were blotted and probed with anti-p63 as indicated. *b,* extracts from SCC011 cells were immunoprecipitated with anti-p63 antibodies, and the immunocomplexes were blotted and probed with anti-YB-1. Samples with no antibody (*no Ab*) or irrelevant α-mouse and α-rabbit antibodies were included as controls. *IB*, immunoblot.

SNAIL1 amplification was performed using Quantitect Primers/Hs *SNAIL1* from Qiagen (GmbH, Hilden, Germany). The amplification sequence consisted of 30 cycles of 94 °C for 1 min, 55 °C for 1min, and 72 °C for 1 min. PCR products were resolved by 2% agarose electrophoresis. RT-PCR amplification results were analyzed by Quantity One software (Bio-Rad). Real time PCR was performed with a 7500 RT-PCR Thermo Cycler (Applied Biosystem) as already described (22). *HPRT* was used for normalization. The results were expressed with the value relative to *HPRT* (set at 1) for each mRNA sample.

Immunofluorescence—A431, SCC011, and SCC022 cells (2.5×10^5) were plated in 35-mm dishes and grown on micro cover glasses (BDH). 24 h after seeding, cells were washed with cold phosphate-buffered saline (PBS) and fixed with 4% para-

formaldehyde (Sigma) for 15 min at 4 °C. Cells were permeabilized with ice-cold 0.1% Triton X-100 for 10 min and then washed with PBS. p63 was detected using a 1:200 dilution of the monoclonal antibody 4A4.

YB-1 was detected using 1:100 dilution of the YB-1 antibody (Ab12148). After extensive washing in PBS, the samples were incubated with Cy3-conjugated anti-mouse IgGs and Cy5-conjugated anti-rabbit IgGs at room temperature for 30 min. After PBS washing, the cells were incubated with 10 mg/ml 4′,6′-diamidino-2-phenylindole (DAPI) (Sigma) for 3 min. The glasses were mounted with Moviol (Sigma) and examined under a fluorescence microscope (Nikon). Images were digitally acquired and processed using Adobe Photoshop software CS.

H1299 and MDA-MB-231 cells (5.0×10^5) were plated in 35-mm dishes, grown on micro cover glasses (BDH), and transfected with 0.2 μg of pcDNAYB-1/GFP plasmid with or without 0.6 μg of ΔNp63α or ΔNp63γ plasmid. The GFP empty vector was used as control (data not shown). 24 h after transfection, cells were subjected to the immunofluorescence protocol as described above.

Cytoskeleton Analysis—Actin bundles were stained with TRITC-conjugated phalloidin. Cell fixation was performed with 4% paraformaldehyde for 20 min and then permeabilized with 0.1% Triton X-100 (Sigma) in PBS one time for 10 min. Actin staining was done by incubating sample with TRITC-phalloidin (Sigma) in PBS for 30 min at room temperature. Images of fluorescent cells were collected with a fluorescent inverted microscope (IX81, Olympus, Tokyo, Japan) equipped with an ORCA 2.8 digital camera (Hamamatsu Photonics, Japan).

Time-lapse Microscopy—SCC011 cells were cultured on 35-mm dishes (Corning, NY) at 2×10^4 cells/dish density. ΔNp63α transient silencing was performed as described under "Experimental Procedures." At 48 h from the addition of ΔNp63α si-RNA, the culture dishes were placed in a mini-incubator connected to an automated stage of an optical microscope (Olympus Co., Japan). Images of selected positions of the cell culture were collected in bright field every 10 min for 12 h. The bright field images were mounted to obtain 72-frame time lapse video for each position. Cell trajectories were reconstructed from time lapse video using Metamorph software (Molecular Device, CA). Root mean square speed (*S*) and persistence time (*P*) were chosen as relevant parameters to describe the macroscopic features of cell migration in the different experimental conditions. These parameters were calculated according to the procedure reported by Dunn (24). Briefly, mean-squared displacement of each cell was calculated according to overlapping time interval methods (25). Subsequently, *S* and *P* were estimated by fitting the experimental data of the mean-squared displacement to a linear approximation of the persistent random walk model. The upper limit for the data fitting was set at approximately 200 min for each cell because of the deviation from linearity that was observed at higher time points. The fitting procedure provided (*S*, *P*) pairs for each cell and the statistical significance between *S* and *P* values of the different experimental setups was assessed by performing a nonparametric Kruskal-Wallis test in Matlab (MathWorks, MA). p values < 0.05 were considered significant.

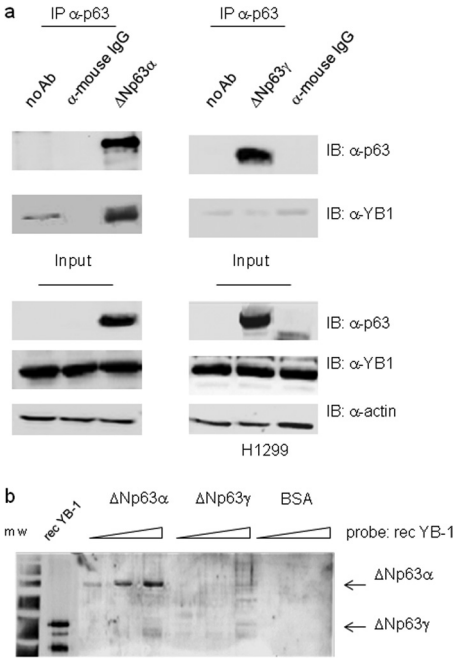

FIGURE 3. **ΔNp63α but not ΔNp63γ interacts with YB-1.** *a,* H1299 cells were transiently transfected with 5 μg of ΔNp63α (*left panel*) or ΔNp63γ (*right panel*) expression vectors. Equal amounts (1 mg) of extracts were immunoprecipitated (*IP*) with anti-p63 antibodies (4A4) or unrelated α-mouse IgG. The immunocomplexes were blotted and probed with anti-p63 and anti-YB-1 antibodies, as indicated. *b,* far Western analysis. Increasing amounts of purified recombinant ΔNp63α (0.2, 0.5, and 1.5), ΔNp63γ (0.2, 0.5, and 1.5), or BSA (0.5 and 1.5) were subjected to SDS-PAGE. After Coomassie staining to monitor equal loading, the proteins were transferred to a PVDF membrane, and the filter was incubated with purified YB-1 recombinant protein (0.8 μg/ml). After extensive washing, the membrane was subjected to immunoblotting (*IB*) with YB-1 antibodies followed by ECL detection. Recombinant YB-1 protein (0.1 μg) was used as positive control. *m.w.,* molecular weight markers.

Cell migration in H1299 cells was evaluated with a similar approach. Briefly, cells were cultured on 35-mm dishes (Corning, NY) at a density of 2×10^4 cells/dish. ΔNp63α expression was induced with 2 μg/ml doxycycline for 48 h. 16 h after transfection, cell dishes were placed in a mini-incubator connected to an automated stage of an optical microscope (Cell[caret]R, Olympus Co., Japan). Time 0 images of selected position were collected in fluorescence to localize transfected cells. Then, at the same positions, images were recorded in bright field every 10 min for 12 h. Data analysis was performed as described above.

RESULTS

YB-1 Interacts with ΔNp63α in Vitro and in Vivo—As a result of a comprehensive screening for ΔNp63α interactors, using affinity purification followed by mass spectrometry, we identified a set of proteins with DNA/RNA binding activity, including YB-1 (26). We decided to confirm the interaction between ΔNp63α and YB-1 in SCC as in this cellular context the *TP63* gene is often amplified and/or overexpressed (27). Immunoblots and immunofluorescence assays performed in A431, SCC022, and SCC011 cell lines showed intense signals for both proteins thus confirming that endogenous YB-1 and ΔNp63α are abundantly co-expressed in human squamous carcinoma cells (Fig. 1, *a* and *b*).

We next performed co-immunoprecipitation experiments in SCC011 cells. Immunocomplexes containing ΔNp63α and

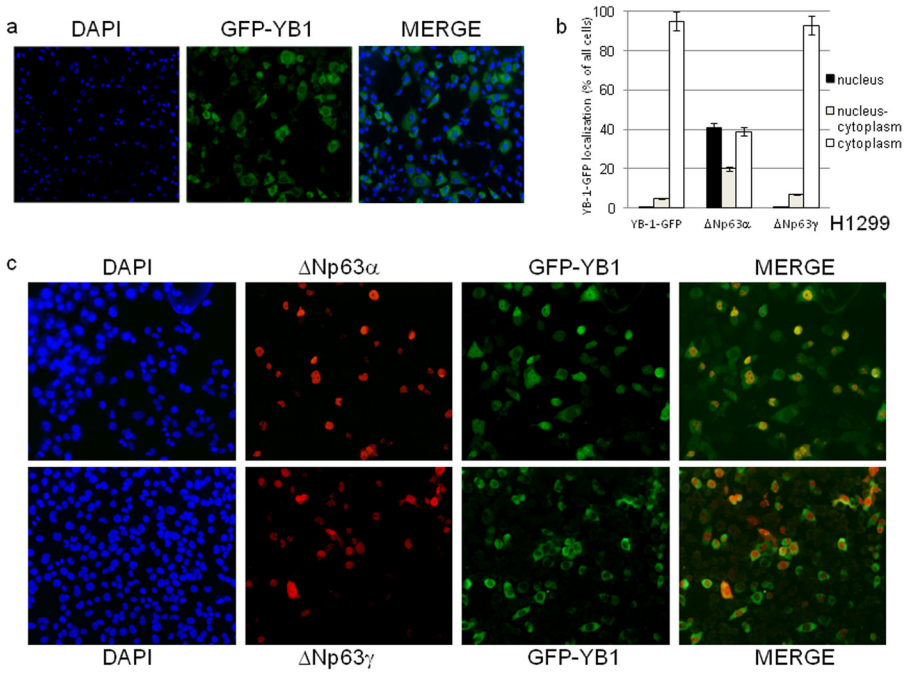

FIGURE 4. **ΔNp63α induces YB-1 nuclear accumulation.** *a*, H1299 cells (2.3×10^5) were seeded at 60% confluency in 24 × 24-mm sterile coverglasses placed in 60-mm dishes and transiently transfected with GFP-YB-1 expression vector (0.3 μg). GFP-YB-1 was detected by direct immunofluorescence. *b*, H1299 cells (2.3×10^5) were seeded as described in *a* and transiently transfected with GFB-YB-1 (0.3 μg) along with 1 μg of ΔNp63α or ΔNp63γ expression vectors. Plot shows the percentage of nuclear (*dark gray*), nucleo-cytoplasmic (*gray*), and cytoplasmic (*white*) GFP-YB-1 in cells transfected with ΔNp63α or ΔNp63γ expression vectors. Each experimental point is the average of counts performed on 100 cells in five independent fields. Each *histogram bar* represents the mean and standard deviation of values from three biological replicates. *c*, H1299 cells (2.3×10^5) were transfected as described in *b*. GFP-YB-1 was detected by direct immunofluorescence (*green*), and p63 was detected using anti-p63 antibodies and secondary anti-mouse Cy3-conjugated (*red*). DAPI was used to stain nuclei.

YB-1 were isolated from total cell lysates, using either antibodies against YB-1 or antibodies against p63 thus confirming the interaction inferred by mass spectrometry (Fig. 2, *a* and *b*). To determine whether YB-1 interacts specifically with the α-isoform of ΔNp63, we transfected p63 null H1299 cells with ΔNp63α or ΔNp63γ to perform co-immunoprecipitation assays. As shown in Fig. 3*a*, YB-1 associates with ΔNp63α but not ΔNp63γ. This result was also confirmed by far Western blot analysis using ΔNp63α, ΔNp63γ, and YB-1 recombinant proteins purified by affinity chromatography (Fig. 3*b*). The obtained results indicate that the α-isoform C-terminal region is involved in the association with YB-1, and the interaction between the two proteins requires no additional factors.

ΔNp63α Induces YB-1 Nuclear Accumulation—It has been reported that YB-1 is ubiquitously expressed and predominantly localized to the cytoplasm (2), ΔNp63α is mainly expressed by basal and myoepithelial cells in skin and glands and is almost completely restricted to the nuclear compartment (29). Because we noticed some overlapping between the p63 and YB-1 immunofluorescence signals in the nucleus of squamous carcinoma cell lines, we sought to determine whether ΔNp63α has an effect on YB-1 subcellular localization. Fusion of YB-1 with the green fluorescent protein (YB-1-GFP) was transfected in H1299 cells. H1299 cells are p63 null and express moderate levels of endogenous YB-1. GFP-positive cells were counted, and 95% showed a strong cytoplasmic signal, although in the remaining 5%, the signal was nuclear or distributed between the nucleus and cytoplasm (Fig. 4, *a* and *b*). A very similar result was observed following ΔNp63γ co-transfection (Fig. 4, *b* and *c*, *lower panel*). Remarkably, combined expression of YB-1-GFP and ΔNp63α caused a dramatic change of YB-1-GFP subcellular localization. In fact, among the GFP-positive cells, more than 40% showed an intense nuclear signal (Fig. 4, *b* and *c*, *upper panel*); an additional 20% exhibited YB-1-GFP almost equally distributed between the nucleus and cytoplasm, and the remaining 40% exhibited exclusively cytoplasmic YB-1-GFP (Fig. 4*b*). As expected, ΔNp63α and ΔNp63γ immunofluorescence signals were almost exclusively nuclear (Fig. 4*c*).

ΔNp63α is a selective nuclear marker of human breast myoepithelial cells. ΔNp63α persists in benign lesions of the breast, although it consistently disappears in invasive carcinomas (30). We transfected ΔNp63α in MDA-MB-231 cells, human metastatic breast carcinoma cells lacking p63 but expressing high level of endogenous YB-1. As shown in Fig. 5, in cells with no detectable p63 signal, YB-1 exhibited a largely prevalent cytoplasmic localization (Fig. 5*a*, *white arrows*), although 95% of ΔNp63α-expressing cells showed a strong YB-1 nuclear staining (Fig. 5*a*, *yellow arrows*). We verified this observation by nuclear/cytoplasmic fractionation of MDA-MB-231 cells transfected with ΔNp63α or ΔNp63γ. Endogenous YB-1 protein, in MDA-MB-231 cells, was detectable as 50- and 36-kDa immunoreactive forms. Both forms of YB-1 appear to accumulate in the nuclear compartment of cells transfected with ΔNp63α but not ΔNp63γ (Fig. 5*b*). Immunoblots with antibodies against PARP-1 (nuclear) and AKT (cytoplasmic) were performed to check for the quality of the fractionation. Interestingly, although the amount of total AKT was comparable, phosphorylated AKT, at serine 473, was enhanced in ΔNp63α but not ΔNp63γ-transfected cells (Fig. 5*b*). This observation was in line with previous data showing the specific

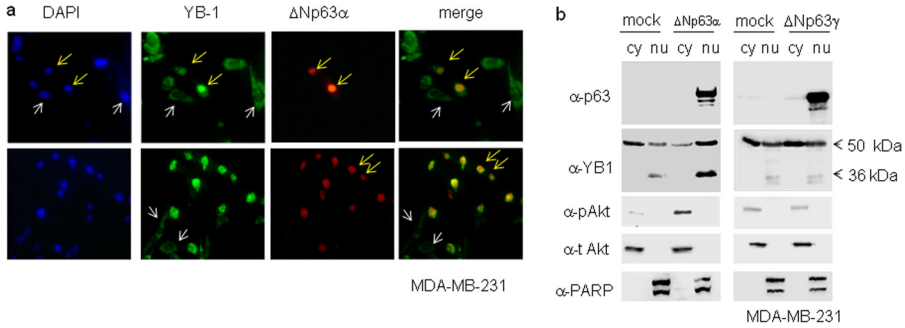

FIGURE 5. **Endogenous YB-1 accumulates in the nucleus of breast cancer cells expressing ΔNp63α.** *a,* MDA-MB-231 cells were seeded at 60% confluency (2.3×10^5) on 24 × 24-mm sterile coverglasses placed in 60-mm dishes and transiently transfected with 1 μg of ΔNp63α expression vector. Cells were fixed and subjected to double indirect immunofluorescence using rabbit primary YB-1 antibody and Fitch-conjugated secondary antibodies (*green*). p63 protein was detected using mouse anti-p63 and Cy3-conjugated secondary antibodies (*red*). DAPI was used to stain nuclei (*blue*). A representative image is given of a cell expressing ΔNp63α and showing nuclear endogenous YB-1 (*yellow arrows*). A representative image is given showing YB-1 cytoplasmic localization in cells bearing no detectable ΔNp63α expression (*white arrows*). *b,* MB-MDA-231 cells were transiently transfected with a fixed amount (5 μg) of an empty vector (*mock*) and ΔNp63α or ΔNp63γ expression vector in 100-mm dishes. 24 h after transfection, cell lysates were fractionated to obtain cytoplasmic (*cy*) and nuclear (*nu*) fractions. 20 μg of nuclear and cytoplasmic extracts were separated by SDS-PAGE and subjected to immunoblot. Proteins were detected with specific antibodies, as indicated. PARP and total AKT were used as nuclear and cytoplasmic controls, respectively, to check for cross-contamination. Images were acquired with CHEMIDOC (Bio-Rad) and analyzed with the Quantity-ONE software.

ability of the ΔNp63α isoform to promote PI3K/AKT pathway activation (31).

We then evaluated the contribution of ΔNp63α to YB-1 subcellular distribution in SCC011 cells expressing both proteins endogenously. To this aim we analyzed YB-1 subcellular distribution by immunoblot on nuclear/cytoplasmic fractions after depletion of ΔNp63α by siRNA. As shown in Fig. 6, *a* and *b*, following p63 knockdown the YB-1 nuclear pool was dramatically reduced, and the 36-kDa form of YB-1 became detectable (Fig. 6*a*).

ΔNp63α and YB-1 Bind to the PIK3CA Gene Promoter and Cooperate in Its Transcriptional Activation—The *PIK3CA* gene encodes the p110α catalytic subunit of the PI3K and is a well characterized YB-1 direct transcriptional target (32). We speculated that ΔNp63α should increase PIK3CA promoter activity because of its ability to cause YB-1 nuclear accumulation. We tested this hypothesis by luciferase assays. As shown in Fig. 7*a*, ΔNp63α transfection in MDA-MB-231 cells caused a relevant increase of the *PIK3CA* promoter activity that was consistently attenuated by YB-1 knockdown. In addition, we observed that ΔNp63α was able to transactivate the *PIK3CA* promoter in a dose-dependent manner, although ΔNp63γ was completely ineffective (Fig. 7*b*).

The role of ΔNp63α and YB-1 in *PIK3CA* promoter activation was thoroughly investigated by chromatin immunoprecipitation (ChIP). We first performed ChIP assays in MDA-MB-231 cells transfected with ΔNp63α or ΔNp63γ using anti-p63 (4A4) antibodies and PIK3CA promoter-specific primers. As shown in Fig. 8*a*, ΔNp63α, but not ΔNp63γ, binds to the genomic sequence of the *PIK3CA* promoter.

Then we evaluated the effect of ΔNp63α expression on the binding of YB-1 to the *PIK3CA* promoter. FLAG-YB-1 was transfected, in MB-MDA-231 cells, with or without ΔNp63α plasmid. ChIP was carried out with anti-FLAG antibodies and coupled with quantitative real time PCR. As show in Fig. 8*b*, FLAG-YB-1 efficiently binds to the *PIK3CA* promoter, and its binding was substantially increased by ΔNp63α. Finally, by using a sequential chromatin immunoprecipitation assay (Re-ChIP) in SCC011 cells, expressing endogenous ΔNp63α and YB-1, we found that both proteins are recruited to the *PIK3CA*

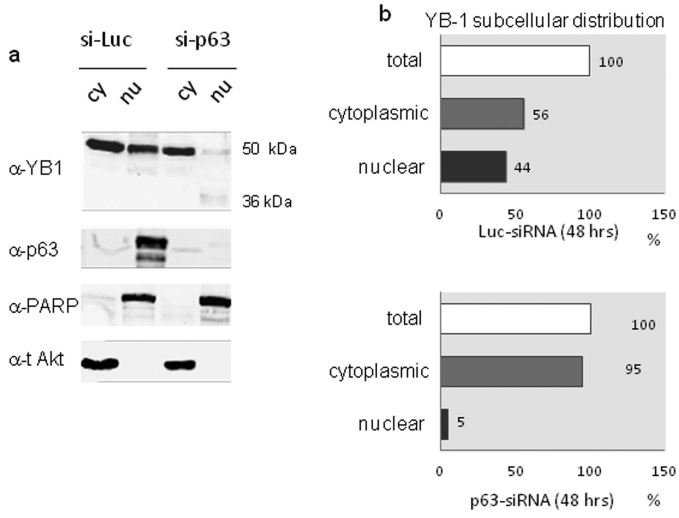

FIGURE 6. **ΔNp63α depletion reduces the pool of nuclear YB-1.** *a,* SCC011 cells were seeded at 60% confluency (1.5×10^6) in 100-mm dishes. 24 h after seeding, cells were transiently silenced with IBONI p63-siRNA pool (20 nm final concentration). 48 h after p63-silencing, cell lysates were fractionated to obtain cytoplasmic (*cy*) and nuclear (*nu*) fractions. Nuclear and cytoplasmic extracts were separated by SDS-PAGE and subjected to immunoblot. Proteins were detected with specific antibodies, as indicated. PARP and total AKT were used as nuclear and cytoplasmic control respectively, to check for cross-contamination. Images were acquired with CHEMIDOC (Bio-Rad) and analyzed with the Quantity-ONE software. *b,* plots show the percentage of YB-1 subcellular distribution in control sample (*upper panel*) and in p63-silenced sample (*lower panel*) considering the total amount of YB-1 between the nucleus and cytoplasm as 100%.

proximal promoter suggesting that they cooperate in *PIK3CA* gene transactivation as a complex (Fig. 8*c*).

ΔNp63α Affects YB-1 Binding to SNAIL and YB-1 mRNAs—Cytoplasmic localization of YB-1 was associated with binding and translational activation of *SNAIL1* mRNA (33). Snail1 protein is a transcriptional repressor of ΔNp63α and E-cadherin and promotes the epithelial-mesenchymal transition in several epithelium-derived cancer cell lines (34). We first observed that ΔNp63α overexpression in MB-MDA-231 caused a reduction of SNAIL1 protein level (Fig. 9*a*). Such a reduction was not associated with a decrease of *SNAIL1* mRNA levels (Fig. 9*b*) thereby suggesting that the SNAIL1 protein was down-regulated at the translational level. We hypothesized that the spe-

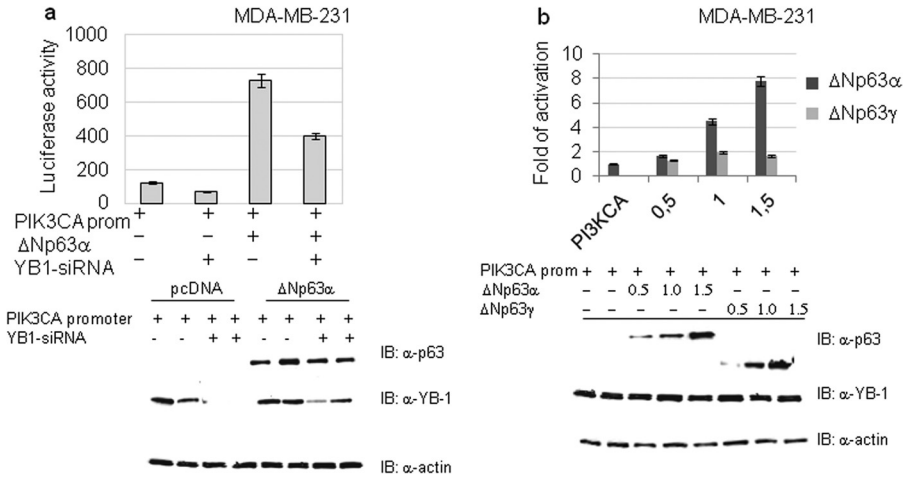

FIGURE 7. **ΔNp63α and YB-1 activates the *PIK3CA* gene promoter.** *a,* MB-MDA− cells were transfected with 1 μg of *PIK3CA* promoter luciferase reporter plasmid. The luciferase activity upon siRNA-mediated knockdown of endogenous YB-1 was measured in the presence or absence of ΔNp63α expression. Values are shown as mean ± S.D. of three biological replicates. The extent of YB-1 knockdown was documented by Western blotting as shown in the *lower panel*. *b,* MB-MDA-231 cells were seeded at 60% confluency (1.2×10^6) in 100-mm dishes and transiently transfected with 1 μg of *PIK3CA* promoter luciferase reporter plasmid and the indicated amounts of ΔNp63α or ΔNp63γ plasmid. Values are the mean ± S.D. of three independent experimental points. *Lower panel,* immunoblotting (*IB*) with indicated antibodies to detect proteins in samples transfected with different amounts of ΔNp63α or ΔNp63γ.

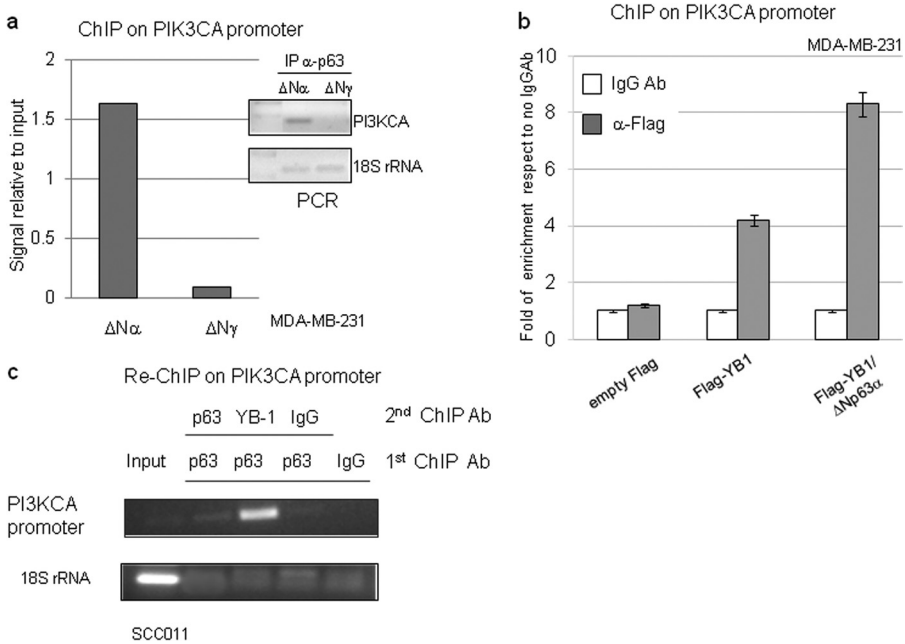

FIGURE 8. **ΔNp63α increases YB-1 binding to the *PIK3CA* gene promoter.** *a,* MDA-MB-231 cells were seeded at 60% confluency (1.2×10^6) in 100-mm dishes and transiently transfected with ΔNp63α or ΔNp63γ plasmid (5 μg). After formaldehyde cross-linking, the DNA-proteins complexes were immunoprecipitated (*IP*) with anti-p63 (4A4) antibody. Immunoprecipitated DNA was PCR-amplified with *PIK3CA* promoter oligonucleotides and 18 S rRNA oligonucleotides (*right*). The data obtained from the ChIP assay were measured by densitometry and are presented as signal relative to the input (*left*). *b,* MDA-MB-231 cells were seeded at 60% confluency (1.2×10^6) in 100-mm dishes and transiently transfected with 3×FLAG empty vector or 3×FLAG-YB-1 (5 μg) plasmid with or without ΔNp63α (2.5 μg) expression vector. The cells were cross-linked with formaldehyde, and DNA-protein complexes were immunoprecipitated with anti-FLAG antibody or irrelevant IgG antibody as negative control. The DNA immunoprecipitates were analyzed by quantitative PCR using *PIK3CA* or *GAPDH* promoter oligonucleotides. Quantitative RT-PCR results were analyzed with the $\Delta\Delta C^T$ method and expressed as fold of enrichment with respect to the IgGAb control samples. Values are represented as the mean of three independent experiments. *c,* SCC011 cells at 85% confluency were fixed with formaldehyde, and the DNA-protein complexes were subjected to sequential ChIP with anti-p63 (4A4), anti-YB-1(Ab12148), or irrelevant IgG antibody as described under "Experimental Procedures." Immunoprecipitated DNA was PCR-amplified with *PIK3CA* promoter primers and 18 S rRNA primers to check the quality of the input chromatin and the cleaning of the other samples.

cific association of ΔNp63α with YB-1 would reduce the amount of YB-1 bound to the *SNAIL1* transcript. To test this hypothesis, we performed RNA-immunoprecipitation coupled with real time PCR to quantitate the amount of *SNAIL1* mRNA bound to endogenous YB-1, in mock and ΔNp63α-transfected MDA-MB-231 cells. The obtained results confirm that ΔNp63α reduces the amount of YB-1 bound to *SNAIL1* transcript (Fig. 9*c*). A similar analysis performed on the *YB-1* transcript gave the same result (Fig. 9*d*).

ΔNp63α Affects Cell Shape and Motility—So far, little attention has been focused on the effects of ΔNp63α on epithelial cancer cell morphology and motility. We have unexpectedly noted a profound change in cell morphology when SCC011 cells were depleted of ΔNp63α by siRNA. SCC011 cells are

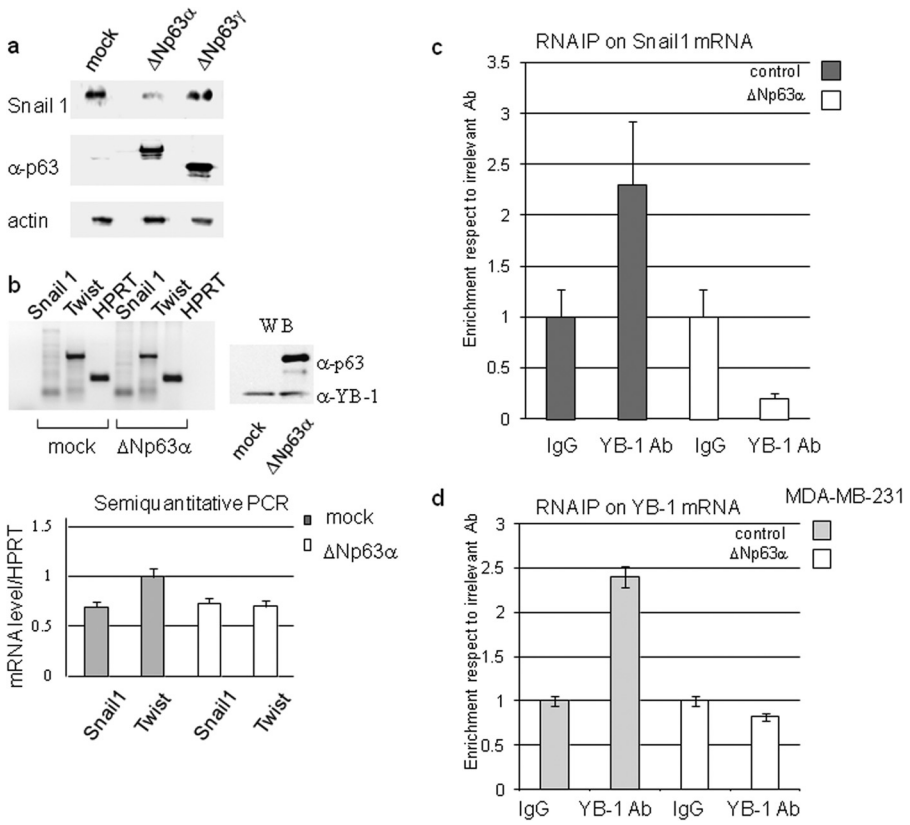

FIGURE 9. **ΔNp63α affects SNAIL1 protein level and YB-1 binding to *SNAIL1* and *YB-1* mRNAs in MDA-MB-231 cells.** *a,* MDA-MB-231 cells were transfected with an empty vector (*mock*) or a fixed amount (1 μg in 60-mm dishes) of ΔNp63α or ΔNp63γ expression vector. 24 h after transfection, cells were harvested, and total extracts were prepared. 20 μg of each extract were loaded on SDS-PAGE and subjected to immunoblot with the indicated antibodies. *b,* MB-MDA-231 cells were transfected with an empty vector or ΔNp63α encoding plasmid. 24 h after transfection, total RNA was purified and retrotranscribed as described under "Experimental Procedures." The expression level of ΔNp63α was checked by immunoblot (*right panel*). *WB,* Western blot. PCR was performed with primers designed to specifically amplify *SNAIL1*, *TWIST*, or *HPRT* transcripts and analyzed by agarose gel electrophoresis (*left panel*). Plot showing the level of *SNAIL1* and *TWIST* transcripts was normalized respect to *HPRT*. Values are the mean of three independent experiments (*lower panel*). Nuclear extracts from ΔNp63α transfected MB-MDA-231 cells were immunoprecipitated with anti-YB-1 antibody. After reverse cross-linking, the YB-1-bound RNA was purified, retrotranscribed, and subjected to quantitative RT-PCR analysis using oligonucleotides designed to specifically amplify *SNAIL1* transcript (*c*) or *YB-1* transcript (*d*). Plots represent the % of enrichment of **SNAIL1/YB-1** transcript normalized as indicated under "Experimental Procedures." 1:50 of the input extract was loaded as control. The values are the means ± S.D. of three biological replicates.

round in shape, and under high density culture conditions, they appear orderly arranged with tight cell-cell contacts. Conversely, ΔNp63α-depleted cells tend to lose their contacts and exhibited an unusual extended phenotype that was distinct from that of the control cells cultured at the same density (Fig. 10*a*). The unusual change in morphology of ΔNp63α-depleted cells indicated possible alterations in actin cytoskeleton organization. Therefore, we examined the status of actin stress fibers at the level of individual cells, in control and ΔNp63α-depleted cells, with TRITC-phalloidin followed by fluorescent microscopy. As shown in Fig. 10*b*, the control cells exhibited a diffuse pattern of actin staining, although ΔNp63α-depleted cells displayed a more substantial enhancement of actin stress fibers suggesting an inhibitory effect of ΔNp63α on cancer cell motility. Remarkably, compared with the control cells, ΔNp63α-depleted SCC011 cells express higher levels of N-cadherin and lower amounts of E-cadherin, suggesting that they were undergoing epithelial to mesenchymal trans-differentiation (Fig. 10*c*).

We determined the influence of ΔNp63α on cell motility by time-lapse microscopy using siRNA-based silencing of endogenous ΔNp63α in SCC011 cells. Silencing efficiency was about 90% as determined by fluorescent staining for p63 protein (data not shown). SCC011 migration was characterized by oscillations of the cells around their initial adhesion site. These oscillations occurred at random directions in space, as reported in the windrose plots of the trajectories (Fig. 10*d*, *inset*). Conversely, ΔNp63α silenced cells display much wider oscillations (Fig. 10*d*). These observations were confirmed by the analysis of the migration parameters "Speed (*S*)" and "persistence time (*P*)" that are computed from cell tracks and are a measure of the frequency of cell steps and of the minimum time that is necessary for a cell to significantly change direction. According to these parameters, SCC011 exhibit lower speeds ($p < 0.05$) and shorter persistence times (0.26 ± 0.03 μm/min and 6.5 ± 0.7 min) with respect to ΔNp63α-depleted cells (0.44 ± 0.05 μm/min and 8.2 ± 2.3 min). These data indicate a role for ΔNp63α in affecting cell motility. In particular, the absence of ΔNp63α causes the cells to migrate faster with less frequent direction changes, which enables the cells to explore larger areas in a fixed time interval.

To gain a better insight into the effects of the interaction of ΔNp63α and YB-1 on cell migration, we used the genetically modified Tet-On-H1299 cells expressing ΔNp63α upon Dox addition (Fig. 11*a*). Cells were transfected with GFP or GFP-

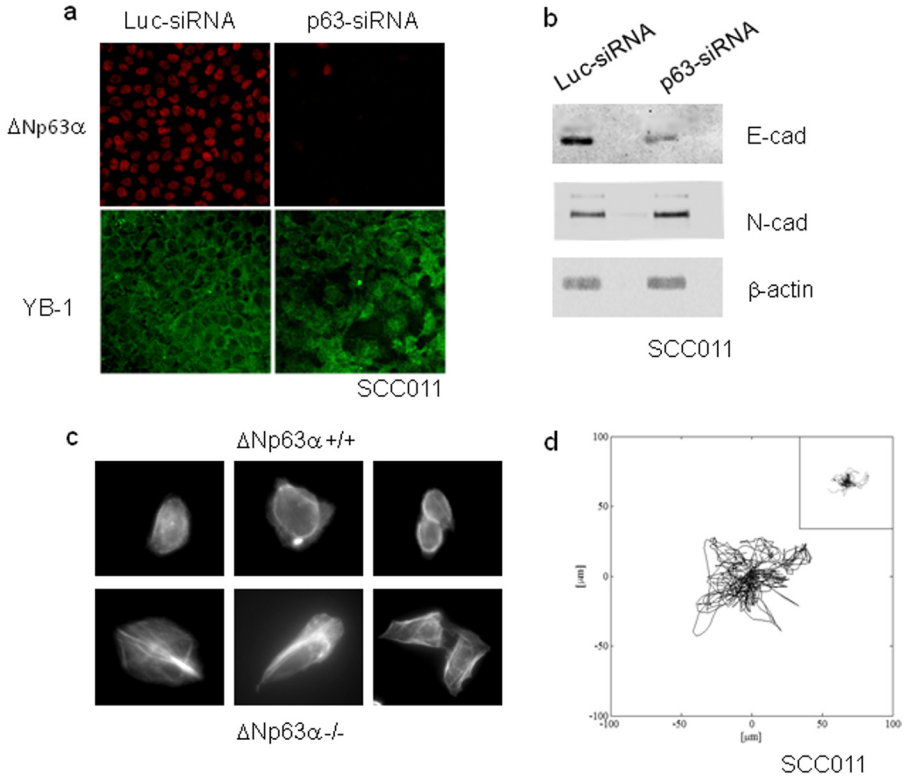

FIGURE 10. **ΔNp63α affects cell shape and motility.** *a,* SCC011 cells were transiently silenced with IBONI p63-siRNA pool (20 nm final concentration). Cells were fixed and subjected to double immunofluorescence 48 h after silencing, as already described. *b,* protein extracts from control and p63-depleted cells were separated by SDS-PAGE and subjected to immunoblot. Proteins were detected with specific antibodies. *c,* actin staining with TRITC-conjugated phalloidin of control and ΔNp63α-depleted SCC011 cells (see "Experimental Procedures"). Cell expressing ΔNp63α displayed a round morphology. Conversely, ΔNp63α-depleted cells had a polarized morphology with more evident lamellipodia and trailing edge. *d,* windrose plot of trajectories described by ΔNp63α depleted SCC011 or SCC011 control cells (*inset*) in 12-h time lapse video. Only 15 cell trajectories were reported in each plot for graphical clarity. *E-cad*, E-cadherin; *N-cad*, N-cadherin.

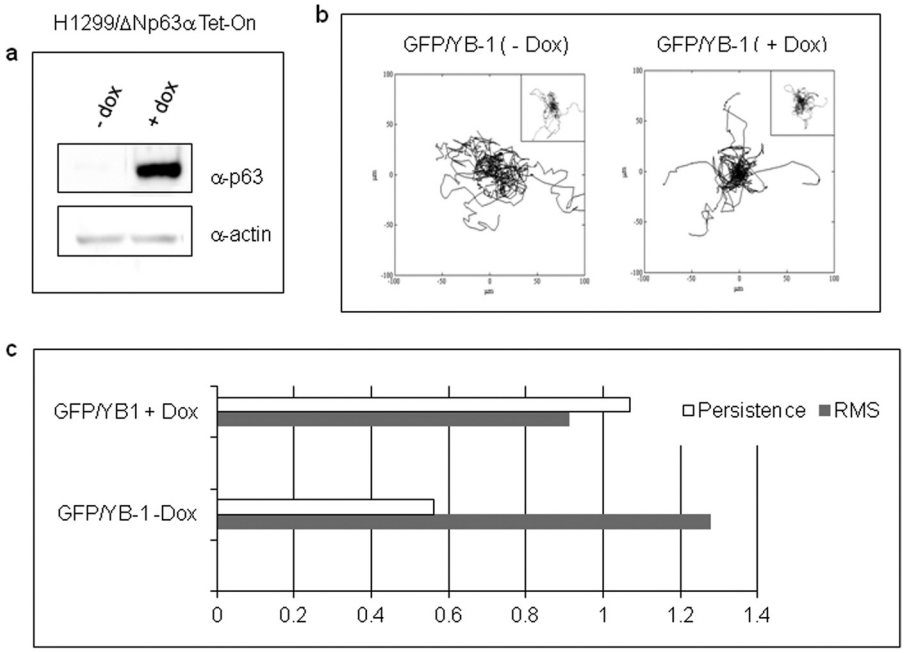

FIGURE 11. **Effects of ΔNp63α and YB-1 on cell migration.** *a,* after being subjected to the migration experiment, extracts from Tet-On H1299 cells, induced (+*dox*) or not (−*dox*) with doxycycline, were prepared and subjected to immunoblot analysis to monitor ΔNp63α induced expression. *b,* trajectories of GFP/YB-1- or GFP (*insets*)-transfected cells. Inducible H1299/ΔNp63α cells were transfected with a fixed amount of GFP-YB-1(1 μg) or GFP empty vector (1 μg). 4 h after transfection, 2 μg/ml doxycycline was added to induce ΔNp63α expression, and 16 h later uninduced (−*Dox*) and induced (+*Dox*) cells were tracked with optical microscopy. Plots represent data from the following number of cells (YB-1/−dox 79; YB−1/+dox 69; control/−dox 44; control/+dox 49). *c*, *bar chart* of speed (*S*; *gray bars*) and persistence ratios (*P*; *white bars*). The ratios are computed by dividing the population average values of speed and persistence for H1299 control cells (− *Dox*) and ΔNp63α-expressing cells (+ *Dox*).

YB-1 plasmid, and unfluorescent and fluorescent cells were tracked separately. Cells migrated describing trajectories that are randomly distributed in plane, as depicted in plots of Fig. 10*b*. In Dox-free medium (−Dox), GFP-YB-1-expressing cells were characterized by a significantly higher *S* and lower *P* (0.69 ± 0.04 μm/min and 8.4 ± 0.5 min) than cells expressing GFP alone (0.54 ± 0.05 μm/min and 15 ± 2.1 min). Remarkably, in Dox-supplemented medium (+Dox), GFP-YB-1-expressing cells exhibited *S* and *P* values (0.62 ± 0.05 μm/min and 9.2 ± 1.0 min), which were not significantly different from those of cells transfected with GFP alone (0.68 ± 0.05 μm/min and 8.6 ± 0.9 min) (Fig. 10*c*). We also noticed that unfluorescent cells were characterized by the highest *S* values suggesting that expression of the green fluorescent protein alters cell migration to some extent (data not shown). However, *S* of unfluorescent cells with or without Dox was comparable. Overall, these data indicate that ΔNp63α expression can revert the increase of cell motility induced by YB-1-enforced expression.

DISCUSSION

In normal epithelium, ΔNp63α protein expression is abundant in basal cells and decreases with differentiation (35). Transient overexpression of ΔNp63α was shown to enhance cell proliferation, inhibit differentiation, and promote malignant conversion of primary keratinocytes (36, 37). However, enhanced and stable expression of ΔNp63α, as seen in human squamous cell carcinomas, is believed to alter skin homeostasis and be directly implicated in the etiology of human cutaneous carcinomas. In normal cells, YB-1 is mainly detected in the cytosol, particularly at the perinuclear region, with a minor pool located in the nucleus (38). Nuclear localization of YB-1 appears to be critical for its role in promoting proliferation. In fact, in the nucleus YB-1 may not only act as a transcription factor of various genes that are closely associated with DNA replication, cell proliferation, and multidrug resistance but also exert SOS signaling against genotoxic factors that could undermine the integrity of highly proliferative basal cells.

This report unveils a novel protein-protein association involving ΔNp63α and YB-1. This specific association results in the accumulation of nuclear YB-1, as shown by immunofluorescence assays and nuclear-cytoplasmic fractionation. Moreover, we have demonstrated that ΔNp63α and YB-1 cooperate in *PIK3CA* gene activation with both being recruited to the *PIK3CA* proximal promoter, thereby supporting the hypothesis that this molecular association can function as a pro-survival mechanism. It's worth mentioning, however, that additional mechanisms have been described to activate and translocate YB-1 to the nucleus (8).

Into the cytoplasm, YB-1 is known to act as a positive translational regulator of SNAIL1, a potent epithelial to mesenchymal transition inducer able to reduce cell-cell adhesion and increase migratory properties of cancer cells (33). Accordingly, we have observed that enforced expression of YB-1 in tumor cells increases their motility and migration speed. Remarkably, we have shown that ΔNp63α-enforced expression reduces the activating binding of YB-1 to the *SNAIL1* transcript and restores a normal migratory behavior to YB-1-overexpressing cells. However, depletion of endogenous ΔNp63α in SCC cells results in SNAIL1 up-regulation, E-cadherin repression, and increased cell motility.

Finally, cytoplasmic YB-1 is known to bind to actin filaments and causes actin fibers to bundle *in vitro* (39). It was also demonstrated that YB-1 plays a relevant role in the organization of the actin cytoskeleton by binding to F-actin and microtubules (40, 41). In normal conditions, SCC011 cells are round in shape and exhibit a more diffuse actin distribution, as determined by phalloidin staining. Here, we show that ΔNp63α depletion in SCC cells promotes morphological changes and causes a profound cytoskeleton reorganization. ΔNp63α-depleted cells had a polarized morphology with more evident lamellipodia and trailing edge. They also exhibited mature stress fibers suggesting a pro-migratory behavior. The alterations in cell morphology and motility of ΔNp63α-depleted SCC cells closely resemble the process of epithelial to mesenchymal transition (28). We can speculate that the absence of ΔNp63α can promote F-actin polymerization by YB-1 thereby promoting the formation of stress fibers.

All together, our data indicate that ΔNp63α-YB-1 association into the nucleus can act as a pro-proliferative/survival mechanism, although the loss of p63 predisposes the acquisition of mesenchymal characteristics at least in part by restoring YB-1 cytoplasmic functions. Moreover, we suggest that the balance between ΔNp63α and YB-1 protein levels could be critical for the transition to a mesenchyme-like phenotype explaining, at least in part, why ΔNp63α depletion promotes cancer cell invasion and spreading (35).

Acknowledgments—We thank Sandra Dunn, Arezoo Astanehe, Karsten Jurchott, and Jill Gershan for kindly providing expression and reporter constructs. We acknowledge Dr. Caterina Missero for providing SCC cell lines.

REFERENCES

1. Matsumoto, K., and Bay, B. H. (2005) Significance of the Y-box proteins in human cancers. *J. Mol. Genet. Med.* **1,** 11–17
2. Homer, C., Knight, D. A., Hananeia, L., Sheard, P., Risk, J., Lasham, A., Royds, J. A., and Braithwaite, A. W. (2005) Y-box factor YB-1 controls p53 apoptotic function. *Oncogene* **24,** 8314–8325
3. Wu, J., Stratford, A. L., Astanehe, A., and Dunn, S. (2007) YB-1 is a transcription/translation factor that orchestrates the oncogenome by hardwiring signal transduction to gene expression. *Translational Oncogenomics* **2,** 49–65
4. Evdokimova, V., Ruzanov, P., Anglesio, M. S., Sorokin, A. V., Ovchinnikov, L. P., Buckley, J., Triche, T. J., Sonenberg, N., and Sorensen, P. H. (2006) Akt-mediated YB-1 phosphorylation activates translation of silent mRNA species. *Mol. Cell. Biol.* **26,** 277–292
5. Sou, P. W., Delic, N. C., Halliday, G. M., and Lyons, J. (2010) Snail transcription factors in keratinocytes. Enough to make your skin crawl. *Int. J. Biochem. Cell Biol.* **42,** 1940–1944
6. Evdokimova, V., Tognon, C., Ng, T., Ruzanov, P., Melnyk, N., Fink, D., Sorokin, A., Ovchinnikov, L. P., Davicioni, E., Triche, T. J., and Sorensen, P. H. (2009) Translational activation of Snail and other developmentally regulated transcription factors by YB-1 promotes an epithelial-mesenchymal transition. *Cancer Cell* **15,** 402–415
7. Jurchott, K., Bergmann, S., Stein, U., Walther, W., Janz, M., Manni, I., Piaggio, G., Fietze, E., Dietel, M., and Royer, H. D. (2003) YB-1 as a cell cycle-regulated transcription factor facilitating cyclin A and cyclin B1 gene expression. *J. Biol. Chem.* **278,** 27988–27996
8. Sutherland, B. W., Kucab, J., Wu, J., Lee, C., Cheang, M. C., Yorida, E., Turbin D., Dedhar, S., Nelson, C., and Pollak, M. (2005) Akt phosphory-

lates the Y-box binding protein 1 at Ser-102 located in the cold shock domain and affects the anchorage-independent growth of breast cancer cells. *Oncogene* **24,** 4281–4292
9. Higashi, K., Tomigahara, Y., Shiraki, H., Miyata, K., Mikami, T., Kimura, T., Moro, T., Inagaki, Y., and Kaneko, H. (2011) A novel small compound that promote nuclear translocation of YB-1 ameliorates experimental hepatic fibrosis in mice. *J. Biol. Chem.* **286,** 4485–4492
10. Zhang, Y. F., Homer, C., Edwards, S. J., Hananeia, L., Lasham, A., Royds, J., Sheard, P., and Braithwaite, A. W. (2003) Nuclear localization of Y-box factor YB-1 requires wild type p53. *Oncogene* **22,** 2782–2794
11. Moll, U. M. (2004) p63 and p73. Roles in development and tumor formation. *Mol. Cancer Res.* **2,** 371–386
12. Yang, A., Kaghad, M., Wang, Y., Gillett, E., Fleming, M. D., Dötsch, V., Andrews, N. C., Caput, D., and McKeon, F. (1998) p63, a p53 homolog at 3q27–29, encodes multiple products with transactivating, death inducing, and dominant-negative activities. *Mol. Cell* **2,** 305–316
13. Yang, A., Schweitzer, R., Sun, D., Kaghad, M., Walker, N., Bronson, R. T., Tabin, C., Sharpe, A., Caput, D., Crum, C., and McKeon, F. (1999) p63 is essential for regenerative proliferation in limb, craniofacial, and epithelial development. *Nature* **398,** 714–718
14. Parsa, R., Yang, A., McKeon, F., and Green, H. (1999) Association of p63 with proliferative potential in normal and neoplastic human keratinocyte. *J. Invest. Dermatol.* **113,** 1099–1105
15. Fukunishi, N., Katoh, I., Tomimori, Y., Tsukinoki, K., Hata, R., Nakao, A., Ikawa, Y., and Kurata, S. (2010) Induction of ΔNp63 by the newly identified keratinocyte-specific transforming growth factor β-signaling pathway with Smad2 and IkB kinase α in squamous cell carcinoma. *Neoplasia* **12,** 969–979
16. Higashikawa, K., Yoneda, S., Tobiume, K., Taki, M., Shigeishi, H., and Kamata, N. (2007) Snail induced down-regulation of ΔNp63α acquires invasive phenotype of human squamous cell carcinoma. *Cancer Res.* **67,** 9207–9213
17. Graziano, V., and De Laurenzi, V. (2011) Role of p63 in cancer development. *Biochim. Biophys. Acta* **1816,** 57–66
18. Adorno, M., Cordenonsi, M., Montagner, M., Dupont, S., Wong, C., Hann, B., Solari, A., Bobisse, S., Rondina, M. B., Guzzardo, V., Parenti, A. R., Rosato, A., Bicciato, S., Balmain, A., and Piccolo, S. (2009) A mutant-p53/Smad complex opposes p63 to empower TGFβ-induced metastasis. *Cell* **137,** 87–98
19. Di Costanzo, A., Festa, L., Duverger, O., Vivo, M., Guerrini, L., La Mantia, G., Morasso, M. I., and Calabrò, V. (2009) Homeodomain protein Dlx3 induces phosphorylation-dependent p63 degradation. *Cell Cycle* **8,** 1185–1195
20. Lefort, K., Mandinova, A., Ostano, P., Kolev, V., Calpini, V., Kolfschoten, I., Devgan, V., Lieb, J., Raffoul, W., Hohl, D., Neel, V., Garlick, J., Chiorino, G., and Dotto, G. P. (2007) Notch1 is a p53 target gene involved in human keratinocyte tumor suppression through negative regulation of ROCK1/2 and MRCKα kinases. *Genes Dev.* **21,** 562–577
21. Lo Iacono, M., Di Costanzo, A., Calogero, R. A., Mansueto, G., Saviozzi, S., Crispi, S., Pollice, A., La Mantia, G., and Calabrò, V. (2006) The Hay Wells syndrome-derived TAp63αQ540L mutant has impaired transcriptional and cell growth regulatory activity. *Cell Cycle* **5,** 78–87
22. Radoja, N., Guerrini, L., Lo Iacono, N., Merlo, G. R., Costanzo, A., Weinberg, W. C., La Mantia, G., Calabrò, V., and Morasso M. I. (2007) Homeobox gene Dlx3 is regulated by p63 during ectoderm development. Relevance in the pathogenesis of ectodermal dysplasia. *Development* **134,** 13–18
23. Cui, S., Arosio, D., Doherty, K. M., Brosh, R. M., Jr., Falaschi, A., and Vindigni, A. (2004) Analysis of the unwinding activity of the dimeric RECQ1 helicase in the presence of human replication protein. *Nucleic Acid Res.* **32,** 2158–2170
24. Dunn, G. A. (1983) Characterizing a kinesis response. Time averaged measures of cell speed and directional persistence. *Agents Actions Suppl.* **12,** 14–33
25. Dickinson, R. B., and Tranquillo, R. T. (1993) Optimal estimation of cell movement indices from the statistical analysis of cell tracking data. *AIChE J.* **39,** 1995–2010
26. Amoresano, A., Di Costanzo, A., Leo, G., Di Cunto, F., La Mantia, G., Guerrini, L., and Calabrò, V. (2010) Identification of ΔNp63α protein interactions by mass spectrometry. *J. Proteome Res.* **9,** 2042–2048
27. Hibi, K., Trink, B., Patturajan, M., Westra, W. H., Caballero, O. L., Hill, D. E., Ratovitski, E. A., Jen, J., and Sidransky, D. (2000) AIS is an oncogene amplified in squamous cell carcinoma. *Proc. Natl. Acad. Sci U.S.A.* **97,** 5462–5467
28. Lee, J. M., Dedhar, S., Kalluri, R., and Thompson, E. W. (2006) The epithelial-mesenchymal transition. New insights in signaling, development, and disease. *J. Cell Biol.* **172,** 973–981
29. Di Como, C. J., Urist, M. J., Babayan, I., Drobnjak, M., Hedvat, C. V., Teruya-Feldstein, J., Pohar, K., Hoos, A., and Cordon-Cardo, C. (2002) p63 expression profiles in human normal and tumor tissues. *Clin. Cancer Res.* **8,** 494–501
30. Barbareschi, M., Pecciarini, L., Cangi, M. G., Macrì, E., Rizzo, A., Viale, G., and Dogliosi, C. (2001) p63, a p53 homologue, is a selective nuclear marker of myoepithelial cells of the human breast. *Am. J. Surg. Pathol.* **25,** 1054–1060
31. Danilov, A. V., Neupane, D., Nagaraja, A. S., Feofanova, E. V., Humphries, L. A., DiRenzo, J., and Korc, M. (2011) ΔNp63α-mediated induction of epidermal growth factor receptor promotes pancreatic cancer cell growth and chemoresistance. *PLoS One* **6,** e26815
32. Astanehe, A., Finkbeiner, M. R., Hojabrpour, P., To, K., Fotovati, A., Shadeo, A., Stratford, A. L., Lam, W. L., Berquin, I. M., Duronio, V., and Dunn, S. E. (2009) The transcriptional induction of PIK3CA in tumor cells is dependent on the oncoprotein Y-box binding protein-1. *Oncogene* **28,** 2406–2418
33. Evdokimova, V., Tognon, C., Ng, T., Ruzanov, P., Melnyk, N., Fink, D., Sorokin, A., Ovchinnikov, L. P., Davicioni, E., Triche, T. J., and Sorensen, P. H. (2009) Reduced proliferation and enhanced migration: Two sides of the same coin? Molecular mechanisms of metastatic progression by YB-1. *Cancer Cell* **15,** 402–415
34. Peiró, S., Escrivà, M., Puig, I., Barberà, M. J., Dave, N., Herranz, N., Larriba, M. J., Takkunen, M., Francí, C., Muñoz, A., Virtanen, I., Baulida, J., and García de Herreros, A. (2006) Snail1 transcriptional repressor binds to its own promoter and controls its expression. *Nucleic Acids Res.* **34,** 2077–2084
35. Barbieri, C. E., Tang, L. J., Brown, K. A., and Pietenpol, J. A. (2006) Loss of p63 leads to increased cell migration and up-regulation of genes involved in invasion and metastasis. *Cancer Res.* **66,** 7589–7597
36. King, K. E., Ponnamperuma, R. M., Yamashita, T., Tokino, T., and Lee, L. A. (2003) ΔNp63α functions as a positive and negative transcriptional regulator and blocks *in vitro* differentiation of murine keratinocytes. *Oncogene* **22,** 3635–3644
37. Ha, L., Ponnamperuma, R. M., Jay, S., Ricci, M. S., and Weinberg, W. C. (2011) Dysregulated ΔNp63α inhibits expression of Ink4a/arf, blocks senescence, and promotes malignant conversion of keratinocytes. *PLoS One* **6,** e21877
38. Koike, K., Uchiumi, T., Ohga, T., Toh, S., Wada, M., Kohno, K., and Kuwano, M. (1997) Nuclear translocation of the Y-box binding protein by ultraviolet irradiation. *FEBS Lett.* **417,** 390–394
39. Ruzanov, P. V., Evdokimova, V. M., Korneeva, N. L., Hershey, J. W., and Ovchinnikov, L. P. (1999) Interaction of the universal mRNA-binding protein, p50, with actin. A possible link between mRNA and microfilaments. *J. Cell Sci.* **20,** 3487–3496
40. Uchiumi, T., Fotovati, A., Sasaguri, T., Shibahara, K., Shimada, T., Fukuda, T., Nakamura, T., Izumi, H., Tsuzuki, T., Kuwano, M., and Kohno, K. (2006) Yb-1 is important for an early stage embryonic development. Neural tube formation and cell proliferation. *J. Biol. Chem.* **281,** 40440–40449
41. Chernov, K. G., Mechulam, A., Popova, N. V., Pastre, D., Nadezhdina, E. S., Skabkina, O. V., Shanina, N. A., Vasiliev, V. D., Tarrade, A., Melki, J., Joshi, V., Baconnais, S., Toma, F., Ovchinnikov, L. P., and Curmi, P. A. (2008) Yb-1 promotes microtubules assembly *in vitro* through interaction with tubulin and microtubules. *BMC Biochem.* 9–23

Original Research Article

Y-Box binding protein-1 is part of a complex molecular network linking ΔNp63α to the PI3K/AKT pathway in cutaneous squamous cell carcinoma[†]

Annaelena Troiano, Irene Schiano Lomoriello, Orsola di Martino, Sabato Fusco§, Alessandra Pollice, Maria Vivo, Girolama La Mantia, Viola Calabrò*

Department of Biology, University of Naples "Federico II", 80128 Naples, Italy

§Center for Advanced Biomaterials for Health Care@CRIB, Istituto Italiano di Tecnologia, Naples, Italy.

Running Title: YB-1, ΔNp63α and the PI3K pathway cross-talk

Keywords: **p53 protein family, Y-box binding protein, PI3K/AKT/PTEN, cell proliferation, squamous carcinoma, skin cancer**.

This work was supported by Progetto "Campania Research in Experimental Medicine" (CREME), POR Campania FSE 2007-2013 to V. C. and Regione Campania L R N°5/2007 to G. L. M.

Corresponding author: Prof. Viola Calabrò, PhD. Dipartimento di Biologia, Università di Napoli, "Federico II", Viale Cinzia, Monte S Angelo, 80126 Napoli, Italy. Phone: +39 081 679069. Fax +39 081 679033. E-mail: vcalabro@unina.it

Additional Supporting Information may be found in the online version of this article.

Received 28 October 2014; Revised 19 December 2014; Accepted 16 January 2015
Journal of Cellular Physiology

DOI 10.1002/jcp.24934

Abstract

Cutaneous squamous cell carcinomas (SCCs) typically lack somatic oncogene-activating mutations and most of them contain p53 mutations. However, the presence of p53 mutations in skin premalignant lesions suggests that these represent early events during tumor progression and additional alterations may be required for SCC development. SCC cells frequently express high levels of ΔNp63α and Y-box binding 1 (YB-1 or YBX1) oncoproteins. Here, we show that knockdown of YB-1 in spontaneously immortalized HaCaT and non-metastatic SCC011 cells led to a dramatic decrease of ΔNp63α, cell detachment and death. In highly metastatic SCC022 cells, instead, YB-1 silencing induces PI3K/AKT signaling hyperactivation which counteracts the effect of YB-1 depletion and promotes cell survival. In summary, our results unveil a functional cross-talk between YB-1, ΔNp63α and the PI3K/AKT pathway critically governing survival of squamous carcinoma cells.

This article is protected by copyright. All rights reserved

Introduction

Squamous cell carcinoma (SCC) is a treatment-refractory malignancy arising within the epithelium of different organs, that is frequently associated with overexpression of ΔNp63α oncoprotein (Rocco et al., 2006, Hibi et al., 2000). ΔNp63α is encoded by the TP63 locus, the ancestral gene of the p53 gene family that gives rise to multiple isoforms that can be placed in two categories: TA isoforms with an acidic transactivation domain and ΔN isoforms that lack this domain. Alternative splicing at the carboxy-terminal (C-terminal) generates at least three p63 variants (α, β and γ) in each class (Rossi et al., 2006, Yang et al., 1999). ΔNp63α is essential for the maintenance of the proliferative capacity of epithelial cell progenitors (Senoo et al., 2004); as these cells start to differentiate, ΔNp63α protein level gradually drops and those that no longer express ΔNp63α, loose the proliferative capacity (Koster, 2010).

In squamous carcinoma, ΔNp63α up-regulation causes skin hyperplasia and abnormal keratinocyte differentiation predisposing to malignant transformation (Hibi et al., 2000; Moll and Slade, 2004). Despite its undisputed relevance in epithelial cancer, the mechanisms through which ΔNp63α executes its pro-oncogenic functions are not fully understood. However, ΔNp63α expression was shown to be induced by activation of downstream targets of EGFR activation including STAT3 (Ripamonti et al., 2013) and the phosphoinositide-3-kinase (PI3K) pathway (Barbieri et al., 2003).

We have recently shown that ΔNp63α interacts with the YB-1 oncoprotein and promotes accumulation of YB-1 into the nuclear compartment (Di Costanzo et al., 2012; Amoresano et al., 2010). YB-1, also named YBX1, is a member of the cold shock domain (CSD) protein family, which is found in the cytoplasm and nucleus of mammalian cells, being able to shuttle between the two compartments (Eliseeva et al., 2011). The YB-1 gene, located on chromosome 1p34 (Toh et al., 1998), encodes a 43 kDa protein having three functional domains: a variable NH2-terminal Alanine/Proline rich tail domain (aa 1-51), involved in transcriptional regulation, a highly conserved nucleic acid binding domain (CSD, aa 51-171), and a COOH-terminal tail (B/A repeat) for RNA/ssDNA binding and protein dimerization (129-324).

YB-1 is a major downstream target of Twist (Shiota et al., 2008) and c-Myc-Max complexes by recruitment to the E-box consensus sites in YB-1 promoter (Uramoto et al., 2002). YB-1 regulates genes promoting cancer cell growth such as EGFR, Her-2, PI3KCA and MET (To et al., 2010) as well as genes linked to cancer stem cells such as those encoding the hyaluronan receptor CD44, CD49f (integrin α6) and CD104 (β4 integrin), implying that YB-1 plays a key role as oncogene by transactivating genes associated with a cancer stem cell phenotype (To et al., 2010). YB-1 protein level drastically increases during progression of several types of tumors including squamous carcinoma, thereby suggesting a role for this protein in the pathogenesis of human epithelial malignancy (Di Costanzo et al., 2012, Kolk et al., 2011).

To mediate gene regulation, YB-1 translocates into the nucleus and interacts with the proximal promoter regions of its target genes (Sutherland et al., 2005; Shiota et al., 2011). Phosphorylation of serine 102 in response to MAPK and PI3K/AKT signaling promotes YB-1 nuclear translocation (Sinnberg et al., 2012). Moreover, YB-1 translocates to the nucleus when cells are exposed to cytokines, anticancer agents, hyperthermia, or UV light irradiation (Schittek et al., 2007).

Herein, we present data showing the existence of a functional cross-talk between YB-1, ΔNp63α and the PI3K/AKT signaling pathway critically governing survival of squamous carcinoma cells.

MATERIALS AND METHODS

Plasmids

The 1.1 Kb EGFR promoter luciferase plasmid was provided by Dr. A.C. Johnson (US National Cancer Institute, Massachusetts, USA). The cDNA encoding human ΔNp63α and ΔNp63α F518L were previously described (Lo Iacono et al., 2006).

Cell lines, transfection and antibodies

SCC011 and SCC022 cell lines were established from cutaneous squamous carcinomas (Lefort et al., 2007). SCC011 and SCC022 cells were cultured in RPMI supplemented with 10% fetal bovine serum at 37°C and 5% CO_2. HaCaT and MDA-MB231 cells were purchased from Cell Line Service (CLS, Germany) and cultured at 37°C and 5% CO_2. HaCaT cells were maintained in DMEM supplemented with 10% FBS. MDA-MB231 cells were maintained in DMEM supplemented with 5% FBS.

Transient transfection

Lipofections were performed with Lipofectammine 2000 (Life Technologies, CA, USA), according to the manufacturer's recommendations.

YB1 transient silencing was carried out with IBONI YB-1siRNA pool (RIBOXX GmbH, Germany) and RNAiMAX reagent (Life Technologies, CA, USA), according to the manufacturer's recommendations. Briefly, cells were seeded at 60% confluence (1.5×10^6) in 100-mm dishes and transiently silenced with IBONI YB1-siRNA at 20 nM final concentration.

YB-1 guide sequences:

UUUAUCUUCUUCAUUGCCGCCCCC;

UUAUUCUUCUUAUGGCAGCCCCC;

UUCAACAACAUCAAACUCCCCC;

UCAUAUUUCUUCUUGUUGGCCCCC.

ΔNp63α transient silencing was carried out with IBONI p63-siRNA pool (RIBOXX GmbH, Germany) at 20 nM final concentration and RNAiMAX reagent (Life Technologies, CA, USA).

p63 guide sequences:

UUAAACAAUACUCAAUGCCCCC;

UUAACAUUCAAUAUCCCACCCCC;

AUCAAUAACACGCUCACCCCC;

AUGAUUCCUAUUUACCCUGCCCCC.

"All Star Negative Control siRNA", provided by Quiagen (Hilden, Germany), was used as negative control.

Transfection efficiency of siRNA was quantified using BLOCK-iT™ Control Fluorescent Oligo (Life Technologies, CA, USA) at a final concentration of 20 nM using Lipofectamine RNAiMAX (Life Technologies, CA, USA). Cells were stained with Hoechst and transfected cells detected by direct immunofluorescence. Transfection efficiency ranged between 70 and 80% .The percentage of transfected cells was estimated as the average of counts performed on 100 cells in five independent fields.

Immunoblot analyses and coimmunoprecipitation

Immunoblots (IB) were performed as previously described (Di Costanzo et al., 2012). Briefly, 30 μg of whole cell extracts were separated by SDS-PAGE, subjected to immunoblot and incubated overnight at 4°C with antibodies.

For nuclear-cytoplasmic fractionation 10 μg of nuclear and 30 μg of cytoplasmic extracts (1:3 rate) were separated by SDS-PAGE and subjected to immunoblot.

All images were acquired with CHEMIDOC (Bio Rad, USA) and analyzed with the Quantity-ONE software.

Coimmunoprecipitation was performed as previously described (Rossi et al., 2006). Briefly, whole HaCaT cell extracts, precleared with 30 μl of protein A-agarose (50% slurry; Roche, Manheim,

Germany), were incubated overnight at 4°C with anti-p63 (2 μg) or α-mouse IgG. The reciprocal experiment was performed with anti-YB-1(3 μg) or α-rabbit IgG (3 μg).

Antibodies and chemical reagents

Anti-p63 (4A4), anti-cytokeratin 1 (4D12B3), anti-GAPDH (6C5), and anti-actin (1-19) were purchased from Santa Cruz (Biotechnology Inc. CA, USA). PARP, PTEN, AKT, pAKT ^{S473}, EGFR and STAT3 antibodies were from Cell Signaling Technology (Beverly, Massachusetts). Rabbit polyclonal YB1 (Ab12148) antibody was purchased from Abcam (Cambridge, UK). Proteasome inhibitor MG132 were purchased from Sigma-Aldrich (St Louis, MO) and used at 10 μM final concentration in DMSO (Sigma-Aldrich, St Louis, MO). LY294002 was purchased from Calbiochem (CA, USA) and used at 50 μM final concentration in DMSO.

Cell Viability assay

Cell viability was determined by the MTT 3-(4,5-dimethylthiazol-2-yl)-2,5-diphenyl tetrazolium bromide assay (Sigma-Aldrich, St Louis, MO). Briefly, cells were seeded in 96-well plates at 2 x 10^3 and transfected with scrambled or YB-1 siRNA oligos, 48h after silencing MTT solution (5mg/ml in PBS, 20 μl/well) was added to cells to produce formazan crystals. MTT solution was substituted by 150 μl DMSO 30 minutes later to solubilize the formazan crystals. The optical absorbance was determined at 570 nm using an iMark microplate reader (Bio-Rad, USA). The experiments were carried out in triplicate for each knockdown and compared to scrambled control (value set at 1.0).

Quantitative Real Time-PCR

For PCR analysis total RNA was isolated using the RNA Extraction Kit from Qiagen (Hilden, Germany) according to the manufacturer's instructions. RNA (2-5μg) was treated with DNAse I (Promega, Madison USA) and used to generate reverse transcribed cDNA using SuperScript III

(Life Technologies, CA, USA), according to the manufacturer's instructions. All samples in each experiment were reverse transcribed at the same time, the resulting cDNA diluted 1:5 in nuclease-free water and stored in aliquots at –80°C until used.

Real Time PCR with SYBR green detection was performed with a 7500 RT-PCR Thermo Cycler (Applied Biosystem, Foster City, USA). The thermal cycling conditions were composed of 50ºC for 2 min followed by an initial denaturation step at 95ºC for 10 min, 45 cycles at 95ºC for 30s, 60ºC for 30s and 72ºC for 30s. Experiments were carried out in triplicate. The relative quantification in gene expression was determined using the $2^{-\Delta\Delta Ct}$ method (Livak and Schmittgen, 2011). Using this method, we obtained the fold changes in gene expression normalized to an internal control gene and relative to one control sample (calibrator). 18S was used as an internal control to normalize all data and the siCtrl was chosen as the calibrator.

Appropriate no-RT and non-template controls were included in each 96-well PCR reaction and dissociation analysis was performed at the end of each run to confirm the specificity of the reaction.

YB1(F):5'CGCAGTGTAGGAGATGGAGAG

YB1(R):5'GAACACCACCAGGACCTGTAA

ΔNp63 (F):5'GGTTGGCAAAATCCTGGAG

ΔNp63 (R):5'GGTTCGTGTACTGTGGCTCA

EGFR (F) :5'TTCCTCCCAGTGCCTGAA

EGFR (R):5'GGGTTCAGAGGCTGATTGTG

STAT3 (F) :5'CCTCTGCCGGAGAAACAG

STAT3 (R):5'CTGTCACTGTAGAGCTGATGGAG

GADD45A (F): 5' TTTGCAATATGACTTTGGAGGA

GADD45A (R): 5' CATCCCCCACCTTATCCAT

18S (F):5'TCGAGGCCCTGTAATTGGAA

18S (R):5'CTTTAATATACGCTATTGGAGCTG

Luciferase reporter assay

MDA-MB231 cells were co-transfected with ΔNp63α, ΔNp63α F518L and EGFR promoter-luciferase reporter vector. Transfections were performed in triplicate in each assay. At 24h after transfection, cells were harvested in 1x PLB buffer (Promega, Madison, USA) and luciferase activity was measured using Dual Luciferase Reporter system (Promega, Madison, USA) using pRL-TK activity as internal control. FireFly-derived luciferase activity was normalized for transfection efficiency. Successful transfection of p63 was confirmed by immunoblotting. The average values of the tested constructs were normalized to the activity of the empty construct.

Immunofluorescence and bright -field images acquisition

HaCaT cells (2.5 x 10^5) were plated in 35 mm dish, grown on micro cover glasses (BDH). At 24 hours after seeding, cells were washed with cold phosphate-buffered saline (PBS) and fixed with 4% paraformaldehyde (PFA) (Sigma-Aldrich, St. Louis, MO) for 15 min at 4°C. Cells were permeabilized with ice-cold 0.1% Triton X-100 for 10 min, washed with PBS and incubated with Thermo Scientific Hoechst 33342 (2'-[4-ethoxyphenyl]-5-[4-methyl-1-piperazinyl]-2,5'-bi-1H-benzimidazole trihydrochloride trihydrate) for 3 min. Images were digitally acquired at 470 nm using Nikon TE Eclipse 2000 microscope and processed using Adobe Photoshop software CS.

SCC022 cells (2.5 x 10^5) were plated in 35 mm dish and grown on micro cover glasses (BDH). At 24 hours after seeding, cells were transfected with scramble , YB-1 or p63 siRNA oligos. 48 hrs after silencing cells were washed with cold phosphate-buffered saline (PBS) and fixed with 4% paraformaldehyde (PFA) (Sigma-Aldrich, St. Louis, MO) for 15 min at 4°C. Cells were permeabilized with ice-cold 0.1% Triton X-100 for 10 min and then washed with PBS. P63 was detected using a 1:200 dilution of the monoclonal antibody D9 (Santa Cruz, Biotechnology Inc., CA, USA). YB-1 was detected using 1:100 dilution of the YB1 antibody (Ab12148). After extensive washing in PBS, the samples were incubated with Cy3-conjugated anti-mouse (red) and Cy5-conjugated anti-rabbit IgGs (green) at room temperature for 30 min. Cells were incubated with

Hoechst 33342 (2'-[4-ethoxyphenyl]-5-[4-methyl-1-piperazinyl]-2,5'-bi-1H-benzimidazole trihydrochloride trihydrate) (Thermo Scientific) for 3 min. Images were digitally acquired and processed using Adobe Photoshop software CS.

Cell motility assay

SCC022 cells were cultured on 35-mm dishes (Corning, NY) at $2x10^4$ cells/dish density. ΔNp63α or YB1 transient silencing were performed as described above. After 24 h from silencing cell migration tests were performed via an Olympus IX81 inverted microscope equipped with a 10X objective and an integrated stage incubator (Okolab, Italy). Images of selected positions of the cell culture were collected in bright field for 16 h with 5-min frame intervals. All of the collected data were processed with the Olympus imaging software Cell^R. To quantify the cell speed (μm/min), time-lapse acquisitions were processed by the dedicated software add-in (TrackIT). The average speed per cell was calculated from the length of the path divided by time. An average number of 60 cells were analyzed for each condition.

Results

YB-1 knockdown in HaCaT cells

We have previously shown that ΔNp63α interacts with YB-1 in human squamous carcinoma cells and promotes accumulation of full length YB-1 protein (50 kDa) in the nuclear compartment (Di Costanzo et al., 2012). We first validated the interaction between YB-1 and ΔNp63α in non transformed HaCaT keratinocytes by co-immunoprecipitation assay (Supplementary Fig. 1). Then, we examined the effect of YB-1 silencing in mitotically active HaCaT keratinocytes. Interestingly, at 48 hrs of silencing we observed massive cell detachment (Figure 1A, upper panel) associated with a high proportion of condensed and fragmented nuclei (Figure 1A, lower panel). Western blot analysis showed a significant reduction of ΔNp63α protein level and PARP1 proteolytic cleavage (Figure 1B, left panel) indicating that YB-1 is critical for keratinocyte survival.

ΔNp63α is known to sustain survival in squamous cell carcinoma (Rocco et al., 2006, Hibi et al., 2000) and up-regulate cell adhesion-associated genes (Carrol et al., 2006). To rule out the possibility that YB-1 silencing induces cell death by merely reducing the level of ΔNp63α, we knocked down ΔNp63α expression in HaCaT cells by RNA interference. According to previous studies (Barbieri et al., 2006), we observed neither cell detachment (Figure 1A, upper panel) nor PARP1 activation (Figure 1B, right panel) clearly indicating that apoptosis, induced by YB-1 depletion, cannot be simply ascribed to the lack of ΔNp63α.

Next, we evaluated the level of ΔNp63α-specific transcript following YB-1 knockdown by Real Time quantitative PCR (RT-qPCR) and we found that it was drastically reduced (Figure 1C). After p63 silencing, instead, YB-1 transcript level was slightly enhanced (Figure 1D) while the mRNA of GADD45A, a gene induced by stressful conditions and used as control, was enhanced in both experiments (Figure 1C and D).

YB-1 knockdown in squamous carcinoma cells

Next, we used RNA interference to explore the function of YB-1 in squamous cell carcinoma (SCC). SCC011 and SCC022 are cell lines derived from cutaneous squamous carcinomas (Lefort et al., 2007). SCC022 are highly metastatic and, when subcutaneously injected in nude mice, form large tumors. SCC011 cells, instead, generate only keratin pearls (C. Missero, personal communication).

Similarly to what observed in HaCaT cells, YB1-depleted SCC011 cells detached from the plate generating abundant cellular debris (Figure 2A, upper panel) and exhibited a reduced level of ΔNp63α protein (Figure 2B). PARP1 cleavage was barely detectable (Figure 2B). On the other hand, we have previously demonstrated that p63 knockdown has no apparent effect on SCC011 cell viability (Di Costanzo et al., 2012).

Surprisingly, SCC022 cells looked healthy and tightly adherent to the plate after YB1 silencing (Figure 2A, lower panel). Moreover, as detected by immunoblot analysis, the expression level of ΔNp63α protein was significantly increased (Figure 2B). Interestingly, ΔNp63α transcript in SCC011 was reduced while in SCC022 it was 2.1-fold higher than control (Figure 2C).

Analysis of cell viability by the MTT assay showed that after 48 hrs of YB-1 knockdown the percentage of viability of SCC022 cells was 70% of the control, while it was reduced to 10% in HaCaT and SCC011 cells (Figure 4C).

We have also performed p63 knockdown in SCC022 cells and, as expected, we observed accumulation of YB-1 in the cytoplasm without any apparent effect on cell viability (Supplementary Fig. 2).

We also determined the influence of ΔNp63α or YB-1 silencing on SCC022 cell motility by time-lapse microscopy using siRNA-based silencing of endogenous proteins. According to our previous observations made on SCC011 cells (Di Costanzo et al., 2012) ΔNp63α silenced cells display higher speeds ($p < 0.01$) than control cells. Conversely, SCC022 cell motility was unaffected by YB-1 depletion (Supplementary Fig. 3).

YB-1 silencing hyper-activates the PI3K/AKT signaling pathway in SCC022 cells

ΔNp63α is a target of the phosphoinositide-3-kinase (PI3K) pathway downstream of the Epidermal Growth Factor Receptor (Barbieri et al., 2003). We hypothesized an involvement of the PI3K/AKT pathway in the upregulation of ΔNp63α observed in SCC022 cells following YB-1 silencing, and we looked for changes in the phosphorylation status of $AKT_{Ser473.}$ Interestingly, unlike HaCaT and SCC011, SCC022 cells exhibited constitutive phosphorylation of AKT_{Ser473} which was reproducibly potentiated following YB-1 depletion (Figure 3A and B) suggesting that YB-1 expression restrains AKT activation. To corroborate this result, we treated YB1-silenced SCC022 cells with Ly294002, a highly selective PI3K inhibitor. Remarkably, Ly294002 treatment counteracted AKT hyperphosphorylation and the increase of ΔNp63α protein level in response to YB-1 silencing (Figure 3B). Moreover, it resulted in cell death and detachment (data not shown). Importantly, Ly294002 treatment alone had no apparent effect on ΔNp63α level and SCC022 cell viability (Figure 3B and data not shown). Quantification of ΔNp63α transcript in YB-1 depleted SCC022 cells, treated or not with LY294002, showed that the increase of ΔNp63α transcription was strictly dependent on the PI3K/AKT pathway (Figure 3B). Moreover, inhibition of the proteasome activity with MG132 did not significantly enhance ΔNp63α protein level in YB1-silenced SCC022 cells, thereby confirming that ΔNp63α up-regulation was almost exclusively at transcriptional level (Supplementary Fig. 4).

The PI3K/AKT signaling pathway is negatively regulated by the phosphatase and tensin homologue PTEN (Song et al., 2012). To further investigate on the ability of SCC022 cells to escape from death following YB-1 depletion, we compared the protein level of PTEN among HaCaT, SCC011 and SCC022 cell lines. Compared to HaCaT and SCC011 cells, the level of PTEN protein in SCC022 cells was very low, accounting for their high basal level of AKT_{Ser473} phosphorylation (Figure 3E). Furthermore, YB-1 silencing resulted in increased levels of cytoplasmic PTEN in

HaCaT and SCC011 cells, while no effects on PTEN protein level was observed in YB-1 silenced SCC022 cells (Figure 3E).

Cross-talk of ΔNp63α and YB-1 with EGFR/STAT3 and PI3K/AKT signaling pathways

In pancreatic cancer cells, ΔNp63α expression was shown to induce the Epidermal Growth Factor Receptor (EGFR) (Danilov et al., 2011). As we observed a PI3K-dependent increase of ΔNp63α in SCC022 cells upon YB-1 silencing, we decided to evaluate the level of EGFR and its direct downstream target STAT3 in SCC022 cells upon YB-1 or ΔNp63α silencing. As shown in Figure 4, along with ΔNp63α, YB-1 depletion up-regulates EGFR and STAT3 both at protein (Figure 4A) and RNA level (Figure 4B). Real Time PCR assay in SCC022 cells clearly shows that YB-1 silencing results in about 2 and 3.5 fold induction of EGFR and STAT3 transcripts, respectively (Figure 4B). Following ΔNp63α silencing, instead, the expression of both EGFR and STAT3 was switched off although the level of YB-1 protein remained unaltered (Figure 4A). These results suggest that ΔNp63α is a major activator of the EGFR/STAT3 axis in squamous carcinoma cells. Accordingly, in SCC011 and HaCaT cells where YB-1 silencing reduces ΔNp63α, EGFR and STAT3 transcription was also reduced (Supplementary Fig. 5A and B).

To confirm the ability of ΔNp63α to regulate EGFR gene expression we performed transient transfection and luciferase reporter assays in MDA-MB231 breast cancer cells expressing no detectable p63. MDA-MB231 cells were transiently transfected with the EGFR promoter-luciferase vector and increasing amount of expression plasmid encoding wild type ΔNp63α or its mutant form bearing the F to L substitution at position 518 of the SAM domain. This mutant was previously described to be transactivation defective (Radoja et al., 2007). Remarkably, wild type but not mutant ΔNp63α protein induced luciferase activity, in a dose-dependent manner (Figure 4C and D). Moreover, Western blot analysis of extracts from MDA-MB231 breast cancer cells

transiently transfected with ΔNp63α showed induction of both EGFR and STAT3 endogenous proteins, confirming that EGFR and STAT3 expression are induced by ΔNp63α (Figure 4E).

DISCUSSION

YB-1 is a versatile protein associated with many malignancies. However, because of its multifunctional character, the role of YB-1 in neoplastic cell growth remains elusive (Bader et al., 2006).

Our previous (Di Costanzo et al., 2012) and present data show that ΔNp63α hyper-expression, as it occurs in squamous carcinoma cells, is associated with YB-1 nuclear localization where it is expected to play a pro-proliferative role. In the present manuscript we show that YB-1 depletion has a strong negative impact on cell survival of both immortalized HaCaT keratinocytes and non-metastatic SCC011 squamous carcinoma cells. Interestingly, in HaCaT and SCC011 cells, YB-1 knockdown causes a significant reduction of ΔNp63α transcription (Yang et al., 1999; Senoo et al., 2004). However, in HaCaT and SCC cells, ΔNp63α knockdown is not sufficient to trigger cell death thereby indicating that YB-1, in keratinocytes, plays additional p63-independent pro-survival functions.

Surprisingly, in highly metastatic SCC022 cells, YB-1 silencing does not result in cell death. Strikingly, in these cells, YB-1 silencing potentiates AKT activation suggesting that YB-1 can act as a negative regulator of the PI3K/AKT signaling pathway and its loss allows PI3K/AKT-dependent induction of pro-survival genes, including ΔNp63α. Interestingly, the low level of endogenous PTEN observed in SCC022 cells can likely explain the constitutive activation of the PI3K/AKT pathway observed in this cell line. Remarkably, we have observed only in HaCaT and SCC011 cells a strong activation of PTEN in response to YB-1 depletion. In SCC022 cells, instead, where PI3K/AKT hyper-activation sustains ΔNp63α protein level, we did not observe any increase

of PTEN after YB-1 depletion. However, at this stage, we can hypothesize that, in this cell line, PTEN cannot be up-regulated because of epigenetic or other inactivating mechanisms.

The evidence that PI3K/AKT hyperactivation in SCC022 cells is responsible for ΔNp63α transcriptional induction is in line with previous studies showing that ΔNp63α is positively regulated by the PI3K pathway (Barbieri et al., 2003). However, it is important to remind that ΔNp63α has been shown to repress the expression of PTEN (Leonard et al., 2011). Accordingly, in PTEN-proficient HaCaT and SCC011 cells, where YB-1 silencing causes a decrease of ΔNp63α, we observed an increase in the level of PTEN protein which is expected to restrain signaling by the PI3K pathway.

In summary, our results indicate that, being able to sustain ΔNp63α gene expression, YB-1 is part of a complex molecular network linking ΔNp63α to the PI3K/AKT/PTEN pathway and that establishment of a positive feedback loop coupling induction of ΔNp63α expression with PI3K/AKT activation may be a relevant step in progression of squamous carcinogenesis.

An important finding of our work is the observation that ΔNp63α controls the expression of the Epidermal Growth Factor Receptor switching-on the entire EGFR/STAT3 axis. Accordingly, in normal adult epidermis, the EGFR is predominantly expressed in basal keratinocytes and signaling events elicited by it are known to affect their proliferation and migration (Bito et al., 2011). ΔNp63α, therefore, represents an important molecular connection between YB-1, the PI3K/AKT and the EGFR/STAT3 signaling pathways. We can postulate that constitutive activation of PI3K/AKT, such as in PTEN-deficient cells, may likely cause persistence of ΔNp63α which can induce keratinocyte hyper-proliferation by impinging on the EGFR/STAT3 pathway. Interestingly, in physiological conditions EGF-dependent and PI3K/AKT pathways are both required for efficient skin wound re-epithelialization (Haase et al., 2003). Moreover, EGFR/STAT3 inhibition was shown to be unable to induce apoptosis (Bito et al., 2003) thereby providing a plausible explanation of why ΔNp63α silencing alone was not sufficient to induce cell death in our experimental settings.

In summary, we have presented clear evidences to suggest that YB-1 can play a role in skin carcinogenesis. However, the molecular basis of cancer can widely vary and the ability of YB-1 to control multiple and overlapping pathways raises concerns about the consideration of YB-1 as an attractive target for therapy against metastatic squamous cancer. In particular, our results indicate that YB-1 knockdown in cells whose oncogenic transformation depends on PI3K/AKT constitutive activation is expected to enhance rather than arrest metastatic progression. Association of YB1-targeted therapy with drugs that target the PI3K and/or EGFR pathway should be evaluated as a valuable strategy to treat squamous carcinoma. *In vivo* experiments will help to clarify this relevant point.

Conflict of interest

The authors declare that they have no conflict of interest.

References

1. Amoresano A, Di Costanzo A, Leo G, Di Cunto F, La Mantia G, Guerrini L, Calabrò V. 2010. Identification of ΔNp63α Protein Interactions by Mass Spectrometry. J. Proteome Res. 9: 2042-48.
2. Bader AG. 2006. YB-1 activities in oncogenesis: transcription and translation. Curr Cancer Ther Rev . 2: 31–39.
3. Barbieri CE, Barton CE, Pietenpol JA. 2003. ΔNp63α expression is regulated by the phosphoinositide 3-kinase pathway. J Biol Chem; 278(51): 51408-51414.
4. Barbieri CE, Tang LJ, Brown KA, Pietenpol JA. 2006. Loss of p63 leads to increased cell migration and up-regulation of genes involved in invasion and metastasis. Cancer Research, 66: 7589- 7597.
5. Bito T, Sumita N, Ashida M, Budiyanto A, Ueda M, Ichihashi M, Tokura Y, Nishigori C. 2011. Inhibition of epidermal growth factor receptor and PI3K/AKT signaling suppresses cell proliferation and survival through regulation of Stat3 activation in human cutaneous cell carcinoma. Journal of Skin Cancer. doi:10.1155/2011/874571.
6. Carrol DK, Carrol JS, Leong CO, Cheng F, Brown M, Mills AA, Brugge JS, Ellisen LW 2006. p63 regulates an adhesion programme and cell survival in epithelial cells. Nat Cell Biol, 8(6): 551-561.
7. Danilov AV, Neupane D, Nagaraja AS, Feofanova E, Leigh AH, Di Renzo J., Kork M. 2011. DeltaNp63alpha-mediated induction of epidermal growth factor promotes pancreatic cancer cell growth and chemoresistence. Plos one: 6(10) e26815.
8. Di Costanzo A, Troiano A, Di Martino O, Cacace A, Natale CF, Ventre M, Netti P, Caserta S, Pollice A, La Mantia G, Calabrò V. 2012. The p63 protein isoforms ΔNp63α modulates Y-box binding protein 1 in its subcellular distribution and regulation of cell survival and motility genes. J Biol Chem, 287(36):30170-80.

9. Eliseeva A, Kim ER, Guryanov SG, Ovchinnikov LP, Lyabin DN. 2011. Y-Box-Binding Protein 1 (YB-1) and its function. Biochemistry (Moscow), 76(13): 1402-1433.
10. Haase I, Evans R, Pofahl R, Watt FM. 2003. Regulation of keratinocytes shape, migration and wound epithelialization by IGF-1-and EGF-dependent signaling pathways. J Cell Sci . 116: 3227-3238.
11. Hibi K, Trink B, Patturajan M, Westra WH, Caballero OL, Hill DE, Ratoviski EA, Jen J, Sidransky D. 2000. Ais is an oncogene amplified in Squamous cell carcinoma. Proc. Natl. Acad. Sci. USA; 97: 5462-5467.
12. Leonard MK, Kommagani R, Payal V, Mayo LD, Shamma HN, Kadakia MP. 2011. ΔNp63α regulates keratinocytes proliferation by controlling PTEN expression and localization. Cell Death Differ. 18(12): 1924-1933.
13. Lefort K, Mandinova A, Ostano P, Kolev V, Calpini V, Kolfschoten I, Devgan V, Lieb J, Rafooul W, Hohl D, Neel V, Garlick J, Chiorino G, Dotto P. 2007. Notch 1 is a p53 target gene involved in human keratinocytes tumor suppression through negative regulation of ROCK1/2 and MRCKα kinases. Genes Dev, 21(5): 562-577.
14. Livak KJ, Schmittgen TD. 2011. Analysis of relative gene expression data using Real-Time Quantitative PCR and the $2^{-DDC}{}_{T}$ method. *Methods*. **25**: 402-408.
15. Lo Iacono M, Di Costanzo A, Calogero RA, Mansueto G, Saviozzi S, Crispi S, Pollice A, La Mantia G, Calabrò V. 2006. The Hay Wells Syndrome-Derived TAp63αQ540L Mutant has Impaired Transcriptional and Cell Growth Regulatory Activity. Cell Cycle, 5(1):78-87
16. Kolk A, Jubitz N, Mengele K, Mantwill K, Bissinger O, Schmitt M, Kremer M, Holm PS. 2011. Expression of Y-box-binding protein YB-1 allows stratification into long- and short-term survivors of head and neck cancer patients. Br J Cancer, 105(12):1864-1873.
17. Koster MI. 2010. p63 in skin development and ectodermal dysplasias. J Invest Dermatol; 130(10): 2352-2358.

18. Moll UM, Slade N. 2004. p63 and p73: roles in development and tumor formation. Mol Cancer Res; 2: 371-386.
19. Radoja N, Guerrini L, Lo Iacono N, Merlo GR, Costanzo A, Weinberg WC, La Mantia G, Calabro V, Morasso MI. 2007. Homeobox gene Dlx3 is regulated by p63 during ectoderm development: relevance in the pathogenesis of ectodermal dysplasias. Development 134(1): 13-18.
20. Ripamonti F, Albano L, Rossini A, Borrelli S, Fabris S, Mantovani R, Neri A, Balsari A, Magnifico A, Tagliabue E. 2013. EGFR through STAT3 modulates ΔNp63α expession to sustain tumor-initiating cell proliferation in squamous cell carcinomas. J Cell Physiol; 228(4): 871-8.
21. Rocco JW, Leong CO, Kuperwasser N, DeYoung MP, Ellisen LW. 2006. p63 mediates survival in squamous cell carcinoma by suppression of p73-dependent apoptosis. Cancer Cell; 9(1): 45-56.
22. Rossi M, De Simone M, Pollice A, Santoro R, La Mantia G, Guerrini L, Calabrò V. 2006. Itch/AIP4 associates with and promotes p63 protein degradation. Cell Cycle; 5(16):1816-22.
23. Schittek B, Psenner K, Sauer B, Meier F, Iftner T, Garbe C. 2007. The increased expression of Y box-binding protein 1 in melanoma stimulates proliferation and tumor invasion, antagonizes apoptosis and enhances chemoresistance. Int J Cancer, 120:2110–2118.
24. Senoo M, Manis JP, Alt FW, McKeon F. 2004. p63 and p73 are not required for the development and p53-dependent apoptosis of T cells. Cancer Cell; 6: 85-89.
25. Shiota M, Izumi H, Onitsuka T, Miyamoto N, Kashiwagi E, Kidani A, Yokomizo A, Naito S, Kohno K. 2008. Twist promotes tumor cell growth through YB-1 expression.Cancer Res, 68(1): 98-105.
26. Shiota M, Zoubeidi A, Kumano M, Beraldi E, Naito S, Nelson C, Sorensen P, Gleave M. 2011. Clusterin is a critical downstream mediator of stress-induced YB-1 transactivation in Prostate Cancer. Mol Cancer Res; 9:1755-1766.

27. Sinnberg T, Sauer B, Holm P, Spangler B, Kuphal S, Bosserhoff A, Schittek B. 2012. MAPK and PI3K/AKT mediated YB-1 activation promotes melanoma cell proliferation which is counteracted by an auto regulatory loop. Exp. Dermatol; 21(4):265-270.
28. Song MS, Salmena L, Pandolfi PP. 2012. The function and regulation of the PTEN tumor suppressor. Nature Reviews Molecular Cell Biology, 13: 283-296.
29. Sutherland BW, Kucab J, Wu J, Lee C, Cheang MC, Yorida E, Turbin D, Dedhar S, Nelson C, Pollak M, Leighton Grimes H, Miller K, Badve S, Huntsman D,Blake-Gilks C, Chen M, Pallen CJ, Dunn SE. 2005. AKT phosphorylates the Y-box binding protein 1 at Ser102 located in the cold shock domain and affects the anchorage-independent growth of breast cancer cells. Oncogene**,** 24(26):4281-4292.
30. To K, Fotovati A, Reipas KM, Jennifer HL, Hu K,Wang J, Astanehe A, Davies AH, Lee L, Stratford AL, Raouf A, Johnson P, Berquin IM, Royer HD, Eaves CJ, Dunn SE. 2010. YB-1 induces expression of CD44 and CD49f leading to enhanced self-renewal, mammosphere growth, and drug resistance. Cancer Res; 70(7): 2840-2851.
31. Toh S, Nakamura T, Ohga T, Koike K**,** Uchiumi T**,** Wada M**,** Kuwano M**,** Kohno K. 1998. Genomic organization of the human Y-box protein (YB-1) gene. *Gene*, 206:93 -97.
32. Uramoto H, Izumi H, Ise T, Tada M, Uchiumi T, Kuwano M, Yasumoto K, Keiko F, Kohno K. 2002. p73 interacts with c-Myc to regulate Y-box-binding protein-1 expression. J Biol Chem, 277: 31694-31702.
33. Yang A, Schweitzer R, Sun D, Kaghad M, Walker N, Bronson RT, Tabin C, Sharpe A, Caput D, Crum C, McKeon F. 1999. p63 is essential for regenerative proliferation in limb, craniofacial and epithelial development. Nature; 398: 714-71.

Figures Legend

Figure 1. YB-1 knockdown affects HaCaT cell survival. (**A) upper panel,** Phase-Contrast imaging and Hoechst staining (**lower panel**) showing HaCaT keratinocyte cells transfected with

scrambled, YB-1 or p63 siRNA oligos. (**B**) Representative immunoblot analyses of HaCaT keratinocytes transfected with YB1 (**upper panel**), p63 (**lower panel**) or scrambled (siCtrl) siRNA oligos, respectively. 48 hours after silencing whole cell extracts were immunoblotted with YB-1, p63 and PARP antibodies. Actin was used as a loading control. Bar graphs are quantitative densitometric analyses of four indipendent Western blots. The blots were normalized to actin and the fold-changes of protein levels are reported in comparison to control (value set at 1.0). P-value <0.05 is represented by *; P-value <0.01 is represented by **. (**C**) Quantitative real-time PCR analysis of HaCaT keratinocytes transfected with scrambled or YB-1 siRNA oligos. GADD45A mRNA level was measured as a control. (**D**) Quantitative Real-time PCR analysis of HaCaT keratinocytes transfected with scrambled or p63 siRNA oligos. In both experiments data were analyzed according to the fold-changes compared to scrambled control (value set at 1.0) using the $2^{-\Delta\Delta Ct}$ method. P-value <0.05 is represented by *; P-value <0.01 is represented by **.

Figure 2. YB-1 knockdown in SCC011 and SCC022 squamous carcinoma cells. (A) Phase-contrast imaging showing SCC011 (**upper panel**) and SCC022 (**lower panel**) cells at 48 hours post-YB1 silencing. (**B**) Representative immunoblot analysis of SCC011 or SCC022 cells transfected with scrambled or YB-1 siRNA oligos. 48 hours after silencing whole cell lysates were immunoblotted with YB-1, p63 and PARP antibodies. GAPDH was used as a loading control. Bar graph is a quantitative densitometric analysis of four indipendent Western blots. The blots were normalized to GAPDH and the fold-changes of protein levels are reported in comparison to control (value set at 1.0). P-value <0.05 is represented by *; P-value <0.01 is represented by **. (**C**) Quantitative Real-time PCR analysis of SCC011 (**left panel**) and SCC022 cells (**right panel**) transfected with scrambled or YB-1 siRNA oligos. Data were analyzed according to the fold-changes compared to scrambled control (value set at 1.0) using the $2^{-\Delta\Delta Ct}$ method. P-value <0.05 is represented by *; P-value <0.01 is represented by **. (**D**) Effect of

YB1 silencing on the viability of HaCaT and SCC cells. Cell viability was assessed by MTT assay following 48 hours of YB-1 silencing. Data are represented as the mean +/- SD from three independent experiments. The asterisk indicates P-value<0.05.

Figure 3. YB-1 knockdown enhances pAKT^{S473} in SCC022 squamous carcinoma. (A) Immunoblot analysis of HaCaT, SCC011 and SCC022 cells transfected with scrambled or YB1-siRNA oligos. 48 hours after silencing whole cell extracts were immunoblotted with YB-1, pAKT^{S473} and AKT antibodies. Actin was used as a loading control. **(B)** SCC022 cells were transfected with scrambled or YB-1 siRNA oligos transfection. After 42 hrs cells were treated with LY294002 for 6 hrs. Whole cell extracts were analyzed by immunoblotting with YB-1, pAKT^{S473}, p63 and AKT antibodies. Actin was used as loading control. (**C**) Quantitative Real-time PCR of ΔNp63 mRNA levels. ΔNp63 mRNA levels were analyzed according to the fold-changes compared to scrambled control (value set at 1.0) using the $2^{-\Delta\Delta Ct}$ method. P-value < 0.05 is represented by *; P-value < 0.01 is represented by **. DMSO was used as control (**D**) Immunoblot analysis of HaCaT, SCC011 and SCC022 cells. Whole cell extracts were immunoblotted with, PTEN, pAKT^{S47} , and AKT antibodies. GAPDH was used as loading control. (**E**) Nuclear and cytoplasmic fractionation of extracts from control or YB-1 silenced HaCaT, SCC011 and SCC022 cells are shown in Figure 5A. Fractions were analysed by immunoblotting with PTEN antibody. GAPDH and PARP were used as cytoplasmic and nuclear controls, respectively.

Figure 4. Cross-talk of ΔNp63α and YB-1 with EGFR/STAT3 pathway. (A) Immunoblot analysis of SCC022 cells transfected with scramble, YB-1 or p63 siRNA oligos. Whole cell extracts were immunoblotted with, YB-1, p63, EGFR, STAT3 antibodies. Actin was used as a loading control. **(B)** Quantitative Real-time PCR analysis of SCC022 cells transfected with

scrambled or YB-1 siRNA oligos. YB-1, EGFR and STAT3 mRNA levels were analyzed according to the fold-changes compared to scrambled control (value set at 1.0) using the $2^{-\Delta\Delta Ct}$ method. P-value < 0.05 is represented by *; P-value < 0.01 is represented by **. **(C)** Luciferase assay of EGFR-promoter activity in MDA-MB231 cells. Cells were transiently transfected with 1µg of luciferase reporter plasmid and the indicated amounts of ΔNp63α or ΔNp63α F518L plasmids. Luciferase assay was performed at 48 hrs post-transfection. Values are the mean +/- SD of three independent experimental points. **(D**) Representative immunoblotting showing the level of ΔNp63α in transfected MDA-MB231 cell extracts used for the luciferase assay shown in 7C. GAPDH immunodetection was used as loading control. **(E**) MDA-MB231 cells were transfected with empty vector or ΔNp63α plasmids. At 24h post-transfection cells were harvested and whole cell extracts were analyzed by immunoblotting with p63, STAT3 and EGFR antibodies. Actin was used as a loading control.

Supplementary Figures

S1. YB-1 and ΔNp63α coimmunoprecipitation in HaCaT cells. (**A**) Extracts from HaCaT cells were immunoprecipitated with anti-p63 antibodies and the immunocomplexes were blotted and probed with anti-YB-1, as indicated. (**B**) Extracts from HaCaT cells were immunoprecipitated with anti-YB-1 antibodies and the immunocomplexes were blotted and probed with anti-p63. Samples with no antibody (no Ab) or irrelevant α-mouse and α-rabbit antibodies were included as controls. (**C**) Immunoblot analysis of YB-1 level in HaCaT cells treated with proteasome inhibitor MG132 for 6h (5µM final concentration). 36kDa and 43kDa YB-1 forms are reduced with concomitant accumulation of full-length YB-1 50kDa band showing the identity of YB-1 bands.

S2. **YB-1 and p63 knockdown in SCC022 cells. (A)** Immunofluorescence assay in SCC022 cells transfected with scrambled, YB-1 or p63 siRNA oligos. YB1 was detected using anti-YB-1 and secondary anti-rabbit Cy5-conjugated (green) antibodies. p63 was detected using anti-p63 and secondary anti-mouse Cy3-conjugated (red) antibodies. Hoechst was used to stain nuclei**. (B)** (upper panel**)** SCC022 cells were incubated with normal mouse serum and secondary anti-mouse Cy3-conjugated (red) antibodies; (lower panel) SCC022 cells were incubated with normal rabbit serum and secondary anti-rabbit Cy5-conjugated (green) antibodies.

S3. Effect of p63 and YB-1 silencing on SCC022 cells migration speed. (A) Motility assay on SCC022 cells after transient silencing of p63 and YB-1 performed by time-lapse microscopy. After 24 h of incubation with siRNA oligos, cell migration assay was performed. Averaged cell speeds after 16 h of observation are reported. Horizontal lines and boxes and whiskers represent the medians, 25th/75th, and 5th/95th percentile, respectively. P-value < 0.01 is represented by **. Only statistically different doubles are marked. (**B**) Immunoblot analysis of ΔNp63α and YB-1 protein levels in SCC022 cells after 40 h of ΔNp63α or YB-1 silencing and used in cell migration assay. Cell extracts were blotted and probed with anti-p63 or anti-YB-1 antibodies. GAPDH was used as a loading control. ΔNp63α protein band was almost undetectable while YB-1 protein was reduced to 40%, as assed by densitometric scanning.

S4. Proteasome activity is not involved in ΔNp63α up-regulation upon YB-1 silencing. Immunoblot analysis of SCC022 cells transfected with scrambled or YB1-siRNA oligos and treated with MG132 (6 hrs) after 42 hours of YB-1 silencing cells. Whole cell extracts were immunoblotted with YB-1 and p63 antibodies. Actin was used as loading control.

S5. Effect of YB-1 silencing on EGFR/STAT3 mRNA levels in SCC011 and HaCaT cells. Quantitative Real-time PCR analysis of **(A)** SCC011 cells and **(B)** HaCaT cells transfected with scrambled or YB-1 siRNA oligos. YB-1, EGFR and STAT3 mRNA levels were analyzed according to the fold-changes compared to scrambled control (value set at 1.0) using the $2^{-\Delta\Delta Ct}$ method. P-value < 0.05 is represented by *; P-value < 0.01 is represented by **.

Figure 1

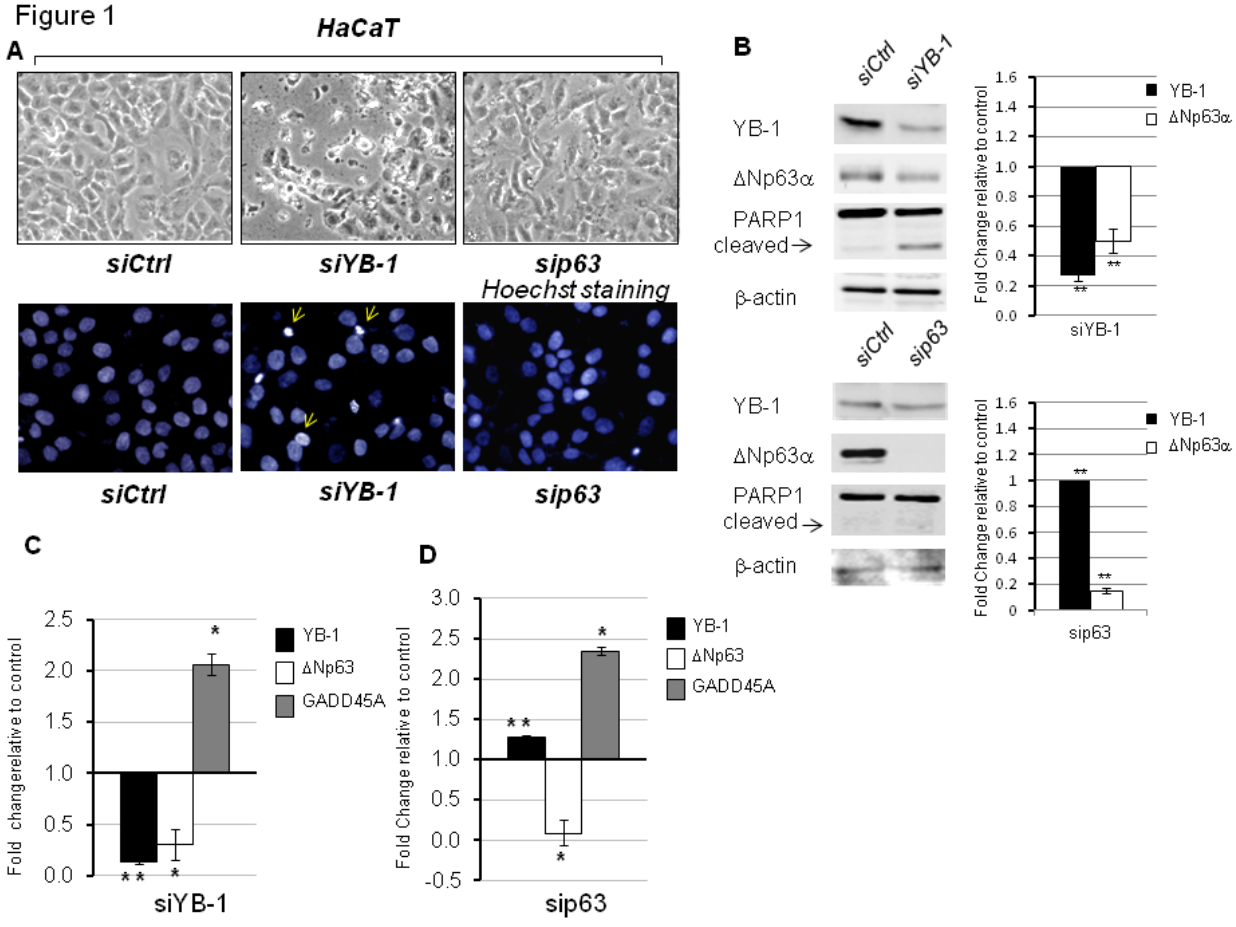

Figure 2

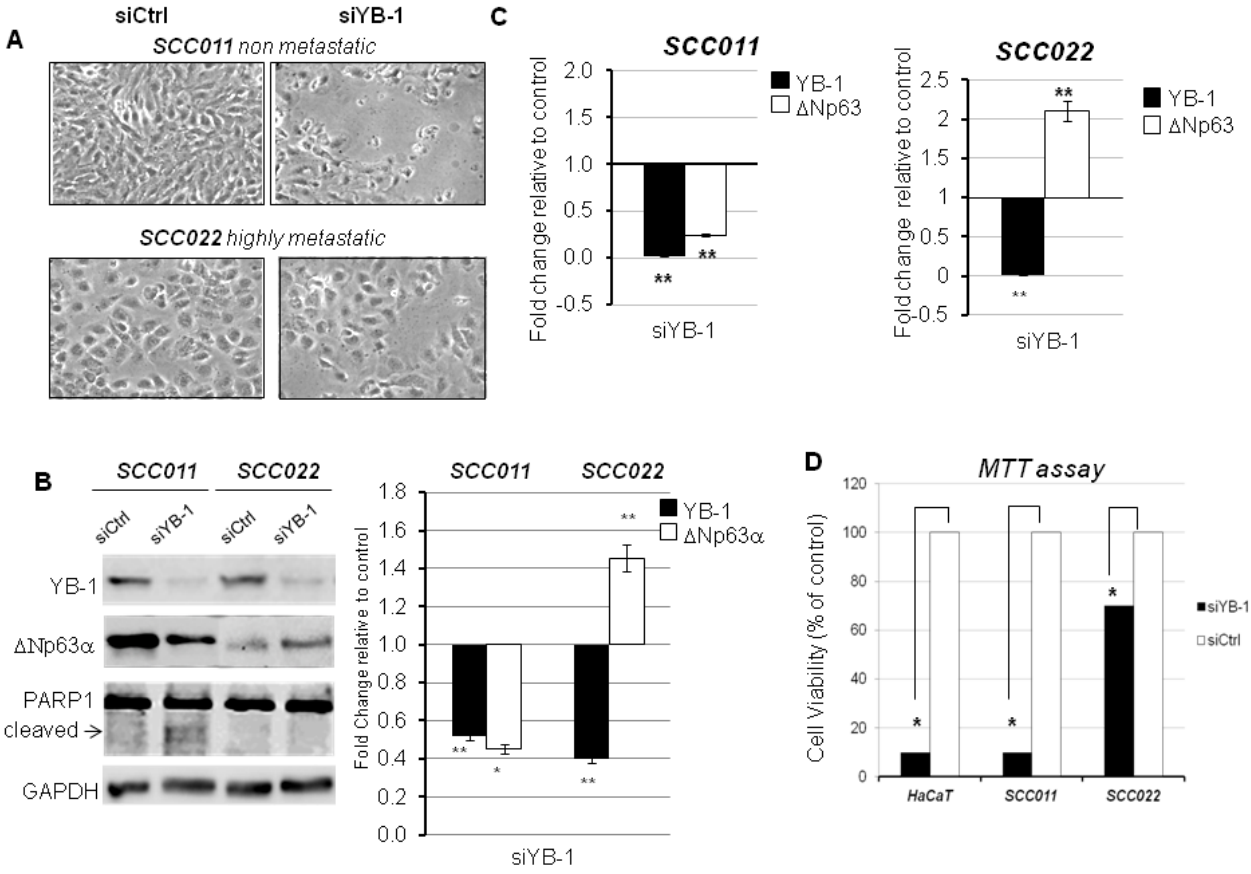

Figure 3

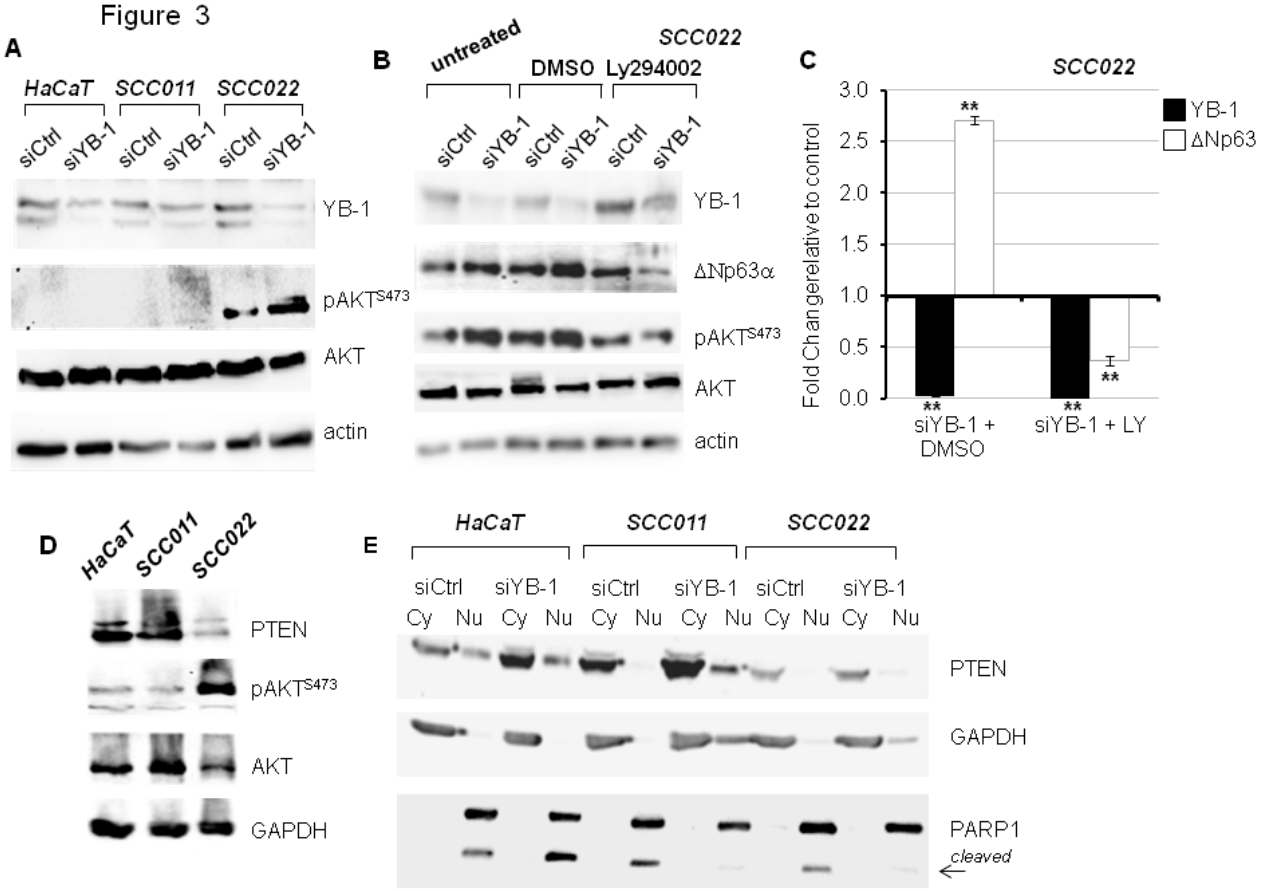

Figure 4

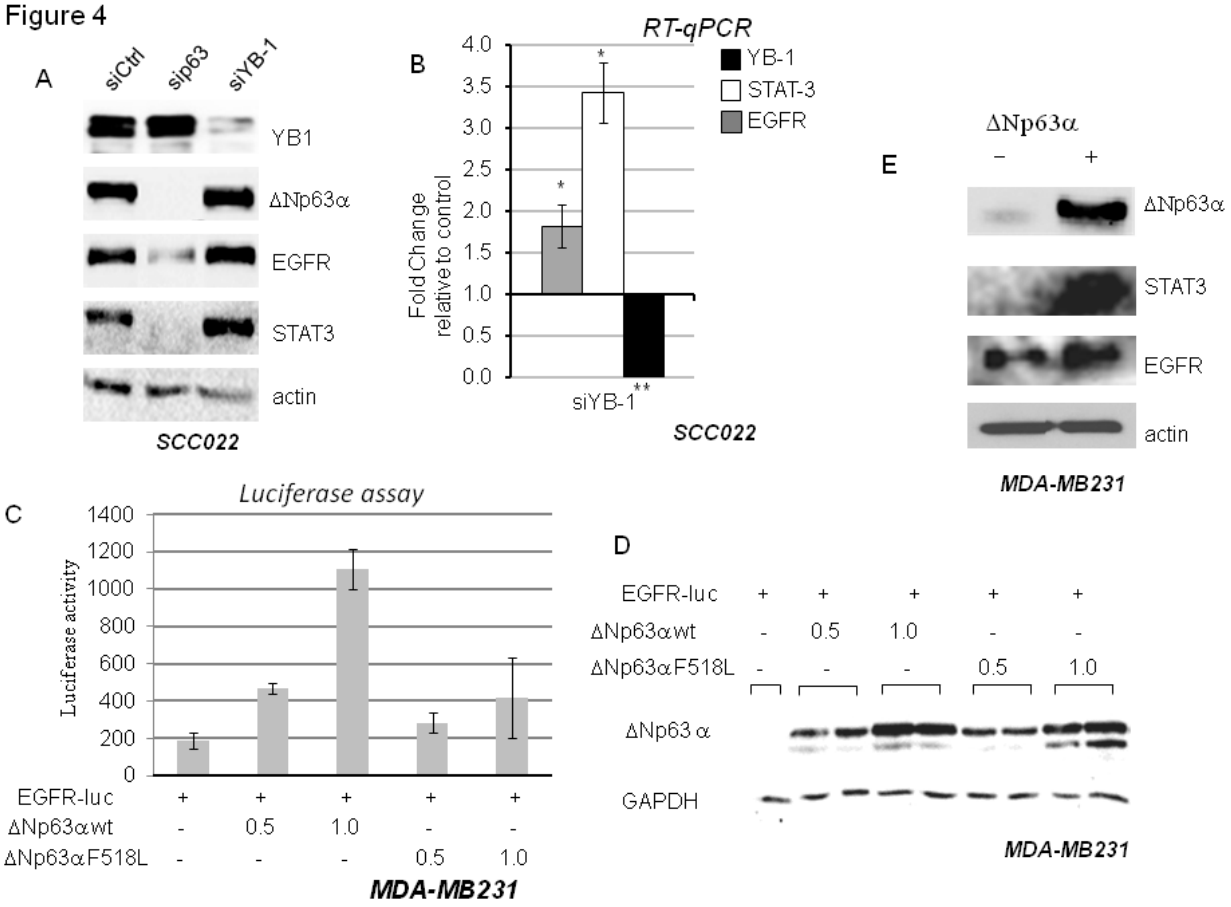

Biochemical Pharmacology 85 (2013) 999–1006

Contents lists available at SciVerse ScienceDirect

Biochemical Pharmacology

journal homepage: www.elsevier.com/locate/biochempharm

p63 involvement in poly(ADP-ribose) polymerase 1 signaling of topoisomerase I-dependent DNA damage in carcinoma cells

Daniela Montariello, Annaelena Troiano, Maria Malanga, Viola Calabrò, Piera Quesada *

Department of Biology, University of Naples "Federico II", Italy

ARTICLE INFO

Article history:
Received 18 December 2012
Accepted 22 January 2013
Available online 29 January 2013

Keywords:
TOP I inhibitors
PARP1 inhibitors
P53
P63
Carcinoma cells

ABSTRACT

Poly(ADP-ribose)polymerase 1 (PARP-1) inhibitors are thought as breakthrough for cancer treatment in solid tumors such as breast cancer through their effects on PARP's enzymatic activity. Our previous findings showed that the hydrophilic PARP inhibitor PJ34 enhances the sensitivity of p53 proficient MCF7 breast carcinoma cells to topotecan, a DNA Topoisomerase I (TOP 1) inhibitor.

In the present study, we combine the classical TOP 1 poison camptothecin or its water-soluble derivative topotecan with PJ34 to investigate the potentiation of chemotherapeutic efficiency in MCF7 ($p53^{WT}$), MDA-MB231 ($p53^{mut}$) breast carcinoma cells and SCC022 ($p53^{null}$) squamous carcinoma cells.

We show that, following TPT-PJ34 combined treatment, MCF7 cells exhibit apoptotic death while MDA-MB231 and SCC022 cells are more resistant to these agents. Specifically, in MCF7, (i) PJ34 in combination with TPT causes a G2/M cell cycle arrest followed by massive apoptosis; (ii) PJ34 addition reverts TPT-dependent PARP-1 automodification and triggers caspase-dependent PARP-1 proteolysis; (iii) TPT, used as a single agent, stimulates p53 expression while in combination with PJ34 increases p53, TAp63α and TAp63γ protein levels with a concomitant reduction of MDM2 protein.

The identification of p63 proteins as new players involved in the cancer cell response to TPT-PJ34 is relevant for a better understanding of the PARP1-dependent signaling of DNA damage. Furthermore, our data indicate that, in response to TPT-PJ34 combined chemotherapy, a functional cooperation between p53 and TAp63 proteins may occur and be essential to trigger apoptotic cell death.

1. Introduction

Poly(ADP-ribose)polymerase (PARP) inhibitors are touted as a breakthrough for cancer treatment in solid tumors such as triple negative breast cancer and ovarian cancer through their effects on PARP-1's enzymatic ADP ribosylation activity [1]; however, less characterized PARP-1 additional functions have also been reported and they can be critical for successful anticancer therapies.

PARPs are involved in the regulation of many cellular processes such as DNA repair, cell cycle progression and cell death [2]. PARP-1 and PARP-2 are constitutive factors of the DNA damage surveillance network, acting as DNA break sensor [3] and several observations indicate that poly(ADP-ribosyl)ation plays an early role in DSB signaling and repair pathways [4,5]. PARP-1 and 2 are highly activated upon binding to DNA strand interruptions and synthesize, within few seconds, large amounts of ADP-ribose polymer (PAR) on several nuclear proteins including themselves, histones, DNA-Topoisomerase 1 (TOP 1) and DNA-dependent protein kinase (DNA-PK) [6,7]. Furthermore, in response to DNA damage, PARP-1 interacts with both ATR and ATM kinases suggesting another susceptible pathway for PARP inhibitors induced apoptosis. [8].

Cell cycle checkpoint activation and growth arrest in response to DNA damage rely on the ATM/ATR kinases and their downstream targets like p53 [9–11]. p53 activates p21WAF which binds PARP-1 during base excision repair [12].

Certain PARP inhibitors including PJ34 induce a G2/M arrest when used in conjunction with methylating agents [13] cisplatin [14] and TOP I poisons such as camptothecin (CPT) or its water-soluble derivative topotecan (TPT) [15], highlighting the existence of potentially different outcomes from PARP inhibition whose molecular mechanisms have not yet been conclusively determined.

In brief, TOP I inhibitors reversibly abolish the DNA religation activity of TOP I generating single strand breaks (SSBs) to which the protein is covalently linked. Double strand breaks (DSBs) arise when replication forks collide with the SSBs and run off. Thus, CPT/TPT-induced DSBs are replication dependent or S phase specific and are usually repaired by the HR pathway [16,17]. According with previous findings poly(ADP-ribos)ylated PARP-1 and PARP-2 counteract CPT through non covalent but

* Corresponding author. Tel.: +39 081 679165; fax: +39 081 679233.
E-mail address: quesada@unina.it (P. Quesada).

0006-2952/$ – see front matter © 2013 Elsevier Inc. All rights reserved.
http://dx.doi.org/10.1016/j.bcp.2013.01.019

specific interaction of PAR with some TOP I sites which results in inhibition of DNA cleavage and stimulation of the religation reaction [6].

We have previously shown that PJ34 can positively or negatively modulate p53 and its target p21WAF depending of the cell genetic background or DNA damage stimulus (i.e. cisplatin or TPT) [18–20]. Indeed, regulating p21WAF expression is one model whereby PARP inhibitors, following the activation of different checkpoint pathways, can cause cell cycle arrest. It has recently been reported that in breast carcinoma MCF7 cells, PJ34 causes a p21WAF-dependent mitotic arrest and that neither PARP-1 nor p53 is required for this mechanism [21]. Furthermore, in triple negative breast cancer cell lines, PJ34 synergizes with cisplatin by reducing the levels of ΔNp63α with a concurrent increase of p21WAF [22].

ΔNp63α is a member of the p53 protein family highly expressed in squamous cell carcinoma and invasive ductal breast carcinoma [23,24]. ΔNp63α and p53 have been shown to inversely regulate target genes such as p21WAF in the context of DNA damage [22,25]. Owing to the presence of two promoters, the p63 gene encodes two major classes of proteins: those containing a transactivating (TA) domain homologous to the one present in p53 (i.e. TAp63) and those lacking it (i.e. ΔNp63) [24]. In addition, alternate splicing at the carboxy-terminal (C-terminal) generates at least three p63 variants (α, β and γ) in each class. The TAp63γ isoform resembles most p53, whereas the α isoforms include a conserved protein–protein interaction domain named Sterile Alpha Motif (SAM). TAp63 proteins mimic p53 function including transactivating many p53 target genes and inducing apoptosis, whereas the ΔNp63α protein, has been shown to repress p53-target genes acting as an oncogene [24,26].

On the light of all these evidences, the use of chemical inhibitors of PARP in combination with TOP I inhibitors CPT or TPT appears to be a promising approach to enhance the antitumour activity of these compounds.

Here, we have investigated the effect of PJ34 used as a single agent or in association with CPT or TPT in the DNA damage response of mammary breast cancer cells (MCF7^{p53wt} and MDA-MB231^{p53mut}) and squamous carcinoma cells (SCC022^{p53null}) showing an active involvement of p63 in the cellular response to these agents. We postulate that the sensitivity to combined treatments is mediated by sustained DNA damage/inefficient DNA repair triggering p53 and p63-mediated apoptosis.

2. Materials and methods

2.1. Drugs, media, antibodies and chemicals

CPT and TPT was from Glaxo Smith-Kline (Verona, Italy) and PJ34 [N-(6-oxo-5,6,-dihydrophenanthridin-2-yl)-(N,N-dimethylamino) Acetamide] from Alexis Biochemicals (Vinci-Biochem, Firenze, Italy). The cocktail of protease inhibitors was from ROCHE-Diagnostic (Milano, Italy).

MCF7, MDA-MB231 and SCC022 cells were from CLS Cell Lines Service (Eppelheim, Germany) Dulbecco's modified Eagle's medium (DMEM), heat-inactivated foetal bovine serum (FBS) and Roswell Park Memorial Institute (RPMI) medium were from Invitrogen (GIBCO, Milano, Italy); penicillin, streptomycin and L-glutamine were from LONZA (Milano, Italy).

Nicotinamide adenine [adenylate-^{32}P] dinucleotide-[^{32}P]-NAD$^+$ (1000 Ci/mmole, 10 mCi/ml) was supplied by GE Healthcare (Milano, Italy).

PVDF (poly-vinylidene-fluoride) membrane was from MILLIPORE S.p.A. (Milano, Italy). Not-fat-milk power was from EUROCLONE (Milano, Italy). Anti-DNA TOP I (Scl-70) human antibody from Topogen (ABCAM, Cambridge, UK). Anti-PARP1 mouse monoclonal antibody (C2-10), anti-p63 (4A4), anti-p53 (DO-1), anti-p21WAF (F-5), anti-cyclin B1 (V152), anti AIF (E-1) and anti-GAPDH (6C5) mouse monoclonal antibodies and anti-actin (H-196) rabbit polyclonal antibody were from Santa-Cruz Biotechnology (DBA, Milano, Italy). Anti-γH2AX (ser139, 2577) and anti-Bax (D2E11) rabbit polyclonal antibodies were from Cell Signaling (Invitrogen, Milano, Italy). Anti-MDM2 (Ab-2) mouse monoclonal antibody was from Oncogene Research Products (Boston, USA). Anti-PAR (10H) mouse monoclonal antibody was from Alexis Biochemicals (Vinci-Biochem, Firenze, Italy). Goat anti-mouse and goat anti-rabbit IgG HRP-conjugated antibodies were from Sigma–Aldrich (Milano, Italy).

All other chemicals analytical grade were of the highest quality commercially available.

2.2. Cell cultures

Breast cancer-derived MCF7^{p53wt} and MDA-MB231^{p53mut} cells were maintained in Dulbecco's modified Eagle's medium (DMEM) containing 10% (v/v) heat-inactivated foetal bovine serum (FBS), while squamous SCC022$^{p53\ null}$ carcinoma cells were maintained in Roswell Park Memorial Institute (RPMI) medium containing 10% (v/v) FBS, 100 U/ml penicillin, 100 g/ml streptomycin, 5 mM L-glutamine and incubated at 37 °C in a humidified atmosphere, *plus* 5% CO_2.

2.3. Cell treatments

Cells were seeded at 1×10^6 cells in 10 ml and 24 h after seeding, treated with 1 μM CPT (stock solution 1 mM DMSO) or 5 μM TPT,10× concentration inhibiting cellular growth by 50% (IC_{50}) [27]. 10 μM or 20 μM PJ34 alone and in combination, for 48 h in fresh medium. Culture medium was removed and, after PBS wash, cells were recovered 6×10^6 cells/ml in 50 mM Tris–HCl pH 7.5, 150 mM NaCl, 5 mM EDTA, 1% NP40 (Lysis Buffer) plus 2 mM PMSF and 1:25 dilution of protease inhibitors cocktail solution. After 40 min of incubation on ice, cellular suspensions were scraped and centrifuged at 16,000 × *g* for 20 min at 4 °C.

Cell growth inhibition was assessed by cell counting at different time points (0–24 48 h) or by the 3-[4,5-dimethylthiazol-2-yl]-2,5-diphenyltetrazolium bromide (MTT) assay using 1×10^4 48 h treated cells. The experiments were performed in triplicate.

2.4. Isolation of nuclear and post-nuclear fractions

To isolate sub-cellular fractions, 3×10^6 cells were suspended in 200 μl of 30 mM Tris–HCl pH 7.5 buffer, containing, 1.5 mM $MgCl_2$, 10 mM KCl, 1% (v/v) Triton X-100, 20% glycerol, 2 mM PMSF and 1:25 dilution of protease inhibitors cocktail solution. After 30 min of incubation on ice, cellular suspensions were centrifuged at 960 × *g* for 90 s at 4 °C and the nuclear fractions recovered in the pellet. The supernatant represents the cytoplasmic fraction.

Nuclear fractions were resuspended in 50 μl of 20 mM HEPES pH 7.9 buffer, containing 20 mM KCl, 0.2 mM EDTA, 1.5 mM $MgCl_2$, 25% glycerol and the protease inhibitors cocktail solution. Protein concentration was determined using the Bradford protein assay reagent (BIO-RAD Milano, Italy) with bovine serum albumin as a standard.

2.5. Cytofluorimetric analysis

Control and treated cells were fixed in 70% ethanol and stored at −20 °C until analysis. After a washing in PBS w/o Ca^{2+}/Mg^{2+}, cells were stained in 2 ml of propidium iodide (PI) staining solution [50 μg/ml of PI, 1 mg/ml of RNAse A in PBS w/o Ca^{2+}/Mg^{2+}, pH 7.4] overnight at 4 °C and DNA flow cytometry was performed in

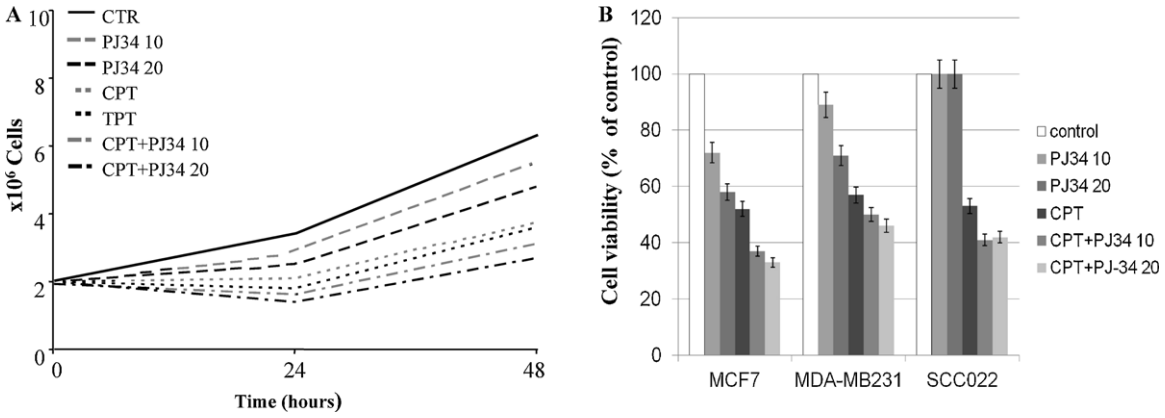

Fig. 1. Cell growth inhibition in MCF7, MDA-MB231 and SCC022 cells treated with CPT/TPT and PJ34 as single agents or in combination. Cells (10^4 cells/plate) were treated 48 h with CPT 1 μM or TPT 5 μM and 10 or 20 μM PJ34 alone or in combination: (A) MCF7 cell growth was measured by cell counting at different time points. Data refer to at least three experiments giving similar results. (B) 48 h treated MCF7, MDA-MB231 and SCC022 cells were used for determination of cell growth inhibition by MTT assay. Each plot represents the media of triplicates from three independent experiments.

duplicate by a FACScan flow cytometer (Becton Dickinson Franklin Lakes, NJ, USA) coupled with a CICERO work station (Cytomation). Cell cycle analysis was performed by the ModFit LT software (Verity Software House Inc., Topsham, ME, USA). FL2 *area* versus FL2 *width* gating was done to exclude doublets from the G2/M region. For each sample 15,000 events were stored in list mode file.

2.6. Analysis of [^{32}P]-PAR synthesis

Following treatment with CPT/TPT ± PJ34 of intact cell (5×10^4cells/plate), [^{32}P]-PAR synthesis was determined by substituting the culture medium with 1 ml of 50 mM HEPES pH 7.5 buffer, containing 28 mM KCl, 28 mM NaCl, 2 mM $MgCl_2$, 0.01% digitonin, 0.1 mM PMSF, 1:25 dilution of a cocktail of protease inhibitors, 0.125 μM NAD^+ and 5 μCi [^{32}P]-NAD^+ (1000 Ci/mmole). After incubation at 37 °C for 15 mins, cells were scraped, transferred to eppendorf tubes and mixed with TCA at 20% (w:v) final concentration. After 90 min standing on ice, samples were collected by centrifugation at 12000 rpm for 15 min, washed twice with 5% TCA and three times with ethanol. [^{32}P]-PAR incorporated in the TCA-insoluble fraction was measured by Cerenkov counting using a LS8100 liquid scintillation spectrometer (Beckman Coulter S.p.A. Milano, Italy). Finally, TCA protein pellets were resuspended in Laemmli buffer; proteins were separated by 10% SDS-PAGE and after electroblotting on PVDF membrane, [^{32}P]-PAR acceptors were visualized by autoradiographic analysis by the PhosphorImager (BIO-RAD). Immunodetection of specific proteins was accomplished on the same blots after autoradiography.

2.7. Immunological analyses

Aliquots of 10 μl of cellular proteins (approx 50–100 μg) were separated by 10% SDS-PAGE and transferred onto a PVDF membrane using an electroblotting apparatus (BIO-RAD). The membrane was subjected to immunodetection after blocking with 5% non-fat milk in TBST 1 h, with anti-PARP1 (C2-10; diluted 1:2500), anti-TOP I (Scl-70; diluted 1:1000), anti-PAR (10H; diluted 1:500), anti-p63 (4A4; diluted 1:2000), anti-p53 (DO-1; diluted 1:5000), anti-p21WAF (F-5; diluted 1:1000), anti-MDM2 (Ab-2; diluted 1:1000), anti-cyclin B1 (V152; diluted 1:1000), anti-γH2AX (2577; diluted 1:1000), anti-Bax (D2E11; diluted 1:1000), anti AIF (E1; diluted 1:2000), anti-GAPDH (6C5; diluted 1:5000), anti-actin (H-196; diluted 1:2000) overnight at room temperature.

As secondary antibodies goat-anti-mouse or goat-anti-rabbit IgG HRP-conjugate (diluted 1:5000–1:10,000) in 3% (w/v) non-fat milk in TBST were used. Peroxidase activity was detected using the ECL Advance Western Blot Kit of GE Healthcare (Milano, Italy) and quantified using the Immuno-Star Chemiluminescent detection system GS710 (BIO-RAD) and the Arbitrary Densitometric Units normalised on those of the GAPDH loading control.

3. Results

3.1. Effect of PJ34 on TPT/CPT-induced growth inhibition in human carcinoma cells

The concentrations of the agents and the time points used in this study were chosen on the basis of previously published data [20,27]. Preliminary experiments, in breast carcinoma MCF7^{p53wt} cells, showed that 1 μM CPT inhibits cell growth similarly to 5 μM TPT (Fig. 1A). To potentiate the CPT/TPT cytostatic effect, PJ34 concentrations were used in a sub-lethal range (10–20 μM). A 48-h of exposure, corresponding approximately to two rounds of MCF7^{p53wt} cell replication, was used according to the administration procedure during anticancer therapy. As shown in Fig. 1A, at 24 h CPT/TPT treatment has a cytostatic effect, while PJ34 induces growth retardation in a dose-dependent way, whereupon cells start to recover but the rate of recovery was significantly affected by CPT-PJ34 combined treatment (Fig. 1A).

We next investigated the impact of CPT on MDA-MB231 and SCC022 cell survival. MDA-MB231 express a mutant p53 (p53R280 K) while SCC022 cells are p53 null. Cells were plated, treated with CPT for 48 h and subjected to the MTT assay to compare viability of treated and untreated cells. As shown in Fig. 1B, CPT significantly reduces cell viability of all cell lines tested (around 50% of control). Moreover, treatment with PJ34 alone affects MCF7 and MDA-MB231 cell viability, in a dose-dependent way, whereas SCC022 cells remain almost unaffected. Interestingly, compared with single drug treatments, combination of PJ34 with CPT results in a significant enhancement of cytotoxicity in MCF7 cells (37–33% of cell survival) while in MDA-MB231 and SCC022 cells addition of PJ34 to CPT has a lower impact on cell survival (Fig. 1B). Similar results are observed when PJ34 is added to TPT (data not shown).

We have previously reported that TPT at concentrations higher than 1 μM promptly arrested the cells in S phase while concentrations equal or lower than 1 μM cause a G2/M arrest [20]. To gain insight into the molecular mechanism of TPT-PJ34 interactive cytotoxicity we analysed the cell cycle distribution of MCF7 cells treated with 10 or 20 μM PJ34 alone or in combination with 1 μM TPT. As shown in Fig. 2, after 48 h treatment, 1 μM TPT

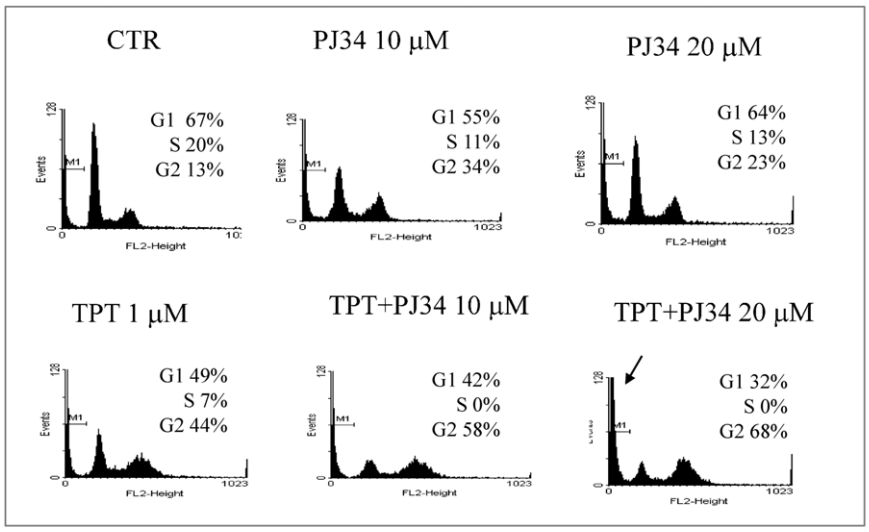

	% subG1 cells
Untreated	6
TPT 1 μM	14
PJ34 10 μM	16
PJ34 20 μM	19
TPT 1 + PJ34 10μM	22
TPT 1 + PJ34 20μM	55

Fig. 2. Cell cycle analysis of MCF7 cells subjected to TPT and PJ34 single and combined treatments. MCF7 cells were treated 48 h with TPT 1 μM and 10 or 20 μM PJ34 alone or in combination. Control and treated cells (1×10^6) were fixed in 70% ethanol and used for flow cytometric analysis (see Section 2). Determination of DNA content after PI staining is shown and cells in G1, S and G2 phase are indicated as percentage (excluded sub-G1 cells). The table reports sub-G1 cells as the percentage of the entire population of cells. Data refer to one of three experiments giving similar results.

as well as 10 or 20 μM PJ34 induce accumulation of cells in G2/M phase and the cell cycle distribution is less affected by treatment with PJ34 (10 or 20 μM) than TPT used as single agents. Furthermore, addition of 10 or 20 μM PJ34 to 1 μM TPT causes a significant increase of G2/M cells, while S-phase cells are drastically reduced. Fig. 2 (table) also shows that single treatments cause an increase of cells with a sub-G1 DNA content (from 6 to 19%), probably due to induction of apoptotic cell death. Remarkably, an increase up to 55% of sub-G1 cells is observed with TPT 1 μM + PJ34 20 μM combined treatment, showing a 2× potentiation factor of PJ34 on TPT cytotoxicity.

3.2. Analysis of CPT- or TPT-dependent TOP I inactivation

It is already known that CPT and TPT abolish the religation activity of TOP I generating an abortive complex to which the enzyme is covalently linked [16]. Therefore, we determined the efficacy of TOP I inhibitors by looking at their capacity of trapping the enzyme in the abortive complex. This was detected, by looking at the disappearance of the immunoreactive band of the TOP I soluble fraction by western blot analysis. After 48 h of treatment, both 1 μM CPT and 5 μM TPT are able to block, almost completely, the TOP I enzyme in the abortive complex, in all cell lines tested (Fig. 3).

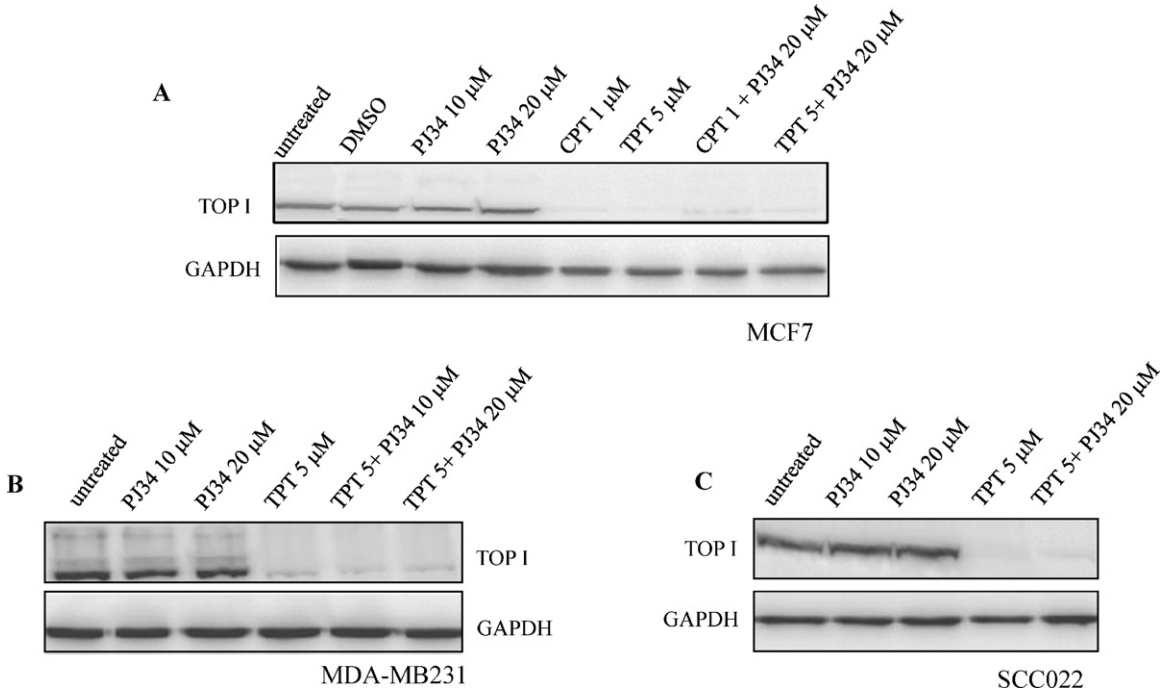

Fig. 3. Western blot analysis of TOP I soluble fraction in carcinoma cells untreated or 48 h treated with the indicated drugs. Untreated and treated whole cell extracts (50–100 μg of proteins) were subjected to 10% SDS-PAGE, electroblotted on PVDF and incubated with the anti-TOP I antibody.
Immunodetection in MCF7 (A), MDA-MB231 (B) and SCC022 (C) cells is shown. 0.1% DMSO treated cells were analysed as CPT internal control. GAPDH was used as loading control.

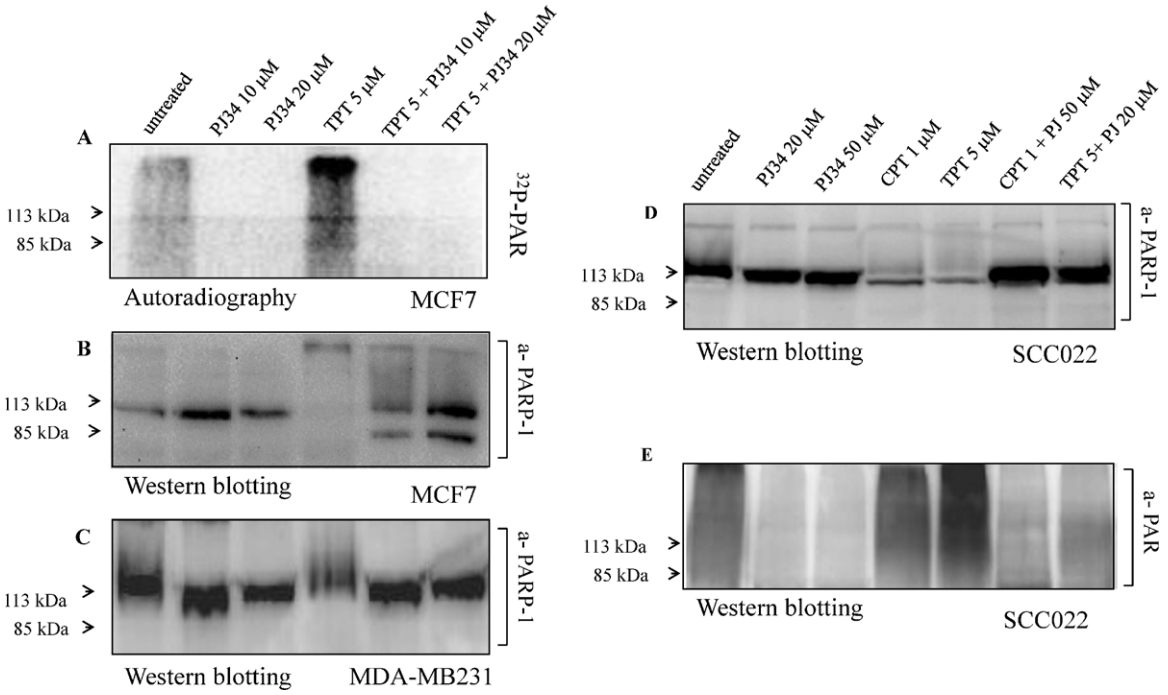

Fig. 4. Analysis of TPT-dependent PARP-1 activation or PJ34-dependent PARP-1 inhibition in carcinoma cells untreated or 48 h treated with the indicated drugs. Whole cell extract (50–100 μg of proteins) after 10% SDS-PAGE and electroblotting on PVDF were either analysed by autoradiography or incubated with the different antibodies. (A) Autoradiographic analysis, of whole cell protein extract from untreated and treated MCF7 cells incubated with 0.125 μM [^{32}P]-NAD$^+$ (see Section 2); (B) immunodetection of PARP-1 on the blot shown in (A); (C) immunodetection of PARP-1 in whole cell protein extract from untreated and treated MDA-MB231cells; (D) immunodetection of PARP-1 in whole cell protein extract from untreated and treated SCC022 cells; (E) immunodetection of PAR on the blot shown in (D)

According to previous findings [20], PJ34 does not affect TOP I enzyme trapping when used in combination with CPT or TPT.

3.3. Analysis of PAR synthesis in carcinoma cells after treatment with TPT ± PJ34

PJ34 efficacy as PARP inhibitor was assessed by looking at its effect on PARP-1 automodification. Proliferating MCF7 cells were exposed to the drugs and PAR synthesis was measured in situ by incubation in the presence of 0.01% digitonin with 0.125 μM [^{32}P]-NAD$^+$. Samples were then analysed by SDS-PAGE followed by autoradiography. As shown in Fig. 4A, a smear of the signal above the PARP-1 molecular weight (113 kDa) is strongly increased in TPT treated cells compared to the untreated sample (Fig. 4A, lane 4). As previously reported [2] such a behaviour indicates automodification of PARP-1 by long and branched ADP-ribose polymers (up to 200 residues in chain) on several sites (up to 25) of the automodification domain. This process gives raise to higher molecular weight PARP-1 forms that do not enter the polyacrylamide gel matrix. The identity of the PAR modified protein was confirmed by western blotting using a PARP-1 antibody showing a mobility shift of the immunoreactive band at the top of the gel (Fig. 4B, lane 4). According to our observation, the autoradiographic signals are absent in cells treated with the PARP-1 inhibitor alone (Fig. 4A, lanes 2 and 3) or in combination with TPT (Fig. 4A, lanes 5 and 6). Interestingly, TPT–PJ34 co-treatment in MCF7 cells induced apoptosis as demonstrated by the appearance of the 85 kDa fragment generated by the caspase-dependent cleavage of PARP-1 (Fig. 4B, lanes 5 and 6).

Immunoblot analysis with PARP-1 antibody was also performed in MDA-MB231 cells subjected to the same treatments. As shown in Fig. 4C, in TPT-treated cells PARP-1 is automodified to a lower extent (lane 4) and there are no signs of apoptosis induction after TPT-PJ34 combined treatment (Fig. 4C, lanes 5 and 6).

Furthermore, we analysed the response of SCC022 squamous carcinoma cells to PJ34 and TPT treatment. Immunoblot with the PARP-1 specific antibody reveals that PARP-1 is modified since the unmodified 113 kDa band is strongly reduced (Fig. 4D, lanes 4 and 5). Accordingly, immunoblot using a PAR antibody shows a smeared signal of long and branched polymers above the PARP-1 molecular weight (Fig. 4E, lanes 4 and 5). PJ34 co-treatment drastically reduces TPT/CPT-induced PARP 1 automodification thus leading to the accumulation of the 113 kDa band of PARP-1. However, we did not observe PARP-1 specific cleavage, thereby suggesting that cells were not undergoing apoptosis albeit up to 50 μM PJ34 was used (Fig. 4D, lanes 6 and 7). All together, our results suggest that, compared to MCF7, MDA-MB231 and SCC022 cells are less sensitive to the drugs combination and do not respond immediately with apoptosis to TOP I and PARP-1 inhibitors co-treatment.

3.4. Involvement of p63 in the cell response to TPT ± PJ34 treatment

To get insight into the molecular mechanism underlying the response of MCF7 cells to TPT ± PJ34 treatment, we analysed the expression of p53, p63 and other cell cycle markers such as p21WAF, MDM2 and cyclin B1. In MCF7 cells we found that PJ34 addition to TPT strongly enhances the TPT-dependent stimulation of p53 expression. Remarkably, the p53 negative regulator MDM2 was down-regulated only upon combined treatment (Fig. 5A). Furthermore, using the 4A4 monoclonal antibody which recognizes all p63 isoforms, we only detected bands corresponding to the pro-apoptotic TAp63 α and γ isoforms; both isoforms are up-regulated by TPT–PJ34 co-treatments (Fig. 5A). Quantitation of proteins by densitometric scanning, reveals a 19–20-fold increase of the expression level for both p53 and p63 proteins after TPT–PJ34 20 μM treatment (Fig. 5B). The increase of p21WAF expression level was concomitant to a decrease of cyclin B1 thereby supporting the G2/M cell cycle arrest observed by cytofluorimetric analyses.

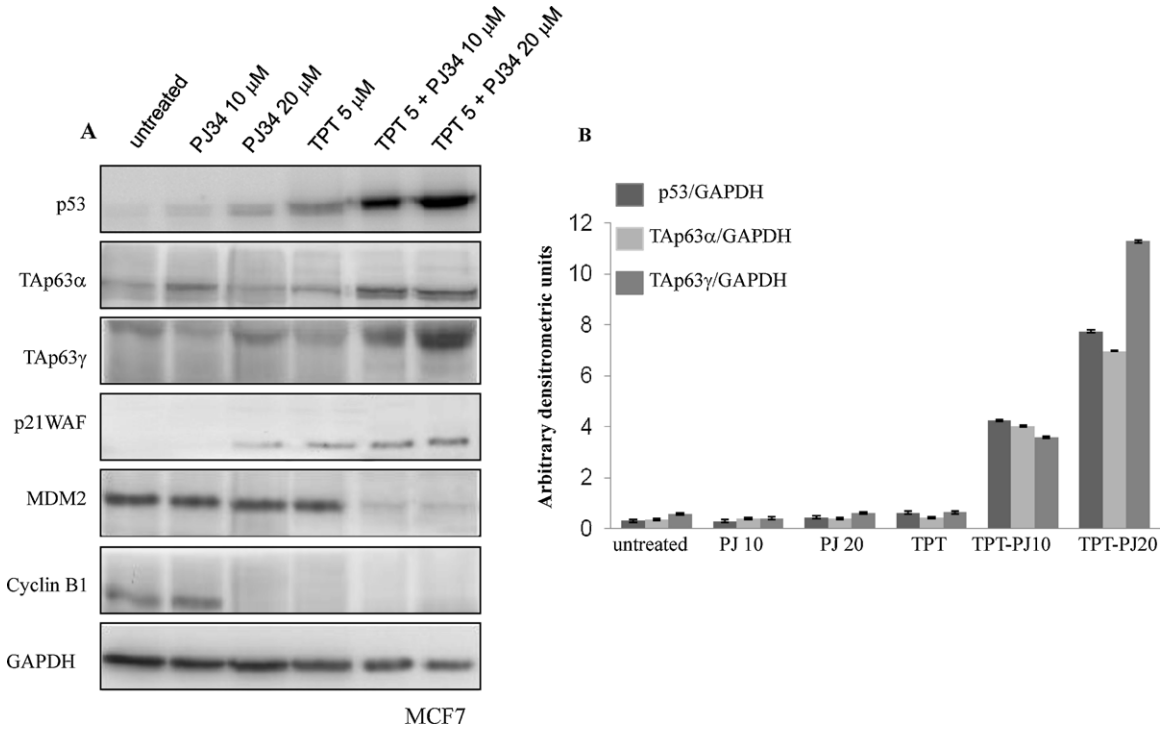

Fig. 5. Western blot analysis of p53, p63, p21WAF, MDM2 and cyclin B1 expression in MCF7 cells untreated or 48 h treated with the indicated drugs. Whole cell extract (50–100 μg of proteins) after 10% SDS-PAGE and electroblotting on PVDF were incubated with the different antibodies. (A) Immunodetection of p53, p63, p21WAF, MDM2, cyclin B1.GAPDH was used as loading control; (B) p53 and TAp63 α and γ band intensities were quantified by densitometric scanning. Data expressed as Arbitrary Densitometric Units (ADU) were normalized to the internal control GAPDH. Shown are the mean of three different experiments ± S.E.

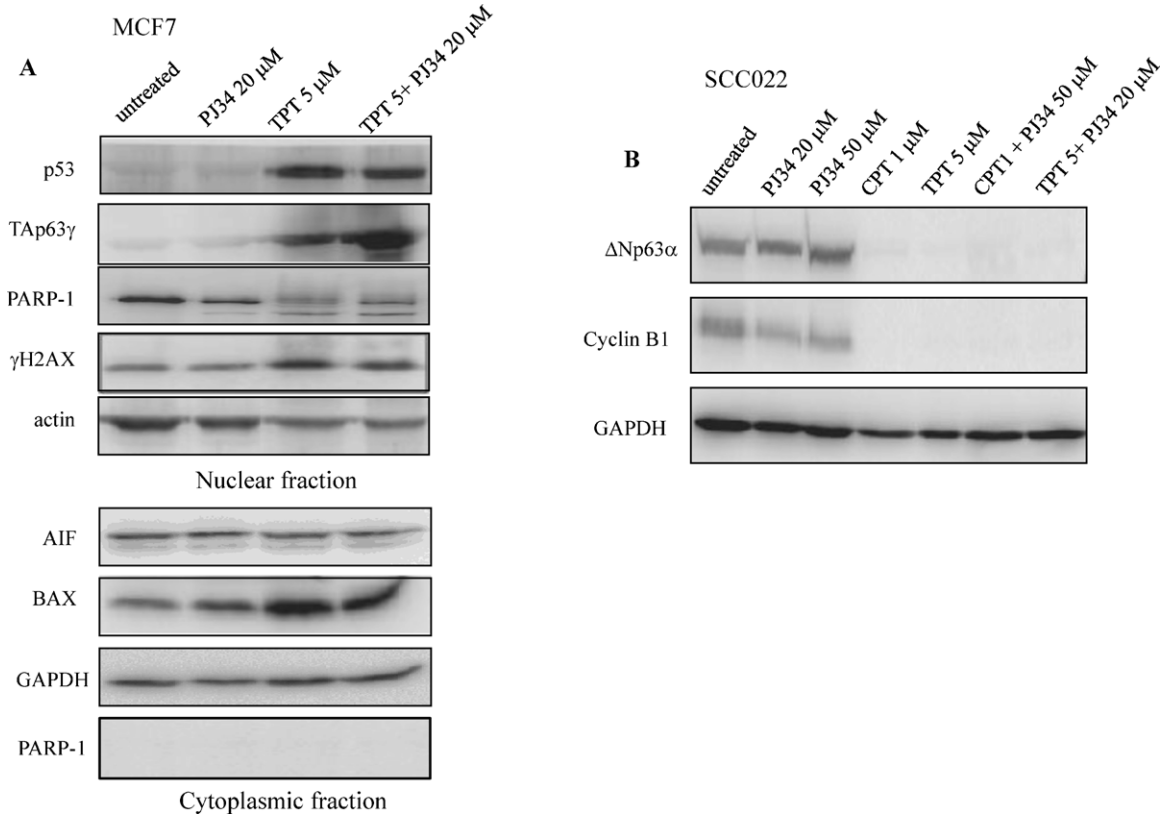

Fig. 6. Western blot analysis of protein extract from nuclear and cytoplasmic fraction of MCF7 cells and from SCC02 cells untreated or 48 h treated with the indicated drugs. Whole extract (50–100 μg of proteins) after SDS-PAGE and electroblotting on PVDF were incubated with the different antibodies. (A) Immunodetection of p53, p63, PARP-1, γH2AX, BAX, AIF in nuclear (upper panel) and cytoplasmic (lower panel) fractions from MCF7 cells. Actin and GAPDH were used as loading controls, respectively; (B) immunodetection of p63 and cyclin B1 in SCC022 cell extract. GAPDH was used as loading control.

We also performed immunoblot analysis of MCF7 nuclear and cytoplasmic fractions. Fig. 6A shows that following TPT ± PJ34 treatment both p53 and TAp63γ accumulate in the nuclear compartment. Nuclear γH2AX expression and PARP-1 specific cleavage were monitored as markers of dsDNA damage and caspase-dependent apoptosis, respectively (Fig. 6A, upper panel). Furthermore, the expression level of the pro-apoptotic BAX protein, whose gene is transcriptionally activated by p53 and TAp63, increases in the cytoplasmic fraction by either TPT alone or TPT–PJ34 combined treatment, while the level of the mitochondrial apoptosis inducing factor AIF is unaffected (Fig. 6A, lower panel).

Finally, as shown in Fig. 6B, in p53 null SCC022 cells, the ΔNp63α anti-apoptotic isoform is dramatically down-regulated by CPT/TPT treatment with or without PJ34. Cyclin B1 appears to be concomitantly reduced suggesting a G2/M cell cycle arrest. Importantly, using the 4A4 antibody, we were unable to detect p63 isoforms other than ΔNp63α both in untreated and TPT ± PJ34 treated SCC022 cells (data not shown). It has previously been demonstrated that ΔNp63α is required for the survival of SCC cells [27]. Interestingly, as shown in Fig. 4D, CPT/TPT ± PJ34 treatments was not sufficient to induce apoptosis in these cells thereby suggesting the existence of an alternative anti-apoptotic pathway able to overcome ΔNp63α depletion. In MDA-MB231 cells, no p63 immunoreactive bands were seen in all experimental conditions (data not shown) thereby excluding a possible role for p63 in TPT ± PJ34-induced cytotoxycity in this cellular context.

4. Discussion

The efficacy of PARP inhibitors as chemosensitizers has led to the development of a multitude of such molecules with different bioavailability and pharmacokinetic properties that are currently under investigation in clinical trials [1]. However, a clear understanding of how PARP inhibitors potentiate the activity of antineoplastic agents is still lacking.

The hydrophilic PARP inhibitor PJ34 has already been reported to synergize with cisplatin- and TPT-dependent apoptotic induction in triple-negative breast cancer and human carcinoma cells expressing wild type p53 [19–22]. We have already shown that PJ34, at a concentration of 5 μM, inhibits PARP-1 activity without cytotoxic effects. Furthermore, in HeLa and MCF7 cells we found that TPT toxicity was higher when PAR synthesis was reduced by either PARP-1 silencing or PJ34 administration [20].

In the present study, we compared the response of MCF7^{p53wt}, MDA-MB231^{p53mut} and SCC022^{p53null} cells to treatment with higher concentration of PJ34 (up to 20 μM) in combination with 1 μM CPT or 5 μM TPT. According to the previously reported specificity of PARP inhibitors for breast cancer [1,29], we observed a higher sensitivity to PJ34 in MCF7^{p53wt} cells. In such cells we confirmed that TPT, which is known to be S-phase specific [30], causes a G2/M cell cycle arrest when used at a lower concentration (1 μM). In addition, the TPT-dependent G2/M cell cycle arrest was enhanced by TPT + PJ34 combined treatment and resulted in a remarkable increase of cells with sub-diploid DNA, confirming a synergic cytotoxic effect of TOP I and PARP-1 inhibitors.

Consistent with the idea that poly(ADP-ribosyl)ation plays a role in the response to CPT/TPT-induced DNA damage we observed the disappearance of a TOP I soluble/active fraction and the PARP-1 automodification in MCF7, MB-MDA231 and SCC022 cells thereby indicating that the response to DNA damage, induced by TOP I inhibitors, in skin squamous carcinoma cells is similar to that observed in breast carcinoma cells [31].

On the other hand, we found that prevention of PARP-1 automodification by PJ34 induces PARP-1 proteolysis only in MCF7^{p53wt} implying that apoptosis induced by inhibition of PAR synthesis requires the p53 wild type activity. Given the similarity between p53 and p63 it was of interest to look at the effect of TOP I + PARP-1 inhibitors on p63 protein isoforms. Interestingly, TPT + PJ34 treatment in MCF7 cells causes a remarkable increase of TAp63 α and γ protein levels. TAp63γ in particular, was reported to be a potent apoptosis inducer [32]. Both p53 and TAp63γ accumulated in the nuclear fraction where the proteins can functionally interact in the control of transcription. Consistently, TPT + PJ34 combined treatment caused a dramatic reduction of MDM2, a negative regulator of p53 transcriptional activity and protein level.

Remarkably, this is the first evidence of a PJ34-inducible pro-apoptotic response involving both p53 and p63 family members in breast carcinoma cells. Furthermore, in SCC022^{p53null} cells we show that CPT/TPT single or combined treatments suppressed the endogenously expressed ΔNp63α anti-apoptotic isoform together with cyclin B1. It has previously been demonstrated that ΔNp63α is required for the survival of SCC cells by virtue of its ability to suppress p73-dependent apoptosis [28]. However, CPT/TPT ± PJ34 treatments is not sufficient to induce apoptosis in these cells thereby suggesting either the presence of a non-functional p73 or the existence of an alternative anti-apoptotic pathway able to overcome ΔNp63α depletion. Similarly, it has been reported that in MDA-MB468 cells expressing high level of ΔNp63α, PJ34 reduced ΔNp63α level, with a concomitant increase of p73. However, in that manuscript, apoptosis induction was not evaluated [22].

Therefore, it can be postulated that carcinoma cells, depending on their genetic background (p53/p63 null versus p53/p63 proficient), can trigger a p53-dependent pathway to induce cell cycle arrest and apoptosis, as a results of concomitant inhibition of PARP-1 and TOP I. To this respect, the particular p63 isoform expressed may sustain (TAp63α and γ) or inhibit (ΔNp63α) the execution of the apoptotic program.

Recently, it has been shown that PARP activity is required for TOP I poisoning-mediated replication fork slowing [33] and reversal [34]. In fact, PARP-1 is able to slow replication fork progression in response to CPT-dependent HR DNA repair. Furthermore, these data identify fork reversal as a means to prevent chromosome breakage upon exogenous replication stress and implicate still undefined proteins involved in fork reversal or restart as factors modulating the cytotoxicity of replication stress-inducing chemotherapeutics.

We have identified p63 as a new player of the PARP1-dependent signalling of DNA damage. Interestingly, in the p63 DNA binding domain, both the PAR binding motif and the glutamic acid residues showed to act as covalent PAR acceptor sites are conserved [35,36]. Our findings contribute to the understanding of the molecular events triggered by TOP I and PARP-1 inhibitor-dependent genomic damage and provide a rationale for the development of new approaches to sensitize cancer cells to chemotherapy.

Acknowledgements

This work is dedicated to the memory of Dr Maria Malanga who died in November 2011, her good spirit, her ideas, her friendship and her energy are greatly missed by all her colleagues. We acknowledge Dr. Daria Maria Monti and Dr. Angela Arciello for their help with cell cultures.

References

[1] Rouleau M, Patel A, Hendzel MJ, Kaufmann SH, Poirier GG. PARP inhibition: PARP1 and beyond. Nat Rev Cancer 2010;10:293–301.
[2] Burkle A. Poly(ADP-ribosyl)ation. LANDES Biosci 2005.
[3] .Malanga M, Althaus FR. The role of poly(ADP-ribose) in the DNA damage signaling network. Biochem Cell Biol 2005;83(3):354–64.
[4] Schreiber V, Dantzer F, Ame JC, de Murcia G. Poly(ADPribose): novel function for an old molecule. Nat Rev Mol Cell Biol 2006;7:517–28.

[5] Sugimura K, Takebayashi S, Taguchi H, Takeda S, Okumura K. .PARP1 ensures regulation of replication fork progression by homologous recombination on damaged DNA. J Cell Biol 2008;183:1203–12.
[6] Malanga M, Althaus FR. Poly(ADP-ribose) reactivates stalled DNA topoisomerase I and induces DNA strand break resealing. J Biol Chem 2004;279(7):5244–8.
[7] Mitchell J, Smith GC, Curtin NJ. Poly(ADP-Ribose) polymerase-1 and DNA-dependent protein kinase have equivalent roles in double strand break repair following ionizing radiation. Int J Radiat Oncol Biol Phys 2009;75(5):1520–7.
[8] Haince JF, Kozlov S, Dawson VL, Dawson TM, Hendzel MJ, Lavin MF, et al. Ataxia telangiectasia mutated (ATM) signaling network is modulated by a novel poly(ADPribose)-dependent pathway in the early response to DNA-damaging agents. J Biol Chem 2007;282:16441–53.
[9] Yoon JH, Ahn SG, Lee BH, Jung SH, Oh SH. Role of autophagy in chemoresistance: regulation of the ATM-mediated DNA-damage signaling pathway through activation of DNA-PKcs and PARP1. Biochem Pharmacol 2012;83(6):747–57.
[10] Nguyen D, Zajac-Kaye M, Rubinstein L, Voeller D, Tomaszewski JE, Kummar S, et al. Poly(ADP-ribose) polymerase inhibition enhances p53-dependent and -independent DNA damage responses induced by DNA damaging agent. Cell Cycle 2011;10(23):4074–82.
[11] Wieler S, Gagne' JP, Vaziri H, Poirier GG, Benchimol S. Poly(ADP-ribose) Polymerase-1 is a positive regulator of the p53-mediated G1 arrest response following ionizing radiation. J Biol Chem 2003;278:18914–21.
[12] Cazzalini O, Donà F, Savio M, Tillhon M, Maccario C, Perucca P, et al. p21CDKN1A participates in base excision repair by regulating the activity of poly(ADP-ribose) polymerase. DNA Repair 2010;9(6):627–35.
[13] Tentori L, Graziani G. Chemopotentiation by PARP inhibitors in cancer therapy. Pharmacol Res 2005;52:25–33.
[14] Sandhu SK, Yap TA, de Bono JS. Poly(ADP-ribose) polymerase inhibitors in cancer treatment: a clinical perspective. Eur J Cancer 2010;46(1):9–20.
[15] Smith LM, Willmore E, Austin CA, Curtin NJ. The novel poly(ADP-Ribose) polymerase inhibitor, AG14361, sensitizes cells to topoisomerase I poisons by increasing the persistence of DNA strand breaks. Clin Cancer Res 2005;11:8449–57.
[16] Pommier Y. Topoisomerase I inhibitors: camptothecins and beyond. Nat Rev Cancer 2006;6:789–802.
[17] Arnaudeau C, Lundin C, Helleday T. DNA double-strand breaks associated with replication forks are predominantly repaired by homologous recombination involving an exchange mechanism in mammalian cells. J Mol Biol 2001;307:1235–45.
[18] Cimmino G, Pepe S, Laus G, Chianese M, Prece D, Penitente R, et al. Poly(-ADPR)polymerase-1 signaling of the DNA damage induced by DNA topoisomerase I poison in D54(p53 wt) and U251(p53mut) glioblastoma cell lines. Pharmacol Res 2007;55(1):49–56.
[19] Gambi N, Tramontano F, Quesada P. Poly(ADPR)polymerase inhibition and apoptosis induction in cDDP-treated human carcinoma cell lines. Biochem Pharmacol 2008;75(12):2356–63.
[20] D'Onofrio G, Tramontano F, Dorio AS, Muzi A, Maselli V, Fulgione D, et al. Poly(ADP-Ribose) Polymerase signaling of topoisomerase 1-dependent DNA damage in carcinoma cells. Biochem Pharmacol 2011;81:194–202.
[21] Madison DL, Stauffer D, Lundblad JR. The PARP inhibitor PJ34 causes a PARP1-independent, p21 dependent mitotic arrest. DNA Repair (Amst) 2011;10(10):1003–13.
[22] Hastak K, Alli E, Ford JM. Synergistic chemosensitivity of triple-negative breast cancer cell lines to PARP inhibition, gemcitabine and cisplatin. Cancer Res 2010;70(20):7970–80.
[23] Di Costanzo A, Troiano A, di Martino O, Cacace A, Natale CF, Ventre M, et al. The p63 Protein Isoform {Delta}Np63α Modulates Y-box Binding Protein 1 in Its Subcellular Distribution and Regulation of Cell Survival and Motility Genes. J Biol Chem 2012;287(36):30170–80.
[24] Di Costanzo A, Festa L, Roscigno G, Vivo M, Pollice A, Morasso M, et al. A dominant mutation etiologic for human Tricho-Dento-Osseus syndrome impairs the ability of DLX3 to downregulate ΔNp63α. J Cell Physiol 2011;226(8):2189–97.
[25] Schavolt KL, Pietenpol JA. p53 and Delta Np63 alpha differentially bind and regulate target genes involved in cell cycle arrest, DNA repair and apoptosis. Oncogene 2007;26:6125–32.
[26] Yang A, Kaghad M, Wang Y, Gillett E, Fleming MD, Dötsch V, et al. p63, a p53 homolog at 3q27–29, encodes multiple products with transactivating, death-inducing, and dominant-negative activities. Mol Cell 1998;2(3):305–16.
[27] Devy J, Wargnier R, Pluot M, Nabiev I, Sukhanova A. Topotecan-induced alterations in the amount and stability of human DNA topoisomerase I in solid tumor cell lines. Anticancer Res 2004;24(3a):1745–51.
[28] Rocco JW, Leong CO, Kuperwasser N, DeYoung MP, Ellisen LW. p63 mediates survival in squamous cell carcinoma by suppression of p73-dependent apoptosis Cancer Cell 2006;9(1):45–56.
[29] Bryant HE, Schultz N, Thomas HD, Parker KM, Flower D, Lopez E, et al. Specific killing of BRCA2-deficient tumours with inhibitors of poly(ADP-ribose) polymerase. Nature 2005;434(7035):913.
[30] Feeney GP, Errington RJ, Wiltshire M, Marquez N, Chappell SC, Smith PJ. Tracking the cell cycle origins for escape from topotecan action by breast cancer cells. Br J Cancer 2003;88(8):1310–7.
[31] Davis PL, Shaiu WL, Scott GL, Iglehart JD, Hsieh TS, Marks JR. Complex response of breast epithelial cell lines to topoisomerase inhibitors. Anticancer Res J 1998;18(4C):2919–32.
[32] Yang A, Kaghad M, Wang Y, Gillett E, Fleming MD, Dötsch V, et al. p63. a p53 homolog at 3q27–29 encodes multiple products with transactivating death-inducing and dominant-negative activities Mol Cell 1998;2(3):305–16.
[33] Sugimura K, Takebayashi S, Taguchi H, Takeda S, Okumura K. PARP-1 ensures regulation of replication fork progression by homologous recombination on damaged DNA. J Cell Biol 2008;183:1203–12.
[34] .Chaudhuri AR, Hashimoto Y, Herradori R, Neelsen KJ, Fachinetti D, Bermejo R, et al. Topoisomerase I poisoning results in PARP-mediated replication fork reversal. Nat Struct Mol Biol 2012;19(4):417–24.
[35] Malanga M, Pleschke JM, Kleczkowska HE, Althaus FR. Poly(ADP-ribose) binds to specific domains of p53 and alters its DNA binding functions. J Biol Chem 2000;275:40974–80.
[36] Kanai M, Hanashiro K, Kim So H, Hanai S, Boulares HA, Miwa M, et al. Inhibition of Crm1–p53 interaction and nuclear export of p53 by poly(ADP-ribosyl)ation. Nat Cell Biol 2007;9(10):1175–83.

Biochemical Pharmacology 94 (2015) 212–219

Contents lists available at ScienceDirect

Biochemical Pharmacology

journal homepage: www.elsevier.com/locate/biochempharm

Effect of poly(ADP-ribose)polymerase and DNA topoisomerase I inhibitors on the p53/p63-dependent survival of carcinoma cells

Daniela Montariello [a], Annaelena Troiano [a], Daniela Di Girolamo [a], Sascha Beneke [b], Viola Calabrò [a], Piera Quesada [a,*]

[a] Department of Biology, University of Naples "Federico II", Naples, Italy
[b] Institute of Pharmacology and Toxicology, University of Zurich-Vetsuisse, Zurich, Switzerland

ARTICLE INFO

Article history:
Received 5 December 2014
Accepted 21 January 2015
Available online 7 February 2015

Keywords:
Apoptosis
Carcinoma cells
p53/p63 targets
PJ34
Topotecan

ABSTRACT

Depending on their genetic background ($p53^{wt}$ versus $p53^{null}$), carcinoma cells are more or less sensitive to drug-induced cell cycle arrest and/or apoptosis. Among the members of the p53 family, p63 is characterized by two N-terminal isoforms, TAp63 and ΔNp63. TAp63 isoform has p53-like functions, while ΔNp63 acts as a dominant negative inhibitor of p53. We have previously published that TAp63 is involved in poly(ADP-ribose)polymerase-1 (PARP-1) signaling of DNA damage deriving from DNA topoisomerase I (TOP I) inhibition in carcinoma cells.

In the present study, we treated MCF7 breast carcinoma cells ($p53^{+}/\Delta Np63^{-}$) or SCC022 ($p53^{-}/\Delta Np63^{+}$) squamous carcinoma cells with the TOP I inhibitor topotecan (TPT) and the PJ34 PARP inhibitor, to compare their effects in the two different cell contexts.

In MCF7 cells, we found that PJ34 addition reverts TPT-dependent PARP-1 auto-modification and triggers caspase-dependent PARP-1 proteolysis. Moreover, TPT as single agent stimulates $p53^{ser15}$ phosphorylation, p53 PARylation and occupancy of the p21WAF promoter by p53 resulting in an increase of p21WAF expression. Interestingly, PJ34 in combination with TPT enhances p53 occupancy at the BAX promoter and is associated with increased BAX protein level.

In SCC022 cells, instead, TPT + PJ34 combined treatment reduces the level of the anti-apoptotic ΔNp63α protein without inducing apoptosis. Remarkably, in such cells, either exogenous p53 or TAp63 can rescue the apoptotic program in response to the treatment.

All together our results suggest that in cancer cells PARP inhibitor(s) can operate in the choice between growth arrest and apoptosis by modulating p53 family-dependent signal

1. Introduction

Poly(ADP-ribose)polymerases (PARPs) and p53 play relevant roles in fundamental biological processes such as replication, transcription, cell cycle progression and apoptosis. Because of their protective role against oxidative and DNA damage stress, PARP and p53 are both named "guardians of genome stability" [1].

PARP enzymes catalyse the synthesis of poly(ADP-ribose) chain (PAR) whose concentration in the nucleus increases 500 fold after DNA damage [2]. The highly abundant PARP-1 is responsible for production of most of the cellular PAR, leading to poly-ADPribosylation (PARylation) of chromatin-associated proteins. Moreover, PARP-1 auto-modification, as well as covalent and non-covalent binding of PAR to several nuclear proteins, including DEK, XPA, ATM and p53, has emerged as a key mechanism to control a wide array of cellular processes [3].

As first suggested by Malanga and Althaus [4] PARP-associated polymers may recruit proteins to sites of DNA damage and regulate their functions. Remarkably, the p53 protein is able to strongly interact with PAR by means of three polymer binding motifs [5]; Fahrer et al. [6] defined the PAR binding affinity of several proteins as a function of chain length.

On the other hand, as reported by Kanai et al. [7] in response to DNA damage, covalent p53 PARylation is able to promote accumulation of p53 in the nucleus, where it exerts its transactivation function.

The p53 signaling pathway is one of the most relevant pathways in cancer biology. In the past, research has mainly be focused on

* Corresponding author.
E-mail address: quesada@unina.it (P. Quesada).

http://dx.doi.org/10.1016/j.bcp.2015.01.012
0006-2952/

the mechanism of p53-dependent regulation of apoptotic cell death [8]. It has been asserted that p53 post-translational modifications and transcriptional induction, allow p53 to increase its safeguard function against cancer [9]. Indeed, in response to cellular stressors such as DNA damage, p53 is phosphorylated, accumulates in the nucleus and up-regulates the expression of pro-apoptotic factors (*i.e.* BAX), by directly binding to the p53 response elements within the promoters of its target genes. However, p53 was also shown to have cytoplasmic functions: for instance it can directly activate BAX at the mitochondrial membrane [10].

It is relevant to remind that the p53 protein belongs to a gene family including p63 and p73. However, although p63 and p73 are structurally related to p53 and have been shown to cooperate in p53-dependent apoptosis, they have not been directly linked to tumor suppression [11]. Moreover, the molecular network through which p53 interacts with its family members to execute their cellular function is far to be completely understood. Importantly, the p63 protein is expressed as three isoforms (TAp63α, β and γ) which differ in their C-termini. All three isoforms can be alternatively transcribed from a cryptic promoter located within intron 3, producing ΔNp63α, β and γ. However, while TAp63 proteins appear to promote p53-dependent apoptosis, ΔNp63α, mainly expressed in epithelial, inhibits the endogenous p53 transcriptional functions required for inducing apoptosis via a dominant negative effect [12–14].

It is now generally accepted that p53 functions are regulated by PARP-1. It seems that the functional consequences of p53-PARP-1 interaction largely depend on the severity of the cellular stress. For instance, during DNA repair, p53 PARylation occurs to activate p53-transcriptional targets that control cell cycle arrest and eventually apoptosis. Under extreme genotoxic conditions, instead, p53 itself, can stimulate PARP-1 activity, leading to NAD depletion and necrosis [15,16]. In this scenario, chemotherapy protocols based on PARP inhibitors can be useful to restore the apoptotic cell death.

DNA topoisomerase I (TOP I) is another example of protein whose functions can be reprogrammed by PARP-1. In brief, TOP I is involved in the control of DNA supercoiling, allowing topological changes that are necessary for DNA transactions [17]. TOP I inhibitors, like the water-soluble campothecin derivative Topotecan (TPT), have been approved as chemotherapic agents since they reversibly abolish the DNA re-ligation activity of TOP I generating single strand breaks (SSBs) to which the protein is covalently linked. Double strand breaks (DSBs) arise when the replication forks collide with the SSBs and run off [18,19].

According with previous findings PARylated PARP-1 counteracts TPT through non-covalent but specific interaction of PAR with some TOP I sites resulting in DNA cleavage inhibition and stimulation of the re-ligation reaction [20]. Therefore, PARP inhibitors can be used as adjuvant of TOP I inhibitors.

The water soluble PARP inhibitor PJ34 has already been reported to synergize with cisplatin in triple-negative breast cancer cells: mechanistic investigations revealed that PJ34 reduced the levels of ΔNp63α with a concurrent increase of its downstream target p21WAF [21]. More recently it has been published that PJ34 has cytotoxic effects in six non small cell lung cancer cell lines: PJ34 treatment likely induces apoptosis through an intrinsic pathway as suggested by its effects on protein expression level [22].

By cell cycle analysis, in HeLa and MCF7 carcinoma cells, we have already shown, that inhibition of PAR synthesis by either PARP-1 silencing or PJ34 inhibition potentiates TPT toxicity, in terms of G2/M cell's accumulation and DSBs level [23]. Furthermore, in MCF7^{p53WT}, MDA-MB231^{p53mut} and SCC022^{p53null} carcinoma cells, we observed changes of p53 and ΔNp63/TAp63 expression levels associated to TPT + PJ34 combined treatments [24].

Here, using MCF7 (p53^{+}/ΔNp63^{-}) and SCC022 (p53^{-}/ΔNp63^{+}) cells subjected to the same agents, we looked at p53 post-translational modifications and levels of pro-arrest or pro-apoptotic proteins implicated in the p53/p63-dependent pathway (*i.e.* p21WAF, MDM2, BAX).

2. Materials and methods

2.1. Drugs, media, antibodies and chemicals

TPT was from Glaxo Smith-Kline (Verona, Italy) and PJ34 [N-(6-oxo-5,6,-dihydrophenanthridin-2-yl)-(*N*,*N*-dimethylamino) Acetamide] from Alexis Biochemicals (Vinci-Biochem, Firenze, Italy). The cocktail of protease inhibitors was from ROCHE-Diagnostic (Milano, Italy).

MCF7 cells were from CLS Cell Lines Service (Eppelheim, Germany), SCC022 cells were provided by C.Missero. Dulbecco's modified Eagle's medium (DMEM), heat-inactivated fetal bovine serum (FBS), Roswell Park Memorial Institute (RPMI) medium and Lipofectamine 2000 were from Invitrogen (GIBCO, Milano, Italy); penicillin, streptomycin and L-glutamine were from LONZA, (Milano, Italy).

PVDF (poly-vinylidene-fluoride) membrane was from MILLIPORE S.p.A. (Milano, Italy). Non-fat-milk powder was from EUROCLONE (Milano, Italy).

Anti-DNA TOP I (Scl-70) human antibody was from Topogen (ABCAM, Cambridge, UK). Anti-PARP-1 (C2-10), anti-pan-p63 (D-9), anti-p53 (DO-1), anti-p21WAF (F-5), anti-GAPDH (6C5) mouse monoclonal antibodies, anti-p53 (FL-393), anti-actin (H196) rabbit polyclonal antibody and protein A/G PLUS Agarose were from Santa-Cruz Biotechnology (DBA, Milano, Italy). Anti-phospho-p53(ser15) (9284), anti-PARP-1 (9542), anti-BAX (D2E11) rabbit polyclonal antibodies were from Cell Signaling (Invitrogen, Milano, Italy). Anti-MDM2 (Ab-2) mouse monoclonal antibody was from Oncogene Research Products (Boston, USA). Anti-PAR (4335) mouse monoclonal antibody was supplied by TREVIGEN (TEMA Ricerca, Bologna, Italy). Goat anti-mouse and goat anti-rabbit IgG HRP-conjugated antibodies were from Sigma-Aldrich (Milano, Italy). All other chemicals analytical grade were of the highest quality commercially available.

2.2. Cell cultures and transfections

Breast cancer-derived MCF7^{p53wt} cells were maintained in Dulbecco's modified Eagle's medium (DMEM) containing 10% (v/v) heat-inactivated fetal bovine serum (FBS), while squamous SCC022$^{p53\ null}$ carcinoma cells were maintained in Roswell Park Memorial Institute (RPMI) medium containing 10% (v/v) FBS, 100 U/ml penicillin, 100 g/ml streptomycin, 5 mM L-glutamine and incubated at 37 °C in a humidified atmosphere, *plus* 5% CO_2. Cell transfection was performed using Lipofectamine 2000 (Invitrogen, Milano, Italy) following the manufacturers' protocols.

2.3. Cell treatments

TPT and PJ34 were dissolved in Milli-Q water, stored as per the manufacturers' recommendations and diluted into cell culture media at the indicated concentrations. Cells were seeded at 1×10^6 cells in 10 ml and 24 h after seeding, treated with 5 μM TPT, 10× concentration inhibiting cellular growth by 50% (IC_{50}) [17], and 10 μM PJ34 alone and in combination for 6 or 24 h in fresh medium. Cell culture medium was removed and, after PBS wash, cells were recovered 6×10^6 cells/ml in 50 mM Tris–HCl pH 7.5, 150 mM NaCl, 5 mM EDTA, 1% NP40 (Lysis Buffer) plus 2 mM PMSF and 1:25 dilution of protease inhibitors cocktail solution. After

40 min of incubation on ice, cellular suspensions were centrifuged at 16,000 × *g* for 20 min at 4 °C.

2.4. Isolation of nuclear fractions

To isolate sub-cellular fractions, 3×10^6 cells were suspended in 200 μl of 30 mM Tris–HCl pH 7.5 buffer, containing, 1.5 mM $MgCl_2$, 10 mM KCl, 1% (v/v) Triton X-100, 20% glycerol, 2 mM PMSF and 1:25 dilution of protease inhibitors cocktail solution. After 30 min of incubation on ice, cellular suspensions were centrifuged at 960 × *g* for 90 s at 4 °C and the nuclear fractions recovered in the pellet. The supernatant represents the cytoplasmic fraction.

Nuclear fractions were resuspended in 50 μl of 20 mM HEPES pH 7.9 buffer, containing 20 mM KCl, 0.2 mM EDTA, 1.5 mM $MgCl_2$, 25% glycerol and the protease inhibitors cocktail solution. Protein concentration was determined using the Bradford protein assay reagent (BIO-RAD Milano, Italy) with bovine serum albumin as a standard.

2.5. Immunological analyses

Aliquots of 10 μl of cellular or nuclear proteins (approx 100 μg) were separated by 10% SDS-PAGE and transferred onto a PVDF membrane using an electroblotting apparatus (BIO-RAD). The membrane was subjected to immunodetection after blocking with 5% non-fat milk in TBST 1 h, with anti-PARP-1 (C2-10; diluted 1:2500), anti-TOP 1 (Scl-70; diluted 1:1000), anti-pan-p63 (D-9; diluted 1:200), anti-p53 (DO-1; diluted 1:5000), anti-p21WAF (F-5; diluted 1:1000), anti-MDM2 (Ab-2; diluted 1:1000), anti-BAX (D2E11; diluted 1:1000), anti-GAPDH (6C5; diluted 1:5000) and anti-actin (H196; diluted 1:2000) overnight at 4 °C.

As secondary antibodies goat-anti-mouse or goat-anti-rabbit IgG HRP-conjugate (diluted 1:5000–1:10,000) in 3% (w/v) non-fat milk in TBST were used. Peroxidase activity was detected using the ECL Lite Ablot TURBO (Euroclone, Milano, Italy) and quantified using the Immuno-Star Chemiluminescent detection system GS710 (BIO-RAD) and the Arbitrary Densitometric Units normalized with those of the GAPDH or actin loading controls.

2.6. Co-immunoprecipitation

Samples of MCF-7 cells ($1–2 \times 10^6$) 24-h treated with 5 μM TPT alone or in combination with 10 μM PJ34 were resuspended in 50 mM Tris–HCl buffer pH 7.5, containing 150 mM NaCl, 5 mM EDTA, 0.5% NP40, 10% glycerol, 1 mM PMSF and 1:25 dilution of the cocktail of protease inhibitors. Protein A/G plus Agarose was equilibrated in the same buffer by 3 washes and centrifugations at 960 × *g* 5 min at 4 °C: 40 μl aliquots were incubated with 1 mg of protein extract in 1 ml final volume, by buffer addition. Anti-p53 (DO-1), anti PARP-1 (C2–10) or anti-PAR (4335) monoclonal antibodies were added (3 μl) and the suspensions were incubated overnight at 4 °C on a rotator.

Co-immunoprecipitated samples were washed 3 times with the same buffer, mixed 1:1 with 4× Laemmli Buffer and, together with total protein extracts (30 μg), were subjected to 10% SDS PAGE, transferred onto a PVDF membrane using an electroblotting apparatus (BIO-RAD) and subjected to immunodetection, after blocking with 5% non-fat milk in TBST for 1 h, with anti-PARP-1 (9542; diluted 1:1000), anti-p53 (FL-393; diluted 1:5000) and anti PAR (4335 diluted 1:1000) antibodies. As secondary antibodies goat-anti-mouse or goat-anti-rabbit IgG HRP-conjugate (diluted 1:5000–1:10,000) in 3% (w/v) non-fat milk in TBST were used. Peroxidase activity was detected using the ECL Advance Western Blot Kit of GE Healthcare (Milano, Italy) and using the Immuno-Star Chemiluminescent detection system GS710 (BIO-RAD).

2.7. RNA extraction and real-time PCR

Total RNA was isolated using PureLink RNA Mini Kit (Ambion, Monza, Italy). 5 μg RNA each sample was reverse transcribed using SuperScript III Reverse Transcriptase (Invitrogen, Milano, Italy) according to manufacturer's protocol. Real-Time PCR was performed with Power SYBR Green PCR Master Mix (Applied Biosystems, Monza, Italy) using 100 ng cDNA in a 20 μl reaction mixture. The relative amounts of amplified transcripts ($2-\Delta CT$) were estimated by the comparative CT ($-\Delta CT$) method and normalized to an endogenous reference (18S) relative to a calibrator. RT-PCR data were obtained from three independent experiments (biological replicates); each experiment was performed in triplicate. Primers are described in the following table.

	Primer sequence forward/reverse (5′–3′)
p63	GGTTGGCAAAATCCTGGAG/GGTTCGTGTACTGTGGCTCA
p21WAF	TCACTGTCTTGTACCCTTGTGC/GGCGTTTGGAGTG GTAGAAA
BAX	CCGCCGTGGACACAGAC/CAGAAAACATGTCAGCTGCCA

2.8. Chromatin immunoprecipitation (ChIP) assay

According to Beneke [25] cells were cross-linked for 10 min at room temperature with 4% formaldehyde into the medium and neutralized by the addition of 1.25 M glycine/PBS for 2 min. Then the solution was removed and plates were washed twice with PBS (2 min each). To yield chromatin suspension, cells were collected after incubation for 5 min at 4 °C in 0.5 ml of lysis buffer 50 mM Tris–HCl pH 8.0, 10 mM EDTA, 1% SDS (LB) supplemented with protease inhibitors. Suspensions were sonicated on ice using Bioruptor Diagenode (Liège, Belgium) on high setting (30 s on and 30 s off) for 50 cycles. Protein concentration was adjusted to 1 μg/μl with lysis buffer and stored at 4 °C.

For ChIP, suspensions were brought to room temperature and 160 μl were spun down for 5 min at maximum speed. 150 μl supernatant was mixed with 1.35 ml of dilution buffer 20 mM Tris–HCl pH 8.0, 2 mM EDTA, 150 mM NaCl, 1% Triton-X-100 (DB) supplemented with protease inhibitors, incubated with 1.5 μg of p53 (DO-1) monoclonal antibody or 1.5 μg of irrelevant IgG and rotated overnight at 4 °C.

100 μl of G Protein immobilized on agarose-beads (Thermo-Scientific, Rockford/IL, USA) were, resuspended in 1 ml 9:1 dilution buffer:lysis buffer mix (DB:LB) and pre-absorbed with 100 μg/ml BSA and 500 μg/ml sheared salmon sperm DNA overnight at 4 °C on a rotator. Beads were washed twice with DB:LB and resuspended in 1 ml DB:LB.

50 μl of the beads suspension was added to each cell lysate and incubated for at least 2 h at 4 °C on a rotator. Suspensions were spun down 10 min at 1000 × *g* and supernatant was aspirated. Beads were washed 3 times in 0.5 ml wash buffer (150 mM NaCl, 20 mM Tris–HCl (pH 8.0), 2 mM EDTA, 1% Triton-X-100, 0.1% SDS) supplemented with protease inhibitors and centrifuged as above; Beads were washed in 0.5 ml of 20 mM Tris–HCl pH 8.0, 500 mM NaCl, 2 mM EDTA, 1% Triton-X-100, 0.1% SDS, supplemented with protease inhibitors and immune-complexes were eluted by addition of 160 μl elution buffer, 100 mM $NaHCO_3$, 1% SDS, 5 min at room temperature. 500 μg/ml of Proteinase K and RNAse A were added to each sample and incubated for 30 min at 37 °C and for 1 h at 56 °C. DNA–protein crosslinks were reversed by NaCl addition to a final concentration of 200 mM and incubation overnight at 65 °C. DNA was isolated by Phenol/Chloroform procedure and subsequent ethanol precipitation.

DNA fractions were subjected to PCR with primers specific for p21WAF and BAX promoter regions and with KOD Hot Start polymerase (Novagen/Merck, Darmstadt, Germany) according to manufacturer's instructions.

PCR was performed in 32 cycles (20 s 95 °C/10 s annealing temperature/5 s 70 °C) and products were resolved by 2.5% agarose gel electrophoresis. Primer sequences and respective annealing temperatures are listed in the following table:

	Primer sequence fwd/rev (5′–3′);	Annealing (°C)
p21WAF	GTGGCTCTGATTGGCTTTCTG/ GCTAAGGTTTACCTGGGGTCTTTA	55
BAX	ATAACGTCCTGCCTGGAAGC/ CCCCAGCGCAGAAGGAATTA	59

ChIP experiments were performed as three independent biological replicates and each experiment was performed in triplicate. Promoter occupancy was calculated with the percent input method by using the Image J software.

2.9. Statistics

Statistical Analysis was performed by using the Graph Pad software and the unpaired Student's *t*-test. *P*-value of <0.05 were considered statistically significant (*); *P*-value of <0.01 were considered extremely statistically significant (**).

3. Results

3.1. Analysis of TOP I and PARP-1 inhibition following TPT, PJ34 and TPT + PJ34 treatments

We first confirmed by western blot the efficacy of TPT in trapping the TOP I enzyme in the abortive complex by looking at the disappearance of the TOP I band corresponding to the soluble fraction of the enzyme. As shown in Fig. 1A, 6–24 h treatment of MCF7 cells with 5 μM TPT significantly decreased the amount of soluble TOP I thereby indicating that the majority of the TOP I enzyme was already blocked into the abortive complex.

Next, we assessed the efficacy of PJ34 as PARP inhibitor by looking at its effect on PARP-1 auto-modification. We have previously reported that 10 μM PJ34 has not citotoxic effect *per se*, indeed it does not alter p53 protein level and cell cycle kinetics [23,24].

We performed immunoblot analysis of TPT and TPT + PJ34 treated MCF7 cell lysates using PARP-1 antibodies. As shown in Fig. 1A, after 6 h of 5 μM TPT treatment a band (PAR-PARP-1) was evident at the top of the gel. Such behavior indicates auto-modification of PARP-1 by long and branched PAR molecules (up to 200 residues in chain) on several sites (up to 25), that gives raise to higher molecular weight PARP-1 forms (up to 250 kDa) that do not enter the polyacrylamide gel matrix [4]. At the same time of incubation, TPT + PJ34 treatment, instead, was able to induce apoptosis as demonstrated by the appearance of the 89 kDa fragment generated by the caspase-dependent cleavage of PARP-1. After 24 h of TPT treatment the PARP-1 proteolytic cleavage was detectable and it was more pronounced after TPT + PJ34 treatment clearly indicating that cells were undergoing massive apoptosis (Fig. 1A).

3.2. Analysis of the effects of TPT, PJ34 and TPT + PJ34 treatments on pro-arrest or pro-apoptotic p53 target proteins

We have previously shown that TPT treatment leads to p53 up-regulation [23,24], therefore we looked, by immunoblot analysis, at the expression level of relevant p53-target proteins, as MDM2, p21WAF and BAX, in MCF7 cells ($p53^+$) treated with TPT, PJ34 and TPT + PJ34. BAX is considered a pro-apoptotic protein, p21WAF is a

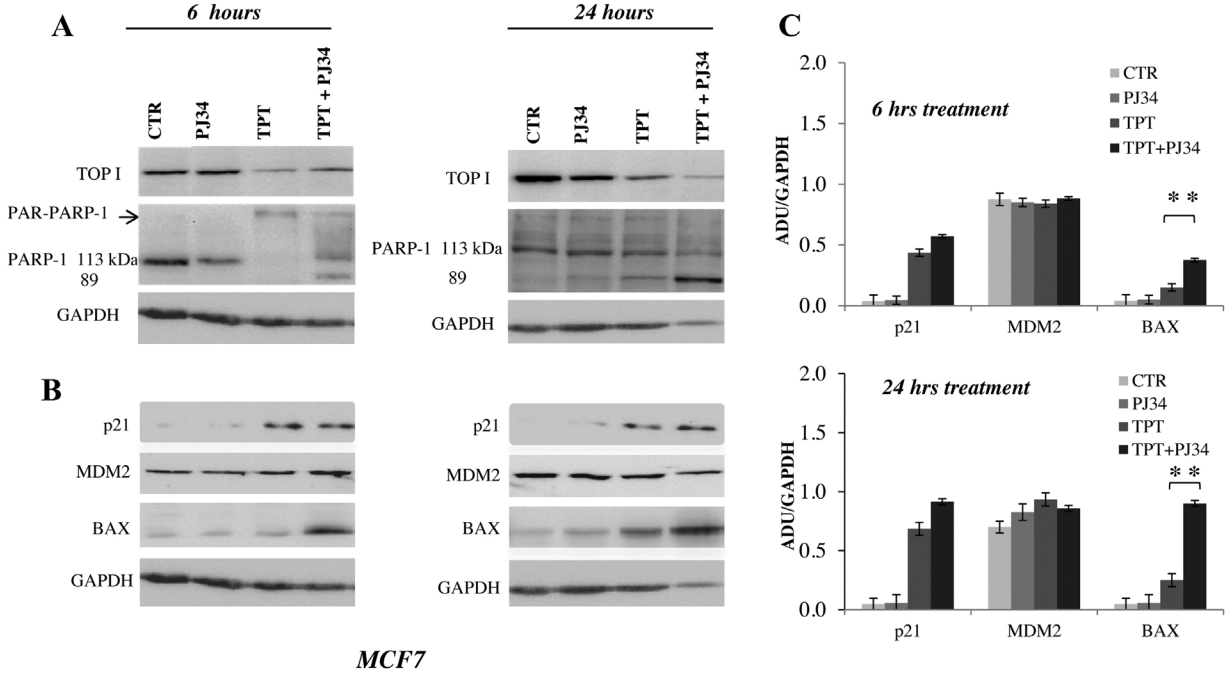

Fig. 1. *Analysis of TPT-dependent TOP I inhibition and PJ34-dependent PARP-1 inhibition and their effects on endogenous levels of p53 target proteins.* Total MCF7 cell extracts untreated or 6 and 24-h treated with the indicated drugs were subjected to 10% SDS-PAGE, electroblotted on PVDF and incubated with different antibodies. (A) Immunodetection of TOP I and PARP-1; (B) immunodetection of p21WAF, MDM2, BAX. GAPDH was used as loading control; (C) p21WAF, MDM2 and BAX band intensities were quantified by densitometric scanning. Data expressed as Arbitrary Densitometric Units (ADU) were normalized to the internal control GAPDH. Data are presented as the mean ± S.E.M. of three independent experiments on three biological replicates. Unpaired Student's *t*-test was conducted to determine whether protein's level was higher in cells induced with TPT compared with TPT + PJ34 at the same time points. ** $P < 0.01$.

well known cell cycle inhibitor while MDM2 is the major negative regulator of p53 [8].

As shown in Fig. 1B, TPT and TPT + PJ34 treatments up-regulated p21WAF both at 6 and 24 h. Moreover, according to the appearance of a distinctive PARP cleavage signature, the pro-apoptotic BAX protein appeared significantly increased mainly upon TPT + PJ34 treatment. Densitometric analysis of three independent experiments indicates a significant (2 to 4 fold) increase of BAX protein level at 6 and 24 h (Fig. 1C). Unexpectedly, we did not detect any significant alteration of the MDM2 protein levels (Fig. 1B and C).

Next, we tested the ability of TPT + PJ34 to induce apoptosis in p53 null SCC022 squamous carcinoma cells following 24 h of incubation with the drugs. Such experiment was performed in p53 and/or TAp63γ transfected cells.

Immunoblot analysis showed that SCC022 cells responded to TPT + PJ34 treatment by reducing ΔNp63α protein level (Fig. 2A). By RT-PCR analysis we measured the level of ΔNp63α mRNA in untreated (CTR) and TPT + PJ34 treated SCC022 cells and we found that it was comparable thus suggesting that ΔNp63α down-regulation was exclusively at protein level (Fig. 2B).

Furthermore, as demonstrated by the appearance of the PARP-1 89 kDa proteolytic fragment (Fig. 2A and C), p53 and TAp63γ are able to induce the caspase-dependent cleavage of PARP-1 and caused a further decrease of endogenous ΔNp63α protein after TPT + PJ34 treatment. Immunoblot analysis with a pan-p63 antibody was used to reveal both endogenous ΔNp63α and transfected TAp63γ proteins (Fig. 2C). This result indicates that reduction of ΔNp63α in SCC022 cells *per se* is not sufficient to induce apoptosis but it seems to cooperate with exogenous p53 or TAp63γ in the restoration of apoptosis upon TPT + PJ34 treatment. However, as ΔNp63α levels are reduced upon by p53 or TAp63γ expression the individual contribution of these proteins on apoptosis is difficult to assess.

Furthermore, apoptosis induction was sustained by a strong BAX up-regulation (Fig. 2C).

3.3. Analysis of the effects of TPT, PJ34 and TPT + PJ34 treatments on p53 post-translational modifications

Activation of p53 transcriptional function by genotoxic stimuli imposes a variety of p53 post-translational modifications; one of the best characterized is phosphorylation at Serine 15 by ATM [26]. We analyzed the effect of TPT and TPT + PJ34 on p53 protein phosphorylation by using a phospho-specific antibody that recognizes ^{15ser}p-p53 (Fig. 3A).

As estimated by densitometric analysis, TPT treatment caused a 10 fold increase of the steady state level of endogenous p53 protein and its phosphorylated form at serine 15. Interestingly, a further increase was observed after TPT + PJ34 treatment form (12 folds compared to untreated) (Fig. 3A). Immunoblot analysis showed that phosphorylated ^{ser15}p53 was located in the nucleus (Fig. 3B).

It was previously demonstrated that p53 exhibits a high affinity for auto-modified PARP-1 [5]. However, whether p53 undergoes "*in vivo*" covalent or non-covalent post-translational modification by PARP-1 (PARylation) is still a matter of debate.

To look at the TPT-dependent p53 PARylation we performed co-immunoprecipitation experiments in MCF7 cells treated with TPT and TPT + PJ34 for 24 h. Same aliquots of total cell extracts were immunoprecipitated with p53, PARP-1 or PAR antibodies (Fig. 4). Protein immunocomplexes were then analyzed by western blot and revealed with the same antibodies.

The p53 immunoprecipitated sample from TPT treated cells, revealed with PARP-1 antibodies (Fig. 4A panel 1), shows a slow migrating broad band can be ascribed to auto-modified PARP-1 (PAR-PARP-1) since it was also detectable in the input sample together with two bands corresponding to the native enzyme (113 kDa) and the PARP-1 apoptotic fragment (89 kDa). The same bands were detected by immunoblot of PARP-1 immunoprecipitate using PARP-1 antibody (Fig. 4A panel 2). Fig. 4B panel 1 confirms the presence of p53 protein in p53-immunocomplexes.

Furthermore, after anti-PAR immunoprecipitation, immunodetection with PAR antibodies shows a sharp band corresponding to PAR polymers of different length linked to PARP-1 (Fig. 4A, panel

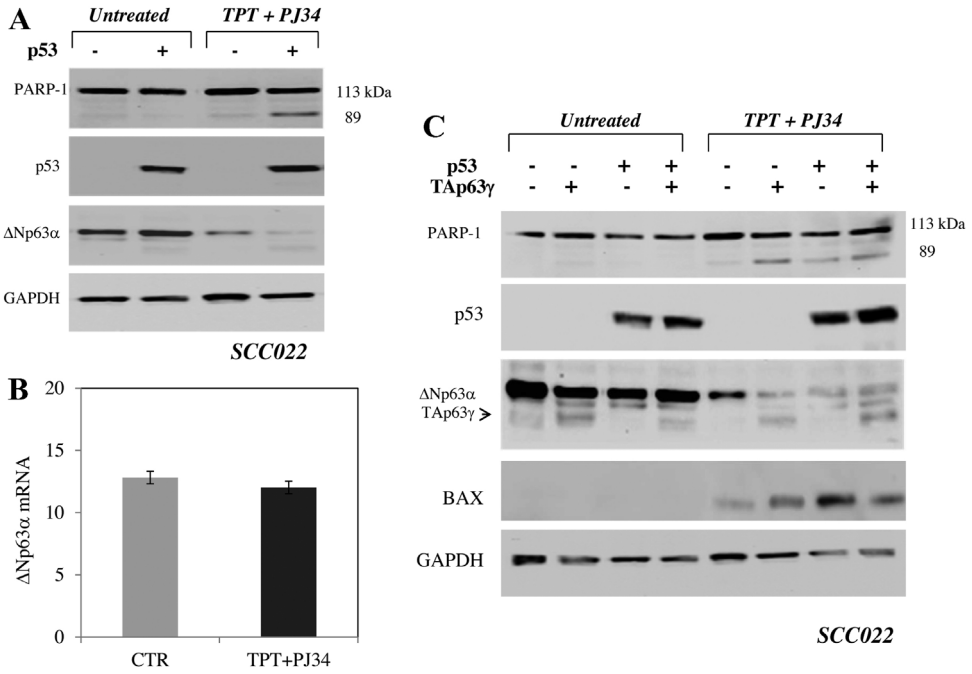

Fig. 2. *Analysis of the effects of TPT + PJ34 treatment in SCC022^{p53null} cells p53+/−TAp63γ transfected.* (A) and (C) Immunodetection with anti-PARP-1, anti-p53, anti-pan p63, anti-BAX antibodies. GAPDH was used as loading control. (B) Quantitative RT-PCR analysis of ΔNp63α mRNA levels in untreated and 24-h treated cells. Data are presented as the mean ± S.E.M. of three independent experiments on three biological replicates.

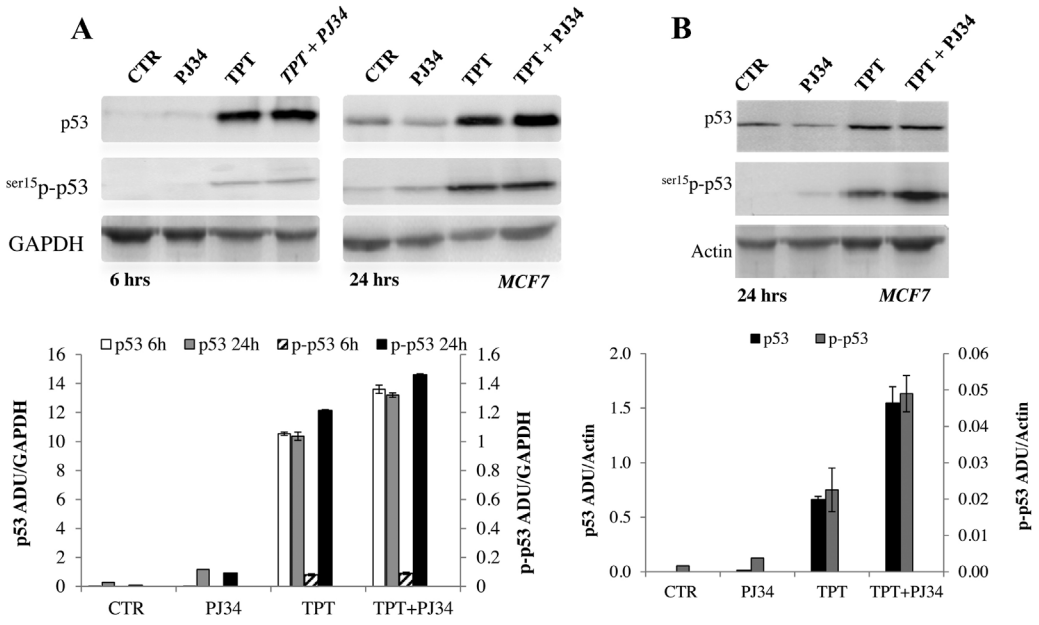

Fig. 3. *Analysis of TPT+/−PJ34 dependent p53 phosphorylation in MCF7 cells.* (A) Western blot analysis of MCF7 cells (A) and isolated nuclei (B), untreated or 6 and 24-h treated with the indicated drugs. Immunodetection of ^{ser15}-p-p53 and p53 band intensities were quantified by densitometric scanning. Data expressed as Arbitrary Densitometric Units (ADU) were normalized to GAPDH and Actin internal controls. Data are presented as the mean ± S.E.M. of three independent experiments on three biological replicates.

4). Immunodetection with p53 antibodies confirms the presence of such protein in PAR immuno-complexes (Fig. 4B panel 3).

Moreover, lysates from MCF7 cells treated with TPT + PJ34 for 24 h were immunoprecipitated with p53 antibodies and analyzed by immunoblot with PARP-1 and p53 antibodies. As shown in Fig. 4C, upper panel, immunoreactive bands corresponding to the native PARP-1 and its apoptotic fragment were present in the input sample but not in p53 immunoprecipitates, thereby confirming that, as a consequence of PAR synthesis inhibition, interaction between p53 and PARP-1 does not occur (lane 2). Fig. 4C lower panel shows p53 bands in the input and immunoprecipitated samples.

3.4. Analysis of p53-dependent p21WAF and BAX genes expression following TPT and TPT + PJ34 treatment

Next, we quantified the level of p21 and BAX transcript on TPT and TPT + PJ34 treated cells that showed comparable levels of p53 and ^{ser15}p-p53 protein (Fig. 3).

Total RNA was purified from cells treated for 6 or 24 h with the indicated drugs and subjected to qRT-PCR assays. As shown, we found a 4.5 fold increase in p21WAF mRNA level in cells subjected to TPT treatment that was strongly reduced by PJ34 addition (Fig. 5A). Concerning BAX mRNA level the increase of BAX mRNA was detectable only after 24 h of treatment with TPT + PJ34 (Fig. 5B).

Then we analyzed the effects of TPT and TPT + PJ34 treatments on p53 binding to promoters of p21WAF and BAX genes, by using the Chromatin Immunoprecipitation (ChIP) approach. Since it was previously shown that standard ChIP is flawed by PAR that may cause changes in promoter-occupancy dependent on artificial formation of polymers [25] we modified the standard protocol, as described in Section 2, to prevent artificial polymer synthesis.

Interestingly, according to the observed increase of p21WAF transcript (Fig. 5A), p53 occupancy of p21WAF promoter was strongly increased in TPT treated cells compared to control cells and significantly reduced by addition of PJ34 (Fig. 5C). Occupancy

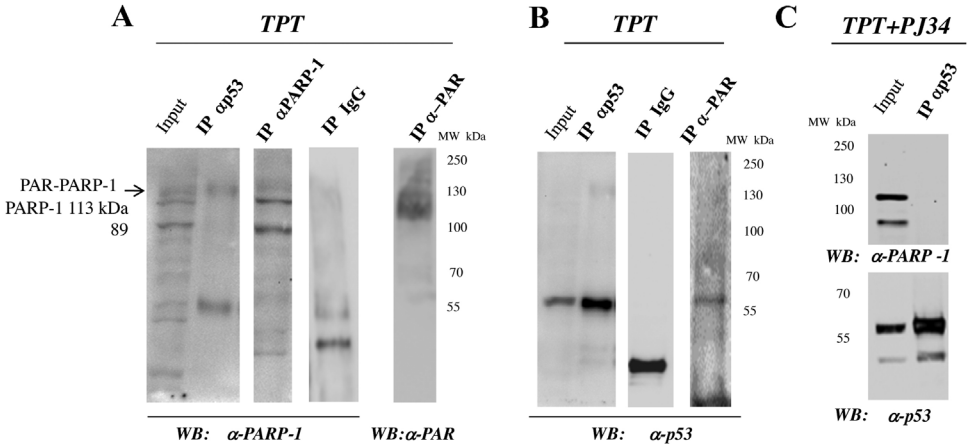

Fig. 4. *Analysis of TPT+/− PJ34 dependent p53-PAR interaction by co-immunoprecipitation.* (A) Total extract from TPT treated MCF7 cells (Input) immunoprecipitated with p53, PARP-1 or PAR antibodies and immunodetected with PARP-1 or PAR antibodies. (B) Total extract from TPT treated MCF7 cells (Input) immunoprecipitated with p53 or PAR antibodies and immunodetected with p53 antibodies. (C) Total extract from TPT + PJ34 treated MCF7 cells (Input) immunoprecipitated with p53 antibodies and immunodetected with PARP-1 antibodies (upper) or p53.antibodies (lower). Immunodetections of irrelevant IgG immunoprecipitated samples are also shown.

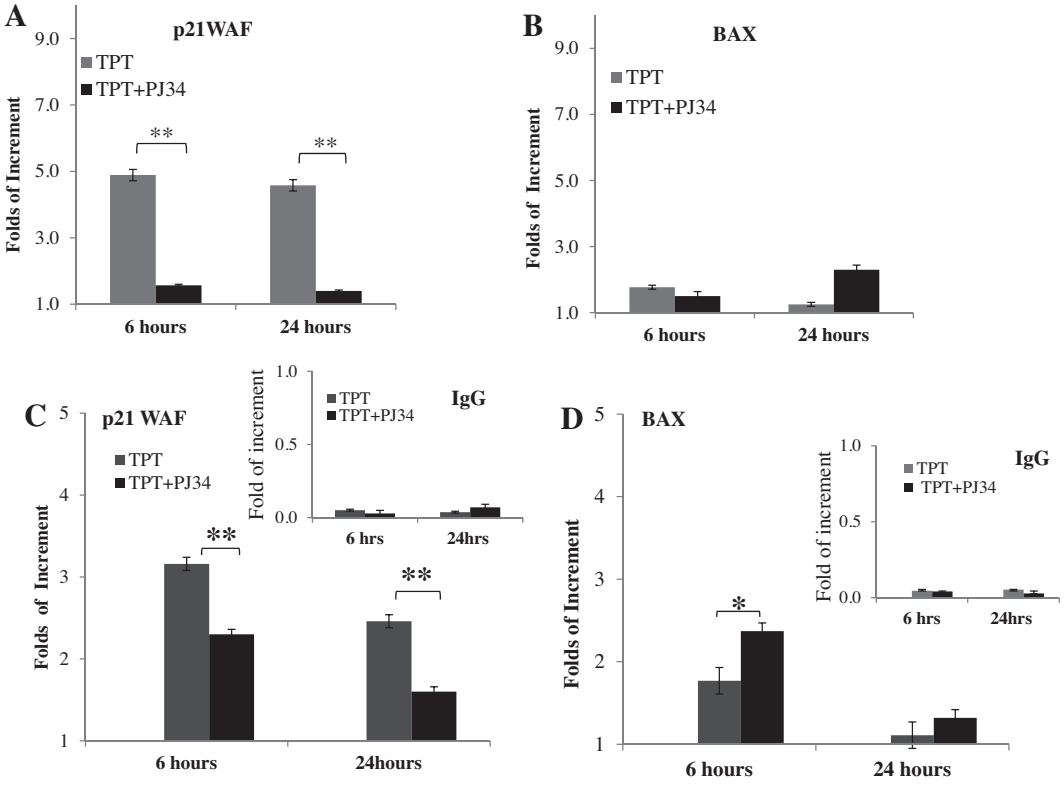

Fig. 5. *Analysis of p53-dependent p21WAF and BAX genes expression following TPT and TPT + PJ34 treatment.* Real-time-PCR analysis of mRNA levels of p21WAF (A) and BAX (B) genes in MCF7 cells 6 and 24-h treated with the indicated drugs. Data normalized with respect to 18S are reported as increment's fold of controls and represent the mean ± S.E.M. of three independent experiments on three biological replicates. Unpaired Student's *t*-test was conducted to determine whether mRNA level was higher in cells induced with TPT compared with TPT + PJ34 at the same time points. ** $P < 0.01$. Chromatin Immunoprecipitation in MCF7 cells 6 and 24-h treated with the indicated drugs. Chromatin was immunoprecipitated with p53 or irrelevant immunoglobulin G (IgG) antibodies and quantified by PCR on p21WAF (C) or BAX (D) promoter. Data normalized with respect to control samples are reported as folds of increment and represent the mean ± S.E.M. of three independent experiments on three biological replicates. Unpaired Student's *t*-test was conducted to determine whether promoter occupancy was higher in cells treated with TPT compared with TPT + PJ34 at the same time points. * $P < 0.05$ and ** $P < 0.01$.

of BAX promoter by p53, instead, was significantly increased by TPT + PJ34 after 6 h of treatment, while at 24 h of treatment we could not detect significant changes (Fig. 5D).

4. Discussion

In the present study we investigate the PARP-1/p53(p63) functional relationship as apoptosis inducers by looking at the transcriptional regulation of their target genes.

It is known that one mechanism that affects the outcome of p53 activation is the abundance of the protein itself [27]: according to the proposed affinity model, at low levels p53 preferentially binds to high-affinity p53 response elements (RE) in promoters of pro-arrest genes, whereas high levels are necessary for p53 to bind low affinity p53 RE in pro-apoptotic promoters [28].

Our findings agree with such a model since MCF7 cells respond to TOP I or TOP I and PARP-1 combined inhibition by p53 increase, phosphorylation at serine 15 and transcriptional activation. Conversely, PARP-1 inhibition by treatment with PJ34 alone has no effect on p53 level, and transcriptional activation compared to control cells.

Moreover, in p53 proficient cells such as MCF7, as a consequence of TPT-dependent DNA damage, the pro-arrest p21WAF protein is rapidly up-regulated. Indeed, both p53 binding to p21WAF promoter and p21WAF mRNA appeared to be enhanced after 6 h of TPT treatment. Concomitant PARP-1 auto-modification is indicative of a DNA repair attempt.

Under more severe DNA damage conditions induced by 6 h of TPT + PJ34 treatment, the p53 binding to the p21WAF promoter was reduced while occupancy of BAX promoter was enhanced. However, the increase of BAX transcript was delayed and the protein level was clearly detectable only after 24 h. Under this condition, PARP-1 undergoes caspase-dependent cleavage.

These data indicate a selective binding and control of pro-arrest or pro apoptotic gene promoters by p53 occurring under specific stimuli which may reflect the severity of DNA damage.

Our previous results point to a role for p63 in the cell response to treatment with TOP I and PARP-1 inhibitors. In MCF7^{p53WT} cells the endogenously expressed TAp63γ isoform, which closely mimics p53, is up-regulated upon TPT + PJ34 treatment [24]. Herein we show that transfection of TAp63γ or wild-type p53 is necessary to trigger caspase-dependent apoptosis in apoptosis-resistant SCC022 cells by inducing BAX expression and degradation of the endogenous anti-apoptotic ΔNp63α protein.

Remarkably, the decrease of ΔNp63α protein was enhanced by expression of wild type p53 and TAp63γ suggesting that they can cooperate in the mechanism of TPT + PJ34 mediated p63 degradation.

We also present evidences that p53 interacts with PAR linked to PARP-1 and that p53 PARylation can be induced by TPT-dependent DNA damage. Our finding contributes to the debate on covalent or non-covalent p53 PARylation using an in cell approach and endogenous proteins. So far, most of the previous evidences were obtained *in vitro*, or as for Kanai et al. [7] by the use of mutants.

Intriguingly, the three PAR binding motifs present in the DNA binding domain of p53 [5] are conserved in the TAp63γ sequence [29], thereby suggesting that, like p53, also this p63 isoform can be subjected to PARylation.

In conclusion, we contribute to the literature describing the role of p53 in mediating cellular sensitivity to apoptosis, along with directly regulating numerous critical components of the extrinsic and intrinsic pathways. In particular, we provide further evidences that in response to TPT-dependent DNA damage, PARylation can be added to post-translational modifications that modulate p53 action on its target promoters.

Moreover, our findings underline the role of PAR and PARP-1 in the differential recruitment of p53 on its target promoters upon DNA damage. Indeed, while TPT treatment induces p53 recruitment on p21/WAF gene promoter with its consequent up-regulation, TPT + PJ34 combined treatment acts as a switch in the cell fate decision by inducing the pro-apoptotic BAX gene expression.

While the regulation of p53 by PARP-1 activity has been widely described, the regulation of PARP-1 activity by p53 reported by Montero et al. [10] is novel and related to a non-apoptotic cell death induction.

It has been shown that PARP-1 and p53 reciprocal regulation acts in different mechanisms of cell death (*i.e.* autophagy, necrosis, apotoptosis) [16]. Indeed, a balance exists between apoptotic and necrotic signaling pathways in response to cellular stress and these pathways likely regulate each other to ensure death of damaged cells.

Moreover, the restoration of apoptosis is considered a chemotherapic strategy that can be based on PARP-1 and p53 joint tumor suppressor function. Our results indicate that modulation of other components of the p53 family (*i.e.* TAp63γ and/or ΔNp63α) can be involved and significantly contribute to the cell response to DNA damage stimuli thus adding further complexity to this phenomenon [29].

Our studies highlighting the different outcome (*i.e.* cell cycle arrest *vs* apoptosis) of PARP-1 activation/inhibition, give right of the use of PARP inhibitor as chemotherapic adjuvant and/or in monotherapy even in TAp63/ΔNp63α proficient cancer cells.

Interestingly, it has been recently published that PARP inhibitors actualize the biological concept of synthetic lethality in the clinical practice, yielding a paradigmatic example of translational medicine [30].

Acknowledgments

This work is dedicated to the memory of Dr Maria Malanga, her ideas, her friendship and her energy are greatly missed by all her colleagues.

The authors wish to thank Prof. Felix R. Althaus for his support to the project.

Dr Montariello and Dr Di Girolamo acknowledge fellowships obtained by P.O.R. Campania FSE 2007–2013, Progetto CREME, CUP B25B09000050007.

Appendix A. Supplementary data

Supplementary data associated with this article can be found, in the online version, at http://dx.doi.org/10.1016/j.bcp.2015.01.012.

References

[1] Tong WM, Cortes U, Wang ZQ. Poly(ADP-ribose)polymerase: a guardian angel protecting the genome and suppressing tumorigenesis. Biochim Biophys Acta 2001;1552(1):27–37.
[2] Burkle A, Virag L. Poly(ADP-ribose): PARadigms and PARadoxes. Mol Aspects Med 2013;34(6):1046–65.
[3] Krietsch J, Rouleau M, Pic É, Ethier C, Dawson TM, Dawson VL, et al. Reprogramming cellular events by poly(ADP-ribose)-binding proteins. Mol Aspects Med 2013;34(6):1066–87.
[4] Malanga M, Althaus FR. The role of poly(ADP-ribose) in the DNA damage signaling network. Biochem Cell Biol 2005;83(3):354–64.
[5] Pleschke JM, Kleczkowska HE, Strohm M, Althaus FR. Poly(ADP-ribose) binds to specific domains in DNA damage checkpoint proteins. J Biol Chem 2000;275:40974–80.
[6] Fahrer J, Popp O, Malanga M, Beneke S, Markovitz DM, Ferrando-May E, et al. High affinity interaction of poly(ADP-ribose) and the human DEK oncoprotein depends upon chain length. Biochemistry 2010;49(33):7119–30.
[7] Kanai M, Hanashiro K, Kim SH, Hanai S, Boulares AH, Miwa M, et al. Inhibition of Crm1-p53 interaction and nuclear export of p53 by poly(ADP-ribosyl)ation. Nature Cell Biol 2007;9(10):1175–83.
[8] Chipuk JE, Green DR. Dissecting p53-dependent apoptosis. Cell Death Differ 2006;13:994–1002.
[9] Vousden KH, Prives C. Blinded by the light: the growing complexity of p53. Cell 2009;137:413–31.
[10] Montero J, Dutta C, van Bodegom D, Weinstock D, Letai A. p53 regulates a non-apoptotic death induced by ROS. Cell Death Differ 2013;20:1465–74.
[11] Flores ER, Tsai KY, Crowley D, Sengupta S, Yang A, McKeon F, et al. p63 and p73 are required for p53-dependent apoptosis in response to DNA damage. Nature 2002;416(6880):560–4.
[12] Liefer KM, Koster MI, Wang XJ, Yang A, McKeon F, Roop DR. Down-regulation of p63 is required for epidermal UV-B-induced apoptosis. Cancer Res 2000;60(15):4016–20.
[13] Di Costanzo A, Troiano A, di Martino O, Cacace A, Natale CF, Ventre M, et al. The p63 protein isoform ΔNp63α modulates Y-box binding protein 1 in its subcellular distribution and regulation of cell survival and motility genes. Biol Chem 2012;287(36):30170–80.
[14] Vivo M, Di Costanzo A, Fortugno P, Pollice A, Calabrò V, La Mantia G. Down-regulation of DNp63a in keratinocytes by p14-ARF-mediated SUMO-conjugation and degradation. Cell Cycle 2009;8(21):3545–51.
[15] Dai C, Gu1 W. p53 post-translational modification: deregulated in tumorigenesis. Trends Mol Med 2010;16(11):528–36.
[16] Elkholi R, Chipuk JE. How do I kill thee? Let me count the ways: p53 regulates PARP-1 dependent necrosis. Bioessays 2014;36(1):46–51.
[17] Wang JC. Cellular roles of DNA topoisomerases: a molecular perspective. Nat Rev Mol Cell Biol 2002;3(6):430–40.
[18] Pommier Y. Topoisomerase I inhibitors: camptothecins and beyond. Nat Rev Cancer 2006;6:789–802.
[19] Devy J, Wargnier R, Pluot M, Nabiev I, Sukhanova A. Topotecan-induced alterations in the amount and stability of human DNA topoisomerase I in solid tumor cell lines. Anticancer Res 2004;24(3a):1745–51.
[20] Malanga M, Althaus FR. Poly(ADP-ribose) reactivates stalled DNA topoisomerase I and induces DNA strand break resealing. J Biol Chem 2004;13–279(7):5244–8.
[21] Hastak K, Alli E, Ford JM. Synergistic chemosensitivity of triple-negative breast cancer cell lines to poly(ADP-Ribose)polymerase inhibition, gemcitabine, and cisplatin. Cancer Res 2010;70(20):7970–80.
[22] Gangopadhyay NN, Luketich JD, Opest A, Landreneau R, Schuchert MJ. PARP inhibitor activates the intrinsic pathway of apoptosis in primary lung cancer cells. Cancer Invest 2014;32(7):339–48.
[23] D'Onofrio G, Tramontano F, Dorio AS, Muzi A, Maselli V, Fulgione D, et al. Poly(ADP-Ribose)polymerase signaling of topoisomerase 1-dependent DNA damage in carcinoma cells. Biochem Pharmacol 2011;81:194–202.
[24] Montariello D, Troiano A, Malanga M, Calabro' V. Quesada P. p63 involvement in poly(ADP-ribose)polymerase 1 signaling of Topoisomerase I dependent DNA damage in carcinoma cells. Biochem Pharmacol 2013;85:999–1006.
[25] Beneke S. Improving chromatin immunoprecipitation (ChIP) by suppression of method-induced DNA-damage signaling. In: Hancock R, editor. The nucleus methods in molecular biology, vol. 1228. New York, NY: Springer Science+-Business Media; 2015. p. 67–81.
[26] Dumaz N, Meek DW. Serine15 phosphorylation stimulates p53 transactivation but does not directly influence interaction with HDM2. EMBO J 1999;18(24):7002–10.
[27] Oren M. Decision making by p53: life death and cancer. Cell Death Differ 2003;10(4):431–42.
[28] Kracikova M, Akiri G, George A, Sachidanandam R, Aaronson SA. A threshold mechanism mediates p53 cell fate decision between growth arrest and apoptosis. Cell Death Differ 2013;20:576–88.
[29] Costanzo A, Pediconi N, Narcisi A, Guerrieri F, Belloni L, Fausti F, et al. TP63 and TP73 in cancer, an unresolved family puzzle of complexity, redundancy and hierarchy. FEBS Lett 2014;588(16):2590–9.
[30] Lupo B, Trusolino L. Inhibition of poly(ADP-ribosyl)ation in cancer: old and new paradigms revisited. BBA 2014;1846:201–15.

Acceptance Letter

19-Feb-2015

Dear Professor Calabrò:

Ref: Regulation of Stearoyl Coenzyme A Desaturase 1 gene promoter in bovine mammary cells

Our referees have now considered your paper and have recommended publication in Animal Biotechnology. We are pleased to accept your paper in its current form which will now be forwarded to the publisher for copy editing and typesetting. The reviewer comments are included at the bottom of this letter, along with those of the editor who coordinated the review of your paper.

You will receive proofs for checking, and instructions for transfer of copyright in due course.

The publisher also requests that proofs are checked and returned within 48 hours of receipt.

Thank you for your contribution to Animal Biotechnology and we look forward to receiving further submissions from you.

Sincerely,
Dr Schook
Editor, Animal Biotechnology
schook@illinois.edu

Reviewer(s)' Comments to Author:

Reviewer: 1

Comments to the Author
I have no further comments

Regulation of Stearoyl Coenzyme A Desaturase 1 gene promoter in bovine mammary cells

Journal:	*Animal Biotechnology*
Manuscript ID:	LABT-2014-0097.R1
Manuscript Type:	Articles
Date Submitted by the Author:	20-Dec-2014
Complete List of Authors:	di Martino, Orsola; Università di Napoli Federico II, Troiano, Annaelena; Università di Napoli Federico II, Addi, Laura; Università di Napoli Federico II, Guarino, Andrea; Università di Napoli Federico II, Calabrò, Serena; Università di Napoli Federico II, Tudisco, Raffaella; Università di Napoli Federico II, Murru, Nicoletta; Università di Napoli Federico II, Cutrignelli, Monica; Università di Napoli Federico II, Infascelli, Federico; Università di Napoli Federico II, Calabrò, Viola; Università di Napoli Federico II,
Keywords:	stearoyl coenzyme A desaturase, regulation of gene expression, bovine mammary cells, fatty acids, insulin

Regulation of Stearoyl Coenzyme A Desaturase 1 gene promoter in bovine mammary cells

O. Di Martino , A. Troiano[§], L. Addi[#], A. Guarino[§], S. Calabrò[#], R. Tudisco[#], N. Murru[#], M.I.Cutrignelli[#] F. Infascelli[#] and V.Calabrò[§*].

[§]Department of Biology, University of Naples "Federico II", Via Cinzia, Monte S. Angelo, 80126 Naples, Italy.

[#]Department of Veterinary Medicine and Animal Production, University of Naples "Federico II", Via F. Delpino 1, 80137 Naples, Italy.

*** Corresponding author**: Viola Calabrò, e-mail address: vcalabro@unina.it.

Running head: SCD1 gene promoter activity in bovine mammary cells

Acknowledgement

We thank Prof. Antonella Baldi of the Laboratory of Cell Culture-Department of Veterinary Science and Technologies for Food safety at the Veterinary Medicine Faculty (University of Milan) for providing the BME-UV1 cells.

This work was supported by Progetto "Bovlac" - PSR 124 2007-2013 "Cooperazione per lo sviluppo di nuovi prodotti, Processi e tecnologie nei settori agricolo e alimentare e settore forestale" Regione Campania.

Conflict of Interest

The authors declare that they have no competing interests.

ABSTRACT

Stearoyl-Coenzyme A desaturase 1 (SCD1) belongs to the fatty acid family of desaturases. In lactating ruminants, the SCD1 protein is highly expressed in the mammary gland and is relevant for the fatty acid composition of milk and dairy products. Bovine mammary epithelial cells (BME-UV1), cultured in vitro, have been proposed as a model to reproduce the biology of the mammary gland. The present study was designed to investigate the responsiveness of bovine SCD1 promoter to serum, insulin, oleic acid and NFY transcription factor in BME-UV1 cells. A luciferase-based reporter assay was used to monitor the transcriptional activity of the SCD1 promoter region in BME-UV1 cells treated or not with insulin and/or oleic acid. The level of endogenous SCD1 mRNA was evaluated by Real time PCR. Insulin (20 ng/mL) induced a 2.0 to 2.5-fold increase of SCD1 promoter activity. Additionally, the effect of insulin was inhibited by oleic acid, serum components, and NFY enforced expression. Serum and NFY showed no synergistic or additive effect on SCD1 promoter activity suggesting that they repress SCD1 transcription through the same responsive element.

Key words: stearoyl coenzyme A desaturase; regulation of gene expression; bovine mammary cells; fatty acids; insulin.

INTRODUCTION

Understanding the basis of lipid homeostasis is fundamental for developing new strategies to combat obesity, diabetes and other diseases of abnormal lipid metabolism. Stearoyl CoA desaturase 1 **(SCD1**, also called Δ^9-desaturase**)** (EC 1.14.99.5) is a short-lived endoplasmic reticulum-bound enzyme that catalyzes the Δ^9-*cis* desaturation of saturated fatty acyl-CoA substrates **(SFAs)** to monounsaturated fatty acids **(MUFAs)**, primarily palmitoyl-CoA and stearoyl-CoA into palmitoleoleyl-CoA and oleyl-CoA, respectively (1). Oleic acid, the main product of SCD1 reaction, is the predominant fatty acid of human adipose tissue triacylglycerols, associating SCD1 with the development of obesity and metabolic syndrome. Moreover, as the SFA/MUFA ratio affects membrane phospholipid composition and fluidity; it has been implicated in obesity, diabetes, neurological disease, skin disorders and cancer (2). Stearoyl CoA desaturase 1 gene homologs have been identified in a range of species, many of which express multiple isoforms, with SCD1 being the most abundant isoform in lipogenic tissues (3; 4). The SCD1 gene plays an important role in converting *trans-11* C18:1 vaccenic acid into *cis-9, trans-11* C18:2 CLA (5) and is highly expressed in the mammary gland of lactating ruminant (6). Early after parturition, the SCD1 activity in adipose tissue decreases while increasing in mammary gland (7).

Activity and expression of SCD1 have been reported to be regulated by fatty acids, although the responses appear to vary among the species. For instance, oleic acid was shown to reduce rat and bovine SCD1 promoter activity (8; 9) but had no effect on

human SCD1 mRNA synthesis (10). Promoter elements that are responsible for the PUFA repression localize with the promoter elements for SREBP-mediated regulation of the SCD gene (11). In *Bos Taurus,* the PUFA response region (PUFA-RE, 60 bp) is essential for the control of SCD1 expression by PUFA (12). This region encompasses the binding sites for Sp1 and NFY transcription factors and the Sterol Response Element (SRE) which is the binding site for the SREBP1 protein. Recently, it has been demonstrated that SREBP1 cooperates extensively with NFY in the control of genes involved in lipid metabolism. Moreover, promoters of genes involved in lipid metabolism were preferentially occupied by the combination of SREBP1 and NFY factors while genes involved in carbohydrate metabolism were enriched among targets of SREBP1 alone (13). In the present study, we have explored the ability of oleic acid and serum to repress SCD1 promoter activity in control and insulin-stimulated BME-UV1 immortalized cells that can mimic the in vivo response of bovine mammary cells. Moreover, since oleic acid was reported to have no effect on human SCD1 mRNA synthesis (10) we performed similar experiments in MCF7 cells, a human breast cancer cell line previously defined as a model for the study of insulin action on mammalian cell metabolism (14).

MATERIALS AND METHODS

Cell Culture

The BME-UV1 cell line was established from primary bovine mammary epithelial cells by stable transfection with a plasmid, carrying the sequence of the simian virus 40 early region mutant tsA58, encoding the thermolabile large T antigen (15). BME-UV1 cells were provided to us by the Laboratory of Cell Culture-Department of Veterinary Science and Technologies for Food safety at the Veterinary Medicine Faculty (University of Milan) and cultured according to Cheli et al., 1999. Human breast cancer MCF7 cells were purchased from Cell Line Service (CLS, Germany). MCF7 cells were routinely grown into 100 cm^2 plates (Corning Life Science, Corning, NY, USA) as a monolayer culture in Dulbecco's modified Eagle's medium (DMEM) (EuroClone, Pero, MI) supplemented with 10% (v/v) fetal bovine serum (FBS) (EuroClone), in humidified incubator with 5% CO_2 at 37° C.

Construction of SCD1_PGL3 reporter plasmid containing the bovine SCD1 promoter

A 600 bp genomic fragment containing the SCD1 proximal promoter region, -590 from the transcription start site (+1) was amplified by PCR. The amplified region is shown in Figure 1A and contains the SP1, SRE and NFY binding sites (Figure 1A and B). Whole genomic DNA was isolated from leucocytes of cow peripheral blood and used as template for PCR using bovine SCD1-promoter specific primers: *Forward* 5'**GCATGGTA**CCCCAGTGCCCATC and *Reverse*

*5'*GGTACCGCGCTGCACGGTGC. The primers included a 8 extra-bases (indicated by small caps) to generate protected *XhoI* or *KpnI* restriction sites. The PCR conditions are given as follows: 94°C for 30 s, 40 cycles of 57°C for 1 min and a final extension step at 72°C for 1 min. The PCR fragment was gel purified and appropriately digested with *XhoI* or *KpnI* restriction enzyme (Roche diagnostics, MI, Italy) to produce cohesive ends. After a step of purification, the digested DNA insert was directionally cloned into the promoter-less luciferase reporter vector, pGL3-Basic (Promega, Madison USA), using *XhoI* and *KpnI* cloning sites. Ligation reaction was set up at a vector to insert ratio of 1:5, using 50 ng of pGL3-Basic vector. T4 DNA ligase and 1X ligase buffer were used according to manufacturer's instructions. Positive clones were first selected for the presence of the *XhoI* and *KpnI* 600 bp restriction fragment, by agarose gel electrophoresis, and then sequenced.

The 2.4 Kb fragment containing the p21WAF promoter was retrieved from the p21WAF-CAT plasmid (16) and ligated into the HindIII site of pGL3-basic Vector (Promega) to obtain the p21WAF-Luciferase reporter construct.

cDNAs encoding human NFYA, NFYB and NFYC proteins cloned in pBK-CMV expression vector (Stratagene) were provided to us by Dr. Maria Morasso (NIH, Bethesda).

Transient transfections and luciferase assay

MCF-7 or BME-UV1 cells were counted and seeded in 6-well plates at a density of $2.5X10^5$ cells/well in 4 mL of complete medium. For luciferase assay, each

experimental point was transfected with 1 µg of PGL plasmid (SCD1_PGL3, p21WAF_PGL3 or PGL3 basic vector). Briefly plasmid DNA was diluted in 250 µl of DMEM serum free and mixed with 2,5 µl of Lipofectamine 2000 (Life Technologies, CA, USA) in 250 µl DMEM serum free. Transfection master mixtures were incubated at room-temperature for 20 min, prior to drop-wise addition to MCF7/BME-UV1 cells. Complexes were added to the cells containing 1 mL of DMEM and 0, 5 or 10% FBS/FCS). After 24 h transfection, the medium was removed, cells were washed twice with PBS and then lysed using the Lysis Buffer (Promega) according to manufacturer's instructions. *Firefly* luciferase activity in cell lysates was measured using Dual Luciferase Assay kit (Promega), according to the manufacturer's instructions. Results were normalized against protein concentration (Bradford Assay, Biorad).

To evaluate the effect of NFY transcription factor, MCF7 cells were co-transfected with 0.5 γ of SCD1_PGL3 basic construct and 0.5 γ of each NFY subunit (NFY-A, NFY-B, NFY-C). Four hours after transfection, the cells were incubated with 0%, 5% or 10% FBS, for 24 h. The promoter activity was evaluated by Luciferase assay.

To evaluate the effect of insulin on SCD1 promoter activity, insulin was added to MCF7 and BME-UV1 cells, at a concentration of 20 ng/mL (3.4 10^{-9} M), 4 h after transfection. Physiologic concentrations of insulin range between 10^{-8} and 10^{-11} (14) therefore treatment with 3.4 10^{-9} M insulin is expected to induce a physiological response in mammalian cells.

Cells were then incubated for 24 hours. To evaluate the promoter response to MUFA, oleic acid (≥ 99% purity, Calbiochem) was added to a concentration of 30 and 50 μM according to a previously published manuscript (17).

Immunoblot

Immunoblots (IB) was performed as previously described (18). NF-YA (G2, sc-17753) and NF-YB (FL207, sc13045) antibodies (Santa Cruz Biotechnology Inc.) were used to specifically detect expression of NFYA or B subunits and used at 1:200 dilution. The anti-GAPDH (6C5) was purchased from Santa Cruz (Biotechnology Inc.).

mRNA quantification by qPCR

SCD1 specific transcript was amplified by quantitative PCR. The primers designed for qPCR reaction are: *Forward* TCCGACCTAAGAGCCGAGAA and *Reverse* AGCACAACAACAGGACACCA (NCBI Reference Sequence: NM_173959.4, from 751 to 823, amplified fragment 72 bp). Total RNA was extracted from BME-UV1 cells maintained in culture with FCS 0% or 10%, with or without insulin (20 ng/mL) (Sigma-Aldrich, St. Louis, MO) using Cells to Ct™ kit (Ambion, Life Technologies), according to the manufacturer's instructions. To evaluate the response of SCD1 endogenous gene in BME-UV1 cells to MUFA, oleic acid ≥ 99% purity (Calbiochem, Millipore, Germany) was added to a concentration of 30 and 50 μM.

For PCR analysis total RNA was isolated using the RNA Extraction Kit from Qiagen (Hilden, Germany) according to the manufacturer's instructions. RNA (2-

5µg) was treated with DNAse I (Promega, Madison USA) and used to generate reverse transcribed cDNA using SuperScript III (Life Technologies, CA, USA) and random examers in 20 µl of total reaction volume. All samples in each experiment were reverse transcribed at the same time and the resulting cDNA diluted 1:5 in nuclease-free water and stored in aliquots at –80°C until used.

Real Time PCR with SYBR green detection was performed with a 7500 RT-PCR Thermo Cycler (Applied Biosystem, Foster City, USA). The thermal cycling conditions were composed of 50ºC for 2 min followed by an initial denaturation step at 95ºC for 10 min, 45 cycles at 95ºC for 30s, 60ºC for 30s and 72ºC for 30s. For the qPCR the relative quantification in gene expression was determined using the $2^{-\Delta\Delta Ct}$ method (19). As previously suggested, Eukaryotic translation initiation factor 3 subunit K (EIF3K) and Glyceraldehyde-3-phosphate dehydrogenase (GAPDH) were used as an internal controls to normalize all data (20). After normalization, the data were presented as fold change relative to the control sample. Appropriate no-RT and non-template controls were included in each 96-well PCR reaction and dissociation analysis was performed at the end of each run to confirm the specificity of the reaction.

Statistical analysis

All experiments were performed in triplicate and repeated at least two times. Quantitative data were presented as mean ± standard deviation (SD). Comparison between data was analyzed using t-tests. Significant differences were accepted when P values is less than 0.05

RESULTS

The effect of Fetal Bovine Serum and Insulin on SCD1 promoter activity

The sequence of full length SCD1 promoter in *Bos Taurus* (1880 base pairs) is annotated in the (EMBL BANK) with the accession number AY241932 while a partial promoter region of *Bubalus bubalis* SCD1 is included in the ENA database (EMBL gene BANK) with the accession number FM876222. Comparison of the SCD1 proximal promoter region of several mammalian species, using the TFBIND and the TRANSFAC (ver.3.4) software, reveals high homology. The SCD1 proximal promoter sequences of *Bos Taurus* and *Bubalus bubalis* share 97% of identity. Figure 1a shows the PUFA-responsive SCD1 promoter region encompassing the perfectly conserved binding sites for Sp1, the SREBP-1c and NF-Y transcription factors, as previously described (8).

To evaluate bovine SCD1 promoter activity we generated the SCD1_PGL3 luciferase reporter construct. The bovine SCD1 promoter region including the PUFA-RE was PCR amplified from genomic cow DNA and appropriate primers (see Materials and Methods). The 600 bp amplified fragment was cloned upstream of the luciferase gene in the PGL3 promoter-less vector (Promega) to generate the SCD1_PGL3 reporter construct.

Cell culture conditions can have a profound impact on intracellular signaling cascade and may be a fondamental source of variability accounting, at least in part, for the conflicting results in the SCD1 litterature. For instance, oleic acid was reported to

reduce rat and bovine SCD1 promoter activity (8; 9) while having no effect on human SCD1 mRNA synthesis (10). To determine the extent to which serum affects SCD1 promoter activity, MCF7 cells were grown in serum-free or serum-supplemented medium (5-10% FBS) and transiently transfected with the SCD1_PGL3 construct or the p21WAF_PGL3 plasmid, containing a serum-independent promoter (our previous observations). The promoter-less pGL3 basic vector was used to evaluate the background signal. At 24 hrs after transfection, cells were collected, whole cell extracts were prepared and subjected to luciferase assay. As shown in Fig. 2a, in presence of serum, the p21WAF promoter activity was unaffected while the SCD1 promoter activity was significantly reduced ($p < 0.02$). In 10% FBS the SCD1 promoter activity was about 4.3 folds lower than in serum-free medium, with a residual activity ranging between 15 and 25 %. The background activity of pGL3 basic construct was negligible in both serum conditions (4.3 +/- 1.5 RLU, arbitrary units of luciferase activity).

Next, we monitored the effect of insulin on SCD1 promoter activity. The experiments were performed in serum-free condition or 10% serum as this is the most commonly used condition for the growth of mammalian cell lines. Insulin was added to the medium at the concentration of 20 ng/mL. In serum-free medium, insulin treatment caused a 2.5-fold induction of the SCD1 promoter reporter (Fig. 2b). After FBS-supplementation, the SCD1 promoter basal activity was reduced and insulin treatment was unable to evoke any response (Fig. 2b). The results demonstrate that serum components exert a strong repression on the SCD1 promoter and that insulin appears to be unable to overcome this repression.

Role of NFY transcription factor in the regulation of SCD1 promoter activity.

NFY factor has been suggested to be a PUFA-specific transcription factor for SCD1 gene repression (11). The transcription factor NFY is a hetero-trimeric protein, composed of three subunits NFY-A, NFY-B and NFY-C. NF-YB and NF-YC must interact and dimerize for association with NF-YA and consequent binding to CCAAT motifs in the promoter regions of a variety of genes. NFY interacts with the Sterol Regulatory Element-Binding Proteins (SREBPs). SREBPs, indeed, are weak transcriptional activators on their own and interact with their target promoters in cooperation with additional regulators, most commonly including one or both NFY and SP1 transcription factors. To investigate the effect of NFY enforced expression on SCD1 promoter activity, we transiently transfected the SCD1_PGL3 reporter construct into MCF7 cells along with an equal amount of each plasmid encoding NFY subunit A, B or C. Four hours after transfection, the culture medium was replaced and cells were maintained in serum-free, 5% or 10% FBS-supplemented medium for 24 h. The expression of transfected NFY subunit A and B was monitored by immunoblot analysis using NFY specific antibodies (Figure 3A). The SCD1_PGL3 activity was then evaluated by Luciferase assay. As expected, in serum-supplemented media the basal activity of SCD1 promoter was lower than in serum-free medium (Fig. 3A). However, both in absence and 5% serum NFY expression causes a significant decline of luciferase activity ($p < 0.02$) indicating that NFY is a transcriptional repressor of SCD1 gene. However, in 10% serum the residual activity of SCD1 promoter was 50% of the control and NFY caused only a

15 % reduction thereby suggesting that serum and NFY compromise SCD1 promoter activity by acting at the same regulatory element.

Regulation of SCD1 promoter activity in bovine mammalian cells

The regulation of SCD1 expression in bovine mammary cells affects milk yield and fatty acid profile (21). SCD1 is induced by insulin (22). It was interesting to study the effect of insulin on SCD1 gene expression in BME-UV1 cells, immortalized, but not transformed, bovine mammary cells that closely mimic the *in vivo* mammary epithelial cells. The promoter reporter construct was transiently transfected into BME-UV1 grown in serum-free, 5% or 10% FCS with or without insulin (20 ng/mL). BME-UV1 cells were transiently transfected with SCD1_PGL3 construct and after 24 hours whole cell extracts were prepared and subjected to the luciferase assay. According to what observed in MCF7 cells, serum-addition repressed SCD1 activity in bovine mammary cells (Fig. 4A). Again, we observed a 2.5 fold promoter activation by insulin only in serum-starved cells showing that the repressive activity of serum is dominant over the inductive effect of insulin. To corroborate these data, we decided to examine the level of SCD1 endogenous mRNA in BME-UV1 cells by quantitative Real Time PCR. Cells were grown in serum-free or 10% FCS medium and treated or not with insulin (20 ng/mL), for 24 hours. Total RNA was isolated and subjected to quantitative PCR using primers to specifically amplify bovine SCD1 mRNA. The level of SCD1 specific transcript was normalized against the 18S ribosomal RNA and expressed as relative amount respect to the sample obtained in

serum and insulin-free medium. As shown in Fig. 4B, we confirmed that insulin treatment enhanced SCD1 mRNA expression level only in serum-deprived cells.

Regulation of SCD1 promoter by oleic acid is still controversial. Oleic acids concentrations up to 100 μM were previously demonstrated do not affect MCF7 cell proliferation and viability (23). However, we performed preliminary test by treating MCF7 and BME-UV1 with increasing amount of oleic acid (15, 30, 50, 80 and 100 μM) for 24 and 48 hours. In each experimental point the cells behave healthy. Moreover, cells lysates were analyzed by immunoblot with antibodies against Caspase3 and PARP and we did not detect signs of apoptosis neither in terms of Caspase 3 induction nor Poli ADP-ribose polymerase cleavage.

(data not shown). To check the effect of oleic acid in the control of bovine SCD1 promoter we transiently transfected BME-UV1 cells with the SCD1 promoter-luciferase reporter in serum-free medium supplemented or not with 30 or 50 μM oleic acid.

The combined effect of insulin and oleic acid was checked by adding insulin at a concentration of 20 ng/mL in cells treated or not with oleic acid. 24 hours after transfection, whole cell extracts were prepared and subjected to the luciferase assay.

As shown in Fig. 5A, oleic acid alone did not significantly changed the basal activity of SCD1 promoter which was instead efficiently activated by insulin. Interestingly, insulin-dependent activation was almost completely abolished by oleic acid addition to the culture medium showing that, similar to serum, the repressive activity of oleic acid overrides the inductive effect of insulin. To substantiate these data, we decided to examine the level of SCD1 endogenous mRNA in BME-UV1 cells by quantitative

Real Time PCR. Cells were grown in serum-free medium supplemented or not with 30 or 50 μM oleic acid for 24 hours. The combined effect of insulin and oleic acid was checked by adding insulin at a concentration of 20 ng/mL. Total RNA was isolated and subjected to quantitative PCR using primers to specifically amplify bovine SCD1 mRNA. The level of SCD1 specific transcript was normalized against the EIF3K and GAPDH RNA and expressed as relative amount respect to the sample obtained in oleic acid and insulin-free medium. As shown in Fig. 5B, we confirmed the induction of SCD1 endogenous gene transcription by insulin which was completely suppressed by oleic acid.

DISCUSSION

Alignment of the highly conserved region of bovine SCD1 promoter region shows the expected high homology of the putative PUFA-RE between different farm animal species. This region is known to be involved in the response of SCD promoter to insulin, fatty acids and sterols (24). The PUFA-RE contains binding sites for SREBP1, NFY and SP1 transcription factors. Genome-wide analysis of promoter co-occupancy, in human liver cells, have recently shown that SREBP1 cooperates extensively with NFY and SP1 throughout the genome, thereby suggesting that the regulatory circuitry among SREBP, NFY and SP1 is highly interconnected. Concerning the metabolic pathways, combination of all three factors was reported to be involved in the control of cholesterol biosynthesis and aminoacid activation while the combination of SREBP1 and NFY alone was shown to regulate lipid metabolism and RNA processing (13).

The expression of the SCD 1 gene is under complex control mechanisms such as hormones and, possibly, intermediates of carbohydrate and fat metabolism therefore it is difficult to dissect all the agents that regulate SCD1 gene transcription by *in vivo* models. The aim of this study was to investigate the responsiveness of bovine SCD1 promoter to insulin, oleic acid and NFY in BME-UV1 cells, a potential in vitro model for studying biotransformation in bovine mammary gland.

In the mammary gland of ruminants, SCD1 is known to be responsible for the production of about 63-97% of c9t11 CLA coming from vaccenic acid as estimated using either direct (13C-labelled fatty acids) or indirect methods (inhibition of SCD

by sterculic acid or duodenal and milk FA flows) (25). SCD1 activity can be measured by comparing the product/substrate ratios of certain fatty acids. There are four main products of SCD1 activity in the mammary gland of ruminants: c9C14:1, c9C16:1, c9C18:1 and CLA, which are produced from C14:0, C16:0, C18:0 and trans11 C18:1, respectively. According to Lock and Garnsworthy (26), the best indicator of SCD1 activity is the c9C14:1/C14:0 ratio because all of the C14:0 in milk fat is produced via de novo synthesis in the mammary gland; consequently, desaturation is the only source of C14:1. Increasing c9C14:1/C14:0 ratio values would indicate an increase of SCD1 activity.

The regulation of SCD1 by dietary factors has been largely investigated in rodents (11), while in ruminants the results are conflicting. Ahnadi et al. (27) and Harvatine and Bauman (28) found a depression of mammary SCD1 mRNA abundance when lactating cows were fed protected PUFA. Researches effected on goats showed that the supplementation of sunflower seed oil (29) and linseed oil (30) did not affect both SCD1 expression and/or activity in maize silage-based diets while the same supplementation to diets based on grass hay decreased only the SCD1 activity (31). Similar results have been reported supplementing soya beans to lucerne hay-based diets (32). Finally, supplementing grass hay-based diets with formaldehyde-treated linseed decreased mammary SCD1 mRNA without effect on the SCD1 activity (32). Tudisco et al (33) reported higher SCD1 expression in the somatic cells of milk yielded from goats bred according either organic system than those bred in stable. The authors justify the results for the a higher amount of both C18:2 and C18:3

ingested by organic group than the stable group, as registered in previous researches (34; 35) thus probably resulting in an up-regulation of the SCD expression.

Bernard et al. (36) suggest to evaluate the importance of interactions between the composition of the basal diet and lipid supplement with the implication that specific PUFA escaping metabolism in the rumen or specific biohydrogenation intermediates may inhibit SCD1 activity via transcriptional or post- transcriptional regulatory mechanisms.

More recently, Tudisco et al (37) reported that the grazing season as well as lactation stage can affect the SCD1 mRNA abundance determined from milk somatic cells with values that progressively decreased from April until June, increased in July and decreased again in August.

In keeping with previous findings (38), we found that insulin treatment induces a significant increase of SCD 1 gene promoter activity in BME-UV1 cells, providing further evidence of its pro-lipogenic role. However, attention must be paid to the evaluation of SCD1 promoter regulation in serum-supplemented cell culture as the repressive effect of serum on SCD1 promoter activity overcomes induction by insulin and this was consistently shown both in human MCF7 and bovine BME-UV1 cells. Remarkably, oleic acid was also able to repress SCD1 promoter activation only in insulin treated cells thereby providing a possible explanation of the controversial literature about the inhibitory effect of oleic on SCD1 expression (11). We confirmed our data on SCD1 endogenous transcription of BME-UV1 cells, thereby demonstrating that our reporter system truly reflects the response of the endogenous SCD1 gene promoter and can be a useful tool to investigate the modulation of SCD1

promoter activity by nutrients and extracellular stimuli. Finally, our study provides evidences that NFY enforced expression represses SCD1 promoter activity. It has to be mentioned that Tabor and coworkers (22) reported that NFY transcription factor is a SCD1 transcriptional activator in adipocytes; our data are in contrast with Tabor conclusion and this might depend on the specific cell type and growing condition used. However, whether NFY works in cooperation or not with other transcription factors, deserves more attention and will be the subject of further investigations.

References

1. Ntambi, J. M. The regulation of stearoyl-CoA desaturase (SCD). Prog. Lipid Res. 1995; 34, 139-150.
2. Paton, C.M., Ntambi, J.M. Biochemical and Physiological Function of Stearoyl-CoA Desaturase. Am J Physiol Endocrinol Metab. 2009; 297:28-37.
3. Flowers, M. T., Groen A. K., Oler, A. T., Keller, M. P., Choi, Y. J., Schueler, K.L., Richards O.C., Lan, H., Miyazaki M., Kuipers, Kendziorski C. M., J. M. Ntambi and A. D. Attie. Cholestasis and hypercholesterolemia in SCD1-deficient mice fed a low-fat, highcarbohydrate diet. J. Lipid Res. 2006; 47:2668-2680.
4. Bionaz, M. and Loor J. Gene networks driving bovine milk fat synthesis lactation cycle. BMC Genomics 9(1). 2008; 366. doi:10.1186/1471-2164-9-366
5. Bauman, D. E., L. H. Baumgard, B. A. Corl, and J. M. Griinari. Biosynthesis of conjugated linoleic acid in ruminants. Proc Am. Soc. Anim. Sci. 1999; Available at: http://jas.fass.org/cgi/content/abstract/77/E-Suppl/1-ae. Accessed Dec. 5, 2005.
6. Ward, R. J., M. T. Travers, S. E., Richards, R. G. Vernon, A. M., Salter, P. J. Buttery, and M. C. Barber. Stearoyl coenzyme A desaturase mRNA is transcribed from a single gene in the ovine genome. Biochim. Biophys. Acta.1998; 1391:145–156.
7. Griinari, J. M., B. A. Corl, S. H. Lacy, P. Y. Chouinard, K. V. Nurmela and D. E. Bauman. Conjugated linoleic acid is synthesized endogenously in lactating dairy cows by Δ9-desaturase. J. Nutr. 2000; 130:2285-2291.

8. Zulkifli R.M., Parr T., Salter A.M. and Brameld J. Salter and John M. 2010. Regulation of ovine and porcine stearoyl coA desaturase gene promoters by fatty acids and sterols. J.Anim.Sci. M. 2010; 88: 2565-2575

9. Keating, A.F., Kennelly J.J., and F. Zhao. Characterization and regulation of the bovine stearoyl-CoA desaturase gene promoter. Biochem. Biophys. Res. Commun. 2006; 200:763-768.

10. Bené, H., Lasky D. and J.M. Ntambi. Cloning and characterization of the human steroyl-CoA desaturase gene promoter: Transcriptional activation by sterol regulatory element binding protein and repression by polyunsaturated fatty acids and cholesterol. Biochem. Biophys. Res. Commun. 2001; .284:1194-1198.

11. Ntambi, J.M.,. Regulation of stearoyl-CoA desaturase by polyunsaturated fatty acids and cholesterol. J. Lipid Res. 1999; 40, 1549–1558.

12. Waters, K.M., Miller, C.W., Ntambi, J.M.. Localization of a polyunsaturated fatty acid response region in stearoyl-CoA desaturase gene 1. Biochim. Biophys. Acta. 1997; 1349(1):33-42.

13. Reed, B.D., Charos, A.E., Szekeley, A.M., Weissman, S.M., Snyder M. Genome-Wide occupancy of SREBP1 and its partners NFY and Sp1 reveals novel functional roles and combinatorial regulation of distinct class of genes. PLOS Genetics. 2008; DOI: 10.1371/journal.pgen.1000133

14. Osborne, C.K., Bolan, G., Monaco, M.E., Lippman, M.E. Hormone responsive human breast cancer in long-term tissue culture. Effect of insulin. Proc. Natl. Acad. Sci USA 1976; 73(12): 4536-4540.

15. Cheli F, Zavizion B, Todoulou O, Politis I. The effect of calcium on mammary epithelial cell proliferation and plasminogen activating system. Can.J. Anim. Sci. 1999; 277-283.

16. Calabrò, V., Mansueto, G., Parisi, T., Vivo, M., Calogero, R.A., La Mantia, G. The human MDM2 oncoprotein increases the transcriptional activity and protein level of the p53 homolog p63. J. Biol. Chem. 2002; 277(4): 2674-81.

17. Harvey, KA, Walker CL, Xu, Z., Whitley, P., Pavlina, T.M., Hise, M., Zaloga, G.P., Siddiqui, R.A. Oleic acid inhibits stearic-induced inhibition of cell growth and pro-inflammatory responses in human aortic endothelial cells. J. Lipid Res. 2010(12): 3470-80.

18. Rossi, M., De Simone, M., Pollice, A., Santoro, R., La Manti, G., Guerrini, L., Calabrò, V. Itch/AIP4 associates with and promotes p63 protein degradation. Cell Cycle. 2006; 5(16):1816-22.

19. Livak, K.J., Schmittgen, T.D. Analysis of relative gene expression data using Real-Time 436 Quantitative PCR and the 2-DDCT method. Methods. 2011(25): 402-408.

20. Kadegowda, A.K.G., Bionaz, M., Thering, B., Piperova, L.S., Erdman, R.A., Loor, J.J. Identification of internal control genes for quantitative polymerase chain reaction in mammary tissue of lactating cows receiving lipid supplements. J Dairy Sci. 2009; 92(5): 2007–2019.

21. Pauciullo A, Cosenza G, Steri R, Coletta A, La Battaglia A, Di Berardino D, Macciotta NP, Ramunno L. A single nucleotide polymorphism in the promoter region of river buffalo stearoyl CoA desaturase gene (SCD) is associated with milk yield. J Dairy Res. 2012; 79(4):429-35.

22. Tabor, D.E., Kim, J.B., Spiegelman B.M. and Edwards P.A. Identification of conserved cis-elements and transcription factors required for sterol-regulated transcription of stearoyl-CoA desaturase 1 and 2. J. Biol. Chem. 1999; 274:20603-20610.

23. Dailey, O.D. Jr, Wang, X., Chen, F., Huang, G. Anticancer activity of branched-chain derivatives of oleic acid. Anticancer Res 2011, 31 (10):3165-9 .

24. Biddinger, S., Miyazaki, M., Boucher, J., Ntambi, J. and Kahn, C.R. Leptin Suppresses Stearoyl-CoA Desaturase 1 by Mechanisms Independent of Insulin and Sterol Regulatory Element–Binding Protein-1c. Diabetes. 2006; 55, 2032-2041

25. Bernard, L., Leroux, C., Chilliard, Y. Nutritional regulation of mammary lipogenesis and milk fat in ruminant: contribution to sustainable milk production. Revista Colombiana de Ciencias Pecuarias 2013; 26, 292-302.

26. Lock, A.L., Garnsworthy, P.C. Seasonal variation in milk conjugated linoleic acid and D9-desaturase activity in dairy cows. Livestock Production Science. 2003; 79, 47–59.

27. Ahnadi, C.E., Beswick, N., Delbecchi, L., Kennelly, J.J., Lacasse, P. Addition of fish oil to diets for dairy cows. II. Effects on milk fat and gene expression of mammary lipogenic enzymes. J. Dairy Res. 2002; 69, 521–531.

28. Harvatine, K.J., Bauman, D.E. SREBP1 and thyroid hormone responsive spot 14 (S14) are involved in the regulation of bovine mammary lipid synthesis during diet-induced milk fat depression and treatment with CLA. J. Nutr. 2006; 136, 2468–2474.

29. Bernard, L., Rouel, J., Leroux, C., Ferlay, A., Faulconnier, Y., Legrand, P., Chilliard, Y. Mammary lipid metabolism and milk fatty acid secretion in alpine goats fed vegetable lipids. Journal of Dairy Science. 2005; 88, 1478–1489.

30. Bernard, L., Bonnet, M., Leroux, C., Shingfield , K. J., Chilliard, Y. Effect of sunflower-seed oil and linseed oil on tissue lipid metabolism, gene expression, and milk fatty acid secretion in alpine goats fed maize silage–based diets. Journal of Dairy Science. 2009;92, 6083–6094.

31. Bernard, L., Leroux, C., Faulconnier, Y., Durand, D., Shingfield, K.J., Chilliard, Y. Effect of sunflower-seed oil or linseed oil on milk fatty acid secretion and lipogenic gene expression in goats fed hay-based diets. Journal of Dairy Research 2009;76, 241–248.

32. Bernard, L., Leroux, C., Bonnet, M., Rouel, J., Martin, P., Chilliard, Y. Expression and nutritional regulation of lipogenic genes in mammary gland and adipose of lactating goats. Journal of Dairy Research. 2005; 72, 250–255

33. Tudisco, R., Calabrò, S., Cutrignelli, M.I., Moniello, G., Grossi, M., Gonzalez, O.J., Piccolo, V., Infascelli, F. Influence of organic systems on Stearoyl-CoA-Desaturase in goat milk. Small Ruminant Research. 2012; 106, 37-42.

34. D'Urso, S., Cutrignelli, M.I., Calabrò, S., Bovera, F., Tudisco, R., Piccolo, V., Infascelli, F. Influence of pasture on fatty acid profile of goat milk. Journal of Animal Physiology and Animal Nutrition 2008; 92, 405-10

35. Tudisco, R., Cutrignelli, M.I., Calabrò, S., Piccolo, G., Bovera, F., Guglielmelli, A., Infascelli, F. Influence of organic systems on milk fatty acid profile and CLA in goats. Small Ruminant Research. 2010; 88: 151-155.

36. Bernard , L., Leroux , C., Chilliard. Expression and Nutritional Regulation of Stearoyl-CoA Desaturase Genes in the Ruminant Mammary Gland: Relationship with Milk Fatty Acid Composition. In: Ntambi, J.M. (Ed.), Stearoyl-CoA Desaturase Genes in Lipid Metabolism, Springer Science+Business Media New York. Y.2013;161-193.

37. Tudisco, R., Grossi, M., Calabrò, S., Cutrignelli, M.I., Musco, N., Addi, L., Infascelli F. Influence of pasture on goat milk fatty acids and Stearoyl-CoA desaturase expression in milk somatic cells. Small Ruminant Research. 2014; DOI: 10.1016/j.smallrumres.2014.07.016.

38. Mauvoisin, D., Rocque, G., Arfa, O., Radenne A., Boissier P., Mounier C. Role of the PI3-kinase/mTor pathway in the regulation of the stearoyl CoA desaturase (SCD1) gene expression by insulin in liver. J Cell Commun Signal. 2007 ; 1(2), 113-125.

Legends to figures

Figura 1. **The SCD1 gene promoter**. **(A)** Sequence alignment of the PUFA-RE sequence in the SCD1 proximal promoter region underlined the sequences corresponding to the Sp1 protein binding site, the Sterol Responsive Element and the NF-Y/NFI consensus. **(B)** The SCD1 proximal promoter region. The primers used for PCR and subsequent cloning are indicated in italic. Underlined are highlighted the sequences corresponding to the Sp1 protein binding site, the Sterol Responsive Element and the NF-Y/NFI consensus. The transcription start site (+1) is indicated in capital.

Figure 2. Effect of FBS on SCD1 promoter activity. (A) The SCD1_PGL3 or p21WAF_PGL3 promoter constructs were transfected into MCF7 cells and treated with different concentrations of serum (0%, 5%,10%). After 24 h the luciferase assay was performed. The p21WAF_PGL3 promoter, was used as a serum independent control. The basal activity of the promoters at 0% FBS was fixed as 100%. Each experimental point was done in triplicate and the results are presented as the mean of three biological replicates. **(B)** The SCD1_PGL3 promoter construct was transfected into MCF7 cells grown in serum-free or 10% Fetal Bovine Serum. Insulin was added at a concentration of 20 ng/ml. After 24 hr the luciferase assay was performed. The basal activity of the promoters at 0% FBS was fixed as 100%. Each experimental point was done in triplicate and the results are presented as the mean of three biological replicates.

Fig.3 Effect of NFY transcription factor and on SCD1 promoter activity into MCF7 cells.

MCF7 cells were co-trasfected with 0.5 μg of SCD-1-PGL3 construct along with 0.5 μg of each plasmid encoding NFY-A, NFY-B and NFY-C subunits. Cells were grow in serum-free medium or media supplemented with 5 or 10% FBS for 24 hrs. **(A)** Expression of transfected NFYA and NFYB protein was evaluated by immunoblot analysis with specific antibodies. **(B)** Promoter activity was evaluated by luciferase assay. Each experimental point was done in triplicate and the results are presented as the mean of three biological replicates.

Figure 4. Effect of serum and Insulin on SCD1 promoter activity. (A) SCD1_PGL3 promoter construct was transfected into BME-UV1 cells treated with the indicated concentrations of serum (0%, 5%, 10%) with or without insulin (20 ng/mL), as indicated. After 24 hr, the promoter activity was evaluated by luciferase assay. Each experimental point was done in triplicate and the results are presented as the mean of three biological replicates.

(B) BME-UV1 cells were treated with the indicated concentrations of serum (0%, 10%) with or without insulin (20 ng/mL), for 24 h. The SCD1 specific transcript was quantified by Real Time PCR and expressed as the relative amount respect to the level expressed in cells grown in serum and insulin-free medium. The results are presented as the mean of three experimental replicates

Figure 5. Effect of insulin and oleic acid on SCD1 promoter activity

(A) SCD1_PGL3 promoter construct was transfected into BME-UV1 cells cultured in serum-free medium with or without insulin (20 ng/mL), as indicated. Oleic acid (30 and 50 μM) was supplemented to the medium as indicated. After 24 hr, the promoter activity was evaluated by luciferase assay. Each experimental point was done in triplicate and the results are presented as the mean of three biological replicates.

(B) BME-UV1 cells were treated as indicated in (A) for 24 h. The SCD1 specific transcript was quantified by Real Time PCR and expressed as the relative amount respect to the level expressed in cells grown in serum-free medium without insulin and oleic acid. The results are presented as the mean of three experimental replicates.

Figure 1

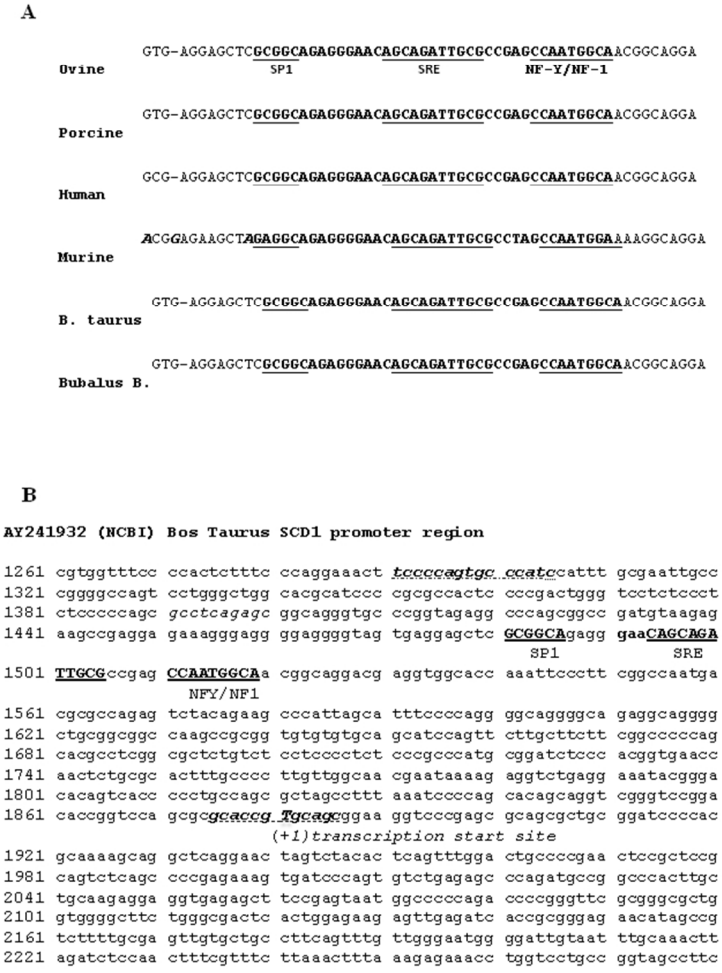

The SCD1 gene promoter. (A) Sequence alignment of the PUFA-RE sequence in the SCD1 proximal promoter region underlined the sequences corresponding to the Sp1 protein binding site, the Sterol Responsive Element and the NF-Y/NFI consensus. (B) The SCD1 proximal promoter region. The primers used for PCR and subsequent cloning are indicated in italic. Underlined are highlighted the sequences corresponding to the Sp1 protein binding site, the Sterol Responsive Element and the NF-Y/NFI consensus. The transcription start site (+1) is indicated in capital.
190x275mm (96 x 96 DPI)

Figure 2

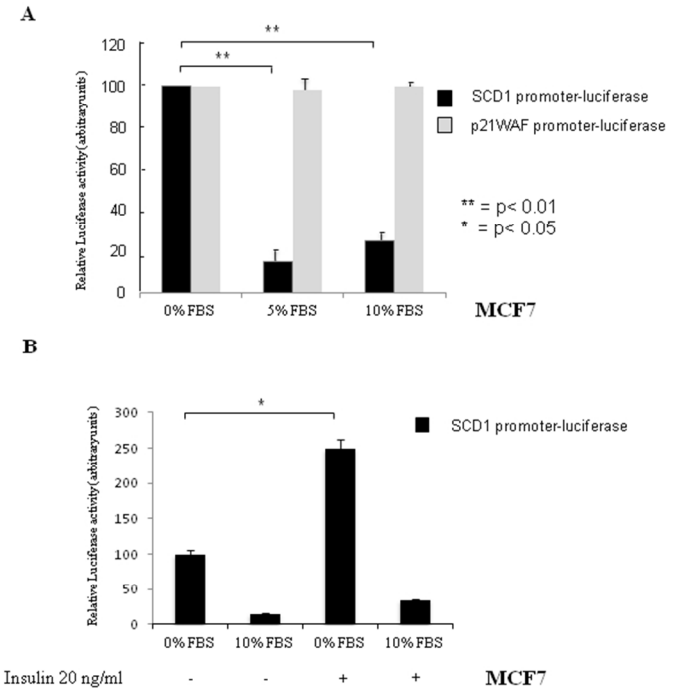

Effect of FBS on SCD1 promoter activity. (A) The SCD1_PGL3 or p21WAF_PGL3 promoter constructs were transfected into MCF7 cells and treated with different concentrations of serum (0%, 5%,10%). After 24 h the luciferase assay was performed. The p21WAF_PGL3 promoter, was used as a serum independent control. The basal activity of the promoters at 0% FBS was fixed as 100%. Each experimental point was done in triplicate and the results are presented as the mean of three biological replicates. (B) The SCD1_PGL3 promoter construct was transfected into MCF7 cells grown in serum-free or 10% Fetal Bovine Serum. Insulin was added at a concentration of 20 ng/ml. After 24 hr the luciferase assay was performed. The basal activity of the promoters at 0% FBS was fixed as 100%. Each experimental point was done in triplicate and the results are presented as the mean of three biological replicates.
190x275mm (96 x 96 DPI)

Figure 3

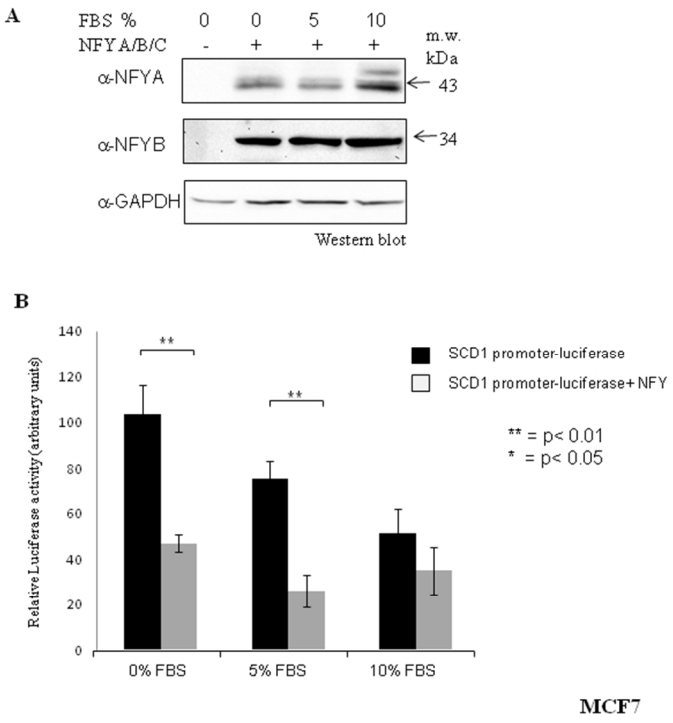

Effect of NFY transcription factor and on SCD1 promoter activity into MCF7 cells.
MCF7 cells were co-trasfected with 0.5 µg of SCD-1-PGL3 construct along with 0.5 µg of each plasmid encoding NFY-A, NFY-B and NFY-C subunits. Cells were grow in serum-free medium or media supplemented with 5 or 10% FBS for 24 hrs. (A) Expression of transfected NFYA and NFYB protein was evaluated by immunoblot analysis with specific antibodies. (B) Promoter activity was evaluated by luciferase assay. Each experimental point was done in triplicate and the results are presented as the mean of three biological replicates.

190x275mm (96 x 96 DPI)

Figure 4

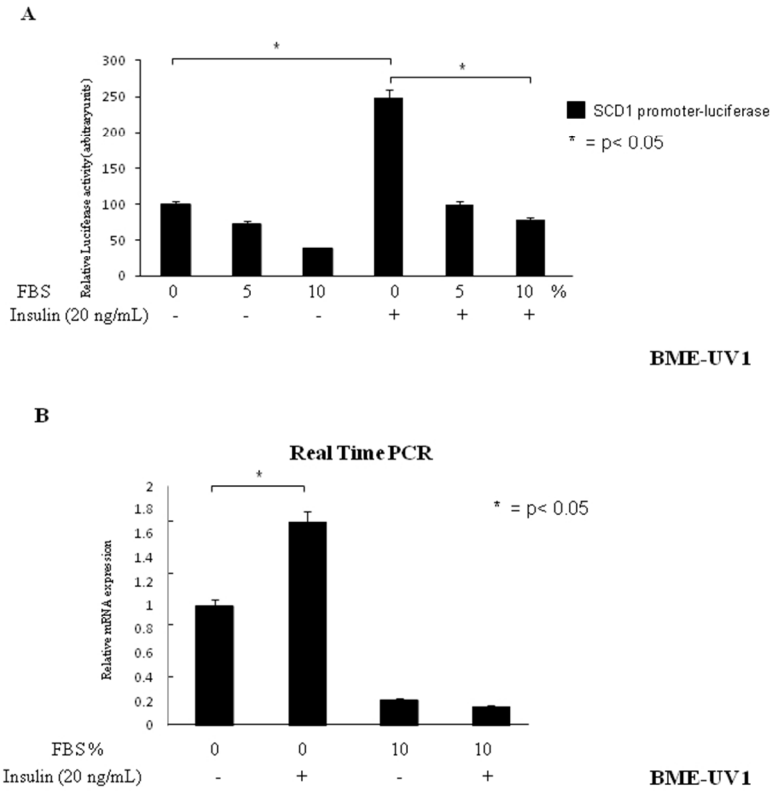

Effect of serum and Insulin on SCD1 promoter activity. (A) SCD1_PGL3 promoter construct was transfected into BME-UV1 cells treated with the indicated concentrations of serum (0%, 5%, 10%) with or without insulin (20 ng/mL), as indicated. After 24 hr, the promoter activity was evaluated by luciferase assay. Each experimental point was done in triplicate and the results are presented as the mean of three biological replicates.
190x275mm (96 x 96 DPI)

Figure 5

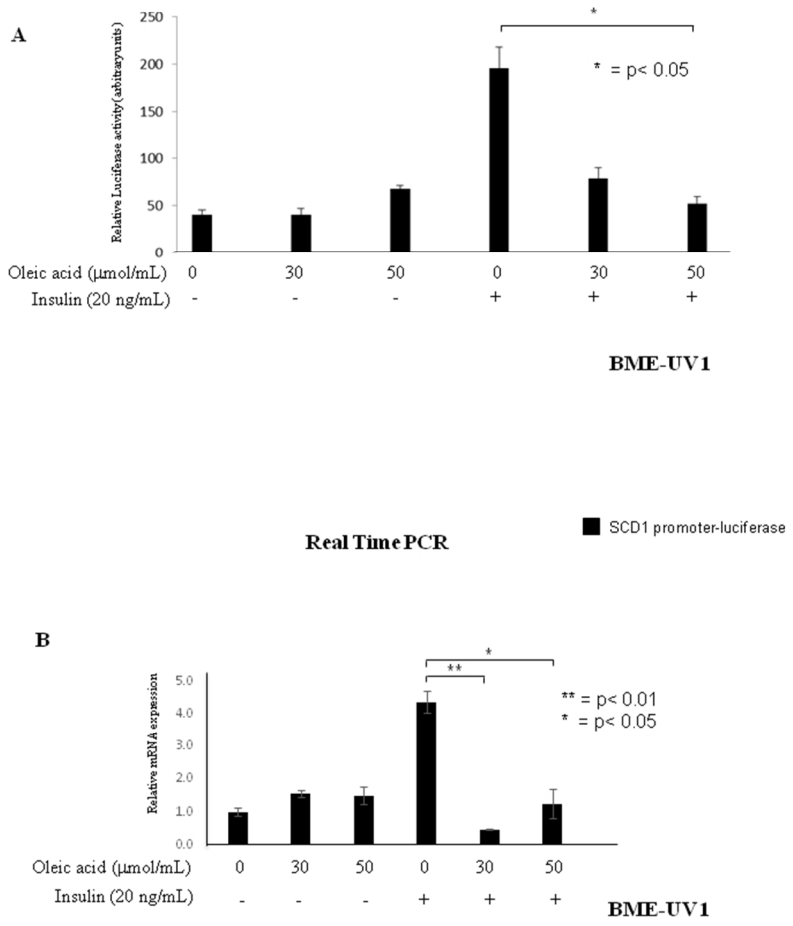

Effect of insulin and oleic acid on SCD1 promoter activity

(A) SCD1_PGL3 promoter construct was transfected into BME-UV1 cells cultured in serum-free medium with or without insulin (20 ng/mL), as indicated. Oleic acid (30 and 50 µM) was supplemented to the medium as indicated. After 24 hr, the promoter activity was evaluated by luciferase assay. Each experimental point was done in triplicate and the results are presented as the mean of three biological replicates.

(B) BME-UV1 cells were treated as indicated in (A) for 24 h. The SCD1 specific transcript was quantified by Real Time PCR and expressed as the relative amount respect to the level expressed in cells grown in serum-free medium without insulin and oleic acid. The results are presented as the mean of three experimental replicates.

190x275mm (96 x 96 DPI)